EXTRAPOLATION OF HIGH WINDS IN COMPLEX TERRAIN: AN APPLICATION IN THE McGREGOR MODEL FOREST, BRITISH COLUMBIA, CANADA

by

Brendan D. Murphy

B.Sc., Saint Mary's University,1987
Cert.Hon., Saint Mary's University,1988
Dip.Sc., University of Alberta, 1992

THESIS SUBMITTED IN PARTIAL FULFILMENT OF

THE REQUIREMENTS FOR THE DEGREE OF

MASTER OF SCIENCE

in

ENVIRONMENTAL SCIENCE

THE UNIVERSITY OF NORTHERN BRITISH COLUMBIA

December 2001

0-612-80709-6

APPROVAL

Name: Brendan D. Murphy

Degree: Master of Science

Thesis Title: EXTRAPOLATION OF HIGH WINDS IN COMPLEX TERRAIN: AN APPLICATION IN THE McGREGOR MODEL FOREST, BRITISH COLUMBIA, CANADA

Examining Committee:

Chair: Dr. Darwyn Coxson
Associate Professor, Biology Program
UNBC

Supervisor: Dr. Peter Jackson
Associate Professor, Environmental Studies Program
UNBC

Committee Member: Dr. Joselito Arocena
Associate Professor, Forestry Program
UNBC

Committee Member: Cliff Raphael, MSc
College Professor, Department of Geography
College of New Caledonia

External Examiner: Dr. John D. Wilson
Professor, Department of Earth & Atmospheric Sciences
University of Alberta

Date Approved: Jan 16 2002

Abstract

This thesis describes the development and application of a technique to estimate high winds in complex and data-sparse terrain. The technique is used to characterize the 2-dimensional near-surface horizontal wind field in the McGregor Model Forest (MMF) of British Columbia under a typical storm scenario. An analysis of historical wind extremes in the Central-Interior of British Columbia reveals that southerly gusts associated with fall and winter cyclones account for most extreme wind events in the region. To determine the climatology of this windy season, daily weather maps of mean sea-level pressure from October through March are averaged for the 25-year period from 1970 to 1994. A storm composite is then constructed by including only those maps where the daily extreme gust speed at the Prince George Airport was from a southerly direction. A pressure anomaly map for strong winds is constructed by subtracting the composite from climatology, and the statistical significance of the composite is tested at the 99% level using a Student's t-test. The analysis is repeated to construct individual composites for moderate (51-70 km/h), strong (71-90 km/h) and severe (>90 km/h) southerly gust events. Map-pattern classification techniques are then used to identify a representative map pattern for each storm scenario. These "keyday" scenarios are then simulated with a 3-dimensional mesoscale numerical model whose output is used to determine wind speed ratios between grid points in the complex forested terrain and a neighbouring airport location. The speed ratios provide an estimate of the winds likely to occur above the forest canopy in the MMF based on a single wind measurement at the Prince George Airport.

Strong gusty winds can knock down trees in forested areas (windthrow) resulting in economic loss to the forest industry, particularly if inappropriate forestry practices are employed in areas prone to high winds. The complex terrain and sparsity of wind data in forested areas is a major obstacle to the development and implementation of wind risk management strategies in British Columbia. By providing a potential-risk surface for terrain prone to high winds, this project represents a first step toward a windthrow-risk assessment model for the McGregor Model Forest.

TABLE OF CONTENTS

Tables **Page**

Figures **Page**

Preface

Funding for this thesis project was provided by the McGregor Model Forest Association (MMFA). The McGregor Model Forest (MMF) is one of ten model forests established under Canada's Green Plan to support the shift toward sustainable forestry management. This shift has required the recognition of forests as complex and dynamic ecosystems sustained by natural renewal processes and disturbance regimes which operate at multiple scales, from individual sites to extensive landscapes. A goal of the MMFA is to develop a knowledge and understanding of the natural processes that have shaped the forest ecosystem and to model these processes, allowing possible future conditions of the landscape to be portrayed and evaluated relative to key social, economic, and ecological concerns (McGregor Model Forest, 1994a). The focus of the initial five-year work plan developed by the MMFA has been a decision support system for analysing forest management options known as the "Brass Ring" (McGregor Model Forest, 1994b). The MMFA made the strategic decision to focus its initial activities toward modelling key ecological processes and human-induced disturbances at the landscape level. To support the development of the Brass Ring, seven research teams were formed, conducting a total of 31 projects (McGregor Model Forest, 1995).

In 1993, the MMFA realized that a better knowledge of ecological patterns and processes that shaped the historical landscape was required. A partnership meeting was held in November 1993 and the decision was made to limit the list of key drivers to be studied to six agents: climate, fire, soils, insect, geomorphology and hydrology. After a detailed request for proposals, a contract was signed with the University of Northern British Columbia to address the deliverables for this program area. An Ecological Processes Team was formed, consisting of UNBC faculty members, graduate students and collaborators having expertise in one or more areas relevant to the key drivers. The work program of the Ecological Processes Team consisted of five projects: Geomorphological and Hydrological Processes; Climate Studies and Monitoring; Fire; Forest Insect and Disease; and Soil and Vegetation Successional Processes.

This thesis has resulted from participation in the Climate Studies and Monitoring project. Climate is a significant determining factor in the development of forests, and indeed, in how an ecosystem functions. Wind, temperature and precipitation (as well as radiation and other parameters) can act to limit or enhance the productivity of the forest. Disturbance events that manifest themselves from extremes in climatic elements include fire, windthrow and floods, which in turn initiate other disturbances such as insect outbreak and disease. These climatic parameters are all dramatically affected by the presence of complex terrain. The assessment of the ways in which complex topography affects these important climatic variables, particularly the wind, is non-trivial. The main goal of the Climate Studies and Monitoring project was to assess the influence of topography on extreme wind behaviour, in order to help the MMFA identify areas of the MMF which are adversely affected by high winds. This thesis describes the development and application of the technique used to extrapolate high wind estimates over the McGregor landscape. The results of this project are intended to complement the efforts of the Forest Practices Team to test and develop a model for extrapolating temperature and precipitation.

Thesis Structure and Overview

For convenience and presentation purposes, the thesis is organized into four parts:

Part I.	PROBLEM STATEMENT & RESEARCH APPROACH	**(Chapter 1)**
Part II.	EXAMINATION OF CENTRAL-INTERIOR WIND REGIME	**(Chapters 2, 3)**
Part III.	EXTRAPOLATION OF HIGH WINDS	**(Chapters 4, 5)**
Part IV.	APPLICATION OF RESULTS	**(Chapters 6, 7)**

Chapters two through six have individual objectives, methods, results and conclusions. Chapters one and seven are introductory and summary chapters respectively. Figures and tables referenced in the text are found in **Appendix A**.

- **Part I** provides the necessary background information on wind and windthrow to establish the rationale for the thesis; identify the main objectives; and gives an overview to the research approach adopted to meet these objectives.

- **Part II** examines the wind regime of the central-interior of British Columbia using historical wind records in order to determine the dominant storm type for the region. In **Chapter 2**, the long-term (30-year) wind normals are described along with related climate normals (temperature, precipitation and frost period) which may have a bearing on windthrow. In **Chapter 3**, the return periods of high wind events are determined by analyzing the observed annual wind extremes. The monthly wind extremes are also examined to determine the directional and seasonal characteristics of high winds. The surface station data are then interpreted by looking at the large scale atmospheric circulation, and conclusions are drawn about the dominant storm type.

- **Part III** addresses the spatial extrapolation of extreme winds. **Chapter 4** examines in closer detail the synoptic climatology of the dominant storm type identified in Part II. Three keyday storms are identified which are representative of moderate, strong and severe winds occurring at the Prince George Airport. The surface weather accompanying these storms is described relative to the climate normals described in Chapter 2. In **Chapter 5**, the three keyday storms are used to initialize a series of numerical weather simulations in order to estimate the maximum mean winds likely to occur across the McGregor Model Forest landscape under each of the three storm scenarios.

- In **Part IV**, the results from the numerical modelling exercise are generalized for application in the McGregor Model Forest. In **Chapter 6**, the simulated wind maximums are used to test a simplified model for extrapolating high winds to the McGregor based on a single wind measurement at the Prince George Airport. **Chapter 7** provides an executive summary of the thesis results, discusses how the results may be used to assess areas of the McGregor which may be adversely prone to windthrow, and makes recommendations for improvements and future work.

<u>Readers may wish to skip to **Chapter 7** for an overview to the thesis.</u>

Acknowledgements

First and foremost, I must thank my supervisor, Dr. Peter Jackson for his infinite patience and understanding. Secondly, this undertaking would not have been possible had it not been for the generosity of the McGregor Model Forest Association who provided a research assistant stipend, and the funds to purchase, install and maintain the climate monitoring network. I would also like to thank my committee, Dr. Joselito Arocena (UNBC) and Clifford Raphael (CNC) for their careful review of the first thesis draft, and the external examiner, Dr. John Wilson (Univ. of Alberta) for his comments.

The following individuals were of great assistance during the preliminary planning stages: Phil Graham, for allowing access to BC Hydro's power interruptions database; Bob Doratty, TFL30 Forester, for assistance in locating and maintaining the temporary climate stations (including arranging for my first ever helicopter ride); Co-op students Adrian Walton and Simon Bickererst at McGregor Model Forest, for providing cutblock topography maps; and summer students Carol Nissila and Lanny Englund, for helping during the field campaigns.

Meteorological and related data were supplied by: Dennis Fudge and Steve Lamble, BC Ministry of Environment; Eric Meyer, BC Ministry of Forest; Mike Jull, Aleza Lake Research Forest; Ross Benton, Canadian Forest Service; Kate Bush, McGregor Model Forest; and numerous "anonymous" individuals at Environment Canada.

I would like to acknowledge the contributions of the following individuals who provided their input and assistance during the analysis stage: Jack Bowling, Environment Canada for his review and comments on the extreme value analysis and synoptic climatology; Dr. Brent Yarnal (Penn. State University) for providing the source code for the keyday analysis, and Dr. Cliff Mass (Univ. of Washington) who provided the original source code for the compositing analysis; Dr. Kevin Tory and Dr. Shucai Guan for their assistance in configuring and running RAMS, and interpreting and displaying the model output; fellow graduate students, Barry Pierce and Nancy Alexander, for providing a smoothed DEM for input into RAMS; Corinna, Elynuik for her help with an award winning poster presentation; Kate Sherren for writing the GIS based routines for displaying the wind vector maximums; Scott Emmons for general computer support and Paul Wilson for continually questioning me about the principle of synoptic climatology; and Dr. Chris Quine, Dr. Steve Mitchell, Dr. John Moore, Mike Jull and Mike Hagan for their comments from a windthrow perspective.

Finally on a personal level, I wish to extend my thanks to the following individuals for providing encouragement throughout, particularly when it came to public speaking: my family (Mom and Dad, Sheila, Nora, Mary Anne, Matthew and Moyna); Maureen Hewlett, Anne Marie MacIsaac, Ron Poirer, Linda Rankin, Aniko Varga, Wendy Vasbinder and Mike Walters; the team of Byran McEwen and Christine Calihoo; my current roommate and climate groupie, Laura Ryser; Grace Cho, who taught me some difficult, but much need lessons about myself; and Maggie Kuntze, for motivating me at a critical stage during the writing process. Last, but not least, Mr. Akin, my grade 7 through 12 general science, math and physics teacher. My graduate experience wouldn't have been possible, had he not supported and encouraged me during my earlier childhood education.

PART I: Problem Statement & Research Approach

1 Wind, Trees and Complex Terrain

1.1 INTRODUCTION

Windthrow or forest blowdown is increasingly recognized as a major natural renewal agent in forested landscapes. Canopy gaps, large pit/mounds and decaying matter that result from windthrow play an important role in soil development and ecological succession (Kimmins, 1997). In managing for a sustainable forest, these processes must be understood and incorporated into forestry practices. While occurring naturally, windthrow is also affected by harvesting and silviculture decisions, particularly in areas prone to high winds. Wind damage in managed forest stands is reported to be steadily increasing in many parts of the world (Navratil, 1995).

One of the reasons for the observed increase in wind damage is the change from natural stand conditions that have resulted from the intensification of forestry management and silvicultural practices. From an economic stand point, windthrow also impacts the productivity of managed forests. In the Prince George Timber Supply Area, the estimated annual loss of timber that cannot be salvaged or recovered due to wind damage is 26,400 m^3/yr, compared with an annual harvest of approximately 18 million cubic metres (B.C. Ministry of Forests, 1995). In addition to these unrecoverable losses, timber which is salvageable is associated with increased harvesting costs and poses a greater hazard to the forest worker. Recently, concern over windthrow has been heightened in British Columbia, as alternatives to clearcutting are being investigated in response to new ecological and social concerns (Chen et al., 1995; Jull, 1996; Coates, 1997). Many foresters are concerned that new partial cutting techniques will leave stands susceptible to windthrow (Mitchell, 1995a). The windiness of a region, particularly the probable occurrence of severe winds and their directional and seasonal characteristics, must be known before wind risk management strategies can be implemented and appropriate silviculture systems designed.

However, implementation of such strategies is often hindered by three compounding factors: 1) wind measurements tend to be spatially limited, typically restricted to airport locations; 2) local terrain plays a considerable role in modifying wind speed and direction, particularly in mountainous regions; and 3) damage tends to be associated with "extreme events" which by definition lie outside the scope of normal experience and thus normal scientific description. The main goal of this thesis was to assess the influences of topography on extreme-wind behaviour, in order to identify areas prone to high winds in the McGregor Model Forest of British Columbia.

1.2 STUDY AREA

The McGregor Model Forest (MMF) is located 30 km northeast of Prince George and encompasses an area of 182,298 hectares within the boreal forests of British Columbia's central-interior (**Figure 1.1a**). The boundaries of the MMF are contiguous with provincial Tree Farm Licence 30 (TFL 30). The total productive land base is 159,932 hectares, or about 88 percent of the total area. The area is located in the Sub-Boreal Spruce biogeoclimatic zone with small areas of the Interior Cedar-Hemlock in the southeast portion and Engelmann Spruce-Subalpine Fir zones located in the northeast portion (B.C. Ministry of Forests, 1991). The TFL 30 is commercially logged and approximately 386,000 cubic metres of timber are harvested annually, predominantly during the winter months. Based upon data collected by the licensee, the base case analysis includes a net deduction of 3,640 cubic metres per year to account for non-recoverable losses due to fire (1,000 cubic metres), wind damage (1,160 cubic metres) and insects (1,480 cubic metres) (B.C. Ministry of Forests, 1996). Gross losses due to windthrow are significantly higher than 1,160 cubic metres per year , but the licensee has adopted an aggressive salvage approach to minimize the overall net loss. The licensee has indicated that in the past, approximately one quarter of the volume harvested has been damaged timber.

Located on the McGregor Plateau, the TFL 30 is generally characterized by deep soils, heavy snowfalls and substantial summer rainfall. The terrain ranges from rolling hills in the west, to the steep western slopes of the Canadian Rockies in the east (**Figure 1.1b**). The southern portion of the MMF is characterized by a broad east-west drainage basin formed by the confluence of two major river systems. The Fraser River flows northwest out of the Rocky Mountain Trench and traverses the southern edge of the McGregor Plateau, where it turns southward back toward Prince George. The McGregor River flows southwest out of the Rockies and into the Fraser.

1.3 BACKGROUND

The two sections which follow are not intended to be an exhaustive review of the literature on wind and windthrow, but rather to provide the necessary background to establish the rationale behind the focus of this study. For an extensive listing of the literature documenting the impacts of wind on forests, see the bibliography compiled by Everham (1996). A background into atmospheric motions is given in the section on wind and complex terrain for the reader who may be unfamiliar with this subject matter. For a more thorough description of atmospheric motions, see the introductory text by Stull (1995), or Holton (1979) for a more advanced understanding.

1.3.1 Windthrow

If the stem strength of a tree is greater than the pressure exerted by the wind (windload), a tree does not break but may uproot and topple over, carrying with it a massive plate of roots and soil. This occurs when the critical load on a tree surpasses the resistive forces anchoring the tree and is referred to as windthrow.[1] In simple terms, factors which contribute to an increase in windload, or a decrease in the resistive forces anchoring a tree, will be important in determining when, where and how wind damage is likely to occur. In practice, however, windthrow is a complex phenomenon caused by the simultaneous interaction between a number of environmental factors such as rooting depth, soil

[1]Where the windload exceeds the stem strength, windbreak is said to occur. Leaning and bending are considered an intermediate or light stage of windbreak and windthrow.

properties, tree and stand morphology, topography and wind (see reviews by Stathers et al., 1994 and Navratil, 1995). The study of windthrow must therefore be considered a multidisciplinary subject which covers a broad range of basic and applied sciences, such as physics, meteorology and engineering, in addition to soil science and forest physiology, ecology, and pathology. As a result of such multi-discipline research, significant advances have been made in the last decade and the first symposium volume on the topic was written following the "Wind and Wind-Related Damage to Trees" conference held in Edinburgh, England in 1993 (see Coutts and Grace, 1995). This conference, held under the auspices of the International Union of Forestry Research Organisations (IUFRO), was the first of its kind and brought together researchers from seventeen countries. A follow-up conference entitled "Wind and other Abiotic Risks to Forests" was held in Finland in August, 1998 and selected proceeding were published in a special issue of Forest Ecology and Management (Vol. 135, 2000).

Windthrow events can be broadly categorized into two types. Catastrophic windthrow occurs infrequently when exceptionally strong winds cause widespread and extensive damage to large areas. Endemic windthrow occurs more frequently, but on a smaller scale and is often an indirect result of forest management practices. This may occur as a result of numerous lower velocity windstorms, and typically affects individual stems, or small groups of trees. Endemic windthrow also tends to spread progressively from an abrupt, or unstable boundary. The causes and interactions between the various factors affecting windthrow are typically investigated at three levels: the individual tree level, stand level and landscape level (refer to **Figure 1.2**). At the individual tree level (**Fig. 1.2a**), stability is affected by tree morphology and soil conditions. Windthrow is more common in shallow than deep rooted species, and more common in shallow and/or wet soils than deep and/or dry soils (Kimmins, 1997). It is also a common result of damage to root systems by pathogenic organisms, or mechanical disturbance.

Stand height, stand density, species composition and silviculture treatments in conjunction with individual tree stability, determine the overall stability of stand structures (**Fig. 1.2b**). Environmental factors in combination with cutblock location and alignment, have a bearing on the incidence and severity of blowdown (Moore, 1977; Navratil, 1995; Stathers et al., 1994). Stand level features and topography in turn affect windthrow by modifying wind exposure, wind direction, speed and turbulence, causing highly variable wind conditions (**Fig. 1.2c**). The assessment of the way in which complex topography affect extreme wind behaviour is non-trivial. In keeping with the strategic decision of the McGregor Model Forest Association to model landscape level disturbances, this thesis focuses on the role that wind and topography plays in this complex phenomenon.

1.3.2 Wind and Complex Terrain

1.3.2.1 Turbulence:

Windthrow is the result of both the stationary and dynamic windloads on trees. The stationary windload is related to the mean wind around a tree crown. The dynamic windload is very complex and is related to turbulent fluctuations in the wind speed and swaying (oscillation) of the tree. According to Miller (1985), windthrow arises as a result of storm force winds of 70 km/hr and associated gusts of higher wind speeds. Catastrophic damage occurs as the wind speed approaches 100 km/hour. Mean wind speeds of more than 108 km/hr over a 10 minute period will damage trees and stands under almost any stand, site and soil conditions (Mayer, 1989). However, it is generally accepted that windthrow, especially endemic windthrow, is more affected by the turbulent component of the wind, than by the mean wind speed (Gardiner, 1995). In particular, gusts with frequencies that correspond to the natural sway of an object are likely to cause the most severe damage (Navratil, 1995; Stathers et al., 1994). A gust, usually defined as a positive departure from the mean over a specified time, can be an extreme case of the normal fluctuations in the wind. A defining feature of the atmospheric layer adjacent to the earth's surface, commonly called the planetary boundary layer (PBL), is that the flow is generally turbulent, resulting in considerable mixing. The turbulent nature of the lower atmosphere is responsible for sporadically mixing volumes of faster moving air from higher layers of the troposphere to the surface in the form of a gust. The causes of this turbulent mixing may be mechanical (due to vertical wind shear and aerodynamic roughness of the surface) or thermal (due to convective air currents).

1.3.2.2 <u>Synoptic meteorology</u>:

Wind flow in the PBL is in general related to winds aloft in the "free" atmosphere. The forces which establish and sustain the flow aloft are pressure forces arising from non-uniform heating of the globe. The pressure gradient force acts perpendicular to the isobars (lines of equal pressure, or height contours on a constant pressure surface) on a weather map, from high to low pressure (or heights). The Coriolis 'force' plays a role in the wind direction aloft, but performs no work. The Coriolis force is an apparent force caused by the rotation of the earth (a non-inertial frame of reference). The Coriolis force acts perpendicular to the wind direction. In the Northern Hemisphere it acts to the right of the wind direction, causing winds to blow clockwise around a high pressure system and counter-clockwise around Lows. The field of synoptic meteorology is primarily concerned with predicting the day-to-day propagation and development of these large scale (~ 1000 km) pressure systems.

The geostrophic wind is a theoretical wind that results from a steady-state balance between the pressure gradient and Coriolis forces. In regions of straight isobars above the top of the boundary layer and away from the equator (where the Coriolis force vanishes), the actual winds are approximately geostrophic. These winds blow parallel to the isobars (or height contours) with low pressure (heights) to the left in the Northern Hemisphere. The wind is fastest in regions where the isobars are closer together (i.e., where the pressure gradient force is larger). In the boundary layer, turbulent drag slows the wind below the geostrophic value and turns the wind to point at a small angle across the isobars toward low pressure. The angle depends on the magnitude of the frictional force, and is typically 10-20° over flat grasslands, or a smooth water surface, and 25-40° over urban and rolling terrain (Henderson-Sellers and Robinson, 1986; Byers, 1974). The frictional force is at its maximum at the surface and gradually decreases with height until it becomes insignificant aloft in the free atmosphere where the geostrophic wind approximation holds. The decrease with height also leads to a clockwise change in wind direction with height, which is sometimes referred to as the Ekman spiral, although often this "theoretical" spiral is perturbed or masked by non-ideal flow conditions.

Very complex terrain usually creates its own circulation pattern in the lowest air layers, rather than simply modify the geostrophic wind. Local circulations such as the sea breeze, and anabatic and katabatic valley winds, can only occur during anticyclonic (high pressure system) weather conditions when the atmosphere is relatively stable and geostrophic winds are light. They are masked by cyclonic (low pressure system) weather activity and cloudy conditions, which limit the development of thermal differences (horizontal temperature gradients). Under such windy and cloudy conditions, the atmospheric stability is near-neutral, and turbulence is generated mechanically.

1.3.2.3 Mechanical turbulence:

In forests, the generation of mechanical turbulence is affected by topography and stand conditions. In general, the higher the wind speed and the rougher the forest canopy, the greater the degree of mechanical turbulence for a given value of "overhead" wind speed, at (say) $z \sim 1$ km. Topographically induced changes in wind speed may occur, for example, as lee-slope turbulence or valley funnelling (see **Fig. 1.2c**). A narrowing valley can accelerate winds leading to eddy formation. Turbulence also occurs when the flows from two valleys meet at a junction. The effects of vegetation on the wind are similar to those of topography, but at a different scale. Cutblock shape and orientation can accelerate or decelerate winds similar to the effect of valleys, depending on alignment with respect to prevailing winds.

1.3.2.4 Wind and wind gust measurements:

Meteorological data, particularly wind gust measurements, are typically only routinely measured from city airports as part of the synoptic monitoring network. Wind and wind gust measurement are therefore often not available for areas that are sparsely populated, or which have mountainous terrain. In Canada, airport wind speeds are measured at the 10-metre level using a U2A cup anemometer and have a short period of record, beginning in the mid-1950's. Mean winds are recorded every hour and represent a two-minute mean. A wind gust is reported when the instantaneous peak wind speed exceeds the two-minute mean by at least 10 km/hour, and the peak attains a speed of at least 30 km/hour. The hourly two-minute mean wind speed and direction is archived at the Canadian Climate Centre in Downsview, Ontario. However, only the speed and direction of the daily extreme wind gust is included in the archive.

1.3.2.5 Models of the orographic windfield:

Airflow over non-uniform terrain is not easy to generalize and requires the use of either: a) empirical models for extrapolating surface winds to the local surroundings, such as WndCom (Ryan, 1983), or by applying the guidelines like those produced by Walmsley et al. (1989); or b) the simulation of actual atmospheric motions using 3-dimensional dynamical models, such as the Colorado State University Regional Atmospheric Modeling System or CSU RAMS (Pielke et al., 1992).

1.3.3 Winds and Windthrow in British Columbia

Mitchell (1995a) provides a synopsis of windthrow in British Columbia and describes windthrow research as being in its infancy. A quantitative approach to determining the windthrow hazard at a particular site is not yet possible in B.C. because information on the frequency and occurrence of strong winds is not available, nor is there enough information about the response of different species, crown classes, tree heights or stand densities to high winds. A hazard-based classification system is all that is currently possible, given that very little windspeed data has been collected in BC forests and that very little is known about the threshold forces required to overturn the wide range of species and crown classes that comprise stands in B.C.

According to a provincial survey conducted in 1992, windthrow damage accounts for 4% of the provincial annual allowable cut or approximately 3 x10^6 m^3, a level of damage which is similar to that caused by wildfire or insect infestation. With the exception of the provincial survey in 1992, there have been no comprehensive studies of windthrow in BC. There have been a limited number of site specific studies, however no studies could be found for the Central-Interior. No systematic reporting mechanism is in place for monitoring windthrow and prior to the 1992 provincial survey, windthrow occurrence could only be estimated from stumpage receipts for salvage timber, but this represented only a portion of the total windthrow and furthermore did not generally lend itself to determining the exact timing of occurrence which is crucial in identifying the dominant storm type. From a meteorological perspective, a more comprehensive reporting system is maintained by BC Hydro which documents storm-related damage to power lines. However, this database has a limited length (beginning in 1992) and is difficult to utilize because it requires a detailed knowledge of powerline orientation with respect to local tree lines. As a result of the 1992 survey, a unified program of windthrow and administration has been proposed by Stathers et al. (1994), but has not yet been adopted on a province wide basis.

In British Columbia, strong winds are associated with the passage of fronts that originate in the Pacific Ocean or in the Arctic, or from strong winds associated with thunderstorm activity. At recurrence intervals of 10 to 20 years, thousands of hectares in B.C. are windthrown by storm or hurricane force winds, while every year hundreds of hectares are blown over in uncut stands and along cutblock boundaries and road allowances (Stathers et al., 1994). However, because accurate records on windthrow are not being maintained locally, it is impossible to ground truth the importance of any particular storm type.

In a survey of fifty-nine sites on Vancouver Island, the simultaneous occurrence of high rainfall and exposure to winter storm winds from the south was found to be the major cause of blowdown in streamside leave strips (Moore, 1977). Storm winds from a southerly direction during the period from October to March are also reported to have caused the vast majority of blowdown in other studies in

Alaska, Washington and Oregon (cited in Moore, 1977).[2] In the Western-Interior, Coates (1997) examined windthrow damage at Date Creek 2 years after partial cutting and found that the vast majority of trees fell in a northerly direction, suggesting winds from the south caused most of the damage. Two major events were reported to have occurred during the two year study period, one in mid-October 1993 and another in mid-August 1994. While these investigations lend support to the importance of winter storms, caution must be exercised when taking relationships derived in coastal regimes and applying them to the Central-Interior, especially given the differences in forest types, the complexities of windthrow, and the increased frequency of summertime convective storms in the interior.

1.4 PROBLEM STATEMENT

The complex terrain and sparsity of wind data in forested areas is a major obstacle to the development and implementation of wind risk management strategies in British Columbia. A quantitative approach to determining the windthrow hazard at a particular site is not yet possible because information on the frequency and occurrence of strong winds is not available. Detailed wind climatologies for forested areas in North America are rare and hazard-based classification will still play an important role in minimizing wind damage (McCarter et al., 1998). From a forest management viewpoint, very little can be done to prevent losses from major catastrophic storms. Some loss is inevitable and should be factored into the Allowable Annual Cut (AAC) calculations according to wind history and stand conditions. On the other hand, control measures to limit the extent of endemic windthrow related to silviculture activities have been established based on its relationship to individual tree stability, stand stability and external stability factors such as the sheltering and diverting effects of both topography and forest canopies (Navratil, 1995). The most obvious and immediate cause of all windthrow, however is wind. Yet, Stathers et al. (1994) recognize there is not enough known about wind zones in B.C. forests to implement a quantitative windthrow hazard classification scheme.

---

[2]In fall and winter, synoptic scale pressure gradients are larger, implying stronger winds.

Longterm wind records in the Central-Interior are limited to a few airport locations, having an average separation of 150 km (see **Part II**). The nearest longterm wind station to the MMF is the Prince George Airport (**Fig. 1.1a**). The complex terrain of the Central-Interior therefore requires the use of either: a) empirical models for extrapolating surface winds to the local surroundings; or b) the simulation of actual atmospheric motions using a 3-dimensional dynamical model. As empirical models are usually developed for specific terrain-types, a more versatile 3-dimensional model such as RAMS was favoured in this research project. RAMS advances gridded fields of atmospheric variables such as velocity, pressure and temperature through a series of discrete time steps based on the physical equations governing atmospheric motions, and can incorporate the effects of topography and forests on windflow. RAMS is currently used by the Canadian Forest Service to forecast fire danger conditions in Alberta (Anderson et al., 1996). Snook et al. (1998) successfully used RAMS to predict the regions of highest winds during a fall blizzard and severe wind event which blew down 8100 hectares of forest in Steamboat Springs Colorado in October 1997.

Prior to the development of a technique for assessing areas prone to high winds, it was important to assess whether severe-wind events in the MMF are primarily due to convective wind bursts (summertime events mainly), or due to synoptic scale wind storms (wintertime events mainly), as this would affect the type of analysis possible. Because accurate records on windthrow are not being maintained locally, it was impossible to ground truth the importance of any particular storm type in predicting windthrow occurrence. If straight-line synoptic winds are the most important, then extrapolation of extreme winds from an airport location would be a feasible expectation If convective storms are most important, then extrapolation is not realistic because of the spatial inhomogeneity of these storms and difficulties associated with their numerical simulation. From a wind-risk management perspective, it would be extremely difficult to design silviculture systems which could minimize the occurrence of windthrow resulting from convective storms. Synoptic storms on the other hand have greater predictability, and because of their spatial scale, have the potential to cause more pervasive damage. Therefore, after an assessment of the seasonal and directional characteristics of wind gusts in the Interior (see **Part II**), the decision was made to focus on the identification of areas in the MMF which are prone to high winds derived from synoptic scale forcing.

1.5 OBJECTIVES

Windthrow is a complex phenomenon caused by the simultaneous interaction between a number of environmental factors. In keeping with the objectives of the McGregor Model Forest Association (MMFA) to model key landscape level disturbances, this thesis focused on the role that topography plays in this complex phenomenon by trying to assess the influences of topography on extreme-wind behaviour. The thesis, therefore, had a very applied-science objective, namely to characterize the wind field in the McGregor Model Forest under a typical storm scenario, in order to help the MMFA identify potential areas of windthrow-prone terrain. In particular, the research focused on the identification of areas of the MMF which are prone to strong synoptic winds.

Specifically, the objectives of this study were:

1) To determine the synoptic climatology of the prevailing storm winds in the Central-Interior; and
2) To test and develop a model for extrapolating high winds across the MMF landscape under this flow condition.

1.6 METHODOLOGY

The complex terrain and sparsity of wind data in BC's forests would typically demand the use of either empirical extrapolative techniques, or a numerical modelling approach to obtain an estimate of the windfield. This project utilizes both techniques by modelling synoptic composites of severe-wind events to derive wind speed ratios between grid points in the complex forest terrain and a neighbouring airport location.

1.6.1 Overview to Research Approach

An overview to the method used to extrapolate high winds under the prevailing storm condition is shown in **Figure 1.3**. An analysis of historical wind extremes recorded at four airport locations in the Central-Interior was undertaken to determine the dominant storm type for the region (Step 1). Synoptic climatology and map pattern classification techniques were used to identify recurring and representative map patterns for moderate, strong and severe winds under this prevailing flow condition (Step 2). Atmospheric soundings taken at the Prince George airport during these three "keyday" storms were used to initialize a series of 12-hour numerical weather simulations (Step 3). The maximum hourly wind simulated at each grid point was recorded, and gridded wind maximums were constructed for each keyday scenario. Each grid of maximum wind speeds was normalized by the corresponding maximum speed simulated for the airport (Step 4). This provided a gridded set of speed ratios stratified by storm category. To extrapolate high wind estimates under the prevailing flow condition, the synoptically parameterized model multiplies the daily maximum mean surface wind speed at the airport by the appropriate grid of speed ratios.

1.6.2 Working Assumptions

A fundamental working assumption of this research approach is that the atmospheric circulation is a critical determinant of the surface environment. A second assumption is that surface winds at the Prince George Airport are forced by the same large scale atmospheric circulation as surface winds in the MMF. That is also to say, given the proximity of the MMF to the Prince George aerological station, an assumption of this analysis is that the upper level wind flow (i.e. that above the turbulent PBL) at both locations is essentially the same. While the first assumption is widely accepted in the field of synoptic meteorology, the second will require scrutiny and its validity will be borne out in the analysis.

1.6.3 Study Components and Objectives

To meet the objectives of this thesis, six individual studies were identified, each with its own objectives and methodology. The six stages of the thesis were:

1) Deployment of a temporary climate monitoring network;
2) Compilation and presentation of historical climate data;
3) Analysis of the return periods of high wind events;
4) Development of realistic wind storm scenarios;
5) Numerical simulation of keyday storms; and
6) Construction of a synoptically parameterized extrapolation model.

The objectives of the six studies are outlined below.

Study 1: Climate Monitoring

- 1.1 To provide local wind data for validating the numerical simulations in stage 5 of this project; and
- 1.2 To provide temperature, precipitation, radiation and humidity data for validation of the climate model developed by the Forest Practices Team.

Study 2: Climate Normals

- 2.1 Identification and synthesis of historical climate data relevant to the MMF;
- 2.2 To characterize climatic conditions in the region; and
- 2.3 To examine the influence of topography and highlight the challenges of interpolating climatic variables in data sparse terrain.

Study 3: Extreme Value Analysis

3.1 To determine the return periods of extreme winds of various magnitudes;

3.2 To describe the directional and seasonal characteristics of these events; and

3.3 To assess whether severe winds in the region are primarily due to convective wind bursts or synoptic scale wind storms.

Study 4: Synoptic Climatology

4.1 To develop composites of fall and winter cyclones that are associated with moderate, strong and severe southerly winds in the Interior; and

4.2 To identify a representative mean sea level pressure map for each storm composite.

Study 5: Numerical Simulation

5.1 To perform numerical simulations of the three keyday storm events identified as being representative storm scenarios for moderate, strong and severe winds under a synoptic southerly flow condition;

5.2 To use the model output to characterize the wind flow under these conditions and to demonstrate the influences of topography on high winds; and

5.3 To obtain estimates of the speed and direction of the maximum winds which are likely to be observed in the McGregor Model Forest (MMF) under each storm scenario.

Study 6: Extrapolation Model

6.1 To test and develop a model for extrapolating high winds across the MMF landscape under a synoptic southerly flow condition; and

6.2 To use the model to characterize the strength and direction of winds in the MMF under this prevailing flow condition due to topographic variation.

With the exception of the climate monitoring study, each of the individual studies is reflected in chapters two through six, respectively. The climate monitoring study is included in Chapter 5 with the numerical simulation study. Chapter 7 provides an executive summary of the thesis results, discusses how the results may be used to assess areas of the MMF which may be prone to windthrow, and makes recommendations for improvements and future work.

PART II: Examination of Central-Interior Wind Regime

2 Climate Normals

2.1 INTRODUCTION

British Columbia is a land of great variety, with strong relief and bold topography. Climatic differences are larger vertically than horizontally, and even a small area may contain climates of much diversity. Meteorological data are often only measured at city airports which are typically located in valley bottoms, and are not available for areas that are sparsely populated, or which have mountainous terrain. Models must often be used to extrapolate meteorological parameters to these areas. One such model that was applied by Benton (1998) to extrapolate climatic parameters over the complex landscape of the McGregor Model Forest (MMF) is the mountain microclimate simulation model (MTCLIM) (Hungerford, 1989). MTCLIM extrapolates daily air temperature, incoming radiation, humidity and precipitation, making corrections for differences in elevation, slope and aspect between the point of measurement and the site of interest. A main goal of this thesis was to provide a module for extrapolating high winds over the McGregor landscape in order to complement Benton's McGregor Model Forest Climate Model (or MMFCliM). The identification, synthesis and analysis of existing sources of climate data was a logical starting point prior to undertaking both studies. This chapter therefore examines the 30-year climate normals for stations within and surrounding the Prince George Forest District. Climate normals for the McGregor station are specifically highlighted and are compared to the normals for the surrounding stations.

2.2 OBJECTIVES

The objectives of the climate normal study were:

1) Identification and synthesis of historical climate data relevant to the McGregor Model Forest;

2) To characterize climatic conditions in the Central-Interior of British Columbia; and

3) To examine the influence of topography and highlight the challenges of extrapolating climatic variables in data sparse terrain.

2.3 STUDY AREA: Climate Station Location and Local Topography

The McGregor Model Forest is situated near the centre of the Prince George Forest District, an area which covers 3.3 million hectares (**Figure 2.4**). Seven climate stations are located within the forest district: Hixon, Dome Creek, Prince George, McGregor, Aleza Lake, Chief Lake and McLeod Lake. Seven additional neighbouring stations were included in this investigation: MacKenzie and Pine Pass at the northern boundary; Fort St. James and Vanderhoof to the west; and Quesnel, Barkerville and McBride along the southern boundary. There is a notable deficiency in the availability of climate data along the north-eastern boundary. A variety of landscapes characterize the area. A large central plateau is the dominant terrain feature, bounded to the east by the Rocky Mountains. The terrain varies from the gently rolling hills in the southwest, to the deep valleys and steep rugged mountains in the east and north. At its southeastern fringes, the plateau extends into the Fraser River trench, which runs northwest from McBride to Aleza Lake. Beyond Aleza, the Fraser turns southward passing through Prince George, Hixon and Quesnel.

2.4 METHOD: Definition of Climate Normals

The data examined and presented in this chapter are from the 1951-1980 climate normal period. The atmosphere varies naturally, not only from day to day, but from year to year. It is therefore necessary to obtain a sample of conditions which is long enough to incorporate most of the variability. It is customary (although somewhat arbitrary) to describe the climate of a location using weather elements which have been averaged over a thirty year period (so-called climate normals). For example, the daily maximum temperature for any month is the mean of all daily maximum temperatures recorded in that particular month. The normal is an average of the set of 30 monthly means, and the annual maximum daily temperature is obtained by averaging the respective monthly values.

2.5 RESULTS

Climate data were examined for fourteen recording stations in and surrounding the Prince George Forest District. The climate normals included in this summary are wind, temperature, precipitation and frost period (Environment Canada, 1982 a-d). Wind, precipitation and frost period are perhaps most relevant to windthrow, because they can directly influence both the wind forces acting on trees, and tree anchorage. Temperature is also important as it will determine the form of precipitation which in turn influences windload and tree anchorage. Climate normals for the McGregor station are specifically highlighted in the text, and are then compared to the normals for the surrounding stations.

2.5.1 Surface Wind Normals

Only seven of the fourteen reporting climate stations recorded wind measurements, and only four had sufficiently long-term records for the determination of climatic wind normals. The nearest station to the MMF for which wind normals are available is the Prince George Airport. The airport is located on a flat plateau 90 metres above the Fraser River, 5 km southeast of the city. The river valley lies north-south, as does a ridge of higher terrain to the east. This tends to confine the wind in a north-south direction, as can be seen from the windrose diagram in **Figure 2.5**. Near the surface (10 metres), the annual frequencies of southerly and northerly winds are 33% and 19%, respectively, while the frequency of westerly winds is only 7%. Calms are also rather frequent (14% annually). Channelled northerly and southerly winds are prevalent year round, but are even more frequent in winter. Westerlies in contrast, are more frequent in summer. For example, in December the frequencies of southerly and northerly winds are 39% and 24, respectively, while westerlies are at a minimum (3%). In June, westerlies are at a maximum (12%), while the frequency of southerly and northerly winds, a relative minimum (28%

and 14, respectively). Respective calms for January and June are 16% and 12%. Winds are less than 20 kph 85% of the time, and the annual mean is 11 kph. The strongest winds are associated with channelled northerly and southerly winds, and westerlies. Winds are also slightly stronger in winter than in summer as can be seen from **Figure 2.6** which compares the mean wind speed for each month to the maximum hourly speed and maximum gust speed observed that month over the entire period of record.

Windrose diagrams for Fort St. James, MacKenzie and Quesnel are given in **Figure 2.7**. The strong control of the surface air movement by topography is as obvious at these locations as at the Prince George Airport. MacKenzie and Quesnel are in valley-bottoms running northwest-southeast, tending to funnel the wind in these directions. Fort St. James at the western edge of the central plateau, is further removed from the influence of the Rockies: the winds are more evenly distributed and the station has the highest occurrence of easterly winds. MacKenzie and Fort St. James, located on the southeast shores of Williston and Stuart Lake respectively, are also influenced by lake breezes. An indication of the seasonal wind speed by direction is given in **Table 2.1**. A generalization about wind direction is that southerly winds are most frequent in winter and northerly winds in summer. Wind speed tends to be low generally, but highest in winter, with the exception of January which exhibits a relative lull as shown in **Figure 2.8**. This winter-time lull is due to the influence of arctic high pressure systems (see results of temperature correlations in the following section). Wind speeds are particularly low in the deep protected valleys at Quesnel and Dome Creek.

2.5.2 Temperature Normals

The monthly temperature normals for the McGregor station are given in **Figure 2.9**. July is the warmest month with a mean daily maximum of 22.5 °C and a mean daily minimum of 15.3 °C. January is the coldest month with a mean daily maximum of -7.1 °C and minimum of -16.1 °C. The daily temperature is below 0 °C for five months of the year (November through March). The annual mean daily temperature at the McGregor station is 2.5 °C, and the annual maximum and minimum temperatures are

9.3 °C and -2.2 °C, respectively. The annual range of monthly temperatures is 12 °C. Clearer skies, calmer conditions and higher solar elevation angle in summer are conducive to more efficient heating of the ground and of the near-surface air by day, and to rapid cooling after sunset. This produces a greater mean daily temperature range in summer than in winter as is evident from **Figure 2.9a**. However, the daily range in temperature is greater in winter when the circulation may at one time permit cold Arctic air to move in, while at another time produce a southerly flow of relatively warm air from lower latitudes. This annual variation in the temperature range is evident in **Figure 2.9b** which compares the mean daily temperature to the temperature extremes.

Charts of mean temperature fail to portray actual conditions in B.C. as meteorological records are too few, and the topography too varied for satisfactory mapping of actual temperatures. The monthly temperature normals for the surrounding stations are given in **Figure 2.10**. There is very little variation between the monthly and annual means at the McGregor station and the immediately adjacent stations at Aleza Lake, Prince George and Dome Creek. Across the district, temperature decreases with increasing latitude and elevation. The annual mean daily temperature ranges from 4.5 °C at Quesnel to 1.9 °C at MacKenzie. The temperature gradient eastward is not significant, except for where there are drastic changes in elevation, such as at Barkerville and Pine Pass which have annual daily temperatures of 1.4 °C and 0.8 °C, respectively.

A regression analysis of the climate normals found that a 2nd-order linear model was appropriate for explaining the variation in the mean annual maximum and daily temperature with station latitude and elevation. Scatter plots between temperature and the geographical attributes of the climate stations are given in **Figure 2.11**. A total of 44 climate stations from within 53° ±3° latitude and 123° ±3° longitude were included in the regression analysis in order to obtain a normal distribution of the dependent and independent variables. A linear combination of station latitude and elevation accounted for 93% and 71% of the variability in the maximum and daily temperatures, respectively. The results of this modelling exercise are summarized in **Table 2.2** through **Table 2.4**. Results for annual daily temperature are depicted in the contour plot in **Figure 2.12**. Temperature was found to decrease by approximately 1 °C per degree latitude and 0.5 °C per 100 metre rise in elevation. The effects of elevation did not improve the prediction of the annual minimum temperature however, and only 25% of the variability could be explained by changes in latitude. Daily minimum temperature is normally recorded during the night when frost pockets, cold air drainage and temperature inversions prevail so that the details of fine scale topography are likely to dominate the microclimatology.

Seasonal differences were explored through the development of models to explain the variation in maximum temperature for the months of January, May, July and October. The effect of latitude was observed to decrease, while the effects of elevation and longitude increased. For example, May temperatures decreased by 0.6 °C per degree latitude, 0.7 °C per 100 metre rise in elevation and 0.3 °C per degree longitude. A notable exception was the month of January, which is influenced by subsidence inversions associated with the winter anticyclone. An example of this temperature inversion is evident in **Figure 2.13**, which compares the monthly daily temperatures of McGregor, Pine Pass and Barkerville. Though Barkerville, well up in the Caribou Mountains, is 655 metres higher than McGregor, its mean January temperature is 1 °C above McGregor. The explanation is largely the gravitational flow of the surface-cooled air to valley-bottoms in calm clear weather, but another factor may be the shallowness of the layer of continental Arctic air from the northeast, which is responsible for very cold spells in the valleys, but often fails to rise to Barkerville. Barkerville has lower means than McGregor for all other months of the year. The relationship is not observed at Pine Pass, due to its northern latitude.

2.5.3 Precipitation Normals

The monthly precipitation normals for McGregor are given in **Figure 2.14**. On average, the McGregor station experiences 157 days with measurable precipitation (104 days in the form of rain and 55 in the form of snow), and the total annual precipitation at the station is 964 mm (620 mm rain and 328 cm snow). The precipitation is fairly evenly spread over the year, with slightly more precipitation in winter than summer. Spring is definitely the driest season, with a precipitation minimum occuring in April (43 mm). Rain turns to snow in late October and back to rain in mid-March as the mean daily temperature passes the 0 °C line.

Precipitation normals for the surroundings are given in **Figure 2.15** and exhibit slightly more variability than the temperature normals. Precipitation is not heavy, except at higher elevations, Barkerville and Pine Pass receiving a total of 1044 mm and 1916 mm per year, respectively. Stations in the west are at the extreme edge of the rain shadow of the Coast Mountains. Vanderhoof is the driest station, receiving only 464 mm annually. Total annual precipitation increases eastward, to 616 mm at Chief Lake, and 897 mm at Aleza Lake. Snow is measured at all stations from October until April and comes earlier at higher elevations. Lower elevations receive more rain than snow, while at higher elevations snow is greater. Pine pass for example receives 1076 cm of snow and 701 mm of rain. Correlations with station location are not as pronounced as temperature correlations (compare **Fig. 2.16** with **Fig. 2.11**). Rain is most strongly correlated with distance from the Pacific Ocean, or station longitude ($r = 0.56$), while snow is more strongly correlated with elevation ($r = 0.60$).

2.5.4 Frost Normals

The normal frost-free period at the McGregor station is 95 days. The last mean frost date (spring) is June 3, and the first frost (fall) is September 7. Frost normals for the surrounding stations are tabulated in **Table 2.5**. The frost-free period is most strongly correlated with elevation ($r = -0.63$), decreasing by roughly 6½ days per 100 metre rise in elevation, $F(1,11) = 7.30$, $p = 0.021$. Hixon, the station with the lowest elevation has the longest frost-free period (122 days), while Barkerville has the shortest period (48 days). **Figure 2.17** shows how the frost-free period decreases with increasing elevation.

2.6 SUMMARY AND CONCLUSIONS

Climate data were examined for fourteen recording stations in and surrounding the Prince George Forest District. Simple temperature, precipitation and frost models were explored, and the results are summarized below.

- Across the district, temperature decreases with increasing latitude and elevation. The temperature gradient eastward is not significant, except where there are drastic changes in elevation. A 2nd-order linear model was appropriate for explaining the variation in the mean annual maximum and daily temperature with station latitude and elevation. The annual daily temperature was found to decrease by approximately 1 °C per degree latitude and 0.5 °C per 100 metre rise in elevation.
- Precipitation normals exhibit slightly more variability than the temperature normals. Precipitation is not heavy (except at higher elevations), and is fairly evenly distributed over the year, with slightly more precipitation during winter, while spring is the driest time of the year. Stations in the west in particular are drier, because of the rain shadow effect of the Coast Mountains. Snow is measured at all stations from October until April and comes earlier at higher elevations. Lower elevations receive more rain than snow, while at higher elevations snow is greater. Correlations with station location are not as pronounced as temperature correlations. Rain is most strongly correlated with station longitude ($r = 0.56$), while snow is more strongly correlated with elevation ($r = 0.60$).
- The frost free period at the McGregor climate station is 95 days, and for the surrounding terrain, is estimated to decrease roughly by 6.5 days per 100 metre rise in elevation.

Wind stations are few and records are short. Only seven of the fourteen climate stations located in the Prince George Forest District had wind measurements, and only four had sufficiently long-term records for the determination of climatic wind normals. The nearest station to the MMF for which wind normals are available is the Prince George Airport. British Columbia lies full in the Westerlies between the subtropical high pressures and the Aleutian Low. Some generalizations about winds in the Central-Interior are:

- Southerly winds are most frequent during winter, while the prevailing winds during summer are northerly;
- The mean wind speed tends to be low generally, but is highest in winter and lowest in summer; and
- The control of surface air movement by topography is strongly evident at most climatological stations.

In contrast to precipitation, temperature and frost, winds over non-uniform terrain are not as easy to generalize. Winds in the boundary layer are modified by turbulent surface drag. Each location has unique landscape characteristics (hills, valleys, depressions etc.) and creates its own perturbation in the wind flow, so that the detailed wind climate of every landscape is unique. Because the focus of this thesis was to assess the influence of topography on extreme wind behaviour, the seasonal and directional characteristics of wind gusts in the Central-Interior are more closely examined in the next Chapter. The synoptic climatology of these strong winds is examined in Chapter 4, and the weather accompanying these storms is described relative to the climate normals given here.

3 Return Periods of High-Wind Events

3.1 INTRODUCTION

Prior to developing a technique for extrapolating high winds, it was important to determine whether severe-wind events in the McGregor Model Forest (MMF) are primarily due to convective wind bursts (summertime events mainly), or due to synoptic scale wind storms (wintertime events mainly), as this would affect the type of analysis possible. Because accurate records on timing of windthrow were not being maintained locally, it was impossible to determine in advance the relative importance of any particular storm type to windthrow in the Central-Interior. The main goal of this chapter is to determine the dominant storm type for the region. This chapter therefore focuses more closely on the wind regime of the Central-Interior, and contrasts the behaviour of extreme winds to the climate normals given in the preceding chapter. Procedures for estimating the likelihood of extreme winds are presented, and the uncertainties inherent in these procedures are discussed. Knowledge of the typical return period between extreme wind events could benefit the development of wind-risk management practices by providing an estimate of the time window available for tree stability improvement over time, in planning sequenced harvesting passes, or to factor natural losses into the equation for a sustainable harvest. A directional and seasonal categorization of the wind extremes is also provided. Directional categorization of maximum winds is an important consideration in the spatial design of harvesting and silvicultural applications. Seasonal variability in the occurrence of extreme wind events is another important consideration since variable soil moisture and frozen ground affect a tree's ability to withstand wind loads.

3.2 OBJECTIVES

In this chapter, annual and monthly wind extremes from four airport weather stations in the Central-Interior are analysed. The specific objectives of this analysis were:

1) To determine the return periods of extreme winds of various magnitudes;
2) To describe the directional and seasonal characteristics of these events; and
3) To assess whether severe winds in the region are primarily due to convective wind bursts or synoptic scale wind storms.

3.3 METHODS

Determining the likelihood of severe wind gusts is an extreme value problem. A gust, usually defined as a positive departure from the mean over a specified time, is an extreme case of the normal fluctuations in the wind. Gusts are due to turbulent air motions that sporadically bring faster moving air from higher layers of the troposphere to near the surface. Consequently, these winds tend to occur only briefly in sudden bursts, but are nonetheless important because of their ability to damage both human and natural structures such as forests. According to Miller (1985) (cited in Navratil, 1995), endemic windthrow in forests arises as a result of winds with speeds of more than 70 kph and associated gusts of higher wind speeds. Wind measurements, particularly gusts speeds, are typically limited to airport locations and therefore have a short period of record beginning in the mid-1950's. To determine the speed of an extreme wind having a return period longer than the period of record, say the 100-year wind, requires extrapolation from the available observations. The objective of an extreme value analysis is to model the observed data extremes to allow generalizations about the likely recurrence of these events.

3.3.1 Extreme-Value Theory

Extreme value theory has many important and well established applications, particularly in the field of engineering. Wind climatology provides the building designer and the building code writer with information on the extreme winds that might affect a structure during its lifetime. When designing a dam, the interest is in knowing the typical period between extreme rainfall events. In many areas prone to flooding, annual flood series are analysed to estimate the probability and magnitude of future occurrences. The treatment which follows is intended to apply to the prediction of extreme winds in 'well-behaved' climates.[3] In such climates, it is reasonable to assume that a random variable may be defined which consists of the largest annual wind speed U, during a period of N consecutive years.

$$U = U_1, U_2, \dots, U_N \tag{3.1}$$

A statistical analysis of such a series can be expected to yield a useful prediction of long-term extremes.

3.3.1.1 Cumulative frequency:

The first step in the analysis is to rank the observations by increasing wind speed and for each U_i calculate an empirical cumulative frequency $C(U_i)$, commonly given by the following expression:

$$C(U_i) = i / (N+1) \tag{3.2}$$

which represents the probability of a wind speed $U \leq U_i$. It should be noted that several alternative expressions to Eqn (3.2) have been published in the literature (see for example Singh, 1985). The expression given is the one popularized by Gumbel (Linacre, 1991). It is favoured here because it avoids

[3]A well-behaved climate is one in which extraordinary events such as hurricanes are not expected to occur.

the final value in the ranked set as the highest possible, and preserves symmetry by making the last percentile differ from 100 per cent, as much as the first differs from zero.

3.3.1.2 Return period:

A return period is the average time within which a given wind speed will be exceeded just once. The probability that U_i will be exceeded is $E(U_i) = 1\text{-}C(U_i)$. The return period $T(U)$ is the reciprocal of the exceedence, $E(U)$. Therefore,

$$T(U_i) = 1 / [1-C(U_i)] \quad \text{years} \tag{3.3}$$

Unfortunately, wind speed records are relatively short and to determine the speed of an extreme wind having a return period longer than the period of record, say the 100-year wind, requires extrapolation from the available observations. The extrapolation may be either graphical or based on an equation representing the cumulative distribution function.

3.3.1.3 Extreme-value distributions:

The two most common probability curves are the Fisher-Tippet Type I and Type II distributions, more commonly known as the Gumbel and Weibull distributions, respectively. The former is the distribution recommended for analysis of extreme winds by the National Building Code of Canada (1980). Differences in the choice of the model are reported to become more significant as the return period increases, eg. 3-6% for 100-year winds (Simiu and Scanlan, 1978). According to Flesch and Wilson (1993) and others (see for example Linacre, 1992 and Simiu and Scanlan, 1978), the Gumbel distribution is the most appropriate probabilistic model for extreme wind behaviour.

The Gumbel distribution, shown graphically in **Figure 3.18** is given by:

$$C(U) = \exp\{-\exp[-g(U-U_m)]\} \tag{3.4}$$

where U_m is the modal value of the set and $1/g$ is the Gumbel scaling factor which can be determined graphically as follows. Applying the natural logarithm to Eqn (3.4) twice yields:

$$-\ln[-\ln C(U)] = g(U-U_m) \tag{3.5}$$

It can be seen from this equation that a graph of the reduced variate $y = -\ln[-\ln C(U)]$ against the annual maximum wind speed U results in a straight line having slope g and intercept $-(gU_m)$.
Substituting for C(U) from Eqn (3.3) yields the predictive equation:

$$U(T) = U_m - [\ln\{-\ln(1-1/T)\}]/g \tag{3.6}$$

For return periods longer than about 10 years, Eqn (6) can be shown to simplify to:

$$U(T) = U_m + (\ln T)/g \tag{3.7}$$

Knowledge of g and U_m therefore allows rapid estimation of the extreme wind for any specified return period $T > 10$ years.

3.3.1.4 Errors and model assumptions:

Statistical methods for regression analysis place three requirements on the data. The data used in an analysis should: 1) be a random statistical variable, 2) come from a static and homogeneous population, and 3) be statistically independent. Wind speed can be assumed to satisfy the first requirement, and since only the annual extremes are studied, it is reasonable to expect that the data will be statistically independent. The static population requirement remains to be assessed on a station-by -station basis.

Errors include, in addition to those associated with the quality of the data, modelling errors and sampling errors. Modelling errors are due to an inadequate choice of the probabilistic model itself. Sampling errors are a consequence of the limited size of the samples from which the distribution parameters are estimated and become, in theory, vanishingly small as the sample size increases indefinitely. It is usually stipulated that measurements over at least 20 years are needed to estimate long-term extreme values (Linacre, 1992).

3.3.2 Daily Extreme Gust Data

Four airports in the Central-Interior were identified as having records greater than the 20-year minimum period recommended for an extreme value interpolation (**Table 3.6**). Airport locations are shown in **Figure 3.19** together with a brief description of the station exposure. The wind speed at these airport locations is measured at the 10-metre level with a U2A anemometer. A wind gust is reported when the peak wind speed exceeds the two minute mean by at least 10 kph and the peak attains at least 30 kph.

Archives of the daily extreme gust speed were obtained from the Canadian Climate Centre. As outlined above, the analysis requires that only the annual extremes be modelled. The largest annual wind gusts recorded at each station are shown in the time sequences given in **Figure 3.20**. Quesnel, Smithers and Williams Lake exhibited no clear trend and can be assumed to satisfy the static population requirement. Prince George however, appears to exhibit a time trend with wind speeds decreasing over time. The trend, however, is not as evident in the time sequence of the largest monthly gust where the higher speeds observed between 1960-1970 appear to be part of a larger random fluctuation (see **Figure 3.21**). The selected data sets are therefore considered to satisfy the model requirements.

The distributions of the annual extremes are compared in the box plots given in **Figure 3.22**. The bottom and top of the box is closely related to the first and third quartile so that approximately 50% of the values lie within the box, and 25% above and below the box. A horizontal line in each box gives the location of the median. For example, from the box plot for Quesnel, it can be seen that approximately 75% of the annual wind extremes are below 80 kph. In contrast, 100% of the annual wind extremes at Prince George are above 80 kph. Gusts at Prince George and Smithers are seen to be significantly larger than those at Quesnel and Williams Lake. However there is no significant difference between the respective high and low speed stations as is evident by the vertical overlap between boxplots. Smithers has a median value which is approximately equal to the mean (93 kph), suggestive of a normal distribution, while the other stations exhibit a slight positive skew. The two low speed stations also exhibit one or more outliers at speeds greater than 105 kph.

3.4 RESULTS

3.4.1 Extreme Value Analysis

The annual wind extremes were ranked by increasing speed in order to calculate the empirical cumulative frequency $C(U_i)$, exceedence $E(U_i)$ and return period $T(U_i)$ for each station. An example of the calculations is shown for Prince George in **Table 3.7**. A scatter plot of the ranked wind speed against the empirical return period (**Figure 3.23**) suggests that an exponential distribution is an appropriate model. The Gumbel reduced variant $G(U_i)$ was therefore calculated for each station (see for example the last column of **Table 3.7**). A simple least squares regression was performed for each station using the Gumbel reduced variant as the dependent variable and the ranked wind speed as the independent variable. The results of the regression analysis are summarized in **Table 3.8** and shown graphically in **Figure 3.24**.

The results for each station were statistically significant. For example, the result for the Prince George data set was a coefficient of determination $R^2 = 0.975$, significantly different than zero $F(1,22) = 862$, $p < 0.0001$. The velocity corresponding to a zero reduced variate or probability of 0.01, was shown by

Eqn (3.5) to be the modal wind. $U_m = 90.0$ kph. The slope of the line is $g = 0.080$ kph^{-1}. The Quesnel data did not show an impressive conformity to a straight line (**Figure 3.24b**), but had a coefficient of determination $R^2 = 0.913$. The poor fit is believed to be a consequence of Quesnel being located in a deep protected valley. There was also evidence of a possible step change from moderate to high gust speeds in the scatter plot in **Fig. 3.23**. The modal wind is $U_m = 72.0$ kph and the slope is $g= 0.085$ kph^{-1}.

3.4.1.1 Estimated return periods:

Having determined the parameters of the Gumbel distribution, 'best-estimates' of the extreme wind for any specified return period can be estimated from Eqn (3.6) or (3.7). The simplified prediction equations ($T > 10$ years) are:

Prince George:	$U(T) = 90.0 + 12.5 \ln T$	(3.8a)
Quesnel:	$U(T) = 72.0 + 11.8 \ln T$	(3.8b)
Smithers	$U(T) = 84.3 + 13.9 \ln T$	(3.8c)
Williams Lake	$U(T) = 78.7 + 8.5 \ln T$	(3.8d)

where the return period T is to be entered in years and the extreme wind is in kph. Extreme wind speeds associated with return intervals of 5, 10, 20, 50 and 100 years were calculated using the more general form of the prediction equation (3.6). The results are shown on the right-hand side of **Table 3.9**. Return periods for extreme winds of 50, 70,90, 110 and 130 kph given on the left-hand side of the page were computed by solving Eqn (3.6) for T(U).

Some examples of the interpretation of the data in the preceding table are as follows:

- The 100-year wind at Prince George is 148 kph. The 100-year wind is the speed likely to be exceeded only once in a century on average, and corresponds to a cumulative probability of

C(U)=0.99. Therefore the chance of having a wind speed of 148 kph in Prince George in any particular year is 1 per cent.

- Return periods at Quesnel are 5 times larger than at Prince George. On average, wind speeds of 90 kph can be expected to occur in Quesnel every 5 years; while in Prince George the same wind is expected to occur every 1-2 years, thus suggesting more severe limitations for protection of an exposed understory in Prince George based on a five-year harvesting sequence.

3.4.1.2 Confidence intervals:

A measure of the sampling error can be obtained by calculating confidence intervals for the extreme wind predictions. The 95% confidence intervals for the regression parameters (g and $-gU_m$) are included in **Table 3.8**. Confidence intervals for the extreme wind predictions were determined by carrying through the uncertainties in the regression parameters in the calculation of U_m and U(T). A visual inspection showed that adding the uncertainties to the best estimate yielded the lower bounds to both U_m and U(T), and subtracting, the upper bounds. The 95% confidence intervals for the extreme wind predictions given in **Table 3.9** are shown in **Table 3.10**. For example, the 95% confidence interval for the true value of the 100-year wind at Prince George was found to lie within a rather broad interval 131-168 kph. Confidence intervals around the Quesnel estimates were nearly twice as large as those for Prince George. The best results were obtained for Williams Lake where the 100-year wind is 118±10 kph. The intervals can be anticipated to become larger for longer return periods. For instance, comparing the confidence intervals for 5-year wind with those for the 100-year wind, the interval becomes 13% larger for Williams Lake and 15-18% larger for the remaining three stations.

3.4.2 Seasonal Characteristics

Since variable soil moisture and frozen ground affect a tree's ability to withstand wind loads, seasonal variability in the occurrence of extreme wind events is another important consideration. The majority of the annual extreme wind gusts at most stations tends to be either a fall or wintertime event (see **Table 3.11**). For instance, nearly half of the annual extreme wind gusts observed at Prince George occurred during the fall, and one-quarter were wintertime events. An exception is Quesnel, where the highest number of annual maximums were recorded during the spring (37%). All stations exhibited a low frequency of annual extremes occurring during the summer months.

3.4.2.1 Monthly wind extremes:

Seasonal variability was more closely examined by studying the complete set of monthly extremes. The largest monthly gust speeds observed during the period of study, and the mean monthly gust speed, are compared in **Figure 3.25**. Most stations show relative maxima in the mean monthly gust speed during the spring and fall, and a minimum during the summer. Prince George exhibits a single maxima occurring in October and an absolute minimum in August. The greatest variance (as shown by the standard deviation) occur during the spring and fall months (most notably in March and October). An exception is Williams Lake, which has a relative maximum during the summer months as a result of two extreme wind events, one in July of 1965, the other June, 1985.

3.4.2.2 Monthly return periods :

Months having higher gust speeds can be expected to have shorter return periods. To demonstrate, return periods for Prince George were calculated for the months of January, April, July and October. The 'best-estimates' of the return periods appear in **Table 3.12**. The highest wind gusts observed at Prince George occur in October. On average, a wind speed of 110 kph is expected to occur in October every nine years, whereas the same wind speed is only expected to occur in July every sixty years.

3.4.3 Directional Characteristics

Directional categorization of wind maximums is an important consideration in the spatial design of harvesting and silvicultural applications. For instance, it is recommended that longitudinal axes of cutblocks and strips be oriented perpendicular to the prevailing wind directions and that harvest sequences progress against the prevailing winds (Navratil, 1995). The Canadian Climate Centre, only archives the direction and speed of the daily extreme gust. Calculating return periods for different directions therefore was not possible, because this would necessitate a daily extreme gust for each wind direction. The only alternative available was to compute the directional frequency of the extreme wind gusts. Directional frequencies of the wind extremes were determined on an annual and monthly basis for the eight cardinal points: N, NE, E, SE, S, SW, W, NW.

3.4.3.1 Annual wind extremes:

The directional frequencies of the annual wind extremes are shown in **Table 3.13**. Between 80-95% of the annual wind extremes recorded at the four stations had either a southerly and/or westerly component. At Prince George, the prevailing directions were southerly (69%) and westerly (18%). Due to the limited size of the annual data set it was not practical to characterize the directional frequencies as a function of either gust size or time of year. A 'next-best' approach was considered to be a characterization of the monthly extremes.

3.4.3.2 Monthly wind extremes:

Directional frequencies of the monthly extremes were determined both as a function of wind speed class and time of year (season). Results for Prince George are shown graphically as windrose diagrams in **Figures 3.26 and 3.27**. The directional frequency as a function of gust size is given in **Figure 3.26**, and the directional frequency by season in **Figure 3.27**. Both figures depict the fact that more than half

(55%) of all the monthly gust extremes recorded at Prince George were blowing from the south. Westerly gusts in contrast accounted for 25%, and winds from the southwest another 10%. From **Figure 3.27**, it can be determined that 78% of the monthly extremes are between 50-90 kph. Wind speeds in excess of 90 kph account for 15% of the monthly extremes. Wind directions in this 'extreme-of-extremes' category are mainly southerly (70%). **Figure 3.27** shows that approximately 70% of all southerly gusts are either winter or fall events, while westerly gusts tend to be spring (29%) and summer (41%) events.

Results for the other three stations are tabulated together with the directional frequencies for Prince George in **Table 3.14** through **Table 3.21**. Prevailing directions at Quesnel, Smithers and Williams Lake are up and down the mountain valleys in which these stations are situated. However, with the exception of a more pronounced presence of northerly gusts, the stations exhibit similar tendencies to those at Prince George. Monthly extreme gusts having a southerly component remain the most frequent, with frequencies between 52% and 68%. Southerly gusts are more frequent during the fall and winter months, while the number of westerly gusts is at a maximum during spring and summer. Westerly gusts are approximately 50% less frequent than at Prince George (occuring only 8-13% of the time) due to the higher incidence of northerly gusts. Gusts having a northerly component tend to be evenly distributed throughout the year and occur between 22% and 35% of the time.

3.5 DISCUSSION

To benefit the development of wind risk management practices, the results of this analysis must be spatially extrapolated. Flesch and Wilson (1993) found that spatial extrapolation was possible for the province of Alberta in areas well removed from the foothills. The results of the present analysis highlight the potential challenges of extrapolating extreme wind predictions in nonuniform terrain.

3.5.1 Topographic Influences

Two of the stations included in the analysis are in what may be described as well-exposed settings, namely the flat plateau and hilltop stations at Prince George and Williams Lake, respectively. In contrast, the other two stations are in highly sheltered river-valley locations. The highest gust speeds however, were found to occur at Prince George and Smithers, while the lowest speeds were at Quesnel and Williams Lake. The appearance of highest gust at Prince George and Smithers may be explained by the scale of the topographic influences at each station. Smithers, located in a deep mountain valley, is prone to slope winds and funnelling effects. Quesnel and Williams Lake are located in the broader Fraser River valley, and are sheltered by the Caribou mountains. Quesnel is also prone to localized sheltering effects from a hill immediately upstream of the prevailing wind direction. Prince George, located in the southeast corner of the Central Plateau is somewhat outside of the sheltering influence of the Caribou mountains. Another important topographic influence is the generation of mechanical turbulence. The stronger the wind, the greater the degree of mechanical turbulence generated. This effect is not linear, and may have manifested itself in the Quesnel series where there was evidence of a step change from moderate to high gust speeds (**Figure 3.23**). Wind extremes in areas of complex terrain are therefore likely to be site specific making extrapolation to the local surroundings an uncertain exercise.

3.5.2 Climatological Influences

The seasonal and directional characteristics of the maximum wind gusts seem attributable to mean climatological pressure patterns and the position of the polar jet stream. The jet stream is a relatively narrow 'stream' of rapidly moving air (up to 400 km/h) flowing in a meandering path from west to east at roughly 10 km elevation. The mean position of the jet, and the belt of westerlies in which it is embedded, shifts south in winter with the seasonal migration of the polar front. As it moves southward in winter, it also moves to higher altitudes and on average, its speed increases. Cyclonic and frontal activity are associated with the position and intensity of the jetstream. The peak gusts observed in the spring and fall coincide with the transitional period when frontal activity is at a maximum. Average summer and fall mean sea-level pressure patterns for the period 1982 through 1994 are compared in **Figure 3.28**. In summer, the Pacific High is strong and rather far north. Winds over the Central-Interior are light and from the west. In fall and winter, the continent is colder than the ocean and there is a tendency for the denser, stagnating air to form high pressure cells over the continent, while lower pressure exists over the oceans. The Pacific High is weaker and displaced farther south by the Aleutian Low which is well developed. Winds are stronger and have a more southerly component. Stronger weather and precipitation along the west coast during this period is associated with the movement of this low pressure system and with associated rapidly moving lows from the southwest which typically move into the Aleutian Low position while their fronts track across B.C.

The southerly winter gusts are, therefore, most likely associated with the flow ahead of a cyclone and frontal system moving across the Pacific Coast. Summer gusts, in contrast, may be the result of gusty westerly winds typically found behind a cold front, or due to wind bursts from day-time convective storms which are able to develop and propagate in the weak prevailing westerly flow. Summertime westerlies allow the passage of unstable maritime polar air over the warmer land surface, which combined with orographic lift, results in increased thunderstorms as one moves eastward across the Central Plateau toward the Rockies. Thunderstorms are relatively infrequent however, typically occurring 5 days per summer at Smithers, but 20 days per summer in the eastern part to the region.

3.6 SUMMARY AND CONCLUSION

Typical return periods of extreme wind events at four locations in the Central-Interior were estimated by assuming that the set of annual extreme gust speeds can be described by an exponential extreme-value distribution. A summary of the key results from the extreme value analysis for the case of the Prince George Airport station follows.

A 'best-estimate' of the 100-year wind at Prince George is 148 kph, while the 95% confidence interval for the true value of the 100-year wind spans from 131 to 168 kph. Seasonal variability in the return period was examined by estimating typical return periods for annual extreme gusts occurring in January, March, July, and October. On average, a wind speed of 130 kph can be expected to occur in October every twenty-seven years, but is only expected to occur in July once every two-hundred and fifty years. A directional and seasonal categorization of the extreme wind events was undertaken by examining the monthly and annual wind extremes. Wind gusts at Prince George were found to occur most frequently from the south, and to a lesser extent from the west. This was found to be particularly true of winds in the 'extreme-of-extremes' category. The southerly gusts were primarily fall and winter events, while gusts from the west tended to be spring or summer events.

The results of the directional and seasonal categorization of the historical wind extremes suggested that southerly gusts, associated with winter cyclones moving across the Pacific Coast, are statistically the most significant contributor to extreme-wind events. A conclusion that may be drawn from the results of this analysis is that synoptic winds driven by a straight-line geostrophic flow are likely to be the most significant contributor to windthrow events, and that wind bursts from convective storms are likely to play only a secondary role. The importance of fall synoptic scale gusts over summer convective storms cannot be confirmed however, because accurate records of windthrow events do not exist for the Central-Interior. Investigations of windthrow events along coastal locations lend support to the importance of winter storms. In a survey of fifty-nine sites on Vancouver Island, the simultaneous occurrence of high rainfall and exposure to winter storm winds from the south was found to be the major cause of blowdown in streamside leave strips (Moore, 1977). Storm winds from a southerly direction during the period from October to March are also reported to have caused the vast majority of blowdown in other studies in Alaska, Washington and Oregon (cited in Moore, 1977). While these investigations lend support to the importance of winter storms, caution must be exercised when taking relationships derived in coastal regimes and applying them to the Interior, especially given the differences in forests and the complexities of windthrow. Given that windfirmness generally improves with frozen soil and snow cover, this suggests that the window for endemic windthrow in the Central-Interior is rather narrow, possibly limited to the fall months.

If, as the results of this analysis would suggest, straight-line synoptic winds (i.e. a southerly flow) are the most important, then extrapolation of extreme winds from an airport location would be a reasonable approach. However, there are at least two notable limitations to this investigation. Firstly, airport anemometers are designed to measure synoptic winds (which have a large horizontal component), and may not adequately resolve convectively-driven wind gusts (which have a large vertical component). Secondly, convective storms typically manifest themselves at a length scale on the order of 1 km (sub-mesocale), not at the synoptic scale (which is on the order of 1000 km). Therefore, for convective storms, the stations used in this analysis (which have an average separation of 150 km, and are all located in river/mountain valleys running north-south) may not fully capture the significance of certain terrain effects operating in the rolling and mountainous MMF landscape (eg. daytime convective storms caused by topographic lifting). If convective storms are most important, then simple extrapolation may not be realistic because of the spatial inhomogeneity of these storms and difficulties associated with their numerical simulation. From a wind-risk management perspective, it would be extremely difficult to design siliviculture systems which could minimize the occurrence of windthrow resulting from convective storms. Synoptic storms on the other hand have greater predictability, and because of their spatial scale, have the potential to cause more pervasive damage. Therefore, although there is a potential bias toward the frequency of synoptic storms, the decision was made to focus on the identification of areas in the MMF which are prone to severe winds under a synoptic southerly flow.

The fact that the extreme wind events are derived from synoptic scale forcing which is characterized by a prevailing wind direction makes the task of spatial extrapolation more tractable. One way to achieve extrapolation may be via a 3-D mesoscale model like RAMS (Pielke et al., 1992), which can incorporate the effects of topography and forests on windflow. A means to extrapolate high winds is described in the next section. In Chapter 5, the synoptic climatology of the strong wind events is first refined by examination of the surface weather and radiosonde data corresponding to those days on which the annual extremes were recorded. Once archetypical soundings of strong wind events have been identified, the soundings are then used to initialize a series of model runs with RAMS (Chapter 6).

PART III: Extrapolation of High Winds

4 A Synoptic Climatology for High Winds

4.1 INTRODUCTION

This chapter examines the synoptic climatology of severe wind storms which may potentially contribute to forest blowdown in the central-interior of British Columbia. A fundamental working assumption of synoptic climatology is that the large scale atmospheric circulation is a critical determinant of the local surface environment. According to Barry and Perry (1973), a synoptic climatology regards patterns of weather (clouds, rain, wind etc.) as an implicit function of sea-level pressure distribution. In Part II, it was shown that fall and winter are typically the windiest times of the year in B.C. To determine the synoptic climatology of this windy season, daily weather maps of mean sea-level pressure from October through March were averaged for the 25-year period 1970-1994. A storm composite for high southerly winds was then constructed by including only those maps where the daily extreme gust speed at the Prince George Airport was from a southerly direction, and greater than 30 km/h. Six hundred and twenty-six storm cases were subsequently identified. A pressure anomaly map for strong winds was constructed by subtracting the composite from climatology and the statistical significance of the composite was tested at the 99% level using a Student's t-test. The analysis was repeated to construct individual composites for moderate, strong and severe wind storms. Map-pattern classification techniques were then used to identify a recurring and representative map pattern for each storm composite. In Chapter 5, the keyday maps identified in this analysis are used to initialize a series of numerical weather simulations in order to obtain estimates of severe winds in the McGregor Model Forest (MMF).

4.2 OBJECTIVES

The main goal of the synoptic climatology component to this investigation was to develop realistic and representative storm scenarios for initializing the numerical simulations in Chapter 5. The specific objectives identified for this study therefore were:

1) To develop synoptic-composites of fall and winter cyclones that are associated with both moderate, strong and severe southerly winds in the Central-Interior; and
2) To identify a recurring and representative map pattern for each storm composite.

4.3 METHODS

Yarnal (1993) identifies and provides worked examples of the main classification methods used in modern synoptic climatology. According to Yarnal (1993), every synoptic climatology has two stages: 1) classification of the atmospheric circulation; and 2) the assessment of the relationship between those categories and the surface environment. Classifications are usually in the form of synoptic weather maps, and may be manual (subjective) or automated (sometimes called objective). The order in which these stages occur distinguishes the two approaches to developing a synoptic classification. In the circulation-to-environment approach, the atmospheric circulation is classified first and then related to the surface environment. Classifications in this approach tend to be more general and are independent of the surface variable (or variables). In contrast, the environment-to-circulation approach classifies the atmospheric circulation on the basis of surface-based criteria and the synoptic classes are not independent of the environmental response. Both the environment-to-circulation and circulation-to-environment approaches were utilized to develop a synoptic climatology for southerly wind gusts in the Central-Interior. The two synoptic classifications selected for this analysis are described below.

4.3.1 Composite Classifications

Compositing is one of the easiest classification methods to conceptualize and apply. Composites can be viewed as a climatology based on events, rather than means calculated over some period of time. Composites are typically average pressure maps of specific situations, and evoke an environment-to-circulation approach toward synoptic classification. Compositing is often the method of first or last resort, and because of its flexibility, is amenable to almost any research problem (Yarnal, 1993). Compositing also offers a means for determining the variability and significance of the synoptic features accompanying surface-based events, such as severe-southerly winds (eg. Mass and Bond, 1996). While a case study can isolate mechanisms which are important for an individual storm, the compositing of a large number of cases into one data set can identify processes common to most cyclones. Ideally, compositing assumes that a correct temporal and spatial orientation can be chosen which will reveal these common features. This usually involves centering a cyclone along a trough of low pressure and tracking the feature as it evolves. In regions where a significant proportion of features form and/or decay in situ or are persistent, the approach would be to focus on a fixed geographical region rather than on a moving synoptic feature (eg. Achtor and Horn, 1986). This approach is therefore amenable to the Gulf of Alaska since it is often the decay centre for storms in the Pacific. Two potential drawbacks associated with composites are: 1) they are no better than the criteria upon which they are based; and 2) they can average disparate atmospheric settings. These two problems can normally be addressed by manually inspecting the maps or other data used to create the composites. A more objective approach to addressing the second drawback is to calculate and plot standard deviations for each composite.

4.3.2 Correlation-based Map-pattern Classifications

In contrast to compositing, map-pattern classifications employ a circulation-to-environment approach to synoptic climatology. Early map classifications were subjective and labour intensive, requiring a meteorologist to manually categorize daily weather maps. Automated map classifications are considered an improvement over manual techniques because, when based on standardized criteria and data, results can be replicated and studies compared. Automated classifications can be considered a pattern recognition problem involving digitized weather maps. Such techniques are generally based on principal component analysis, factor analysis or pattern correlation techniques. The latter were favoured in this study because: 1) results from eigenvector-based techniques are often difficult to interpret and lack the uncomplicated appeal of a readily interpretable weather map; and 2) correlation-based techniques are typically capable of classifying more than 90 per cent of the weather maps in a sample (Yarnal, 1993). There are two approaches to correlation-based classifications. The first, introduced by Lund (1963), uses chart-to-chart correlation coefficients to determine the most highly correlated and frequently occurring map patterns. Kirchhofer (1973) introduced a variation on this scheme which uses a simple sums-of-squares formula to compare normalized daily pressure grids. The two algorithms are similar, but the Kirchhofer formula is easier to code and Yarnal (1984) provides a computer program based on this technique. A flow diagram of the program is shown in **Figure 4.29**, and a description of the algorithm is given below.

Step 1: Normalize Grids

The data on each grid are first normalized in order to obtain generalized map patterns which are free of seasonal effects according to the equation:

$$Z_i = \frac{x_i - \overline{X}}{s} \tag{4.9}$$

where,

Z_i = the normalized value at grid point I

x_i = the observed value at grid point I

$\overline{X}$ = the mean, and s the standard deviation as calculated from the "population" which is all points of the N-point grid.

Step 2: Calculate Scores

A Kirchhofer score is calculated for all grid-pair combinations using the following sums-of-squares formula:

$$S = \sum_{i=1}^{N} (Z_{ai} - Z_{bi})^2 \tag{4.10}$$

where Z_{ai} and Z_{bi} are the normalized grid values of point I on days a and b, respectively. Two maps are considered similar if S is less than a prescribed threshold. To distinguish between maps which are statistically similar overall, but which have differing patterns in specific sectors, subscores for each row and column of the grids are also computed using (Eq. 4.10). Maps which meet the prescribed grid, row and column thresholds are termed "significant-pairs".

Step 3: Select Keydays

The record of significant-pairs is examined, and the map having the largest number of significant scores associated with it is designated as keyday 1. This map and all the maps associated with it are removed from the data set and the procedure is repeated to find keyday 2, 3 etc. The procedure continues until all days are clustered into a specified group size minimum (eg. 5 or more significant days per keyday). Any maps remaining at this stage are labelled "unclassified".

Step 4: Reclassify Maps

Because any given map may be significantly correlated with more than one other map, it is possible for days to have been misclassified in Step 3. To correct this, each grid is reclassified. In the reclassification procedure, Kirchhofer scores between each grid and each of the keydays identified in Step 3 are calculated. The lowest significant score is recorded for each daily grid, with the associated keyday denoting the synoptic type of that day. The output from this step is a map-pattern catalogue for the entire data set.

Willmott (1987) demonstrated that the Kirchhofer score given by Equation 4.10 is related to the correlation coefficient (r) used by Lund through the equation S=2N(1-r). Selection of the appropriate r-value is critical to the analysis. While higher r-values cause within-group variance to decrease and between-group differences to increase, it also results in more map patterns and a greater number of unclassified days. Many investigators therefore opt for lowering the r-value in order to produce a workable number of map-pattern categories and to increase the number of grids classified. Values are typically chosen to correspond to a correlation coefficient of 0.5 to 0.7 (Yarnal, 1993).

4.3.3 Study Area and Data Selection

Surface maps exhibiting a tight southeast-to-northwest pressure gradient over the Interior (such as in the southeast corner of a cyclone situated off the coast of B.C.), will result in strong southerly winds over the region. The importance of such a map feature is supported by the review of two existing synoptic climatologies for the region and provides a focal point to the current investigation. Overland and Hiester (1980) produced a subjective sea-level climatology for the coastal region of southern Alaska, which they used to stratify coastal winds under strong orographic influence by synoptic map type. Three of the map patterns identified in Overland and Hiester (1980) may be recognized as potential candidates for strong southerly winds in the interior of B.C. In order of annual percent frequency, the three map patterns were the Aleutian Low (33%), a stagnating low off the Queen Charlotte Islands (17%) and a low in the Gulf of Alaska (12%). The Aleutian Low was prevalent during all seasons while the other two map patterns were primarily winter features, but were also common during fall and spring. Blasing and Lofgren (1980) applied map-correlation techniques to the identification of recurring anomaly patterns in sea-level pressure over the North Pacific Sector and Western North America. Five major anomaly patterns were identified for each season. Anomalies of the three noteworthy features from the Overland and Hiester study were identifiable in the winter and fall patterns here. One winter anomaly pattern featured a strong Aleutian Low, and another a strong somewhat southeasterly displaced Aleutian Low. Relevant fall patterns included a negative pressure anomaly over southern Alaska, and a slightly below-normal pressure anomaly off the North American West Coast. In order to resolve all three potential map patterns noted above, the grid selected for this study covered the area from 110° to 190° west longitude and 35° to 70° north latitude (see **Figure 4.30**).

Two types of data were required for determining the synoptic climatology of strong winds; gridded pressure data to classify the large scale atmospheric circulation, and station data to assess the relationship between the atmospheric circulation and the local surface environment. An earlier examination of long-term wind records at the Prince George Airport (see **Fig. 3.20** and **Fig. 3.21**) showed an anomalous increase in wind speed during the period 1960-1970. Yarnal (1985) reports that the Pacific north-west coast experienced a significant change in both temperature and precipitation regimes in the middle of this anomaly, and according to White and Walker (1973) (cited in Yarnal, 1985), abrupt changes in the relationship between equatorial sea surface temperature and Aleutian Low intensity took place at about the same time. To avoid mixing data from two potentially distinct populations, this study was limited to the 25-year period 1970-1994. A description of the two data sets selected for this study is given below.

4.3.3.1 <u>Environmental data</u>:

Periods of gusty winds were taken as a surrogate for strong winds. Records of the direction and speed of the daily extreme gust measured at the Prince George Airport were obtained from the Canadian Climate Centre for the period 1970-1994. Wind direction measurements prior to 1977 were taken to the nearest 20 degrees (eg. 360, 340, 320 etc.), while the remainder of the data was recorded to the nearest

10 degrees or 36 compass points. Gusts were reported when the peak wind speed exceeded the two-minute mean by at least 10 km/hour and the peak attained a speed of at least 30 km/hour. The data set had a 97% availability, and according to the criteria for recording gust measurements, there was no gust activity on 54% of the available days.

4.3.3.2 Atmospheric circulation data & analysis software:

The gridded data used in this study were obtained from model output of the NCEP/NCAR Reanalysis Project (Kalnay et al., 1996). The goal of this project is to produce a 40-year record of global analyses of atmospheric fields. The quality and utility of the re-analyses are considered superior to archives of real-time weather analyses because: 1) the model used a frozen state-of-the art data assimilation routine, eliminating perceived climate jumps associated with changes in data assimilation systems; 2) additional observations are used that were not available for the real-time analyses; and 3) the model output data are temporally and spatially continuous. Reanalysis information and partial model output of selected fields are available free of charge at http://wesley.wwb.noaa.gov/reanalysis.html. Daily-averaged mean sea-level pressure data and 850 hPa and 500 hPa pressure surface data were obtained for the North Pacific sector and western North America for period 1970-1994. The data are stored in GRIB (GRIdded Binary) format and have a spatial resolution of 2.5° latitude, resulting in a grid size for this study of 17x24 (see **Figure 4.30**). The daily grids represent an average of 4 daily assimilation cycles (00Z, 06Z, 12Z and 18Z) and therefore, result in smoothed map features. One drawback to using the daily data is that it was not suitable for studying storm development over time.

The gridded data were studied utilizing the Gridded Analysis and Display System (GrADS), an interactive desktop tool for the analysis and display of earth science data developed by the Center for Ocean-Land-Atmosphere studies, Calverton, MD. The software is GRIB compatible and is freely distributed at http://grads.iges.org. GrADS implements a 4-Dimensional data model, where the dimensions are usually latitude, longitude, vertical level, and time. Operations may be performed on the data directly using a set of built-in functions, or users may add their own functions as external routines written in any language. A programmable scripting language can also be used to automate complex multi-step calculations or displays. Once the data have been accessed and manipulated, the results may be displayed using a variety of graphical output techniques.

4.3.4 Analysis of Fall-Winter Cyclones

Using the environment-to-circulation approach to synoptic climatology, composites for moderate, strong and severe wind storms were constructed. The map composites were used to characterize the storm events and to assess the spatial representativeness of the storm winds. Map-pattern classification techniques were then applied in a nontraditional manner to find archetypical pressure patterns for each storm composite.

4.3.4.1 Development of storm composites:

The compositing-criterion established for this analysis was southerly gusts (greater than 30 km/h) occurring during the fall and winter months. Based on the monthly distribution of the southerly gusts (**Figure 4.31a**), the fall-winter period was defined to be October through March. The distribution of the daily extreme gust speeds satisfying the composite-criteria is shown in **Figure 4.31b**. A total of 626 potential storm cases were identified. Because the typical lifetime of a cyclone is greater than one day, it was possible that the compositing-criteria classified more than one gusts from the same storm event. However, to allow for the possibility of stagnating map features, no corrective measures were taken. **Figure 4.31c** shows that more storm-events were identified per year during the period 1970-1976. This anomaly was most likely due to the change in the number of compass points used to resolve wind direction measurements (as noted above). More events were classified during this period, because a coarser resolution was used to record wind direction. No attempt was made to account for this measurement bias, and it is estimated to account for approximately 15% of the total number of storm cases identified in this study. The effect of maintaining this bias was to allow slightly more variability in the orientation and position of the map features associated with southerly gusts.

The date of each storm-event was entered into a GrADS script which computed the mean and standard deviation of the pressure on the corresponding daily maps (see script **"composite.gs"** in **Appendix B**). Each map was inspected before being included in the composite calculation. Almost all the map patterns were associated with a strong surface low, however, no maps were rejected at this stage as the composites would later be refined (see below). Composite maps were computed for mean sea-level pressure (MSLP) and the 850 hPa and 500 hPa pressure surfaces. To determine the degree of departure from normal climatology, climatological fields were constructed for each map level. The climatological fields were prepared by averaging the entire set of daily grids from October through March (N=4556) (**"climate.gs"**). Pressure and height anomaly maps were then constructed by subtracting the climatology fields from the composites. The statistical significance of the anomalies was computed using a two-tailed Student's t-test. The composite, standard deviation and climatological fields were entered into a third script (see function **"sigfig.gs"**) which calculated the t-values at each grid point. The significance was tested at the 99% level by interpolating from an encoded t-table, and the areas of significance were plotted on the anomaly maps.

Since this research project was primarily concerned with extreme wind events, the above exercise was repeated by focussing more closely on the third and fourth quartile of the distribution shown in **Figure 4.31b**. As synoptic winds are believed to be a function of storm intensity, the composites were stratified according to gust size. This approach would also act to limit the possibility of having multiple map patterns from the same storm event in a single composite unless it was due to a stagnating feature. Composites of MSLP were constructed for each of the following speed categories: moderate (51- 70 km/h), strong (71-90 km/h) and severe (91+ km/h). The number of storm events falling into each category were 202, 70 and 11, respectively. No maps were rejected because in this instance every map was associated with an intense cyclone, suggesting that most of the variability seen earlier was caused by the lower velocity wind storms.

4.3.4.2 Identification of keyday storms:

Map-pattern classification techniques were applied to the set of daily MSLP grids in each of the composite categories. The aim of this analysis was to find the single most recurring and representative map-pattern in each of the three speed class categories. This required selecting a grid threshold value which would minimize the total number of map types, while maintaining the correlation between grids at a reasonable level. A smaller 20x13 grid covering British Columbia and the southern coast of Alaska (**Figure 4.32**) was utilized in this analysis, because the results of the compositing exercise (given below) determined that a low in the Gulf of Alaska was the most significant contributor to strong wind events in the Interior.

A version of the Kirchhofer sums-of-squares technique presented in Yarnal (1984) was obtained from the author. Daily grids of MSLP were exported from GrADS and converted to floating decimal point for input into the map-pattern classification program. The group size minimum and row and column thresholds were set at their default values, namely a group size of 5 and row and column thresholds equal to 2 times the number of columns and rows, respectively. In specifying the overall grid threshold value, the desire was to find a single map pattern which was highly correlated with at least 50% of the maps in any given speed category. A series of preliminary map classification trials were preformed to find the optimal grid threshold. A threshold value corresponding to a correlation coefficient of $r = 0.8$ produced too many map types for the purposes of this study, and left too many days unclassified. A threshold of $r = 0.6$ produced fewer map types in the higher speed class categories, but resulted in too many equally frequent map types in the lowest speed category. As it was desirable to apply the same criteria to each speed category, the optimal grid threshold was determined to be $r = 0.7$.

4.4 RESULTS

4.4.1 Storm Composites

The climatological fields constructed as part of this analysis are given in **Figure 4.33**. The climatology of British Columbia during the fall-winter period is shown to be dominated by a strong westerly maritime air stream (see 500 hPa climatology, **Fig. 4.33a**). The prevailing climatological surface feature is the Aleutian Low. The cyclonic flow around this semi-permanent feature, and the relatively weak pressure gradient over the Interior, explains why the prevailing winds for that region are generally light and from a southerly direction. In the compositing of all southerly gusts (greater than 30 km/h), the importance of the Aleutian Low was diminished and two additional recurring map patterns became readily identifiable: a low in the Gulf of Alaska and a low off the coast of B.C. While the majority of the MSLP maps associated with these three patterns exhibited a strong southeast to northwest pressure gradient over the Interior, the position and orientation of the corresponding surface low was highly variable. The maximum standard deviation in mean-sea level pressure occurred southwest of the Aleutians (16 hPa), while a relative minimum (9 hPa) occurred over the composite-criteria area (Central-Interior). The most frequently occurring of these map patterns, as is evident by the MSLP composite shown in **Figure 4.33b**, was the low in the Gulf of Alaska.

The surface composite representing the average weather conditions during southerly gust events is shown in **Fig. 4.33b**. The composite exhibits a southeast-northwest oriented pressure gradient over the Interior, situated between the low in the Gulf of Alaska to the northwest, and a continental high pressure area to the southeast. In comparing the MSLP composite to climatology, these map features were found to be statistically significant departures from normal climatology (**Fig. 4.33c**). The anomaly in MSLP near the centre of the storm is 8-10 hPa below normal, while the pressure at Prince George is about 4 hPa lower than normal. The 500 hPa composite shows an intensification of the low pressure trough over the northeast Pacific and ridging over the west coast which is indicative of warming due to the flow of warm air from the south. However, there were no significant changes in the 500 hPa heights over the criteria area. For this reason, the stratification of the storm composite according to gust speed was limited to the study of mean sea-level pressure. The removal of the lower velocity storms resulted in a noticeable lowering in the standard deviation of the composite fields, and the variation in map patterns became less in higher speed class categories. While this may be due to the decrease in the number of cases included in each category, it may also be a manifestation of the observation that deviations in wind direction generally become less as wind speed increases. The statistical significance of the difference in map pattern between the speed class categories was not tested. The composites of medium (51-70 km/h), strong (71-90 km/h) and severe (>90 km/h) wind gusts are shown in **Fig. 4.34a.** Each composite shows an incremental intensification of the pressure gradient over the central and southern portions of British Columbia (see **Table 4.22**). The coefficient of determination between mean daily extreme gust speed and the relative strength of the pressure gradient is $R^2 = 0.96$.

Increments in speed class category are also accompanied by decreasing pressure over the criteria area (**Table 4.22**), and can be attributed to the eastward propagation of the map features. For instance, there is a slight northeastward displacement in the position of the storm centre in each of the map composites shown in **Fig. 4.34a**. The trough feature north-east of the low in the composite maps is further evidence of a north-eastward tracking storm system. This distortion in the pressure pattern is more readily identifiable in the anomaly maps (**Fig. 4.34b**), and storm motion is most pronounced in the severe-storm anomaly, where the largest pressure drop is seen to occur over northern B.C. The sea-level pressure at Prince George during severe wind storms is 12 hPa below normal, while the sea-level pressure at the centre of the storm depression is 4 hPa higher than it is for storms in the strong gust category. Taken together, this evidence would suggest that gusts in the severe category are associated with an orographically split storm system. When the surface low encounters the coastal barrier, the upper portion of these storm systems are able to travel over the mountain barrier, while the surface feature decays. As the upper level storm travels over the mountain range, a broad and intense pressure gradient sweeps across the Interior. By constructing composites one day prior and one day after the peak gust event, it was seen that there is a difference in the prevailing storm tracks between the moderate and the strong and severe events. The moderate category storms appear to track eastward through the Central-Interior, causing an anticyclonic shift in the flow to a more northwesterly direction after passage of the system. The strong and severe events are thought to be related to storms tracking northeastward.

4.4.2 Keyday Storms

The aim of this component of the analysis was to find, for each of the speed class categories, the daily map pattern which most closely resembled the composite for that category. The criteria established for meeting this objective was to find a keyday map which was correlated at r=0.7 or higher, with at least 50% of the maps in its respective category. In order to diminish the influence of the Aleutian Low upon the map-pattern classification, the smaller grid shown in **Fig. 4.32** was used in this analysis. Due to the variability of map patterns in the lowest speed category, a map satisfying the criteria adopted for this analysis could not be found. Application of the classification criteria to the moderate storm category resulted in four map types, one of which was correlated with 45% of the maps in this category. To increase the number of days explained to 50% required using a grid threshold of less than r = 0.6. For the purposes of this study, the preference was to maintain the higher map correlation, and designate the first map-type as the keyday for this storm category (see **Table 4.23**). Application of the classification criteria to the strong and severe storm categories resulted in keydays which were correlated with 89% and 73% of the maps in their respective categories.

The keyday maps are shown in **Fig. 4.34c** and their storm characteristics are compared in **Table 4.23.** All three keyday events were fall storms, occurring in either October or November. While the pressure values for the keyday maps are generally lower than their composite values (compare with **Table 4.22**), the pressure patterns in the vicinity of the composite-criteria area are very similar. The daily extreme gust speed for the keydays storms are approximately equal to their mean composite value suggesting that selected maps represent archetypical patterns for moderate, strong and severe winds. Further evidence that strong synoptic winds in the Interior are associated with decaying storms in the Gulf of Alaska are also seen in the results here. Pressure at the centre of the keyday storms are seen to increase with increments in gust speed category, and troughing in the strong and severe keyday maps is indicative of storms propagating over the coastal barrier.

4.4.3 Storm Related Weather

An examination of surface weather records from the Prince George airport for the fall-winter period showed that the peak gust events were also accompanied by peaks in temperature and precipitation. **Table 4.24** provides a demonstration of this trend for the severe gust events. Similar trends were observed for the moderate and strong storm categories, with the exception of snowfall. With the lower speed wind storms, snowfall amounts were high on all three days, but more snow fell before the peak in gust speed, which is typical of warm front weather. The amount of rainfall and warming associated with the storm events was also seen to increase with storm intensity (**Table 4.25**), and the increases in temperature and rainfall were significantly above the climatic normals for the period. For example, the mean daily temperature for the October-March period is -3.6 °C, while the average mean daily temperature during the severe storm events was +3.6 °C.

4.5 DISCUSSION

Following this analysis, it was later learned that there are two errors in the widely distributed Yarnal (1984) code. As pointed out by Blair (1998), the first error interferes with the attempt to ensure that grids classified as similar are sufficiently similar at the sub-grid level. The second error, involves the conversion of the Kirchhofer scores to correlation coefficients which causes a slight lowering of the Kirchhofer scores and might allow some grids to be classified as similar, even though their scores do not satisfy the intended correlation thresholds for similarity. The two errors are not considered problematic for this analysis, however, because of the manner in which the technique was applied. Normally, the Kirchhofer technique is applied to an entire population of maps which will have a large degree of variability, and subgrid scores are therefore critical. Here, the technique was applied to a small sub-population of already similar maps, as dictated by the composite criteria (and as was also verified by a manual inspection of each map entering the analysis). Furthermore, the potential for subgrid differences was minimized by limiting the size of the domain. The second error is also not considered problematic to the current analysis. Because the aim of this analysis was to find a single representative map-pattern for each storm composite, this required selecting a grid threshold value which would minimize the total number of map types, while maintaining the correlation between grids at a reasonable level. The exact value of the correlation coefficient was not as critical. A series of preliminary map classification trials were performed to find the optimal overall grid threshold. An optimal grid threshold corresponding to a correlation coefficient of r=0.7 identified three keyday maps which were highly correlated with 50%, 89% and 73% of the maps in the moderate, strong and severe storm categories respectively. The daily extreme gust speed recorded at the Prince George airport during each of the keyday storms were approximately equal to their mean composite value, suggesting that the selected maps represent archetypical patterns for moderate, strong and severe winds. Further evidence for supporting the representativeness of the three keyday storm is seen the validation of the numerical simulations in Chapter 5, and in the general applicability of the wind speed ratios derived in Chapter 6.

4.6 SUMMARY AND CONCLUSIONS

It was argued in Part II that fall and winter cyclones are the most significant contributor to high winds occurring in the interior of British Columbia. Using the principles of synoptic climatology, a mean sea-level pressure storm composite of these high wind events was constructed. Similar to the mean sea-level pressure pattern for coastal Europe, the storm composite exhibits a strong southeast-to-northwest oriented pressure gradient over the Interior, situated between a deeper than normal low in the Gulf of Alaska, and a stronger than normal Idaho High. An examination of surface weather records from the

Prince George Airport revealed that the peak gust events are also accompanied by above normal temperatures and precipitation, and that the amount of rainfall and warming associated with the storm events increase with storm intensity.

Using the correlation-based map-pattern classification technique proposed by Kirchhofer (1973) and encoded by Yarnal (1984), three daily mean sea-level pressure maps were subsequently identified as model scenarios for moderate (51-70 km/h), strong (71-90 km/h) and severe (>90 km/h) southerly daily extreme gusts occurring at the Prince George Airport. All three keyday storms were fall events. The moderate and severe keyday storms occurred November 21, 1988 and November 12, 1975 respectively, while the strong keyday event occurred October 26, 1994. Two errors in the Yarnal (1984) code reported by Blair (1998) were not considered problematic to this analysis because of the manner in which the technique was applied. The daily extreme gust speed recorded at the Prince George airport during the keyday storms were approximately equal to their mean composite value, suggesting that the selected maps represent archetypical patterns for moderate, strong and severe gust events.

A qualitative approach towards winthrow hazard classification is all that has previously been possible given the sparsity of wind speed data in B.C. forests. The main goal of this research project was to identify areas of the McGregor Model Forest which are prone to high wind speeds. The fact that extreme winds in this region are derived from synoptic scale forcing which is characterized by an extensive zone of straight-line parallel southerly flow, makes spatial extrapolation of the winds possible. In Chapter 5, the three keyday storm scenarios identified in this chapter are used to initialize a series of numerical weather simulations in order to characterize areas of the McGregor Model Forest which are prone to severe winds under a synoptic southerly flow.

5 Numerical Simulation of Keyday Storms

5.1 INTRODUCTION

Numerical weather models are used to simulate the state of the atmosphere by knowing its present condition and solving the mathematical equations which govern atmospheric motions and thermodynamic properties to predict its future state. The physical laws governing atmospheric motions are well known and are described by a set of non-linear partial-differential equations (e.g. Pielke 1984). However, an analytical solution to the full set of governing equations does not exist, so that an approximate solution must be found numerically. A numerical weather model can solve the set of governing equations by evoking finite-difference approximations at discrete grid point locations. The initial, lateral and top boundary conditions may be specified by observations, or during idealised simulations, using typical climatic values. By determining the primary modes of atmospheric circulation, synoptic climatology methods allow for the definition of representative scenarios for model runs (Yarnal 1993). In this chapter, the three keyday storm events identified in Chapter 4 are used to initialize a series of numerical weather simulations. The results of this modelling exercise are employed in Chapter 6 to derive a simplified model for extrapolating high winds across the McGregor landscape on the basis of a single wind measurement taken from the Prince George Airport.

5.2 OBJECTIVES

The objectives of the numerical simulation component of this study were:

1) To perform numerical simulations of the three keyday storm events identified in the previous chapter as being representative storm scenarios for moderate, strong and severe winds under a synoptic southerly flow condition;

2) To use the model output to characterize the wind flow under these conditions and to demonstrate the influences of topography on high winds; and

3) To obtain estimates of the speed and direction of the maximum winds which are likely to be observed in the McGregor Model Forest (MMF) under each storm scenario.

5.3 METHODS

5.3.1 The Regional Atmospheric Modeling System (RAMS)

The numerical weather model used to perform the keyday simulations was the Colorado State University Regional Atmospheric Modeling System, version 3b (CSU RAMS 3b) (Pielke et al. 1992). RAMS is a 3-dimensional, mesoscale model for simulating and forecasting meteorological phenomena in vertical terrain-following coordinates. The model domain size has no lower limit (although in practice the turbulence and other parameterization schemes are optimized for meso-synoptic scales), and widely varying atmospheric phenomena have been successfully studied, ranging from synoptic-scale weather systems to individual thunderstorms and turbulent eddies (Bossert and Poulos, 1993). Two-way interactive nested grid capabilities allow small scale phenomena to be resolved on a finer grid, while the larger systems from which they are derived are simultaneously modelled on a coarser grid. The model advances gridded fields of atmospheric variables such as velocity, pressure and temperature from an initial state through a series of discrete time steps, to a future state based on the set of quasi-Boussinesq equations which govern atmospheric motions. These equations consists of three prognostic equations (two horizontal momentum equations and the thermodynamic energy equation), and three diagnostic equations (continuity, hydrostatic approximation and the equation of state). Optimized parameterization schemes are used for describing the actions of turbulent diffusion, solar and terrestrial radiation, moist processes, sensible and latent heat exchange, multiple soil layers, a vegetation canopy, water surfaces, terrain steering effects and cumulus convection (Walko et al., 1995).

RAMS has three major components: 1) the atmospheric model written primarily in FORTRAN 77; 2) an Isentropic Analysis package (ISAN) which reads in observational data and generates gridded initialization fields; and 3) a postprocessing and analysis RAMS Evaluation and Visualization Utility (REVU). There are two basic methods of initializing the model. With the first method, data from a single sounding is used to construct horizontally homogenous fields of velocity, temperature, pressure and moisture for each model level. The second method is more complex and involves objectively analysing data from one or more sources, and from multiple locations, to produce variable three-dimensional model initialization fields. Variable initialization requires a minimum of either gridded pressure level data or sounding data from one or more locations. Surface observations are also optional. Sounding data offers a higher vertical resolution over gridded pressure level data, but has poor horizontal resolution (one station every 600-800 km^2 in Canada), and is typically only available every 12-hours (00 and 12 Coordinated Universal Time or UTC). For a more detailed description of the model, refer to Pielke et al. (1992). In the section which follows, an overview of the modelling approach and model configuration parameters used in this study is given.

5.3.2 Modelling Approach

While RAMS is a complex model, capable of performing highly sophisticated and detailed weather simulations, a simplified modelling approach was adopted from the outset in this work. The intent was to use the model to diagnose the wind field and obtain a dynamically balanced realization of the flow under each storm scenario, rather than provide a prognostic evolution of the windfield. After trial simulations using a horizontally homogeneous initialization failed to produce a stable solution, an additional level of complexity was introduced and a variable initialization approach was adopted. Surface observations and atmospheric soundings taken at the Prince George Airport during the three keyday storm events were used to initialize three 12-hour numerical simulations using a single grid.

The domain of any mesoscale model must be artificially enclosed and boundary conditions must be specified at the perimeter surface of the model in order to integrate in time the approximate forms of the governing equations.[4] However, it is often difficult to accurately specify the boundary conditions, and this can lead to erroneous solutions being generated along the boundaries. As a practical problem, errors generated in this way are only serious when they propagate from the boundary into the region of interest. It is, therefore, desirable to remove this boundary as far from the region of interest as possible, and expanding the grid in the horizontal is one means to minimize the effect of the lateral boundary. A 120 km x 100 km grid encompassing the up-wind region south and west of the MMF was therefore selected for the modelling exercise (refer to **Fig. 1.1**). To resolve the topographic influences of the main terrain features in the MMF, a horizontal grid size of 1 km was selected. Since a finer grid size would have also demanded a smaller time step in order to preserve numerical stability, a 1 km grid size was also deemed as the finest practicable given computer memory and CPU constraints. Terrain data were obtained from the McGregor Model Forest Association (MMFA) at a resolution of 100 metres (**Fig. 1.1a**) and were smoothed to 1 kilometre using a silhouette averaging scheme that preserved realistic heights and eliminated computational instability associated with $2\Delta x$ topographic wavelengths (see **Figure 5.35a.** for smoothed topography). The model had 29 vertical levels and extended to a height of 16 km (using a spacing of 50 m at the surface which was stretched by a factor of 1.2 for each successive level, to a maximum separation of 1000 m).

The minimum attention necessary to obtain realistic results was given to the model optimization parameters. For example, since the intention here was to model topographic influences on the wind field, and not edge effects of individual cutblocks, a uniform surface roughness corresponding to coniferous forest cover was selected. Other relevant model configuration parameters are summarized in **Table 5.26** Archive sounding data for the Prince George Airport were available on CD ROM from the National Climatic Data Center (1995) in Asheville, North Carolina. Each keyday simulation was initiated at 12 UTC (4:00 a.m PST) and "nudged" toward the subsequent afternoon conditions at 00 UTC

---

[4]Top and lateral perimeters are incorporated because of computational necessity and have no physical meaning (in contrast to the bottom boundary which is real and has physical significance).

(4:00 p.m. PST) using a 5 second time step. In the nudging scheme, the model solution was gradually forced toward the analyzed data during each time integration. The nudging was strong, but was limited to the outer lateral (10 grid points in from lateral edges) and top boundaries (above 12 km). The model was executed on a Silicon Graphics Power Indigo 2 and each time step required approximately 35 seconds of CPU time, making the total run time 84 hours or 3.5 days. In an attempt to simulate wind gust activity, the RAMS code was also modified to record the hourly wind maximum at each grid point in the model domain for the second (k=2) and third (k=3) model levels (corresponding to a mean height of 25 metres and 80 metres respectively). To assist with evaluating the performance of each model run, the code was also modified to output temperature and wind time series data for k=2 and k=3 every hour at grid cells nearest the available climate station locations. It was later learned however, that simulating gusts would require direct numerical simulation of the turbulence and a much finer grid resolution than was feasible for this study. Nevertheless, the information obtained from the modifications to the code proved useful in assessing when the model had reached a dynamically balanced state. After three hours, the hourly time series wind data and one-hour wind maximums simulated for a given location became nearly identical, and the model was assumed to have reached a balanced state. The largest hourly wind maximums recorded in the nine hours beyond the first three hours of simulation were then used as an estimate of the largest wind speed likely to occur under each storm scenario. Gridded wind maximums were subsequently constructed for each keyday storm scenario. In Chapter 6, the estimated wind maximums are used to derive wind speed ratios (relative to the wind speed at the airport), at each grid point in the MMF domain, for winds in each of the three gust categories: moderate, strong and severe.

5.4 KEYDAY MODEL RESULTS

In the preceding chapter, three mean sea level pressure maps were identified which are archetypical of synoptic-scale storms that produce moderate (51-70 km/h), strong (71-90 km/h) and severe (> 90 km/h) southerly wind gusts at the Prince George Airport. Vertical profiles of the atmospheric conditions (temperature, pressure, humidity and wind speed and direction) taken from weather balloons released at Prince George every twelve hours at 00 UTC and 12 UTC were used to initialize three 12-hour simulations using RAMS in order to obtain an estimate of the windfield likely to occur in the MMF during each storm scenario.[5] In this section, the keyday modelling results are briefly presented and discussed, and an estimate of the maximum winds likely to occur under each storm scenario is given. The validity of the keyday simulations is addressed in Section 5.5, while validation of the estimated wind maximums is discussed in Chapter 6. The moderate and strong keyday storms were both fall events (October 22, 1993 and October 25, 1994 respectively). The severe keyday storm was a winter event, occurring January 20, 1973. Results of the three keyday simulations are depicted in the plots shown in **Figure 5.36**. The winds shown are for the third model level (k=3), which corresponds to a mean height of approximately 80 metres. Because erroneous solutions may be generated by the model along the lateral boundaries, especially the inflow (southern) boundary, the plots in **Fig. 5.36** show only the grid interior enclosing the MMF.

Output from the RAMS isentropic analysis package is depicted in the top three frames in **Fig. 5.36** which show the initialization fields interpolated onto the model grid from the 12 UTC sounding taken at the Prince George Airport during the keyday storm events. The three initializing wind fields represent an unbalanced condition, and have not been adjusted for kinematic effects. All three fields exhibit a strong southerly flow characterized by conditions at PGA during the keyday storm events. The moderate initialization wind field is seen to be slightly stronger than the strong keyday field, particularly over the river basin area in the centre of the domain. This is a consequence of the time at which observed winds at PGA reached their daytime maximum. The peak gust during the moderate keyday storm occurred close to 12 UTC, while the peak during the strong keyday storm occurred closer to the 00 UTC sounding. Consequently, the moderate keyday simulation was nudged away from the peak gust event, and the strong keyday simulation was nudged toward the storm peak. The peak wind gust observed

[5]The vertical profiles were incomplete for the moderate (88/11/21) and severe (75/11/12) keyday events identified in Chapter 4. The map-pattern analysis was repeated with these dates removed from the analysis in order to identify alternate moderate (93/10/22) and severe (73/01/20) keydays.

during the severe keyday storm occurred midway between 12 UTC and 00 UTC.

After six hours of simulation (centre row) the winds have been adjusted for terrain effects, and are showing the influences of topography. The strong keyday windfield is generally stronger than the moderate keyday across the entire domain. In most locations, winds are even more intense in the severe keyday simulation. One exception is the wind jet which developed in the strong keyday event where there is a merging wind flow out of the McGregor and Torpy and Fraser river valleys. The most striking feature of the simulated windfield is the nearly easterly flow that develops across the central drainage basin as the southerly synoptic flow encounters the northwest-to-southeast oriented mountains along the eastern boundary and the McGregor Plateau along the northern boundary. The general flow patterns in all three simulations are similar: an easterly flow develops over the broad central drainage basin; winds speed up as air is forced over the McGregor Plateau; and there are strong outflow winds along the deeper McGregor and Fraser river valleys. Winds across the drainage basin appear more easterly for the moderate and strong category where winds appear to be steered around the McGregor Plateau. Differences between the moderate category storm and the strong and severe storms become more apparent at the end of the 12-hour simulation (00 GMT). The moderate keyday winds are lighter and have veered (clockwise shift) by as much as 90 or 180° over the drainage basin. The strong and severe keyday windfields continue to show a southeasterly flow over the Plateau.

The temporal evolution of the simulated windfields is more closely examined in **Figures 5.37a** through **5.37c** which show the speed and direction of simulated winds at discrete grid point locations. Winds are clearly seen to be progressively stronger for each keyday event. Frictional effects are evident in the plots for k=2 (corresponding to a mean height of 25 metres), where winds are significantly lighter and there is more variation in wind direction. However, there is little evidence of winds veering with height due to frictional effects. Simulated winds increase with time in the MMF for the strong and severe storms, but decrease in the moderate category. Veering of the winds with time is also clearly seen in the simulated wind direction for the moderate category storm. Wind speeds in the Prince George Bowl area (not shown) were found to increase with time for the moderate and severe storms, but decreased during the strong keyday simulation.

The speed and direction of the maximum wind simulated at each grid point during the three keyday model runs is shown in **Figures 5.38a** through **5.38c**. The wind maximums did not necessarily occur at the same time at each grid point during the simulations, and the plots therefore should not be interpreted as a snapshot of the windflow. This is particularly true in the case of the moderate keyday scenario, where the strongest winds occurred in the southeast corner of the domain toward the end of the simulation (i.e. after the winds had veered). The plots are shown over a digital elevation model which has a higher resolution (100 m) than was actually modelled (1 km). This was done to aid interpretation of the observed fields presented in the validation section, and in order to simplify orientation with respect to key landscape features. For presentation purposes, wind vectors are only shown every 3 grid points. The wind vectors are colour coded according storm category, with yellow, orange and red denoting moderate, strong and severe winds respectively (blue vectors are less than 50 km/h). Within the MMF, all winds simulated during the moderate keyday were less than 51 km/h. Moderate and strong category winds which occurred during the strong and severe keyday simulations were generally associated with flow over hills, valley funnelling or outflow conditions. Winds greater than 90 km/h occurred along the mountain ridge line located southeast of the McGregor camp station during the severe keyday simulation. The simulated winds are not representative of true gusts however, and are more comparable to hourly winds. For instance, the peak gust speed measured during the strong wind event at the Prince George Airport was 70 km/h, while the peak hourly wind was 43 km/h, which is comparable to the blue zones (see PGA, **Fig. 5.38b**). The peak gust measured during the severe wind event was 92 km/h and the peak hourly wind was near 70 km/h, comparable to orange zones (see PGA, **Fig. 5.38c**). Therefore, actual gust speeds would be even higher than those indicated in **Figure 5.38**. According to Linacre (1992) mean wind to gust ratios are typically in the range of 1.2 - 2.0. The mean wind to gust ratio for southerlies at the Prince George Airport is 1.7. This gust ratio was determined on the basis of the strong correlation ($r = 0.83$, $F(1,243) = 540.46$, $p<0.001$) between daily extreme southerly gusts and the daily maximum hourly wind at the airport between October and March during the period 1972 - 1993.

5.5 MODEL VALIDATION

A direct validation of the keyday simulations was not possible due to the limited availability of meteorological observations during these storm events. The keyday storms selected by the map-pattern analysis in Chapter 4 were drawn from storm events which occurred during the period 1970 - 1994, and preceded wind records at most stations within the model domain. Therefore, three southerly gust events which occurred during the 1995-1997 storm seasons were simulated to assess the representativeness of the keyday storms, and the suitability of RAMS to this application. Wind data from a network of temporary climate stations deployed in the MMF as part of this project during this two year period, supplemented with data from other existing stations were used to assess the validity of these simulations. Ideally, it would have been preferred to have one validating storm for each storm category. However, given the typical return period of severe wind events (2-3 years for gusts of 90-100 km/h), this was not possible. Instead, the three strongest events recorded during the validation period were simulated using the identical model configuration as the keyday storm scenarios. A total of 16 southerly storm events with a daily extreme gust greater than 50 km/hr were observed during the 1995-1997 storm seasons. There were no severe category storms, and only a single strong wind event. In order to increase the number of candidate storms, daily extreme gusts having a wind direction of 180° ± 10° were considered. A single additional strong category storm event was subsequently identified. The three highest wind events are shown in **Table 5.27**.

5.5.1 Station Locations

Meteorological stations located within the model domain are shown in **Figure 5.35b**. In addition to the airport station located in the southwest corner of the domain (PGA), there are three 10-metre towers

(Plaza, PG Pulp and Northwood) operated by the local environment ministry in the Prince George Bowl area. Stations in or near the MMF include: two 10-metre climate research stations (Averil and Aleza) operated by the federal and provincial forest ministries (CFS and MoF, respectively); three 10-metre fire weather stations (Rainbow, Seebach, and Woodall) operated by Northwood Pulp and Timber Limited; and a fourth fire weather/climate station maintained by the MoF (McGregor). Unfortunately, the Northwood fire weather stations are not operated during the fall-winter period, making only six pre-existing stations available for the validation analysis, only two of which are located within the boundaries of the MMF. As part of the MMF Climate Studies and Monitoring Project, data collection was supplemented by the installation of three additional stations within the MMF. Three 3-metre tripod-based stations were deployed at Dojo, Seebach and Flute. A more detailed description of these three stations is included in **Appendix C**.

5.5.2 Validation Methods

Given the modelling approach adopted in this analysis, the temporal evolution of the modelled fields was not expected to be adequately captured. The typical storm duration for both the keyday and validation events (as defined by a period of sustained southerly winds greater than 20 km/h at PGA) was 10-16 hours. Therefore, nudging the numerical solution toward a single sounding (00 UTC) was unlikely to fully capture the synoptic evolution of the storm events. Consequently, a quantitative evaluation of the model's performance using the statistical methods recommended by Willmott et al. (1985) (cited in Jackson and Steyn, 1994) was not considered appropriate to this analysis. Model validation was further confounded by a number of other factors which are highlighted below.

1) **Limited observations:** while it is not realistic to have wind measurements at each grid point, a higher station density than was available would have been necessary to validate all of the major topographic windfield features in the MMF.
2) **Measurement error:** the cumulative errors associated with airport wind speed measurements

(cup anometers) may be as high as 10 percent (Linacre 1992), and wind directions are only reported to 36 compass points. RM Young wind monitors were used at all other stations, and have a wind speed error of 2%, and a 5% error for wind direction. The airport measurements were not used in the validation exercise, but would be a source of initialization error (see item 7 below).

3) **Observational inconsistencies:** the underlying vegetation varied between stations, as did measurement height. Winds are generally observed to increase with height, and the wind profile above a locale is dependant upon the aerodynamic roughness of the underlying surface. Variations in measurement height and surface roughness therefore make it difficult to compare observed winds to model winds at a given height. Given the lack of accurate surface roughness measurements, and the fact that surface conditions also varied between storm events (eg. vegetation height, snow cover etc.), no attempt was made to correct for measurement height differences.

4) **Simulation inconsistencies:** while every attempt was made to maintain consistency between the model runs, there were two differences worth noting. Firstly, some runs were nudged towards the storm peak, while others where nudged away from the storm peak. Secondly, there were differences in sounding resolution (i.e. the number of vertical data points) used to initialize each model run.

5) **Modelled vs. observed fields:** modelled winds are instantaneous and represent a volume averaged value, whereas observations are measured at single point and are typically recorded as either a one-hour average or a two-minute average before the hour (PGA and McGregor).

6) **Subgrid effects**: observations may include the influence of cutblock boundaries resulting from improper exposure, or small scale topographic effects (< 1 km) which may cause localized speed-up or sheltering effects. Such influences would not be resolved by the model.

7) **Initialization errors:** sounding data is assumed to represent an instantaneous vertical profile of the atmosphere above a point. In reality, the sondes take a finite period to ascend (1 - 2 hours), and are carried a considerable distance by winds aloft (on the order of 100 km under strong winds). As noted above (see point 4) the soundings used to initialize each run had different vertical

resolutions. Sounding data for storm events which occurred in 1994 or later were obtained directly from the local aerological station, and were available at much higher resolution (every 10 seconds, or on the order of 400 levels) than data from archived sources (typically on the order of 40 levels). Coarser soundings could be associated with greater interpolative errors. Sensitivity tests showed that using a higher resolution sounding produced (near surface) winds that were 0.5 to 1 m/s faster.

As a result of the above limiting factors, the focus in this chapter therefore is a qualitative evaluation of the model performance, rather than a quantitative validation of the modelling results. A more quantitative validation of the synoptically parameterized extrapolation model derived from the RAMS output was possible however, and is given in Chapter 6. The primary aim in this chapter is to assess whether 1) the numerical simulations reached a stable and balanced solution; and 2) if the model results provide a plausible estimation of the wind field based on theory and experience. Trends in the time series data (temperature and wind speed) and model integral quantities (such as kinetic energy, peak vertical velocities, and surface pressure) were used to determine whether the simulations reached a stable solution. Similarity between model runs, and evidence of topographic influences, were assessed to determine if the wind field was realistic. Modelled wind directions were qualitatively assessed by comparison to the prevailing storm winds observed at each station. For this purpose, a windrose diagram was constructed at each wind monitoring station for the fall-winter period. The magnitude of the simulated wind speeds were qualitatively assessed by comparison to observed winds speeds at each of the wind monitoring stations.

5.5.3 Simulation Results

Results from the numerical simulation of the three validation storms are depicted in **Figure 5.39** which includes the initializing wind field (12 UTC) and a snap shot of the wind flow after six (18 UTC) and after twelve hours (00 UTC) of simulation. The two strong category storms had nearly identical initializing wind fields and were substantially stronger than the moderate counterpart. Similarities between the strong wind storms are still evident after six hours of simulation. After 12 hours, winds simulated for both storms have diminished, but in the case of the October 1996 event, the winds across the drainage basin have veered by approximately 45°. However, variation in wind direction was considerably less during the strong category simulations than during the moderate validation run. After 12 hours, the moderate simulation had undergone substantial veering, as it did during the moderate keyday simulation (compare with **Fig. 5.36**). In general, winds within the MMF resemble the same flow patterns noted in the keyday simulation. Gridded wind maximums were also constructed from model output for the validation simulations (not shown), and exhibited many similarities to the keyday maximums in **Fig. 5.38**. However, during the validation model runs, moderate and strong category winds were seen to occur within the MMF in all three simulations and there were no severe winds simulated for the MMF.

Simulated winds at grid point locations nearest to the monitoring stations are compared to observed winds in **Figures 5.40a through 5.40c** for each of the validation scenarios. Observed winds increased with time in the Prince George Bowl area and decreased in the MMF. A similar trend is observed in the simulations. The Bowl area monitoring stations show an incremental intensification of the wind with each storm. The moderate storm generally had the lowest wind speeds, while the October 1996 event had the strongest winds. The same trend is evident in the simulated wind speeds for the Bowl grid point locations. In contrast, observed winds from the MMF stations had approximately the same magnitude for each storm, yet the simulated winds still exhibited the incremental intensification noted for the Bowl area However, winds near the end of each simulation are similar and comparable in magnitude to observed winds. There is also greater variability between the MMF observations (speed and direction) than in the Bowl area due to the greater variation in topography, station elevation and station separation. This variation between stations is not as evident in the simulations, because the simulated winds are for the same height and the model assumes a uniform surface roughness. With the exception of a few anomalies, both observed and simulated wind directions during the strong category storms remained relatively constant with time. The observed and simulated wind directions during the moderate category storm exhibited a clockwise shift midway through the 12-hour period. A clockwise shift was also noted in the moderate keyday simulation. An examination of daily MSLP maps before, during and after each storm event suggests that the difference between the moderate and higher category storms may be due to a preferred storm track. During moderate storms, the low pressure system tends to track eastward directly through the model domain. This would cause the wind to shift from southerly to easterly as the bottom portion of the low sweeps through the area. The higher category storms tend to track northeastward allowing only the southerly and southwesterly flow in the lower right hand quadrant to sweep over the study domain.

Observed wind directions during the three validation storms were northerly, northeasterly and easterly at Flute, Dojo and Seebach, respectively. A similar clockwise rotation of the wind is evident in the simulation results, but is not as pronounced or as persistent, and the discrepancies between modelled and observed wind directions are greater. Variation in model discrepancies is notably greater at Seebach and Flute. The discrepancies may be partially due to frictional effects given the height difference between the modelled and observed fields. Wind directions in the lower boundary layer typically veer (clockwise shift) with height. A clockwise shift of approximately 45° would make the observed wind at 3-metres agree with the simulated wind direction. However, the discrepancy is greater than can be explained by frictional effects alone, and may also be due to non-ideal station exposure, or localized effects not resolved by the model. For instance, the prevailing northeasterly winds at Dojo are most likely the result of wind funnelling given the orientation of the Fraser River near this location. Simulated winds at Dojo, however were more easterly. The gap through which the Fraser flows is very narrow in the vicinity of Dojo and may not be fully resolved at a scale of 1 km. The prevailing northeasterly winds at Seebach appear to be associated with down slope winds, and local topography near Flute may also cause funnelling of the wind in a northeasterly direction. Also, the location of these two stations along the western edge of the Rockies may be influenced by weather systems not captured by the synoptic climatology at PGA such as Arctic outbreaks and subsequent funnelling of winds through gaps along the mountain barrier. At Seebach, both observed and modelled winds were easterly during the strong validation storms. Observed wind directions at Flute during the validation storms were more variable, but generally had a strong northerly component. Winds simulated for Flute during the two strong category storms were more easterly.

To lend support to the representativeness of the keyday storms, and the ability of RAMS to provide a plausible estimation of the resulting wind field, prevailing wind directions measured during the October 1996 to March 1997 windy season are shown in **Figure 5.41**. The prevailing wind directions are consistent with the wind directions measured during the three validation storm events and with the results of the numerical simulations. With the exception of the 3-metre stations (Dojo, Seebach and Flute), the prevailing wind direction was southerly or southeasterly. Prevailing wind directions at Aleza and McGregor were southeasterly and show good agreement with the results of the numerical simulations. Prevailing winds at Averil were southerly (27%) to southeasterly (20%), and simulated winds were generally southeasterly. Equally strong, but less frequent winds also occurred out of the north at the 10-metre stations, while the prevailing wind direction at each of the 3-metre stations was northeasterly.

5.6 SUMMARY AND CONCLUSION

Atmospheric soundings taken at the Prince George airport during the three keyday storms were used to initialize a series of 12-hour simulations utilizing the Regional Atmospheric Modeling System (RAMS). RAMS was used in a diagnostic mode, to quickly obtain a dynamically balanced realization of the flow. The general flow pattern in all three simulations was similar. An easterly flow developed over the broad central drainage basin. Wind speeds increased where the air was forced over the McGregor Plateau and strong outflow winds occurred along the deeper McGregor and Fraser river valleys. The maximum wind simulated at each grid point were recorded, and gridded wind maximums were constructed for each keyday scenario. Direct validation of the keyday simulations was not possible due to the limited availability of observations during these storm events. Three southerly gust events during the 1995-1997 storm season were simulated to assess the representativeness of the keyday storms, and the suitability of RAMS to this application. Wind data from a temporary climate network deployed in the MMF, supplemented with data from existing stations, were used to assess the validity of these simulations. Simulated winds were comparable to hourly winds and showed general agreement with 10 metre winds in a clear opening. Frictional effects were evident at the 3-metre stations where the observed winds were significantly lower than the simulated value. Prevailing wind directions at the 10-metre towers showed reasonable agreement with the simulated wind field. Simulated directions at the 3-metre stations were plausible when subgrid effects are taken into consideration. While the model validation performed in this section was rather qualitative, the similarities noted between the keyday simulations and the validation runs lend support to both the representativeness of the keyday storms, and the ability of RAMS to provide a realistic estimate of the windfield under each storm scenario.

PART IV: Application of Results

6 A High-Wind Model for the McGregor Model Forest

6.1 INTRODUCTION

The complex terrain and sparsity of wind data in British Columbia forests would typically demand the use of either empirical extrapolation techniques or numerical modelling to estimate winds over the landscape. The model proposed here incorporates both techniques by using model output from the numerical simulation of three keyday storms, to derive speed ratios between grid points in the complex forest terrain and a neighbouring airport location. In Part I, it was shown that prevailing storm winds in the Central-Interior are from a southerly direction and are related to the passing of synoptic scale disturbances. In Part II, three keyday pressure maps were identified as typical of disturbances which cause high southerly winds in the Interior, and three numerical simulations were carried out to determine the maximum wind speeds likely to occur under each storm scenario. In this chapter, an example is given of how the results from Parts I and II of this thesis may be generalized for application in the McGregor Model Forest (MMF). The model described here is intended to provide an estimate of the winds likely to occur above the forest canopy in the MMF based on a single wind measurement at the Prince George Airport (PGA). The model strictly only applies when there is a strong southerly flow with winds gusting higher than 50 km/h, although a relaxation of these constraints is also examined.

6.2 OBJECTIVES

1) To test and develop a model for extrapolating high winds across the MMF landscape under a synoptic southerly flow condition; and
2) To use the model to characterize the strength and direction of winds in the MMF under this prevailing flow condition due to topographic variation.

6.3 METHODS

6.3.1 Model Description

The three keyday numerical simulations in Chapter 5 provide an estimate of the wind field likely to occur in the MMF when winds at PGA are from a southerly direction, and the daily extreme gust speed recorded at the airport falls into one of three categories: moderate (51-70 km/h), strong (71-90 km/h) or severe (90+ km/h). These results were used to construct a more generalized model for extrapolating the maximum wind speeds likely to occur in the MMF for any given wind speed at the airport which was greater than a threshold value of 30 km/h and from a southerly direction (180°). Therefore, as was the case with the numerical simulations, the synoptically parameterized extrapolation model developed here also has a horizontal resolution of 1 km, and provides an estimate of the maximum mean surface wind speed, rather than a gust maximum.

The estimated wind maximums from the three keyday numerical simulations were first used to derive wind speed ratios (relative to the wind speed at the airport), at each grid point in the MMF domain, for winds in each of the three gust categories. Simulated wind maximums at a mean height of 70 metres (model level, k=3) were selected for this purpose. Each grid of maximum wind speeds was normalized by the corresponding maximum simulated for the airport at this level (9.2 m/s, 12.4 m/s and 13.7 m/s for the moderate, strong and severe, respectively). This provided a gridded set of three speed ratios stratified by daily extreme gust speed. To extrapolate high wind estimates under a southerly flow condition, the model multiplies the mean surface wind speed at the airport by the appropriate grid of speed ratios. To determine the appropriate speed ratio category, a mean wind to gust ratio of 1.7 is applied to the observed wind speed at PGA. It was not possible to develop a similar scheme for varying the wind direction within a gust category. The model assumes that wind directions are identical to what was simulated for the keyday which corresponds to the gust category determined by the gust ratio.

6.3.2 Model Validation

A qualitative validation of the keyday numerical simulations was given in Chapter 5, and the difficulties associated with comparing model winds to observed winds were discussed. The same challenges exist here and are compounded by the short period of observations available in the MMF and the long return interval between strong and severe wind events. Nevertheless, a more quantitative validation of the synoptically parameterized extrapolation technique presented in this chapter was possible. Validation of the extrapolated wind speeds was assessed by the comparison of observed daily wind maximums under a strong southerly flow to the extrapolated wind speed determined by application of the appropriate speed ratio. Validation storm dates were identified by the occurrence of southerly gusts (180°) greater than 50 km/hr during the fall and winter months. Six stations in or near the MMF and three stations in the vicinity of Prince George were used to perform the validation (refer to Chapter 5 for a description of each station). Validation of this technique is limited to verifying the magnitude of the wind estimates, as verification of the wind direction was addressed in Chapter 5.

6.4 RESULTS

6.4.1 Speed Ratios

Speed ratios calculated for the wind monitoring stations are shown in **Table 6.28** together with the period of record available at each station. No general trends are distinguishable between stations or storm categories with the possible exception of the three BCMOE stations located in the Prince George Bowl area (Northwood, PG Pulp and Plaza), which exhibit speed ratios less than 1.0 for all storm categories. The period of record available at each station varies from 2 to 8 years, with the stations deployed as part of this project having the shortest record (Averil, Dojo, Flute and Seebach), while the

BCFS climate station at the MMF forest camp site has the longest period of record. However, the MMF forest camp station had extensive periods of missing data during the winter months and this is reflected in the low number of storm dates for this station. The total number of storm events recorded at each station is given in the last column of **Table 6.28**. To increase the sample size for those stations having the shortest period of record, the gust threshold was lowered to 35 km/hour and the allowable wind direction was extended by $\pm 10^{\circ}$. No severe-gust storms were recorded at PGA during the period 1989-97 and only one strong-gust event occurred during the 1996-97 period.

6.4.2 Model Validation

The maximum daily hourly wind which occurred at PGA during each of the identified gust-events was entered into the model and a corresponding wind maximum was extrapolated for each of the wind monitoring stations as described in the previous section. Application of the gust ratio to the maximum daily wind entered into the model increased the number of storms classified as strong gust events. The extrapolated wind maxima are compared to the observed daily maximum at each station in the scatter plots given in **Figure 6.42**. With the exception of Averil and Flute (not shown), the correlation between the observed and extrapolated wind maximums were statistically significant at the 95% level. The correlation for Flute was negative and is not included in **Fig. 6.42**. It should be noted that the wind monitor at this station experienced failures during many of the high wind events. It is suspected that this may have been related to the heavy rainfall and subsequent freezing which typically accompanied the storm events. In the case of Averil, increasing the sample size by lowering the gust threshold and increasing the number of allowable wind directions resulted in a significant decrease in the correlation coefficient. The correlation and test results shown for Averil therefore only include storm events which satisfied the original model criteria. The effects of surface friction are clearly evident at the 3-metre wind stations (Dojo, Seebach and Flute) where the observed wind speeds are significantly lower than the extrapolated value.

The scatter plots in **Fig. 6.42** also suggest that there is a tendency for the strong category speed ratios to over predict winds in exposed areas (Aleza, Averil and McGregor) and under predict winds in sheltered locations (see Northwood and Plaza). In an attempt to correct this bias, two alternative measures were explored. First, speed ratios where calculated for the three numerical simulations of the validation storm scenarios also presented in Chapter 5, and a mean ratio was then calculated for each station. The second alternative explored was to apply the moderate keyday ratios to all storm events since it was most representative of the largest number of storms. Both measures improved the correlation at those stations biased by strong category events, with the exception of Averil. While there were no apparent differences in the correlations between the two schemes, application of the moderate ratios generally yielded results which were closer to the one-to-one line and this approach was therefore adopted (see **Figure 6.43**).

6.4.3 Model Error

The mean absolute error of the extrapolated maximum mean wind speeds using the moderate wind speed ratios at each of the wind monitoring stations is shown in **Table 6.29**. The average mean absolute error for the six 10-metre stations is 1.5 m/s, while the mean absolute error at each of the 3-metre stations is significantly higher (5.65, 3.38, and 5.35 m/s at Dojo, Flute and Seebach, respectively). Assuming a model error of 1.5 m/s for all locations, the difference in wind speed due to measurement height at the 3-metre stations is therefore 4.15 m/s, 1.88 m/s, and 3.85 m/s at Dojo, Flute and Seebach, respectively. However, according to Linacre (1991), the ratio of a wind speed at 3 m, to the wind at 10 m, for a surface roughness of $z_0 = 0.1$ m (between open and rough terrain) is 0.65. Therefore, the wind speed errors at Dojo and Seebach are larger than can be explained by measurement height alone, and are probably also due to topographic influences not resolved by the model. These two 3-metre stations are known to have had poor topographic exposure. Seebach was located on a steep south-westward facing slope, and Dojo had higher terrain located to the north of the station. The Dojo cutblock also experienced significant tree growth during the period of measurement.

The frequency distribution of the mean absolute error at each station is shown in **Figure 6.44**. The frequency distributions at the two poorly exposed 3-metre stations are both positively skewed., while the distribution for Flute (not shown) resembled those of the 10-metre stations. Extrapolated wind speeds at the 10-metre stations were within an absolute error of 3 m/s over 70% of the time; within 2 m/s between 45 and 85% of the time; and within 1 m/s between 20 to 40% of the time (see **Table 6.30**). As seen in **Figure 6.45**, the model shows a slight bias toward overestimating the wind speed at most stations. A notable exception is Averil, which doesn't exhibit any model error bias.

6.5 DISCUSSION AND CONCLUSION

Model output from the numerical simulation of the moderate, strong and severe keydays storm events were used to test and develop a model for extrapolating high winds across the MMF landscape under a synoptic southerly flow condition. Speed ratios derived from the moderate keyday simulation were found to be equally applicable to extrapolating winds in the other two storm categories. The estimated wind maximums correlated well with 10 metre wind speeds in a clear opening, and were within 3 m/s of observed winds at the six 10-metre wind monitoring locations over 70% of the time. Taken together with the qualitative validation of the numerical simulations given in Chapter 5, these results are encouraging and should provide an adequate picture of prevailing storm winds in the MMF.

The second objective of this chapter was to use the extrapolation model to characterize the strength and direction of the prevailing storm winds in the MMF. In this chapter, model validation focused on the magnitude of the wind estimates. In Chapter 5, a comparison of the keyday simulations and three validation scenarios suggested that there are possibly two wind regimes related to a difference in the prevailing storm tracks between the moderate and the strong and severe events. The moderate category storms appear to track eastward through the central interior, which may account for the anticyclonic shift in the flow to a more northwesterly direction behind the storms. The strong and severe events are thought to be related to storms tracking northeastward. Therefore, to complement the extrapolation model, two possible wind directions should be given, one for moderate storms and one to reflect the strong and severe events. A vector average of wind directions and scalar average of wind speeds was performed for the latter case. The final model design is reflected in **Figure 6.46** through **Figure 6.48. Fig. 6.46** provides a contour map of the moderate speed ratios. The contour plot of wind speed ratios also highlights areas prone to high winds: moderate wind speeds over the central drainage basin; higher winds over the McGregor Plateau; and severe winds in areas prone to valley funnelling, merging wind streams and along mountain ridge lines. Wind directions for storm winds in the moderate category are given in **Fig. 6.47** and the average of the strong and severe keydays is given in **Fig. 6.48**. Given the opposing wind directions seen in the southeast corner of the MMF, application of the moderate speed ratios in this region may not be appropriate to strong and severe wind storms. Another limitation is that the stations used to validate the model results were not located in areas prone to extreme winds, having speed ratios lower than or only slightly greater than one. The station at Averil remains deployed and will allow ongoing verification of the model to be performed by the MMFA.

7 Executive Summary and Conclusion

7.1 INTRODUCTION

This thesis resulted from participation in the Climate Studies and Monitoring project, funded by the McGregor Model Forest Association (MMFA). Wind, temperature and precipitation can act to limit or enhance forest productivity. Natural disturbances that manifest themselves from extremes in these climatic elements include fire, windthrow and floods. These climatic parameters are all dramatically affected by the presence of complex terrain. The assessment of the ways in which complex topography affects these important climatic variables, particularly the wind, is non-trivial. The main goal of the Climate Studies and Monitoring project was to assess the influence of topography on extreme wind behaviour, in order to identify areas of the McGregor Model Forest (MMF) which are prone to high winds. This chapter provides an executive summary of the technique developed in this thesis to identify areas prone to high winds, discusses a potential application of this work, and makes recommendations for improvements and future work.

7.2 PROJECT OBJECTIVES

To meet the main objective of the McGregor Model Forest Climate Studies and Monitoring project, six individual studies were identified:

1) Compilation and presentation of historical climate data;
2) Analysis of return intervals between severe wind events;
3) Development of realistic storm scenarios;
4) Deployment of a temporary climate monitoring network;
5) Numerical simulation of keyday storms; and

6) Construction of an extrapolation model for high winds.

7.3 PROJECT OVERVIEW

Strong gusty winds can knock down trees in forested areas resulting in economic loss to the forest industry, particularly if inappropriate forestry practices are employed in areas prone to strong winds. Forest blowdown is also recognized as a natural renewal agent, and therefore poses a complex challenge for establishing sustainable forest management practices. The wind climatology of a region, particularly the probable occurrence of severe winds and their directional and seasonal characteristics, must be known before wind risk management strategies can be implemented and appropriate silviculture systems designed. The MMF is located 30 km northeast of Prince George in the central-interior of British Columbia (**Fig. 1.1**). Long-term wind records in the Central-Interior are limited to a few airport locations having records dating back to the mid-1950's to early-1960's. There has been no detailed description, or analysis of winds in the interior of British Columbia. The identification, synthesis and analysis of existing sources of climate data was therefore a logical starting point to undertaking this study.

7.3.1 Climate Normals

Climate data were obtained for fourteen recording stations in and surrounding the Prince George Forest District (**Fig. 2.4**). Only seven of the fourteen stations identified recorded wind measurements, and only four had sufficiently long-term records for the determination of climatic normals and return intervals. The nearest airport stations to the MMF are Prince George, Fort St. James, MacKenzie and Quesnel. The local winds at each of the four airport locations was characterized by examining the annual and monthly mean wind normals for the 30-year period, 1951-1980. Winds are relatively light across the Interior Plateau which is protected from the west by the Coastal Mountains, and in the east by the Canadian Rockies. Prevailing wind directions are southerly in winter and northerly in summer. Wind speeds tend to be low generally, but are highest in winter and lowest in summer. For instance, at the Prince George Airport, the annual frequency of southerly and northerly winds is 33% and 19%, respectively, while the frequency of westerly winds is only 7% (**Fig. 2.5**). Calms are also rather frequent (14% annually). While Prince George is the windiest of the four stations, winds are less than 20 km/h 85% of the time, and the annual mean wind speed is only 10.9 km/h.

Forests in the interior, therefore, grow and mature in a relatively low wind regime, and are not as wind firm as in coastal locations, where annual mean winds speeds are on the order of 15-20 km/h. Catastrophic damage is, therefore, likely to occur during rare high wind events, or when there are unusually strong winds from a non-prevailing wind direction. Endemic damage is likely to occur more frequently during lower intensity storms in areas were previously sheltered trees have been exposed as a result of harvesting, or are otherwise already adversely susceptible to windthrow. It is therefore important to know the return intervals of both moderate, strong and severe wind events.

7.3.2 Extreme Value Analysis

In British Columbia, strong winds are associated with the passage of fronts that originate in the Pacific Ocean or in the Arctic, or from strong winds associated with thunderstorm activity. Knowledge of the typical return period between extreme wind events could benefit the development of wind-risk management practices by providing an estimate of the window available for tree stability improvement over time, in planning sequenced harvesting passes, or to factor natural losses into the equation for a sustainable harvest. Directional categorization of maximum winds is also an important consideration in the spatial design of harvesting and silvicultural applications. Seasonal variability in the occurrence of extreme wind s is another important consideration since variable soil moisture, snow load and frozen ground affect a trees ability to withstand wind loads.

Typical return periods of extreme wind events at four airport locations in the Central-Interior were estimated by assuming that the set of annual extreme gust speeds can be described by a Gumbel distribution (**Table 3.9**). A directional and seasonal categorization of the extreme wind events was undertaken by examining the monthly and annual wind extremes. The strongest gust on record at the Prince George Airport occurred January 17, 1968. This winter storm resulted in mean winds of 65 km/h and gusts of up to 129 km/h being recorded at the Prince George Airport. A wind gust of this magnitude at the airport has a return period of approximately 25 years. A wind gust of at least 70 km/h can be expected to occur every year, and a 'best-estimate' of the 100-year wind at Prince George is 148 km/h. The 95% confidence interval for the true value of 100-year wind lies within 131-168 km/h. An annual wind extreme was ten times more likely to occur during the fall-winter months than spring-summer. In contrast to the mean winds, which tend to be channelled by local topography and have a prevailing north-south component (**Figs. 2.6** and **2.7**), the strongest daily extreme wind gusts occur most frequently from the south, and to a lesser extent from the west. The southerly gusts were primarily fall and winter events, while gusts from the west tended to be spring and summer events. For example, at the Prince George Airport (**Fig. 3.26**), the prevailing annual wind gust directions are southerly (69%) and westerly (18%), and approximately 70% of all the southerly gusts are either winter or fall events, while westerly gusts tend to be spring (29%) and summer (41%) events (**Fig. 3.27**).

The directional and seasonal patterns observed in the airport wind records can be explained by looking at the large scale (synoptic) atmospheric circulation patterns. A 25-year mean sea level pressure map for summer and fall was constructed using model reanalysis data having a 2.5° latitude resolution (**Fig. 3.28**). In summer, the Pacific High over the ocean is strong and rather far north. The clockwise flow around the high explains why winds over the Central-Interior are light and from the west. This weak westerly flow allows the passage of unstable maritime polar air over the warmer land surface, which combined with orographic lift, results in increased thunderstorms as one moves eastward across the Central Plateau toward the Rocky Mountains. Summer gusts may, therefore, be the result of gusty westerly winds typically found behind a cold front, or due to wind bursts from day-time convective storms which are able to develop and propagate in the weak westerly flow. In winter, the Pacific High is weaker and displaced farther south by the Aleutian Low which is well developed. Winds over the Central-Interior are stronger and have a more southerly component. The southerly winter gusts may therefore be associated with the flow ahead of a frontal system attached to a cyclone moving across the Pacific Coast. Differences in the wind climates between stations (particularly differences in wind speed, direction and return period) would be related to the variability in storm tracks and local topographic influences.

The main conclusion drawn from the analysis of the historical climate data was that the majority of strong wind events recorded in the Central-Interior appear to be due to winter cyclones, while summertime convective storms (thunderstorms) appear to be of less significance. However, it is also possible that the relative importance of convective storms can not be adequately resolved by the airport monitoring network. Although there is a potential bias toward the importance of synoptic storms, in consultation with the available literature, forest practitioners and other researchers, a pragmatic decision was made to focus on extrapolating high winds under this prevailing synoptic storm pattern.

7.3.3 Synoptic Climatology

To further refine the synoptic climatology of the windy season, the mean climatology map **(Fig. 3.28)** was reconstructed for the fall-winter period (Oct-Mar), by including only those days where the daily extreme wind gust at the Prince George Airport was from a southerly wind direction and greater than 30 km/h. The resulting storm composite (**Fig. 4.33b**) exhibited a strong southeast-to-northwest oriented pressure gradient over the Interior, situated between a low in the Gulf of Alaska to the northwest, and a continental high pressure area to the southeast. In comparing the MSLP composite to climatology, these map features were found to be statistically significant departures from normal climatology (**Fig. 4.33c**). The anomaly in MSLP near the centre of the storm is 8-10 hPa below normal, while the pressure at Prince George is about 4 hPa lower-than-normal. The 500 hPa composite shows an intensification of the low pressure trough over the northeast Pacific and ridging over the west coast which is indicative of warming due to the flow of warm air from the south. An examination of surface weather records from the Prince George airport for the fall-winter period showed that the peak gust events were also accompanied by peaks in temperature and precipitation significantly above the climatic normals for the period. For example, the mean daily temperature for the October-March period is -3.6 °C, while the average mean daily temperature during severe storm events is +3.6 °C.

To examine the differences between wind storms of varying intensities, individual composites were constructed for moderate (51-70 km/h), strong (71-90 km/h) and severe (>90 km/h) gust events. Each composite showed an incremental intensification of the pressure gradient over the central and southern portions of British Columbia (**Table 4.22**). The coefficient of determination between mean daily extreme gust speed and the relative strength of the pressure gradient is $R^2 = 0.96$. The amount of rainfall and warming associated with the storm events was also seen to increase with storm intensity (**Table 4.25**). Increments in speed class category are accompanied by decreasing pressure over the Interior, attributable to the eastward propagation of the storm centre. By constructing composites one day prior, and one day after the peak gust event, it was seen that there is a difference in the prevailing storm tracks between the moderate and the strong and severe events. The moderate category storms appear to track westward through the Central-Interior, causing an anticyclonic shift in the flow to a more northwesterly direction. The strong and severe events are thought to be related to storms tracking northeastward.

Since the main goal of this thesis was to characterize the wind field in the MMF under a typical storm scenario, map-pattern classification techniques were used to find a single keyday event which could then be used to initialize a 3-dimensional mesoscale simulation of the storm event. The aim of the map-pattern analysis was to find, for each speed class category, the daily map-pattern which most closely resembled the composite for that category. The criteria established for meeting this objective was to find a keyday map which was correlated at r=0.7 or higher, with at least 50% of the maps in its respective category. Application of this criteria resulted in three keyday maps which were correlated at r=0.7 or higher with 50%, 89% and 73% of the maps in the moderate, strong and severe storm categories respectively. The daily extreme gust speeds recorded at the Prince George airport during the keyday storms were approximately equal to their mean composite value, suggesting that the selected maps represent archetypical patterns for moderate, strong and severe gusts.

7.3.4 Wind Monitoring Network

To provide additional data for validation of the numerical simulations and the speed ratios in the subsequent two studies, three 3-metre tripod-based weather stations were installed in the MMF to supplement the existing stations within the study domain (see Dojo, Seebach and Flute in **Fig. 5.35b**). The stations were installed in the spring of 1996, and remained deployed until the fall of 1997. As a minimum, each station measured wind speed and direction, temperature and rainfall. Daily and hourly averages, and 24-hour and 1-hour extremes were recorded using a 1-minute sampling interval (see **Appendix C** for a more complete description of the monitoring network).

A total of eight southerly high wind events occurred at the Prince George Airport during the MMF monitoring campaign. However, the prevailing wind direction during the windy season (October - March) was northeasterly at all three locations (**Fig. 5.41**). This is due in part to the height of the measurements, and the strong topographic steering which occurs at each location. However, the prevailing northeasterlies may also be the result of gap-like winds from an anticyclone to the east of the Rockies, which would suggest that the Prince George Airport may not totally reflect the synoptic situation in the MMF, particularly along the western boundary.

7.3.5 Numerical Simulation

Atmospheric soundings taken at Prince George during the three keyday storms were used to initialize a series of 12-hour numerical weather simulations utilizing the Colorado State University Regional Atmospheric Modeling System (CSU RAMS) (Pielke et al. 1992). The maximum wind simulated at each grid point was recorded, and gridded wind maximums were constructed for each keyday scenario. Each simulation was initiated at 12 UTC (4:00 a.m PST) and "nudged" toward the subsequent afternoon conditions at 00 UTC (4:00 p.m. PST) using a 5 second time step. To resolve the topographic influences of the main terrain features in the MMF, a horizontal grid size of 1 km was selected (**Fig. 5.35**). (Other key model configuration parameters are given in **Table 5.26**.)

The general flow patterns in the three keyday simulations were similar (**Fig. 5.36**). The most striking feature of the simulated windfield is the nearly easterly flow that develops across the central drainage basin as the southerly synoptic flow encounters the northwest-to-southeast oriented mountains along the eastern boundary, and the McGregor Plateau along the northern boundary. Winds increase where air is forced over the McGregor Plateau, and there are strong outflow winds along the deeper McGregor and Fraser river valleys. Winds across the drainage basin were more easterly for the moderate and strong category where winds appear to be steered around the McGregor Plateau. Differences between the moderate category storm and the strong and severe storms became more apparent at the end of the 12-hour simulation. The moderate keyday winds were lighter and veered (clockwise shift) by as much as 90 or 180° over the drainage basin, and strong winds occurred in the southeast corner of the model domain as winds were funnelled into the Rocky Mountain Trench. The strong and severe keyday windfields continued to show a southeasterly flow over the Plateau. As seen in the storm composites, the moderate gusts tend to come from cyclones that track eastward directly through the Interior. This would result in winds veering as the backside of the low sweeps through the area. The strong and severe gusts are related to storms which track northeastward and winds remain southerly as the warms sector sweeps over the MMF.

The wind maximums recorded during the strong keyday simulation were generally stronger than the moderate keyday maximums across the entire domain (**Fig. 5.38**). Winds were even stronger in the severe keyday simulation. One exception was a wind jet which developed during the strong keyday simulation where there is a merging wind flow out of the McGregor, Torpy and Fraser river valleys.

Within the MMF, all winds simulated during the moderate keyday were less than 51 km/h. Moderate (51-70 km/h) and strong (71-90 km/h) category winds which occurred during the strong and severe keyday simulations were generally associated with flow over hills, valley funnelling or outflow conditions. Winds greater than 90 km/h occurred along the mountain ridge line located southeast of the McGregor camp station during the severe keyday simulation. As seen during the model validation runs discussed below, however, the simulated wind maximums are not representative of true gusts. Actual gust speeds would be even higher than those indicated (**Fig. 5.38.**). According to Linacre (1991) mean wind to gust ratios are typically in the range of 1.2 - 2.0.

Direct validation of the keyday simulations was not possible due to the limited availability of observations during these storm events. Three southerly gust events during the 1995-1997 storm season were simulated to assess the representativeness of the keyday storms, and the suitability of RAMS to this application. The three strongest wind events recorded during the validation period were simulated using the identical model configuration as the keyday storm scenarios. Wind data from a temporary climate network deployed in the MMF, supplemented with data from existing stations (**Fig. 5.35b**), were used to assess the validity of these simulations. Simulated winds showed general agreement with 10 metre winds in a clear opening. Prevailing wind directions at the 10-metre towers showed reasonable agreement with the simulated wind field. Simulated directions at the 3-metre stations were plausible when subgrid effects were taken into consideration. Gridded wind maximums were also constructed from model output for the validation simulations and exhibited many similarities to the keyday maximums.

7.3.6 Extrapolation Model

Results from keyday simulations were used to construct a model for extrapolating high winds across the MMF landscape under a synoptic southerly flow condition. The model is intended to provide an estimate of the winds likely to occur above the forest canopy in the MMF based on a single wind measurement at the Prince George Airport. Each grid of maximum wind speeds was normalized by the corresponding maximum simulated for the airport. This provided a gridded set of speed ratios stratified by storm category. To extrapolate high wind estimates under a southerly flow condition, the model multiplies the mean surface wind speed at the airport by the appropriate grid of speed ratios. The wind speed ratios derived from the moderate keyday simulation were found to be equally applicable to extrapolating winds in the other two storm categories. The final model design is therefore reflected in the contour map of the moderate wind speed ratios (**Fig. 6.46**) and wind directions given by the vector average of the strong and severe keyday simulated wind maximums (**Fig. 6.48**).

Validation of this extrapolation technique was limited to verifying the magnitude of the wind estimates, as verification of the wind direction was addressed during the numerical modelling exercise. The validity of the extrapolated wind speeds was assessed by the comparison of observed daily wind maximums under a strong southerly flow, to the extrapolated wind speed determined by application of the moderate keyday speed ratios. Validation storm dates where identified by the occurrence of southerly gusts (180 $\pm 10^{\circ}$) greater than 30 km/h occurring at the Prince George airport during the fall and winter months. No severe-gust storms were recorded at the airport during the entire validation period. The daily maximum hourly wind which occurred at the airport during each of the identified gust-events was entered into the model, and a corresponding wind maximum was extrapolated for each of the wind monitoring locations. The estimated wind maximums correlated well with 10 metre wind speeds in a clear opening (**Fig. 6.43**). With the exception of two stations (Averil and Flute), the correlation between the observed and extrapolated wind maximums were statistically significant at the 95% level. Extrapolated wind speeds at the six 10-metre wind monitoring stations were within an absolute error of 3 m/s over 70% of the time (**Table 6.30**).

7.4 SUMMARY OF KEY FINDINGS

The key findings of this work are summarized below:

- In British Columbia, strong winds are associated with the passage of fronts that originate in the Pacific Ocean or in the Arctic, or from strong winds associated with thunderstorm activity.

- An analysis of historical wind extremes in the central interior of British Columbia revealed that southerly gusts associated with fall and winter cyclones account for most of the extreme wind events in the region.

- Synoptic climatology and map-pattern classification techniques were used to identify representative map patterns for moderate (51-70 km/h), strong (71-90 km/h) and severe (>90 km/h) southerly wind events in the Central-Interior.

- The keyday storms are characterized by a strong southeast-to-northwest oriented pressure gradient over the Interior, situated between a low in the Gulf of Alaska to the northwest, and a continental high pressure area to the southeast.

- The "keyday" scenarios were simulated with a 3-D mesoscale numerical model whose output was used to determine wind speed ratios between grid points in the complex forested terrain and a neighbouring airport location.

- The speed ratios provide an estimate of the winds likely to occur above the forest canopy in the MMF based on a single wind measurement at the Prince George Airport.

7.5 CONCLUSION

This thesis has described a technique developed to estimate severe winds in complex and data-sparse topography. The technique was used to characterize the 2-dimensional near-surface horizontal wind field in the McGregor Model Forest (MMF) of British Columbia, under a typical storm scenario. The complex terrain and sparsity of wind data in BC's forests would typically demand the use of either empirical extrapolative techniques, or a numerical modelling approach to obtain an estimate of the windfield. This project utilized both techniques by modelling synoptic composites of high-wind events (keydays) to derive wind speed ratios between grid points in the complex forest terrain and a neighbouring airport location. The numerical model used to perform the keyday simulations was the Colorado State University Regional Atmospheric Modeling System (CSU RAMS) (Pielke et al. 1992). RAMS is a complex model capable of performing highly sophisticated and detailed weather simulations. A simplified modelling approach was adopted, however, as the intent was to use the model to diagnose the wind field and obtain a dynamically balanced realization of the flow under each storm scenario, rather than provide a prognostic evolution of the windfield. Given the rather simplistic approach taken in initializing and configuring the RAMS model, the results of the keyday simulations were encouraging. The similarities noted between the numerical simulation of the keyday storms and validation events, supports both the representativeness of the keydays, and the ability of RAMS to provide a realistic estimate of the windfield. Wind speeds extrapolated using the speed ratios derived from the keyday simulations correlated well with 10 metre winds in a clear opening, and wind directions agreed favourably with the prevailing storm winds measured at each monitoring station. Taken together with the qualitative validation of the numerical simulations, the results validate the working assumption that extreme winds can be extrapolated under a straightline synoptic flow condition, and the technique should provide an adequate picture of prevailing storm winds in the MMF. While a sophisticated model such as RAMS is not deemed practical for day-to-day application in the forestry sector, the synoptic-parameterization developed here would allow for realistic wind estimates at all grid points in the MMF simply by knowing the synoptic-type and surface wind at the Prince George Airport.

7.6 EXPECTED BENEFITS

Windthrow involves complex interactions between many factors, including stand development which influences tree stability, site conditions that influence tree anchorage, and topography and stand structure that cause highly variable wind conditions (Navratil, 1995). Until very recently, the predictability of windthrow using a modelling approach was considered to be very low (Mayer, 1989), and most wind risk assessments simply ranked the relative hazards as being either low, medium or high based on a functional understanding of windthrow (Miller 1985; Mayer, 1988; Mitchell, 1995a). However, these hazard-based classifications do not specify the overall likelihood of damage. With an improvement in the understanding of the mechanics of windthrow, recent emphasis has been placed on the development of risk management models.

7.6.1 Role of Risk Management Models

Risk is defined as the probability that a certain hazard will occur (Gardiner, 1998). Quine (1998) identifies four stages to the process of risk management: identification of the risk agent, an estimate of the likelihood that a hazard will occur and its consequences, assessment of alternative responses and implication of chosen course. The prediction of when, where and how frequently damage will occur, is key for decision support management systems. With an improvement in the understanding of the mechanics of windthrow, recent emphasis has been placed on the development of risk management models. One of the main goals of the IUFRO 1998 Conference on "Wind and other Abiotic Risks to Forests" was to consider the degree to which this new understanding could be incorporated into forest management through risk assessment and decision support systems (Peltola, 1998). Risk-based models are reported to be under development in Britain (Gardiner, 1998), the Czech Republic (Lekes and Dandul, 1998), Finland (Kellomäki and Peltola, 1998), and Switzerland (Valinger and Fridman, 1998).

While the models differ in their complexity, they share the following fundamental components: a mechanistic module, a wind module and an integrated geographic information system. The mechanistic module predicts the critical wind speed needed to cause wind damage based on measurements of tree and stand parameters. The wind module describes the wind climate and utilizes wind speeds statistics to determine the probability that the threshold wind speed is exceeded. A geographical database of spatial stand data provides input to each module, and allows the information on critical wind speed, relative wind climate and the annual average wind speed statistics to be linked together making it possible to map the probability of wind damage.

Development of the European windthrow risk models has benefited from the availability of long-term records of wind (early 1900's) and atmospheric pressure (1800's), which Alexandersson et al. (1998) showed could be used as a surrogate for estimating return periods of strong winds. Meteorological observations in Europe also have a higher spatial resolution than is available in any other continent (Stull, 1995). As in British Columbia, the wind climate of the coastal European states is also dominated by extra-tropical cyclones (low pressure systems) which form in the Atlantic, and past west to east across or close to Britain. The strongest winds typically occur during the winter months, and similar to what was found for the Central-Interior, wind speeds are often increased by the presence of an anticyclone (high pressure areas) over the mid- Atlantic or south-western Europe.

7.6.2 A Windthrow Risk Assessment Model for the McGregor Model Forest

Detailed wind climatologies for forested areas in North America are rare, and according to McCarter et al. (1998), hazard-based classification will still play an important role in minimizing wind damage. By determining the synoptic climatology of strong winds in the Central-Interior, and providing a potential-risk surface for terrain prone to severe winds, this project represents a first critical step in moving toward a winthrow-risk assessment model for the MMF. For instance, the information on areas prone to severe winds could be entered into a GIS framework, together with information on soil properties, stand conditions, etc. to provide a threat rating for windthrow occurrence. It is anticipated that the results of this analysis will, at some future stage, be incorporated into a decision support system that includes a data management system for forest representation and forest modelling. The technique developed in this thesis for identifying areas prone to high winds would be equally applicable to other forested areas, especially coastal locations such as Vancouver Island, were the wind climatology is dominated by cyclonic activity and strong winds are driven by straight line synoptic flow.

7.6.3 Related Benefits

The technique developed and described in this thesis for identifying areas prone to high winds would also be of benefit to BC Hydro in minimizing and/or forecast planning for electrical power interruptions. Tree blowdown onto transmission lines is responsible for the majority of severe power disruptions in British Columbia (British Columbia Hydro and Power Authority, 1999). The technique developed here could be used to identify transmission line corridors, and stand edges at risk from blowdown. The winter storms identified and described in Chapter 4 also have the potential to cause ice-damage due to the above normal temperatures and precipitation, and subsequent freezing that occurs following the passage of the cold front. Accurate forecasting of these storms would allow for better budgetary and emergency response planning for dealing with such power interruptions. Maps of terrain prone to prevailing high winds could also aid in the assessment of wind power generation capabilities and in locating future wind turbines. Finally, the synoptic-typing methods employed in this analysis also lends itself to assessing the impacts of climate change scenarios. If a given synoptic type is found to cause the majority of severe wind events, and a climate modelling exercise was to predict an increase (decrease) in this synoptic type, then more (less) wind related damage could be expected.

7.7 RECOMMENDATIONS FOR FUTURE WORK

The focus of this thesis on southerly gusts associated with fall and winter cyclones has recently been supported by Sagar and Jull (2001), who installed ten 10-metre wind towers in northeastern British Columbia between 1995-2000. Extreme wind events (1-sec wind speed > 20 m/s) recorded during the 5-year campaign occurred predominantly during the fall and winter months (October through March). The three most prevailing wind directions were SE, SSE, and S, respectively. In analysing the data, Sagar and Jull (2001) found that the spatial and temporal distribution of extreme wind events were very dependent on local topography. Despite the large scale synoptic forcing, most extreme wind events were isolated to only one of the ten sites on a given date, suggesting to the authors that local topography leads to high winds. However, given the extended size of their monitoring network, this could also be due in-part to variability in prevailing storm tracks. This further highlights the difficulties of attempting to extrapolate extreme winds and directions over a wide area, and supports the limited-area numerical modelling approach adopted in this study. This thesis has demonstrated that extrapolating high winds under a straight-line synoptic flow is a reasonable hypothesis. Therefore, further development of the extrapolation technique developed in this thesis warranted, and the recommendations outlined below should be given consideration by future researchers.

- Synoptic Climatology:

The synoptic climatology of high wind events could be improved with the use of hourly re-analysis data rather than daily assimilated fields. This would provide a clearer picture of the development and propagation of the storm systems, and may allow a map of prevailing storm tracks to be constructed. To assess the influence of Arctic outbreaks, and subsequent funnelling of high winds through gaps along the eastern mountain barrier, a synoptic climatology for high northerly winds could also be constructed, and a typical outbreak scenario could be simulated. To identify terrain prone to high convective winds, the BC Ministry of Forests lightening strike database could be used to construct prevailing storm tracks for summertime thunderstorms.

• Numerical Modelling:

A more detailed numerical simulation of the keyday and validation storms should be undertaken. To obtain wind estimates at a higher resolution than 1 km, a series of nested runs should be initialized and nudged using hourly gridded analysis data in addition to vertical sounding data. The model domain should be expanded to include as many of the stations installed by Sagar and Jull (2001) as feasible within the inner domain. However, caution should be exercised not to over extend the inner grid beyond the region of straight line flow (as dictated by the station used to construct the synoptic composites). The simulation period should also be extended to a minimum of 24-hours to allow adequate time for the model to settle down prior to the peak wind event. These measures would provide more accurate wind estimates, and be caple of capturing the temporal evolution of the winds, thereby allowing for a more thorough validation of the numerical modelling results. While it may not be possible to simulate actual gust speeds, Brasseur (2001) has demonstrated that it is possible to estimate gust speeds based on physical considerations using simulated meteorological fields with an accuracy at least equal to that of other empirical techniques. More importantly however, a physical approach allows for the determination of a bounding interval around gust estimates, which provides a range of likely gust magnitudes, and refinement of the estimates will come with improvements in modelling capabilities. Brasseur's approach may allow return periods of extreme winds events to be eventually mapped.

• Wind Monitoring:

Climate monitoring is essential to the continued development and validation of both the extrapolative climate model (MMFCliM) and the extrapolation model for high winds. A deficiency was noted in the monitoring practices of the fire weather stations maintained by the licensee. While hourly readings are recorded at each station, only the noon parameters are routinely downloaded and archived, and operation of these stations is limited to the fire season. To further test the accuracy of the extrapolation model, more wind stations should be installed. In locating future stations, consideration should be given to both the high (<1.5) and low (>1) speed ratio locations delineated in **Fig. 6.46**. A first step would be to retrofit the existing fire weather stations to record and archive hourly data on a year round basis.

• Windthrow Monitoring:

Finally, in relation to the actual occurrence of windthrow, it was not possible to confirm the contribution of straight-line synoptic winds, because records of windthrow necessary for ground truthing a relationship are not being maintained. It is difficult to assess baseline conditions with respect to windthrow because of the noted record keeping deficiencies. For instance, it is difficult to determine what portion of windthrow is natural, and how much is the result of an intensification of forestry related activities. It is imperative that record keeping methods of windthrow events be immediately established and maintained for future evaluations. Accurate records will be necessary to evaluate whether imposed treatments to limit the extent of windthrow related to harvesting and silviculture activities are effective. A windthrow monitoring database similar to that maintain by BC Hydro to document power interruptions should be maintained using the guidelines provided in the windthrow handbook.

References

Achtor, T. H. & Horn, L. H. (1986). Spring season Colorado cyclones. Part I: Use of composites to relate upper and lower tropospheric wind fields. *Journal of Climate and Applied Meteorology*, 25, 732-43.

Alexandersson, H., Schmith, T., Iden, K. & Tuomenvirta, H. (1998). Long-term trend variations of the storm climate over NW Europe. *Global Atmosphere-Ocean System*, 6, 97-120.

Anderson K., R. Carr, R. Benoit, & M. Desgagné. (1996). A test of two mesoscale meteorological models in Jasper National Park. 12th Conference on Numerical Weather Prediction, American Meteorological Society.

B.C. Ministry of Forests. (1991). Ecosystems of British Columbia. Ministry of Forests Special Report Series 6. Victoria, B.C.: Queen's Printer for British Columbia.

B.C. Ministry of Forests. (1995). *Prince George Timber Supply Area: Timber Supply Review Discussion Paper*. Victoria, B.C.: Queen's Printer for British Columbia.

B.C. Ministry of Forests. (1996). Rationale for Allowable Annual Cut (AAC): Tree Farm Licence TFL30. Victoria, B.C.: Queen's Printer for British Columbia.

Barry, R.G. & Perry, A.H. (1973). *Synoptic Climatology, Methods and Applications*. London: Methuen & Company.

Benton R.A. (1998). *MMFCliM: a GIS based monthly climate model for the McGregor Model Forest: Theory and Model Description, Version 0.9*. McGregor Model Forest Association.

Blair, D. (1998). The Kirchhofer technique of synoptic typing revisited. *International Journal of Climatology*, 18, 1625-1635.

Blasing, T.J. & Lofgren, G.R. (1980). Seasonal climatic anomaly types for the North Pacific Sector and western North America. *Monthly Weather Review*, 108, 700-719.

Bossert, J. E. & Poulos G.S. (1993). Application of an Advanced Atmospheric Mesoscale Model to Dispersion in the Rocky Flats. *The Role of Meteorology in Managing the Environment in the 90s: Colorado Proceedings of the 1991 US EPA/A&WMA International Symposium*, 118-129.

Brasseur, O. (2001). Development and Application of a Physical Approach to Estimating Wind Gusts. *Monthly Weather Review*, 129, 5-25.

British Columbia Hydro and Power Authority. (1999). Annual Report 1998. Burnaby, BC.

Byers, H.R. (1974). *General Meteorology*. New York: McGraw-Hill Book Company.

Chen, J.M., Black, T.A., Novak, M.D., & Adams, R.S. (1995). A wind tunnel study of turbulent airflow in forest clearcuts. In M.P. Coutts & J. Grace (Eds.), *Wind and Trees* (pp. 71-87). Cambridge: Cambridge University Press.

Coates, K.D. (1997). Windthrow damage 2 years after partial cutting at the Date Creek silvicultural systems study in the Interior Cedar-Hemlock forests of northwestern British Columbia. *Canadian Journal of Forest Research*, 27, 1695-1701.

Coutts, M.P. & J. Grace (Editors). (1995). *Wind and Trees*. Cambridge: Cambridge University Press.

Environment Canada. (1982a). *Canadian Climate Normals 1951-1980, Volume 2: Temperature* (Catalogue No. En56-60/2). Minister of Supply and Services Canada.

Environment Canada. (1982b). *Canadian Climate Normals 1951-1980, Volume 5: Wind* (Catalogue No. En56-60/5). Minister of Supply and Services Canada.

Environment Canada. (1982c). *Canadian Climate Normals 1951-1980, Volume 6: Frost* (Catalogue No. En56-60/6). Minister of Supply and Services Canada.

Environment Canada. (1982d). *Canadian Climate Normals 1951-1980, Temperature and Precipitation: British Columbia*. Minister of Supply and Services Canada.

Everham, E.M. (1996). A Bibliography of Catastrophic Wind Impacts on Forest Vegetation. Internet: <http://sunceer.upr.clu.edu/DATA/win/win-dbib.htm> Accessed January 26, 1999.

Flesch, T.K. & Wilson, J.D. (1993). *Extreme Value Analysis of Wind Gusts in Alberta* (Catalogue No. FO42-91/107-1993E). Minister of Supply and Services Canada.

Gardiner, B.A. (1998). Quantifying the risk of damage to forests [abstract]. In: *Wind and other Abiotic Risks to Forests, Joensuu, Finland August 1998* (p. 26).

Gardiner, B.A. (1995). The interactions of wind and tree movement in forest canopies. In M.P. Coutts & J. Grace (Eds.), *Wind and Trees* (p. 41-59). Cambridge: Cambridge University Press.

Henderson-Sellers, A. & P.J. Robinson. (1986). *Contemporary Climatology*. New York: John Wiley & Sons Inc.

Holton, J.R. (1979). *An Introduction to Dynamic Meteorology*. New York: Academic Press, Inc.

Hungerford, R.D., R.R. Nemani, S.W. Funning & J.C. Coughlan. (1989). *MTCLIM: A Mountain Microclimate Simulation Model* (Research Paper INT-414). U.S. Department of Agriculture, Forest Service, Intermountain Research Station.

Jackson, P.L. & D.G. Steyn. (1994). Gap winds in a fjord. Part I: Observations and numerical simulation. *Monthly Weather Review* 122, 2645-2665.

Jull, M. (1996). *Wind-resistant silvicultural systems by design: Identification of windthrow and wind risk factors in central and northern interior partial cuts* (Research Project OP96-053). Forest Renewal BC.

Kalnay E., M. Kanamitsu, R. Kistler, W. Collins, D. Deaven, L. Gandin, M. Iredell, S. Saha, G. White, J. Woollen, Y. Zhu, A. Leetmaa, and R. Reynolds (NCEP Environmental Modeling Center); M. Chelliah, W. Ebisuzaki, W.Higgins, J. Janowiak, K. C. Mo, C. Ropelewski, and J. Wang (NCEP Climate Prediction Center); R. Jenne & D. Joseph (NCAR). (1996). The NCEP/NCAR 40-Year Reanalysis Project. *Bulletin of the American Meteorological Society.*

Kellomäki, S. & Peltola, H. (1998). Forest management strategies and silvicutural risks by wind and snow damage. [abstract]. In: *Wind and other Abiotic Risks to Forests, Joensuu, Finland August 1998* (p. 33).

Kimmins, J.P. (1997). *Forest Ecology/A Foundation for Sustainable Management.* 2nd edition. New Jersey: Prentice Hall.

Kirchhofer, W. (1973). Classification of European 500 mb patterns. *Arbeitsbericht der Schweizerischen Meteorologischen Zentralanstalt* 23.

Lekes, V. & I. Dandul. (1998). Wind damage risk classification (WNDARC). [abstract]. In: *Wind and other Abiotic Risks to Forests, Joensuu, Finland August 1998* (p. 30).

Linacre, E. (1992). *Climate Data and Resources: A Reference and Guide.* London: Routledge.

Lund, I.A. (1963). Map-pattern classification by statistical methods. *Journal of Applied Meteorology*, 2, 56-65.

Mass, C.F. & Bond, N.A. (1996). Coastally-trapped reversals along the U.S. West Coast during the warm season: Part II, synoptic evolution. *Monthly Weather Review*, 124, 446-461.

Mayer, H. (1989). Windthrow. *Phil. Trans. R. Soc. Land*, 324, 267-281.

McCarter, J.B., Wilson, J.S., Baker, P.J., Moffett, J.L., & Oliver, C.D. (1998). Landscape Management through Integration of Existing Tools and Emerging Technologies. *Journal of Forestry*, 9, 17-23.

McGregor Model Forest. (1994a). *The McGregor Model Forest Concept.* McGregor Model Forest, Prince George, British Columbia.

McGregor Model Forest. (1994b). *The McGregor Model Forest Association's Five Year Action Plan.* McGregor Model Forest, Prince George, British Columbia.

McGregor Model Forest. (1995). *Compendium of Projects.* McGregor Model Forest, Prince George, British Columbia.

Miller, K.F. (1985). Windthrow hazard classification. Forestry Commission Leaflet 85.

Mitchell, S.J. (1995a). A synopsis of windthrow in British Columbia: occurrence, implications, assessment and management. In M.P. Coutts & J. Grace (Eds.), *Wind and Trees* (p. 448-459). Cambridge: Cambridge University Press.

Mitchell, S.J. (1995b). The windthrow triangle: A relative windthrow hazard assessment procedure for forest manages. *The Forestry Chronicle*, 71, 446-50.

Moore, M.K. (1977). *Factors Contributing to Blowdown in Streamside Leave Strips on Vancouver Island* (Land Management Report 3). Ministry of Forests, Province of British Columbia.

National Climatic Data Center. (1995). *Radiosonde Data of North America: 1946-1994* [CD-Rom]. Version 1.0, Forecast Systems Laboratory, Boulder Colorado.

National Building Code of Canada. (1980). *Canadian Structural Design Manual, Supplement to the National Building Code of Canada.* Ottawa: Associate Committee on National Building Code and National Research Council of Canada.

Navratil, S. (1995). *Minimizing Wind Damage in Alternative Siliviculture Systems in Boreal Mixedwoods* Canada-Alberta Partnership Agreement in Forestry Report. For. Can., Northwest Reg., North. For. Cent., Edmonton, Alberta, and Alberta For. Lands Wildl., For. Ser., Edmonton, Alberta.

Overland, J.E. & Hiester, T.R. (1980). Development of a synoptic climatology for the northeast Gulf of Alaska. *Journal of Applied Meteorology*, 19, 1-14.

Peltola, H. (1998). Preface. In: *Wind and other Abiotic Risks to Forests, Joensuu, Finland August 1998.*

Pielke, R.A. (1984). *Mesoscale Meteorological Modeling*. New York: Academic Press Inc.

Pielke, R.A., Cotton, W.R., Waldo, R., Tremback, C.J., Lyons, W.A., Grasso, L.D., Nicholls, M.E., Moran, M.D., Wesley, D.A., Lee, T.J. & Copeland, J.H. (1992). A comprehensive meteorological modelling system - RAMS. *Meteor. Atmos. Phys.*, 49, 69-91.

Quine, C.P. (1995). Assessing the risk of wind damage to forests: Practice and pitfalls. In M.P. Coutts & J. Grace (Eds.), *Wind and Trees* (p. 379-403). Cambridge: Cambridge University Press.

Quine, C. P. (1998). Management of forests to reduce the risk of abiotic damage - How can it be done and is it worthwhile? [abstract]. In: *Wind and other Abiotic Risks to Forests, Joensuu, Finland August 1998* (p. 29).

Ryan, B.C. (1977). A mathematical model for diagnosis and prediction of surface winds in mountainous terrain. *Journal of Applied Meteorology*, 16, 571-584.

Sagar, R. M. & Jull, M.R. 2001. Wind climatology of high wind events in northeastern British Columbia 1995-200. In: *Conference Proceedings: Windthrow Assessment and Management in British Columbia - Windthrow Researchers Workshop, Richmond, British Columbia Jan. 31- Feb. 01, 2001.*

Simiu, E. & Scanlan, R.H. (1978). *Wind Effects on Structures: An Introduction to Wind Engineering* New York: John Wiley & Sons.

Singh, K.P. (1985). Floods. In: David D. Houghton (Editor). *Handbook of Applied Meteorology*. (p 520-536). Toronto: John Wiley & Sons.

Snook, J.S., Meyers, M.P., Poulos, G.P. & Wesley, D.A. (1998). A local-area model comparison of the October 1997 Rocky Mountain blizzard and severe wind event. In: *Conference Procedings: 8th Conference on Mountain Meterology, American Meteorological Society, Flagstaff, Arizona* (p. 31-36).

Stathers, R.J., Rollerson, T.P. & Mitchell, S.J. (1994). *Windthrow Handbook for British Columbia Forests* (Working Paper 940) Victoria, B.C.: British Columbia Ministry of Forests.

Stull, R.B. (1995). *Meterology Today for Scientist and Enginners*. San Fransisco: West Publishing Company.

Valinger, E. and J. Fridman. (1998). Models for snow and wind damage assessments in swedish pine, spruce and birch forests [abstract]. In: *Wind and other Abiotic Risks to Forests, Joensuu, Finland August 1998* (p.27).

Walko, R.L., Remback, C.J., & Hertenstein, R.F.A. (1995). *RAMS - The Regional Atmospheric Modeling System Version 3b: User's guide*. Fort Collins, Colorado: ASTeR, Inc.

Walmsley, J.L., Taylor, P.A. & J. Salmon. (1989). Simple guidelines for estimating wind speed variations due to small-scale topographic features - an update. *Climate Bulletin*, 23, 3-14.

White, W.B. & A.E. Walker. (1973). Meridional atmospheric teleconnections over the North Pacific from 1950 to 1972. *Monthly Weather Review*, 101, 817.

Willmott, C.J., S.G. Ackleson, R.D. Davis, J.J. Feddma, K.M. Klink, D.R. Legates, J. O'Donnell, & C.M. Rowe. (1985). Statistics for the evaluation and comparison of models. *Journal of Geophysics Research.* , 90, 8995-9005.

Willmott, C.J. (1987). Synoptic weather-map classification: Correlation versus sums-of-squares. *Professional Geographer*, 39, 205-207.

Yarnal, B. (1984). A procedure for the classification of synoptic weather maps from gridded atmospheric pressure surface data. *Computers and Geosciences*, 10, 397-410.

Yarnal, B. (1985). A 500mb synoptic climatology of Pacific north-west coast winters in relation to climatic variability, 1948-49 to 1977-78. *Journal of Climatology*, 5, 237-252.

Yarnal, B. (1993). *Synoptic Climatology in Environmental Analysis: A Primer: Studies in Climatology Series*. London: Belhaven Press.

Appendix A - Figures & Tables

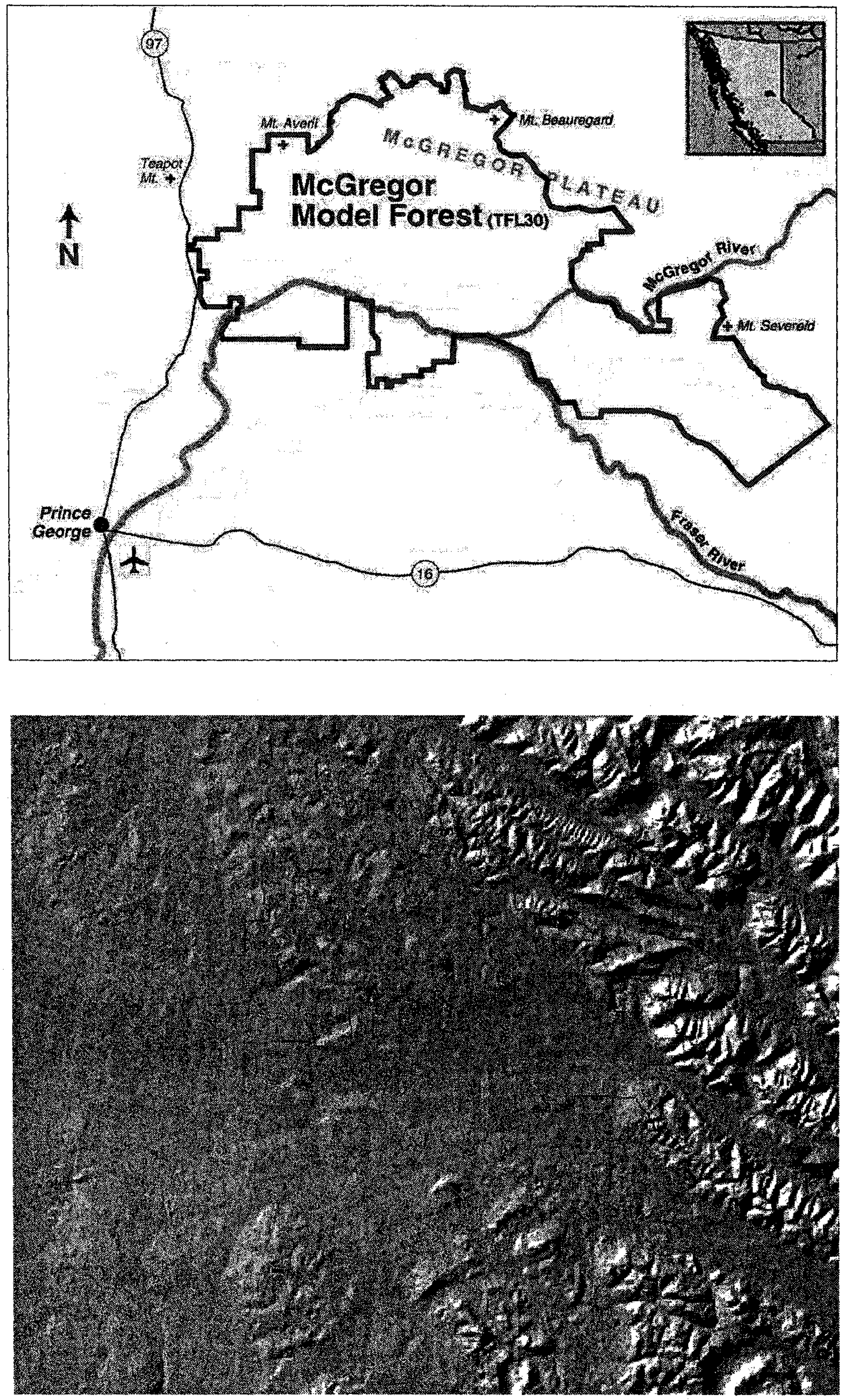

Figure 1.1 Map of Study Area: (a) Location of the McGregor Model Forest in the east central-interior of British Columbia, 30 km northeast of Prince George. (b) Digital elevation model (100 m resolution) of study area shown in (a). (Coverage: 100 x 120 km.)

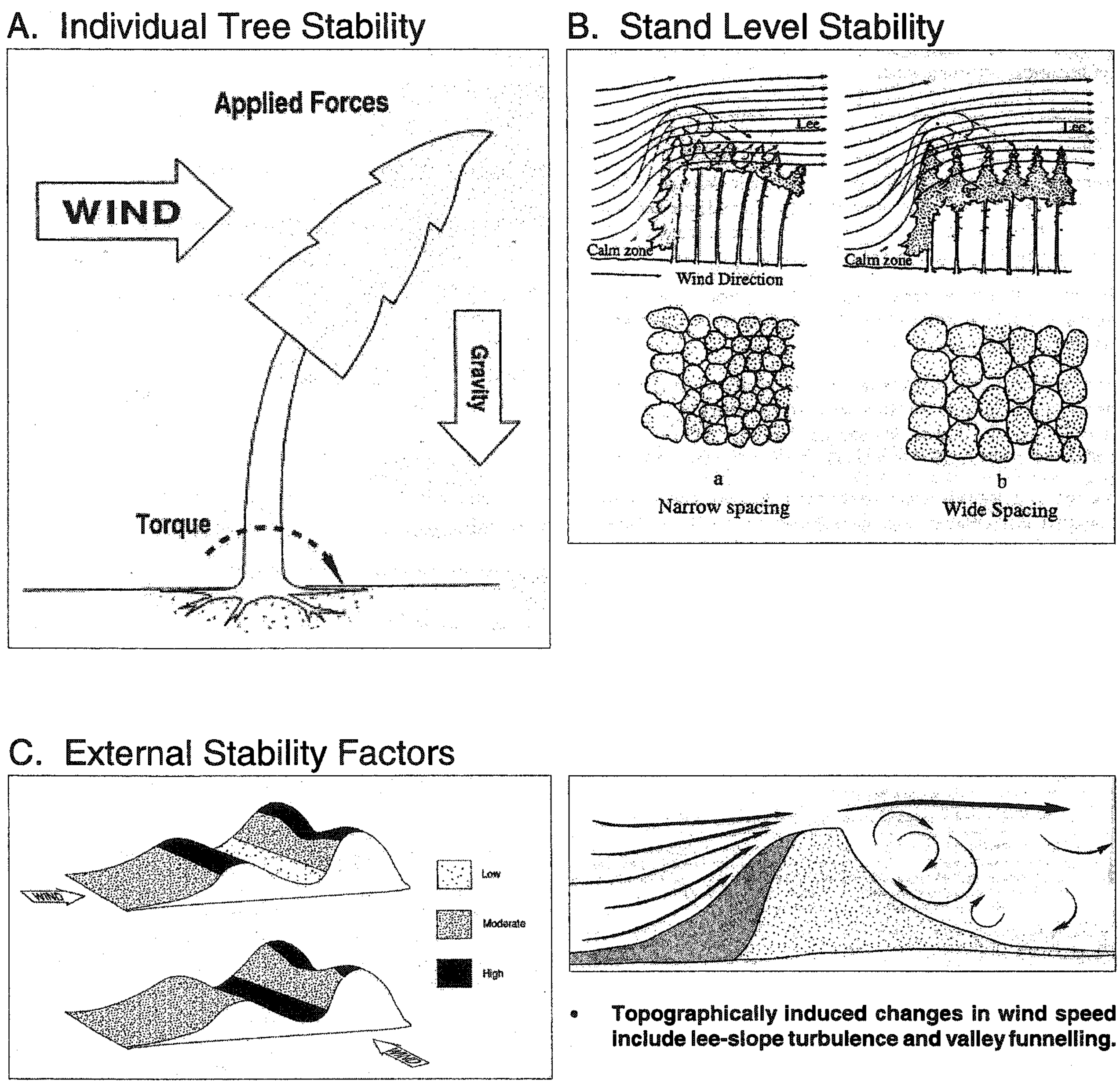

Figure 1.2 Factors Influencing Windthrow: Windthrow involves complex interactions between many factors which operate at multiple scales: (a) individual tree level, (b) stand level and (c) landscape level. At the individual tree level, stability is affected by tree morphology and soil conditions. Stand height, stand density, species composition and siliviculture treatments in conjunction with individual tree stability, determines the overall stability of stand structures. Stand level features and topography in turn affects windthrow by modifying wind exposure, wind direction, speed and turbulence. (Adapted from Stathers et al., 1994; Navratil, 1995.)

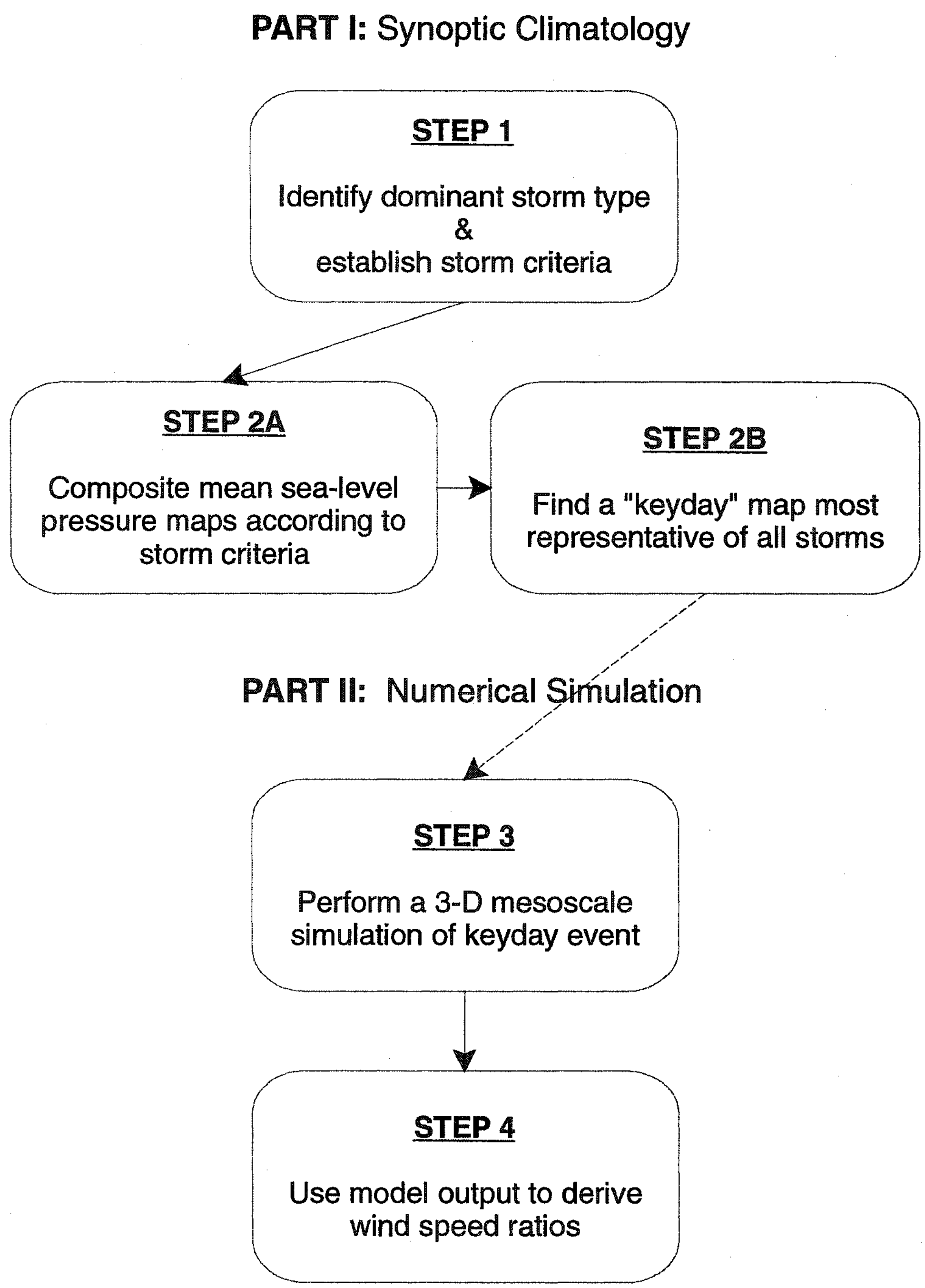

Figure 1.3 Research Method Flow Diagram: Overview of the methodology used to extrapolate high winds from the Prince George Airport, to the McGregor Model Forest.

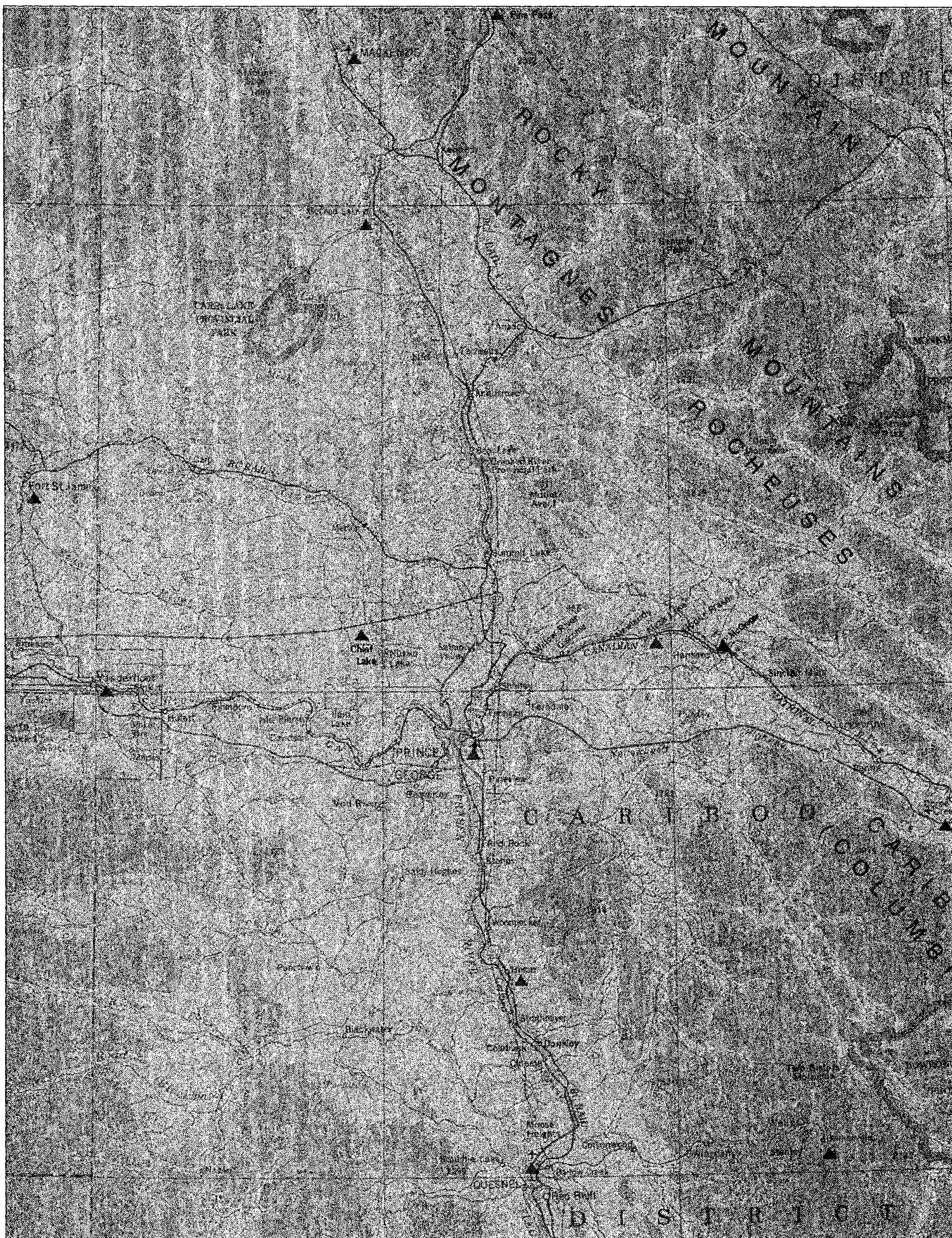

Figure 2.4 Climate Station Location and Local Topography: Map approximating boundaries of the Prince George Forest District, showing location of principal climate stations (▲) and airport wind monitoring stations at Dome Creek, MacKenzie, Quesnel and Prince George. (Scale: 1 cm=14.3 km.)

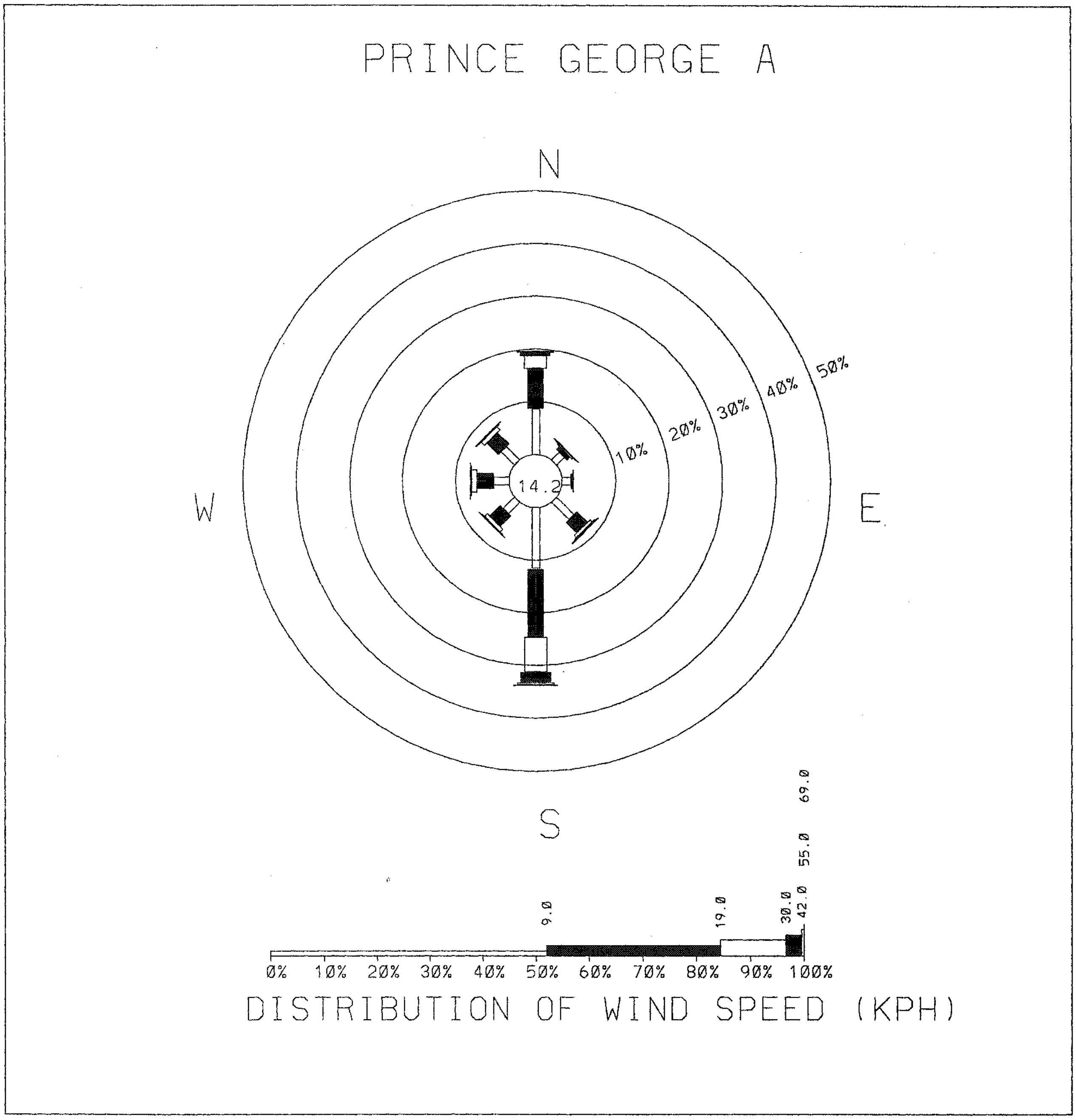

Figure 2.5 Windrose for Prince George Airport: Radial histogram showing directional frequency, and distribution of mean wind speeds during the 30-year climate normal period, 1951-1980. The indicated direction is the direction from which the wind is blowing. The radial length is the percent frequency that the wind blows from the given direction in the following speed classes: 0-8.9, 9-18.9, 19-29.9, 30-42.9, 42-54.9, 55-69 km/h. The bottom bar histogram shows the frequency distribution (in percent) by speed class (in km/h, or kph in figure) for all wind directions.

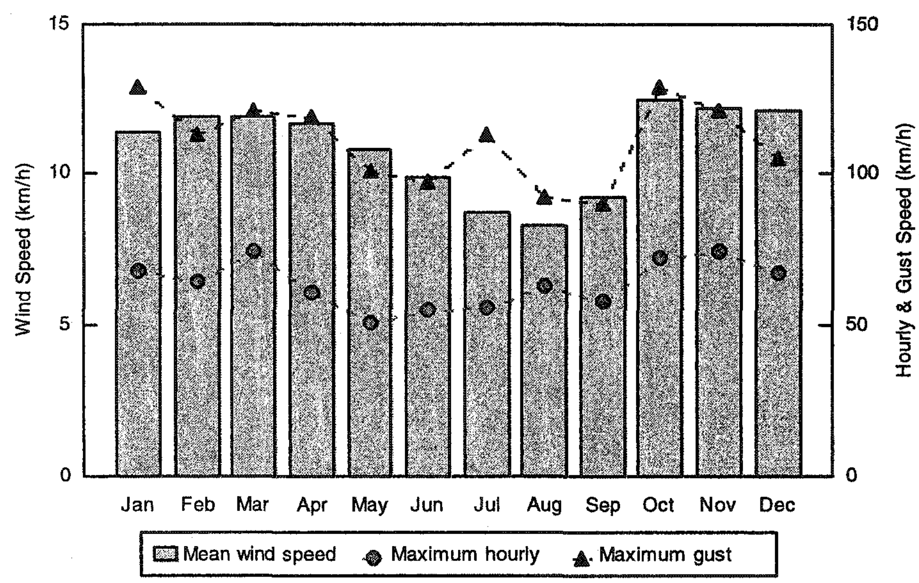

Figure 2.6 Mean Wind Speed and Extremes at Prince George Airport: Mean wind speed (left-axis) compared to the maximum hourly speed and maximum gust speed (right-axis) observed during the period 1955-1980.

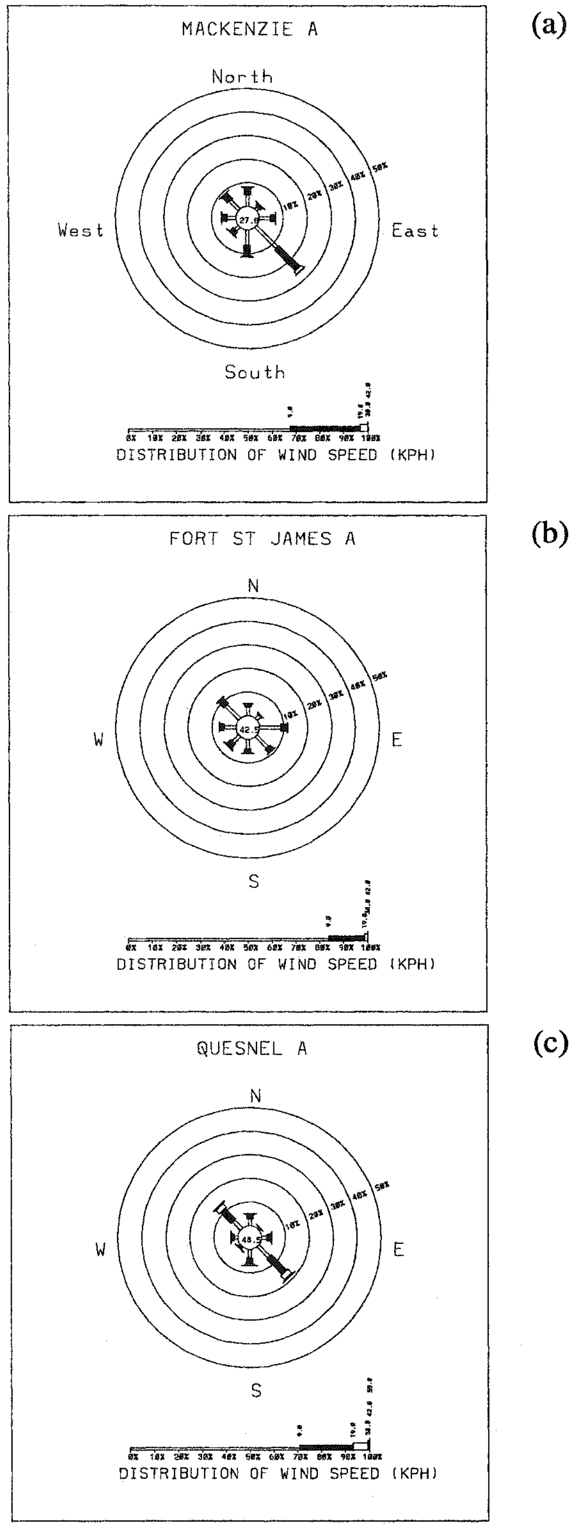

Figure 2.7 Windrose Diagrams for Neighbouring Stations: Radial histograms showing directional frequency, and distribution of mean airport wind speeds at (a) MacKenzie, (b) Fort St. James and (c) Quesnel during the 30-year climate normal period, 1951-1980. (Refer to Fig. 2.5 for interpretation of windrose and definition of speed categories.)

Table 2.1 Wind Directions at Prince George and Neighbouring Stations: Comparison of mean wind speed, by direction and time of year,at four airport locations.†

		N	NE	E	SE	S	SW	W	NW	Mean
MACKENZIE	Jan	8.8	9	5.3	12.6	8.3	9.2	4.6	8.4	8.5
	Apr	7	8.9	4.4	10.3	8.4	9.1	5.8	7.9	7.7
	Jul	6.9	9.1	3.8	8.8	7.8	11	6.8	9	8.1
	Oct	7.5	8.7	3.8	11.5	8.8	9.7	5.2	7.6	9.1
PRINCE GEORGE	Jan	12.1	5.2	3.7	5.6	17.8	9.4	11.5	6.7	11.4
	Apr	13.6	13	7.8	8.9	11.2	11.4	13.3	12.2	11.7
	Jul	10.9	8.6	5.9	6.6	10.2	10.1	11.9	10.9	8.7
	Oct	11.4	8.5	5.2	7.2	17.8	11.1	13.2	9.2	12.5
DOME CREEK	Jan	2.8	4.6	4.1	6.8	2.3	2.6	3.8	5.4	3.3
	Apr	3.1	6.5	3.7	7.3	2.3	3.8	4.7	8.6	4.7
	Jul	2.9	3.7	3.4	4.6	2.4	3.2	5.9	8.3	3.9
	Oct	2.5	3.1	3.6	7.9	2.3	3.2	4	5.9	3.9
QUESNEL	Jan	10.7	5.7	7.1	14	10.4	6.5	7.3	13.9	6
	Apr	10.6	9.2	8.7	13.4	12.7	10.9	11.6	14.3	7.7
	Jul	9.5	7.4	7.6	9.3	9.3	7.2	8.3	11.3	4.8
	Oct	10.2	6	8.7	14.2	11.5	8.3	9.8	12.4	6.7

† Shaded columns indicate prevailing wind direction.

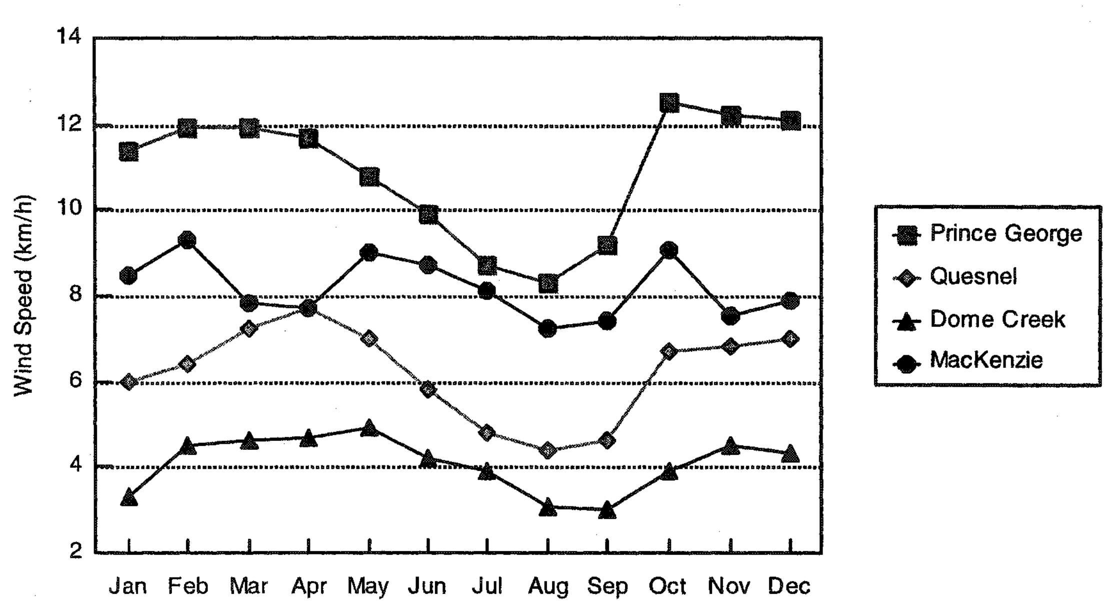

Figure 2.8 Wind Speeds at Prince George and Neighbouring Stations: Comparison of mean monthly wind speed at four airport locations, showing seasonal differences, as well as differences between stations.

(a)

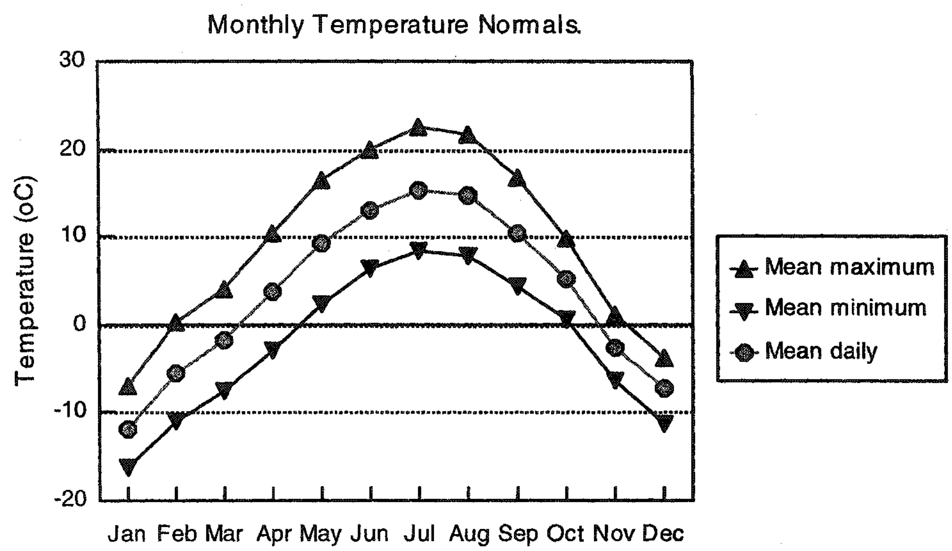

(b)

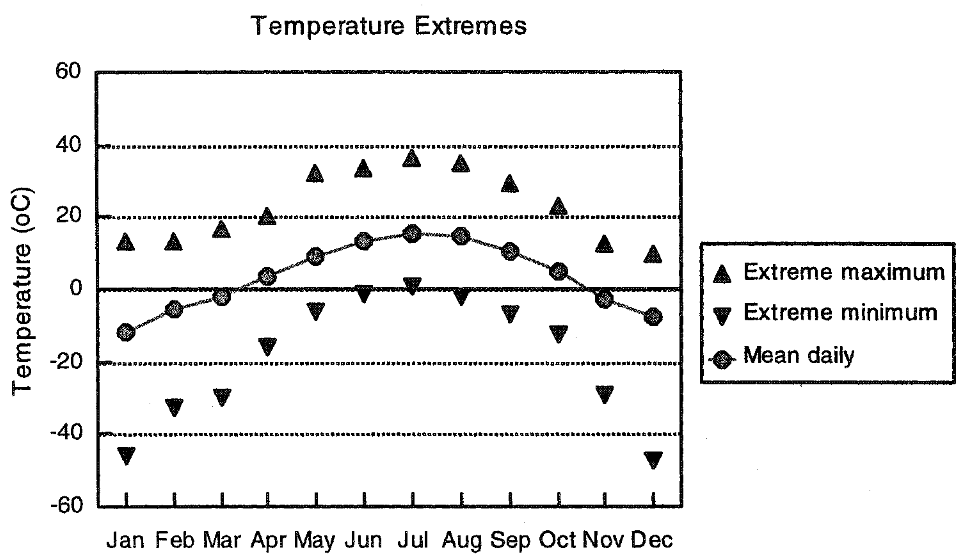

Figure 2.9 Monthly Temperature Normals and Extremes for McGregor Climate Station: (a) daily mean, maximum and minimum temperatures, and (b) daily extreme maximum and minimum temperatures compared to mean daily temperature. Station elevation is 610 m above mean sea-level.

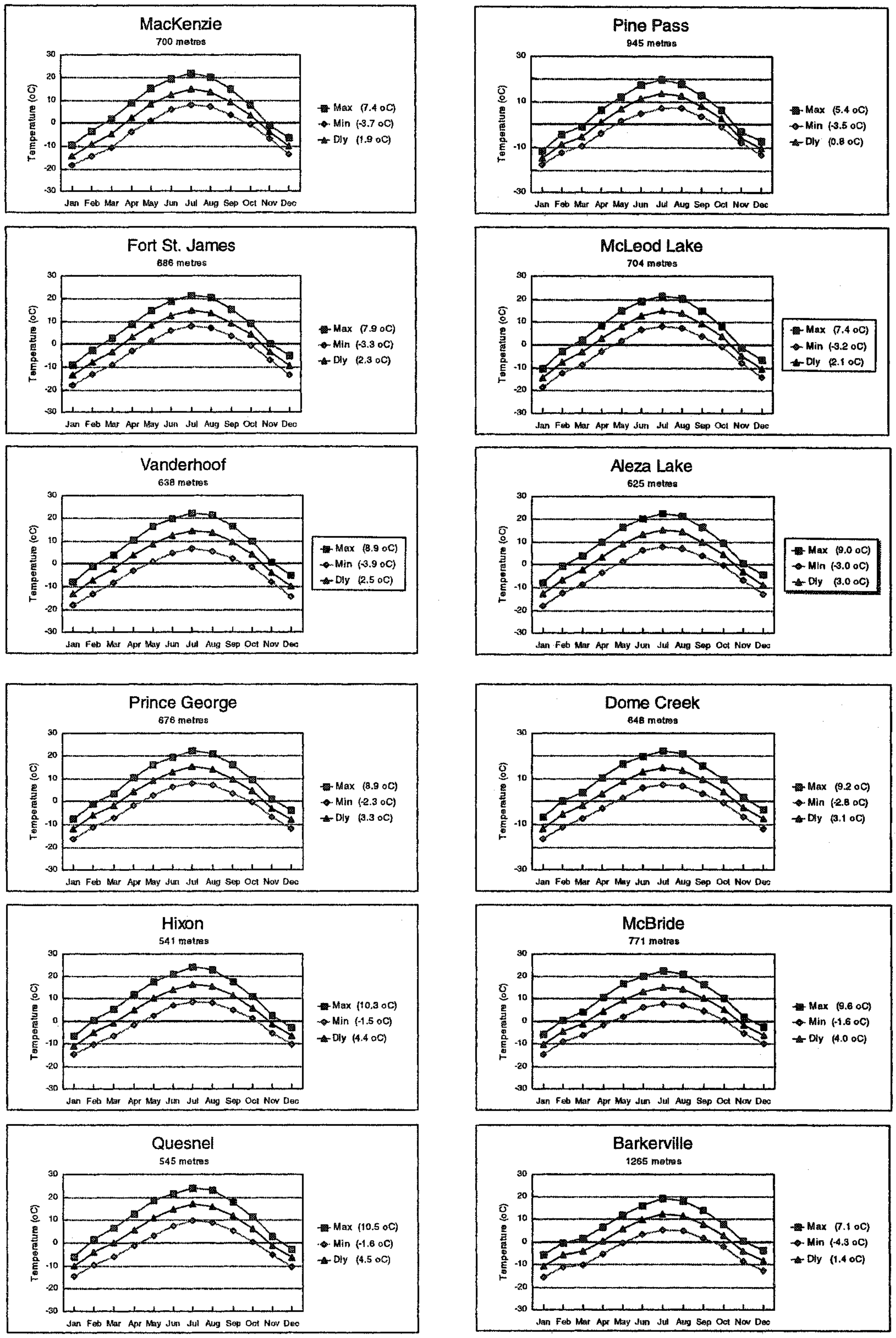

Figure 2.10 Monthly Temperature Normals for Neighbouring Climate Stations: Daily mean (dly), maximum (max) and minimum (min) temperatures. Station elevations are given under station name and annual means shown in parenthesis in the legend.

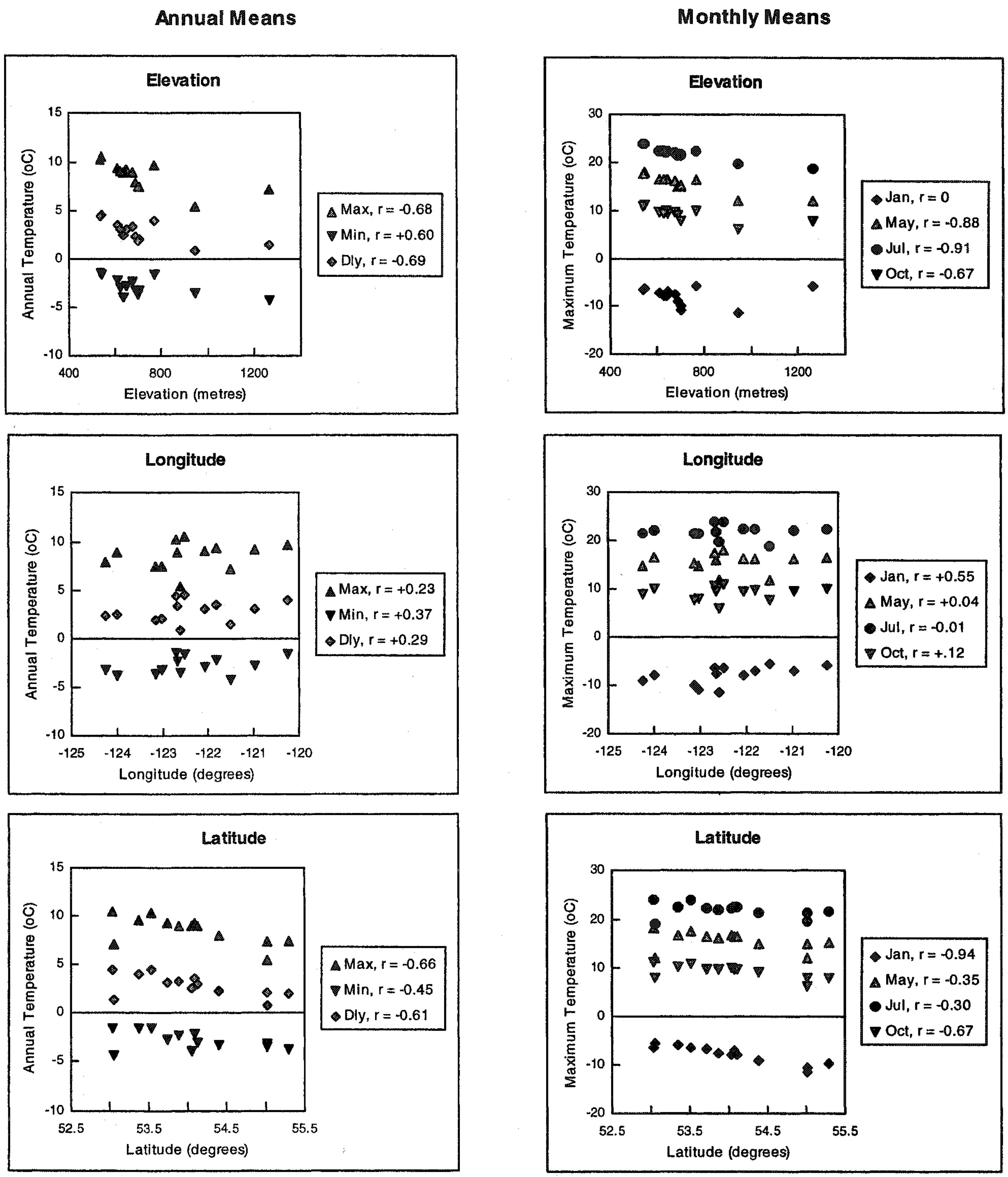

Figure 2.11 Temperature Correlations: Scatter plots between temperature and geographical attributes of climate station location. Plots on the left show the correlation between the annual daily, minimum and maximum temperature with station elevation, longitude and latitude. Plots on the right show the correlation between the monthly maximum temperature for January, May, July and October and station location.

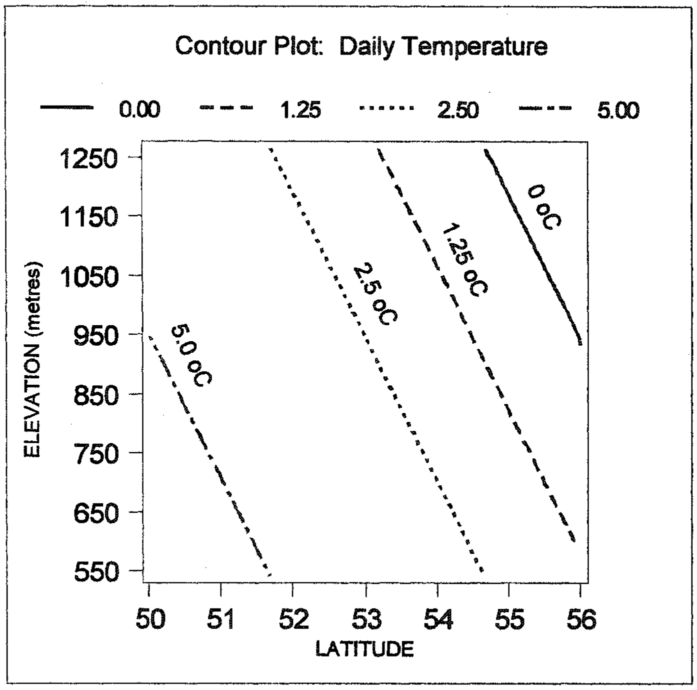

Figure 2.12 Annual Daily Temperature Model: A 2nd-order linear model describing the variation in mean annual daily temperature with station latitude and elevation. The annual mean daily temperature decreases by approximately 1 °C per degree latitude and 0.5 °C per 100 metre rise in elevation.

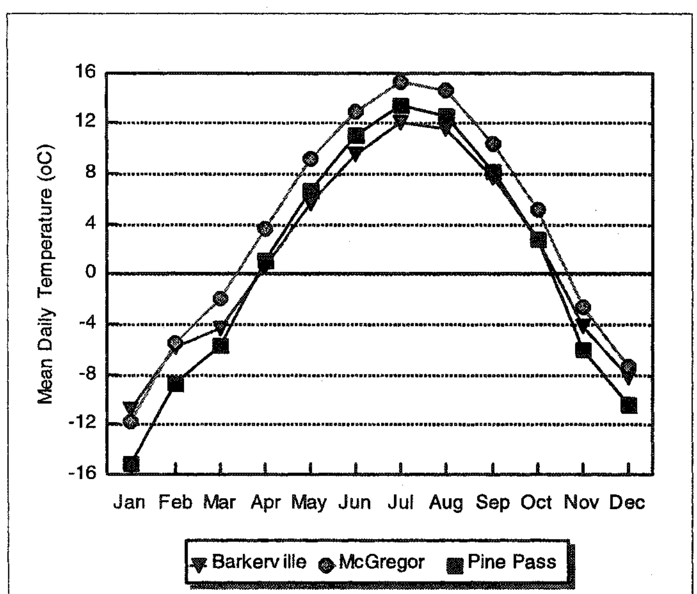

Figure 2.13 Temperature Inversions: Comparison of monthly daily temperatures at McGregor with stations at higher elevations, showing evidence of a climatic temperature inversion at Barkerville in January.

Table 2.2 Annual Temperature Models: Optimal linear regression models for annual daily, maximum, and minimum temperature.

	Optimal Model	R^2 (%)	Significance Test
Maximum	LAT + ELEV	93	F(2,41)=260.5, p<0.00001
Minimum	LAT	25	F(1,42)=14.12, p<0.00001
Daily	LAT + ELEV	71	F(2,41)=49.81, p<0.00001

Table 2.3 Monthly Temperature Models: Optimal linear regression models for monthly daily temperature.

	Optimal Model	R^2 (%)	Significance Test
January	LAT	81	F(1,42)=176.5, p=0.00001
May	LAT + LONG + ELEV	86	F(3,40)=79.83, p=0.00001
July	LAT + LONG + ELEV	91	F(3,40)=138.8, p=0.00001
October	LAT + ELEV	78	F(2,41)=72.2, p=0.00001

Table 2.4 Model Comparison: Regression parameters for annual and monthly linear regression models. (See Table 2.2 and 2.3 for p-values.)

Temperature [°C]	Constant		Latitude [deg]		Elevation [Km]		Longitude [deg]		R^2 [%]
	b0	Err	b1	Err	b2	Err	b3	Err	
Maximum	69.11	3.8	-1.05	4.8	-5.17	7.7	-	-	93
Minimum	24.56	30.1	-0.52	26.9	-	-	-	-	25
Daily	50.24	9.6	-0.84	9.5	-3.44	20.9	-	-	71
January	70.31	8.4	-1.46	7.5	-	-	-	-	81
May	80.07	7.9	-0.61	11.5	-7.2	7.9	-0.28	17.9	86
July	104.3	4.8	-0.83	7.2	-6.22	7.4	-0.27	14.8	91
October	65.93	7.3	-0.97	8.2	-5.66	12.7	-	-	78

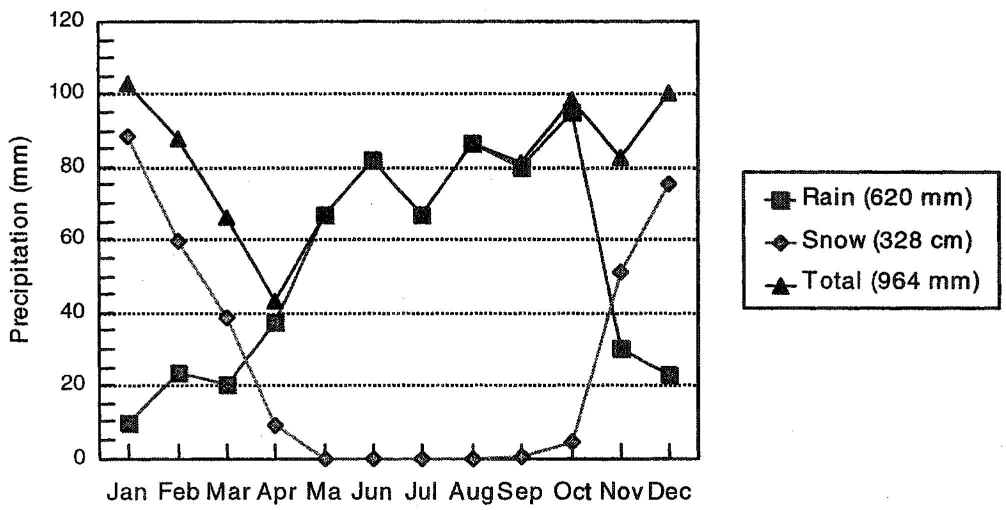

Figure 2.14 Precipitation Normals at McGregor Climate Station: Mean monthly snow (cm), rain (mm) and total precipitation (mm) amounts at the McGregor station during the 30-year period 1951-1980.

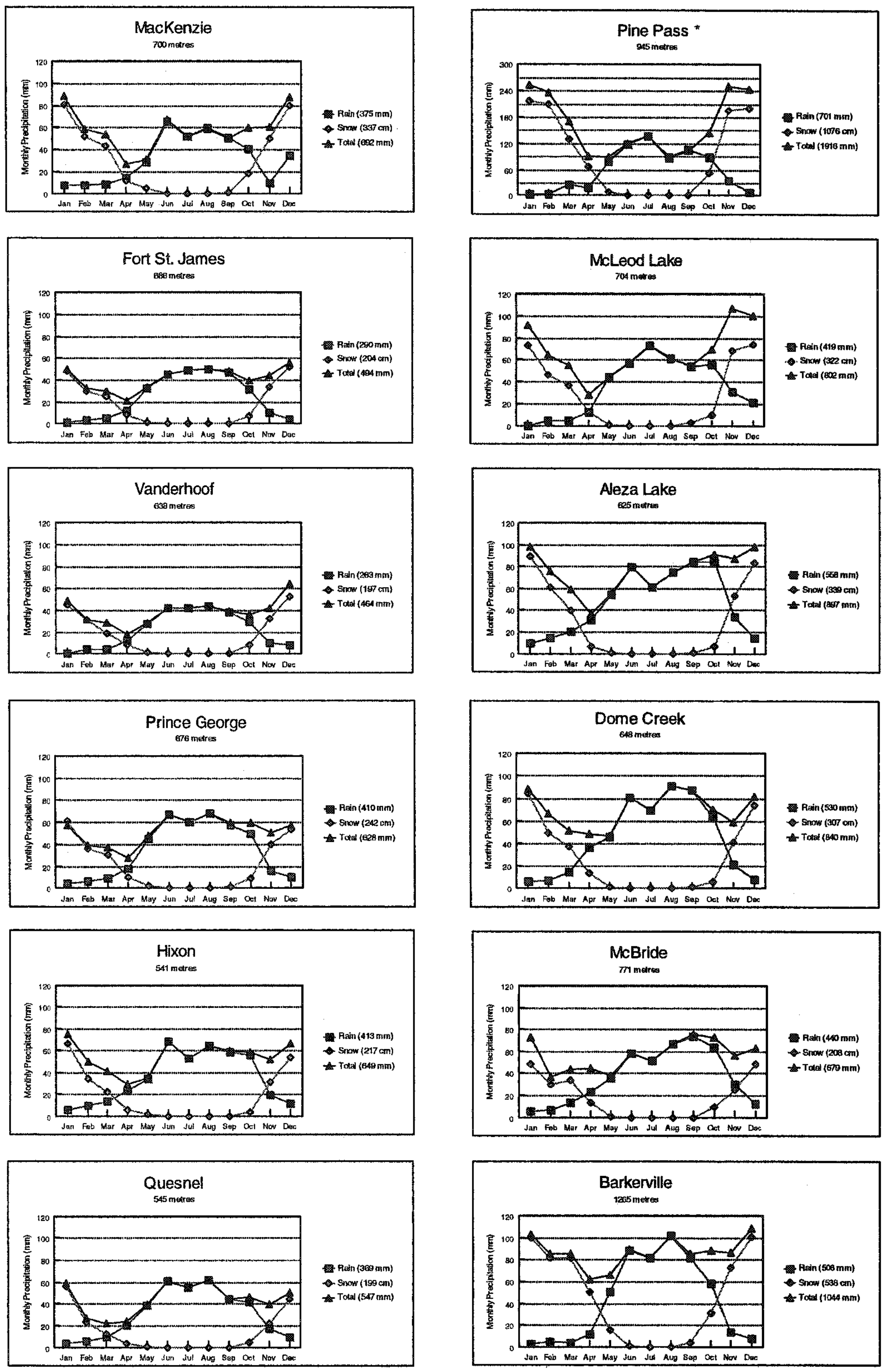

Figure 2.15 Precipitation Normals for Neighbouring Stations: Mean monthly precipitation amounts for surrounding climate stations (see Fig. 2.14). Note change in vertical axis for Pine Pass.

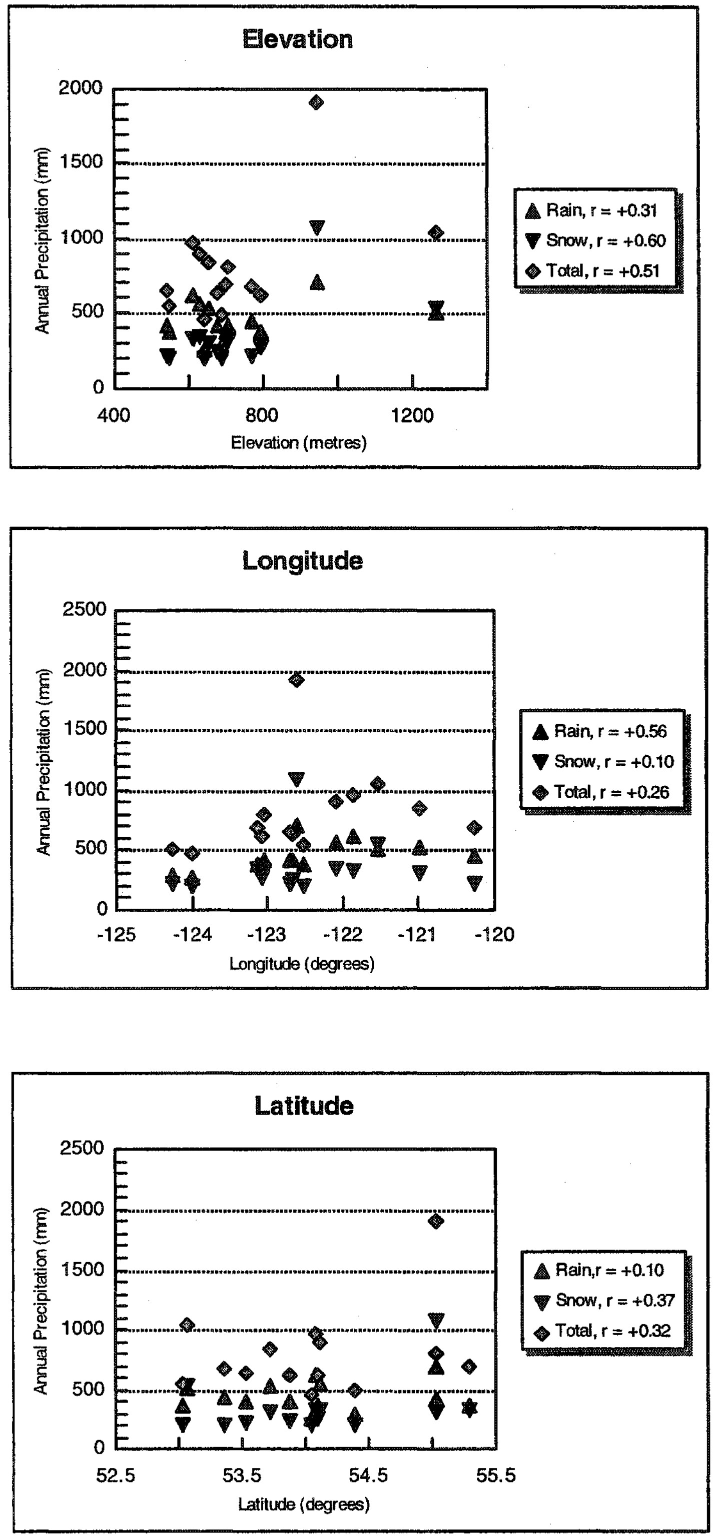

Figure 2.16 Precipitation Correlations: Scatter plots between annual (rain, snow and total) precipitation amounts and station geographical attributes.

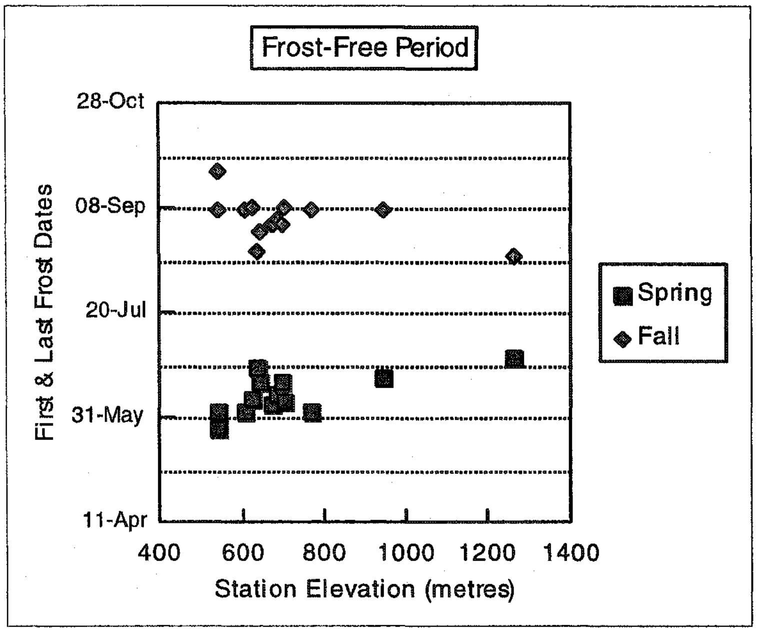

Figure 2.17 Effect of Elevation on Frost Free Period: Scatter plot of spring and fall frost dates and elevation. Frost free period decreases 6.5 days per 100 metre rise in station elevation.

Table 2.5 Frost Normals: Length of frost-free period and average date of first and last frost during for stations in and surrounding the Prince George Forest District.

Station	Frost-free Period (Days)	Last Frost (Spring)	First Frost (Fall)
Aleza Lake	91	June 8	September 8
Barkerville	48	June 28	August 16
Dome Creek	72	June 16	August 28
Fort St. James	83	June 11	September 3
Hixon	122	May 26	September 26
MacKenzie	75	June 16	August 31
MacLeod Lake	92	June 7	September 8
McBride	96	June 2	September 7
McGregor	95	June 3	September 7
Pine Pass	79	June 19	September 7
Prince George	85	June 6	August 31
Quesnel	104	June 3	September 16
Vanderhoof	54	June 24	August 18

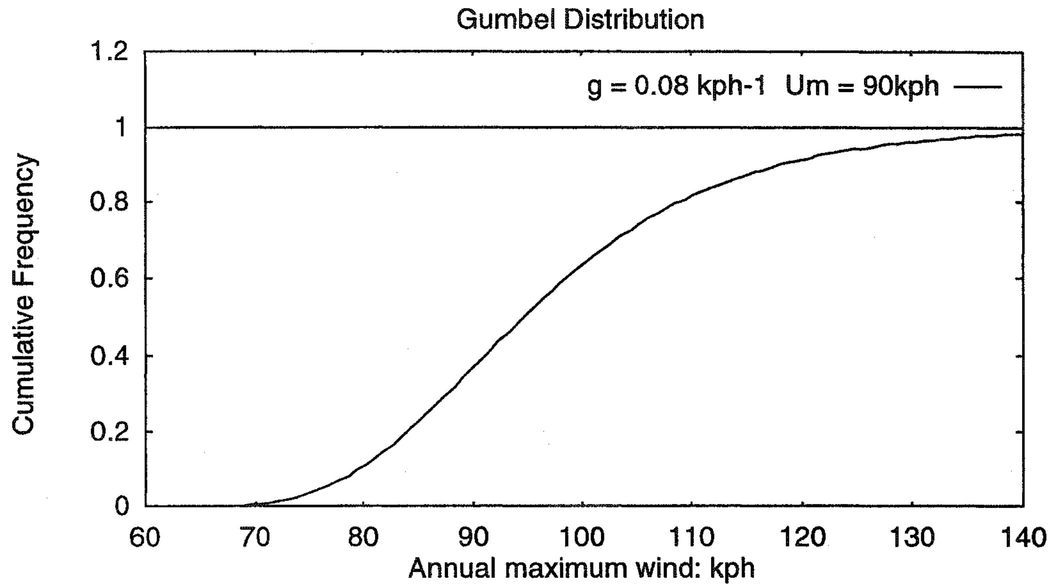

Figure 3.18 Gumbel Distribution, C(U): Extreme-value distribution shown with a Gumbel scaling factor g = 0.08 kph^{-1} and a wind modal value of U_m = 90 kph.

Table 3.6 Airport Wind Stations: List of airport stations included in extreme value analysis, showing period of record and station elevation.

Station	Period of Record	Length of Record (years)	Station Elevation (metres)
Prince George	1956-1994	39	676
Quesnel	1958-1988	31	545
Smithers	1968-1994	27	523
Williams Lake	1961-1994	34	940

Figure 3.19 Location of Airport Stations and Exposure: Map of Central-Interior, showing location of airport wind monitoring stations at Prince George, Quesnel, Smithers and Williams Lake. Airport locations are shown next to city centres by larger light-coloured circles indicated by an '**A**'. Description of station exposure given below. (Scale: 1 cm = 58 km.)

STATION EXPOSURE

Prince George: Located on a flat plateau 90 metres above the Fraser River which runs N-S. Surroundings are heavily wooded with rolling hills rising to an elevation of 1220 metres.

Quesnel: Situated in the Fraser River valley which runs N-S and cuts through rolling and hilly countryside. A hill to the southeast of the airport result in a high frequency of calms.

Smithers: Station is located in the Bulkley Valley of the Skeena Mountains which runs NNW-SSE. The surrounding country is mountainous with peaks reaching 2560 metres.

Williams Lake: Airport is situated on a hill top east of the Fraser River. Winds are reported to be unaffected except for some local effects caused by dense stands of tall trees surrounding the airport.

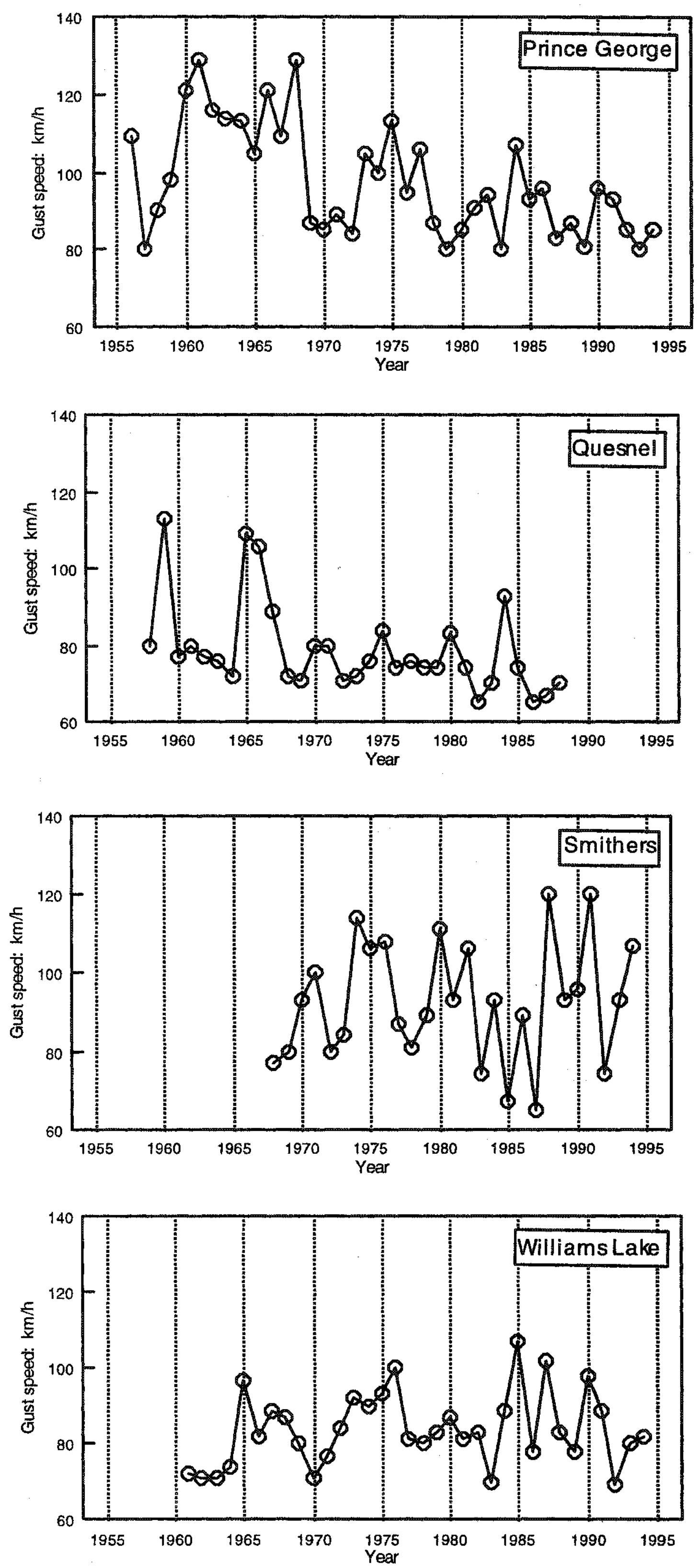

Figure 3.20 Time Series of Annual Wind Extremes: Maximum annual gust speeds observed at Prince George, Quesnel, Smithers and Williams Lake airport wind stations.

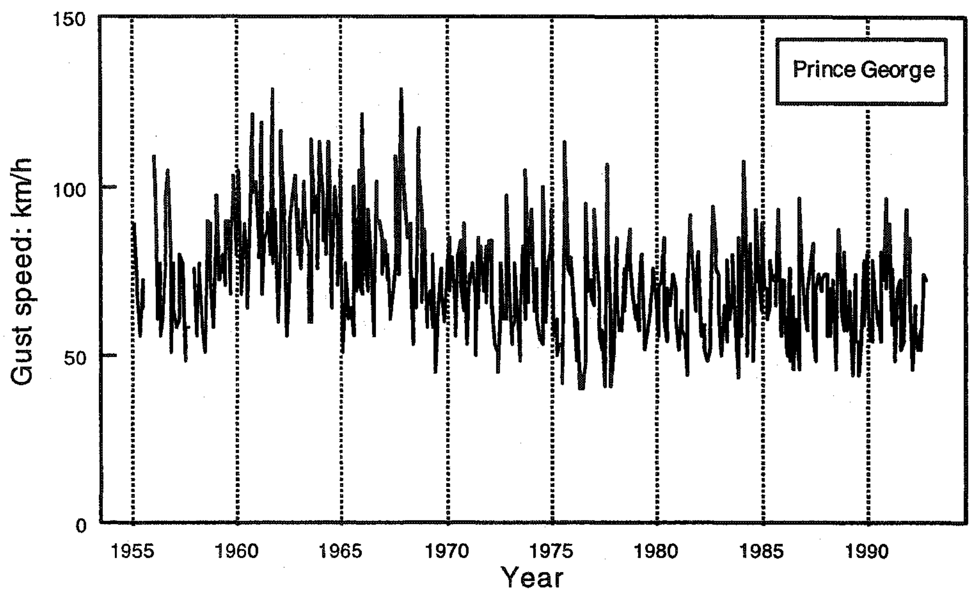

Figure 3.21 Time Series of Monthly Wind Extremes: Maximum monthly gust speed observed at the Prince George Airport during the period of record 1955-1994.

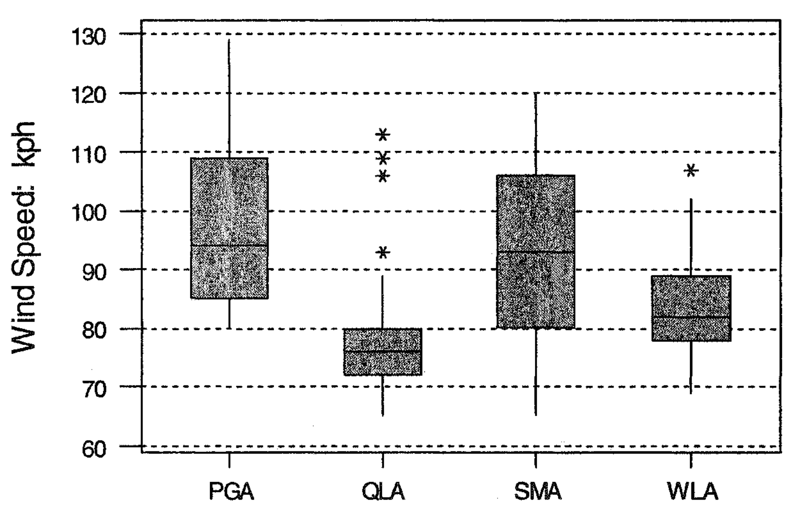

Figure 3.22 Distribution of Annual Wind Extremes: Box plot of maximum annual gust speeds at Prince George (PGA), Quesnel (QLA), Smithers (SMA) and Williams Lake (WLA) airport wind stations. Note outliers (*) at QLA and WLA.

Table 3.7 Extreme Value Analysis Sample Calculation: Ranking of annual wind extremes U and calculation of the empirical cumulative frequency C(U), exceedence E(U) and return periods T(U) for Prince George Airport.

Annual maximum wind U: km/h	Number of values less than or equal to U	100 C(U) percentile	Exceedence 100 E(U)	Return period T(U): years	Gumbel reduced variate
80	4	10.0	90.0	1.11	-0.834
81	5	12.5	87.5	1.14	-0.732
83	6	15.0	85.0	1.18	-0.640
84	7	17.5	82.5	1.21	-0.556
85	11	27.5	72.5	1.38	-0.255
87	14	35.0	65.0	1.54	-0.049
89	15	37.5	62.5	1.60	0.019
90	16	40.0	60.0	1.67	0.087
91	17	42.5	57.5	1.74	0.156
93	19	47.5	52.5	1.90	0.295
94	20	50.0	50.0	2.00	0.367
95	21	52.5	47.5	2.11	0.440
96	23	57.5	42.5	2.35	0.592
98	24	60.0	40.0	2.50	0.672
100	25	62.5	37.5	2.67	0.755
105	27	67.5	32.5	3.08	0.934
106	28	70.0	30.0	3.33	1.031
107	29	72.5	27.5	3.64	1.134
109	31	77.5	22.5	4.44	1.367
113	33	82.5	17.5	5.71	1.648
114	34	85.0	15.0	6.67	1.817
116	35	87.5	12.5	8.00	2.013
121	37	92.5	7.5	13.33	2.552
129	39	97.5	2.5	40.00	3.676

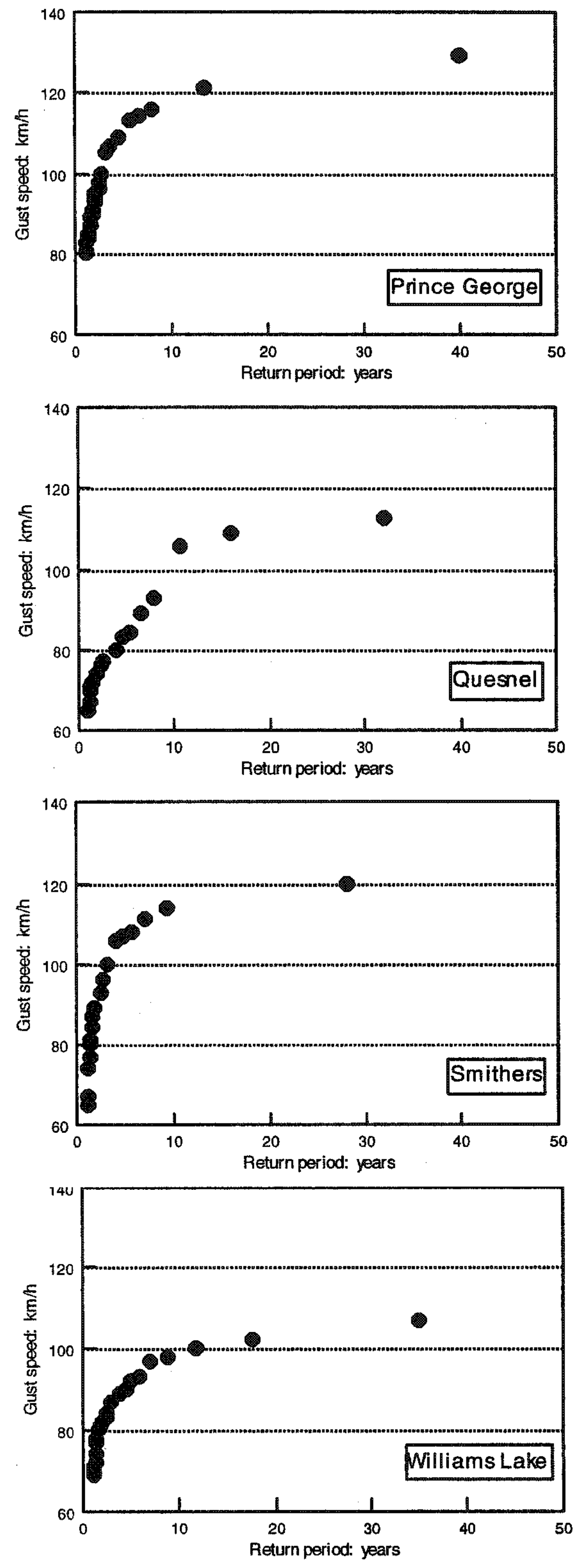

Figure 3.23 Empirical Return Periods: Scatter plots of 'ranked' annual extreme wind speed against the empirical return period at four airport locations.

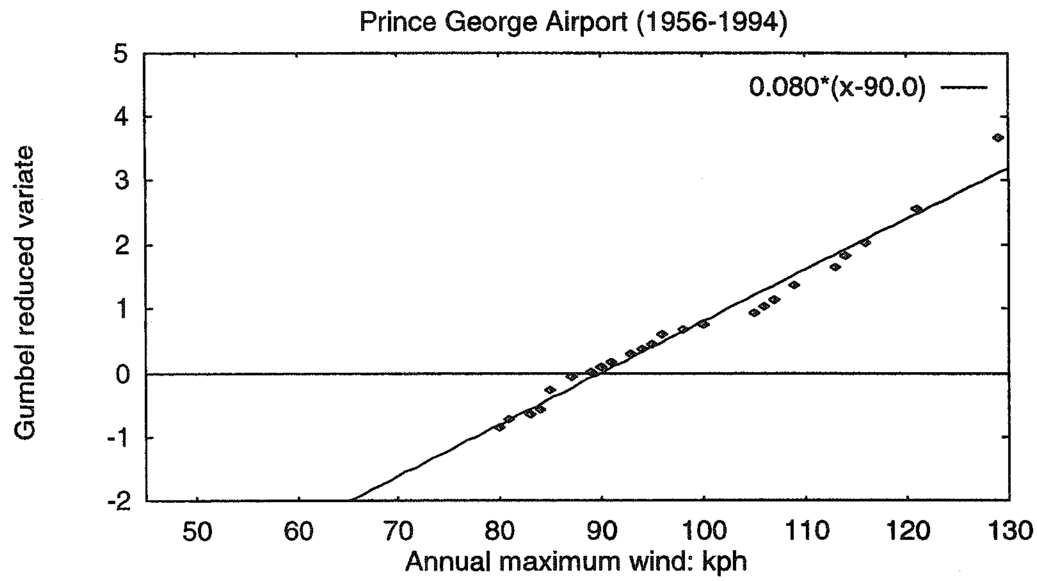

Figure 3.24 (a) 'Best-fit' line to the plot of the Gumbel reduced variate against the annual maximum gust speed at Prince George Airport: Coefficient of determination $R^2 = 0.975$, significantly different than zero $F(1,22) = 862$, $p<0.0001$.

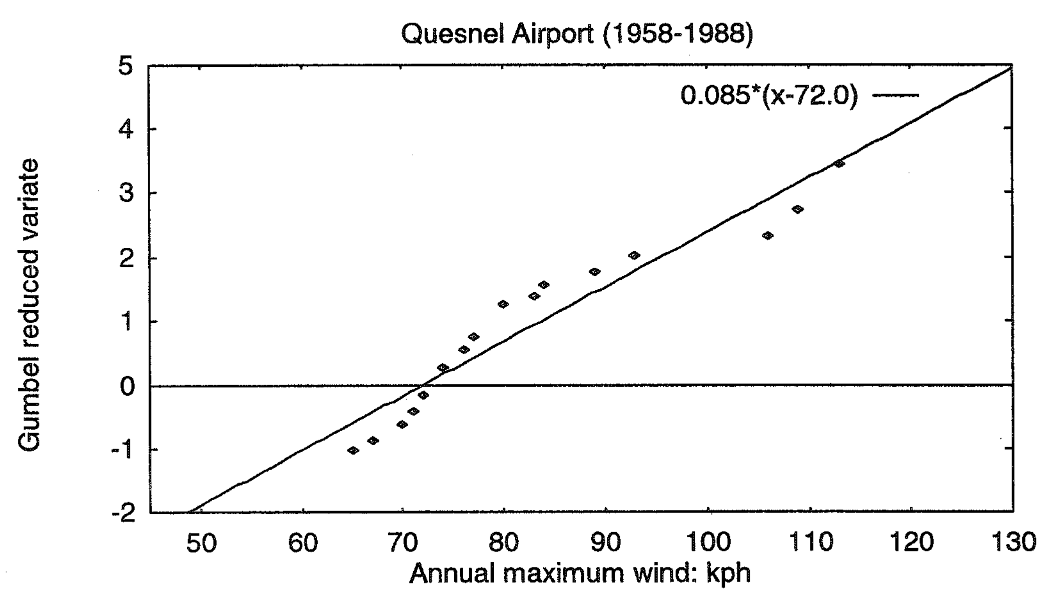

Figure 3.24 (b) 'Best-fit' line to the plot of the Gumbel reduced variate against the annual maximum gust speed at Quesnel Airport: Coefficient of determination $R^2 = 0.913$, significantly different than zero $F(1,14) = 147$, $p<0.0001$.

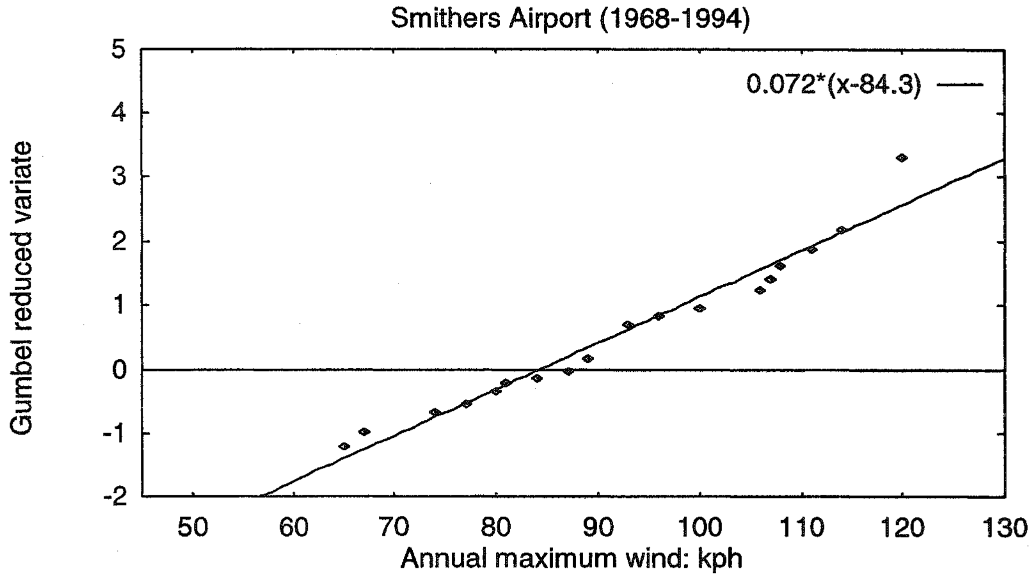

Figure 3.24 (c) 'Best-fit' line to the plot of the Gumbel reduced variate against the annual maximum gust speed at Smithers Airport: Coefficient of determination $R^2 = 0.962$, significantly different than zero $F(1,16) = 403$, $p<0.0001$.

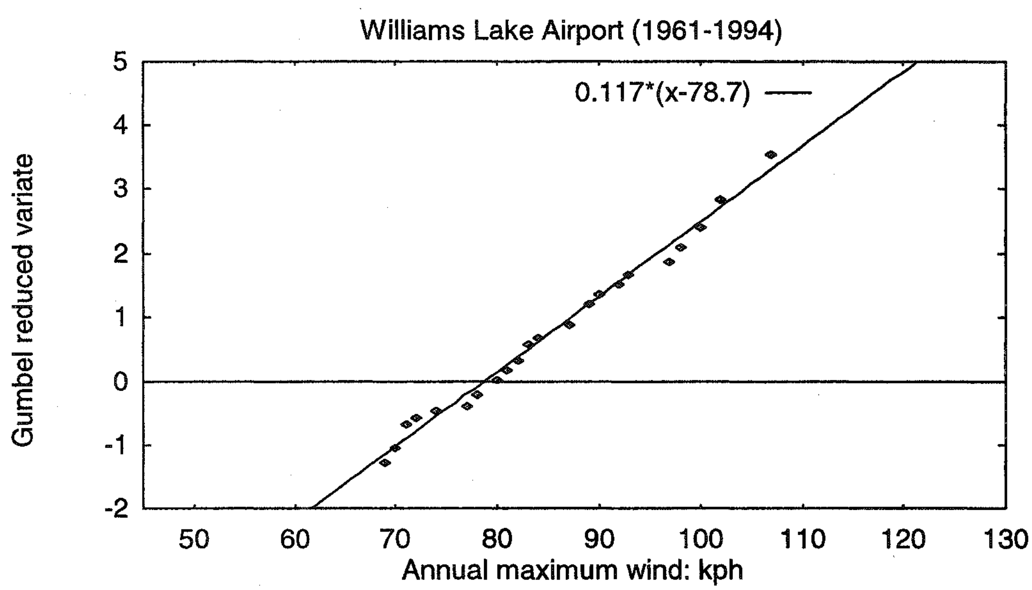

Figure 3.24 (d) 'Best-fit' line to the plot of the Gumbel reduced variate against the annual maximum gust speed at Williams Lake Airport: Coefficient of determination $R^2 = 0.989$, significantly different than zero $F(1,22) = 1782$, $p<0.0001$.

Table 3.8 Summary of Gumbel Least Squares Regression Analysis: Regression parameters are given at the 95% confidence level. Uncertainties in the regression parameters (g and $-gU_m$) were used to determine the upper and lower limits to the 'best' estimate of the modal wind, U_m.

Station:	R^2	Standard Error	Slope g	Y-intercept ($-gU_m$)	Modal Wind U_m lower	upper
Prince George	0.975	0.177	0.080 ±0.006	-7.24 ± 0.565	77.6	105.5
Quesnel	0.913	0.411	0.085 ±0.012	-6.12 ± 1.013	52.6	97.7
Smithers	0.962	0.244	0.072 ±0.008	-6.07 ± 0.711	67.0	106.0
Williams	0.989	0.141	0.117 ±0.006	-9.21 ± 0.496	70.8	87.4

Table 3.9 Extreme wind and Return Period Estimates: 'Best-estimate' of (a) return period for extreme wind gusts of a given magnitude (left column); and (b) extreme wind for a given return period (right column) at selected stations. The true range of the extreme wind estimates are given in Table 3.10 at a 95% confidence level.

Station	Wind speed (kph)	Return period (years)	Return period (years)	Extreme wind (kph)
Prince George	50	1.00	5	109
	70	1.01	10	119
	90	1.58	20	128
	110	5.47	50	139
	130	25.0	100	148
Quesnel	50	1.00	5	90
	70	1.44	10	98
	90	5.14	20	107
	110	25.8	50	118
	130	139	100	126
Smithers	50	1.00	5	105
	70	1.06	10	116
	90	2.06	20	126
	110	6.88	50	138
	130	27.4	100	148
Williams Lake	50	1.00	5	92
	70	1.07	10	98
	90	4.27	20	104
	110	39.4	50	112
	130	405	100	118

Table 3.10 Return Period Confidence Intervals: Upper and lower bounds to the 'best-estimate' within a 95% confidence interval.

Station:	Return Period (T)	Best Estimate U(T)	95% Confidence Interval lower	upper	$\Delta U/2$
Prince George	5	108.7	95.0	125.8	15.4
	10	118.1	103.8	135.9	16.1
	20	127.1	112.1	145.6	16.8
	50	138.8	123.0	158.2	17.6
	100	147.5	131.1	167.7	18.3
Quesnel	5	89.6	68.1	117.4	24.7
	10	98.5	75.8	127.3	25.8
	20	106.9	83.2	136.8	26.8
	50	117.9	92.8	149.0	28.1
	100	126.1	100.0	158.2	29.1
Smithers	5	105.1	85.7	129.4	21.9
	10	115.6	95.1	141.2	23.1
	20	125.6	104.1	152.4	24.2
	50	138.5	115.8	167.0	25.6
	100	148.2	124.5	177.9	26.7
Williams Lake	5	91.5	83.0	100.9	9.0
	10	97.9	89.1	107.7	9.3
	20	104.1	94.9	114.2	9.7
	50	112.0	102.5	122.6	10.1
	100	118.0	108.2	128.8	10.3

Table 3.11 Seasonal Frequencies of Annual Wind Extremes: Frequency (in percent) of annual wind extremes recorded at each airport wind station during winter, spring, summer and fall.

Season:		Prince George	Quesnel	Smithers	Williams Lake
Winter	(Dec-Feb)	26	23	40	35
Spring	(Mar-May)	15	37	30	18
Summer	(Jun-Aug)	10	16	0	9
Fall	(Sep-Nov)	49	24	30	38

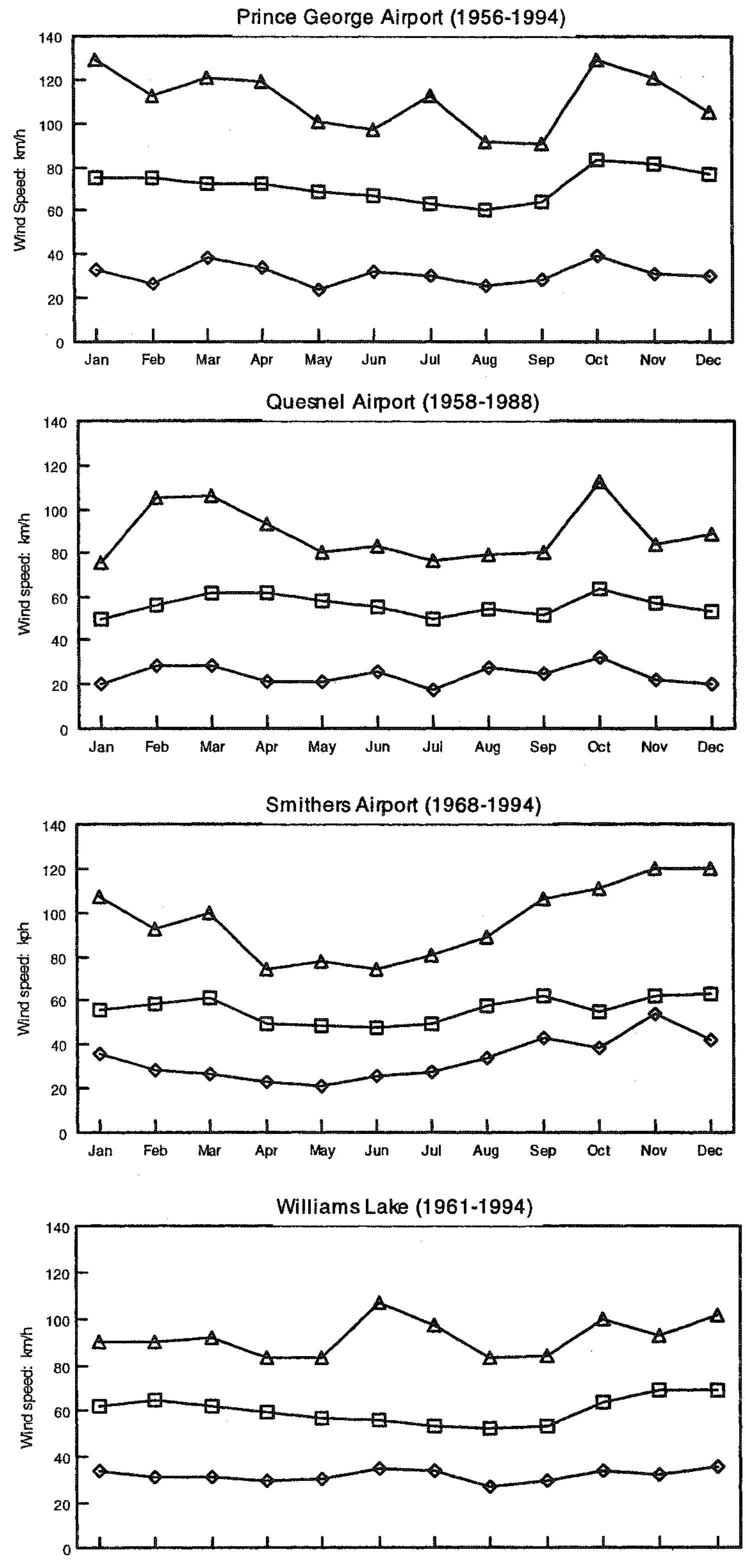

Figure 3.25 Seasonal Characteristics of Monthly Extreme Gust Speeds: (△) maximum gust; (□) mean gust; and (◇) 2 x standard deviation in monthly extreme gust speed.

Table 3.12 Seasonal Return Periods: Estimated return periods for extreme winds of a given magnitude occurring in January, April, July and October at the Prince George Airport.

Wind Speed (kph)	Return Period (Years)				
	January	April	July	October	Annual
50	1.0	1.1	1.2	1.0	1.0
70	1.8	2.1	3.4	1.4	1.0
90	5.5	6.0	13	3.2	1.5
110	20	21	60	8.9	5.5
130	76	74	270	27	25

Table 3.13 Directional Frequencies of Annual Extreme Winds: Frequency (in percent) of annual extreme wind direction recorded at each airport station.

Direction	Prince George	Quesnel	Smithers	Williams Lake
N	0	5	3.7	0
NE	0	0	0	2.9
E	2.6	0	3.7	0
SE	2.6	25	0	64.7
S	69.2	45	11.1	8.8
SW	7.7	0	51.9	2.9
W	17.9	15	29.6	14.7
NW	0	10	0	5.9

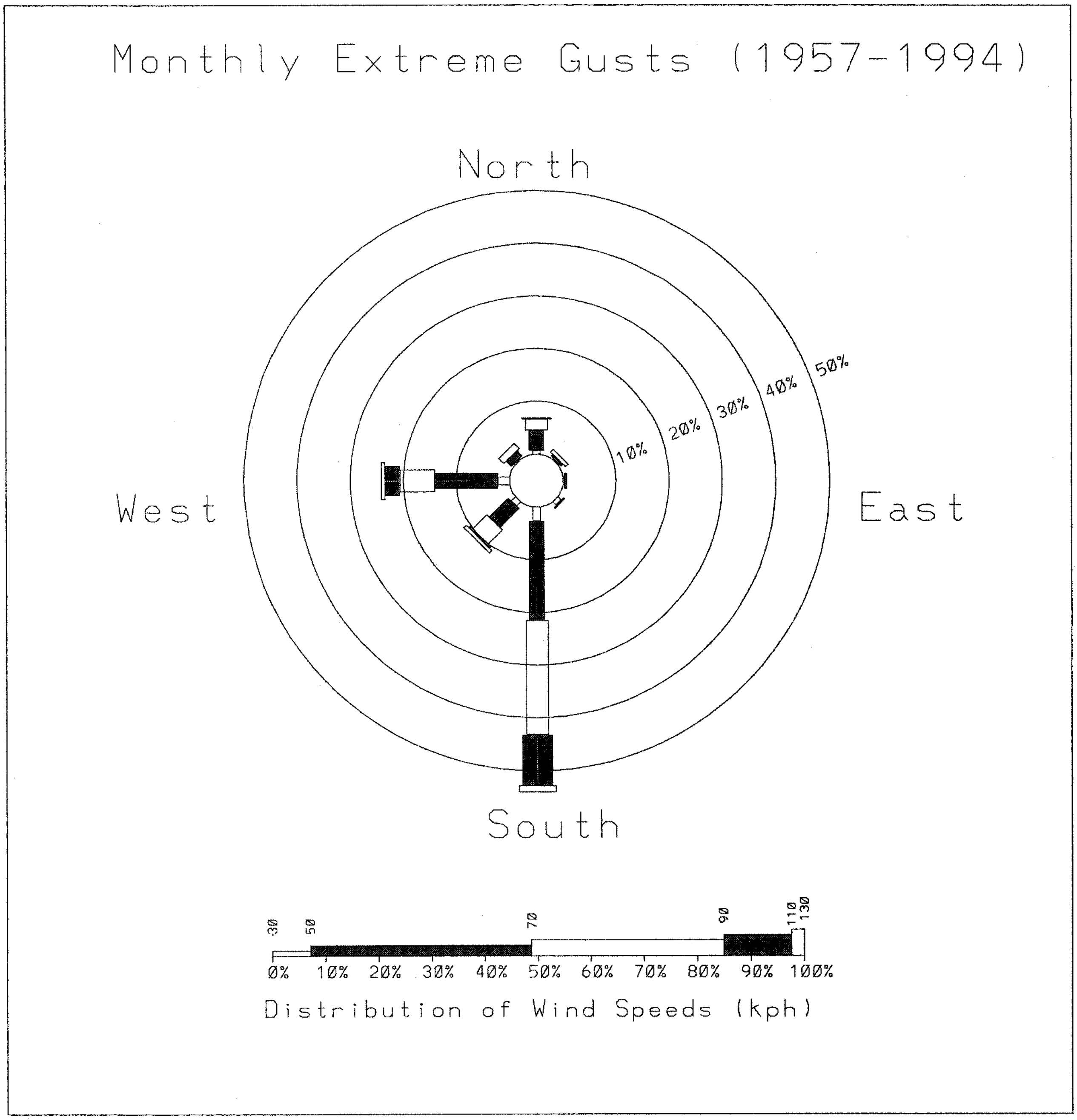

Figure 3.26 Windrose diagram of the monthly extreme gusts at the Prince George Airport (by speed class): Radial histogram showing directional frequency, and distribution of monthly extreme wind gusts during the period, 1957-1994. Gusts are mainly from the south (53%), and both from the south and greater than 70 kph almost 30% of the time.

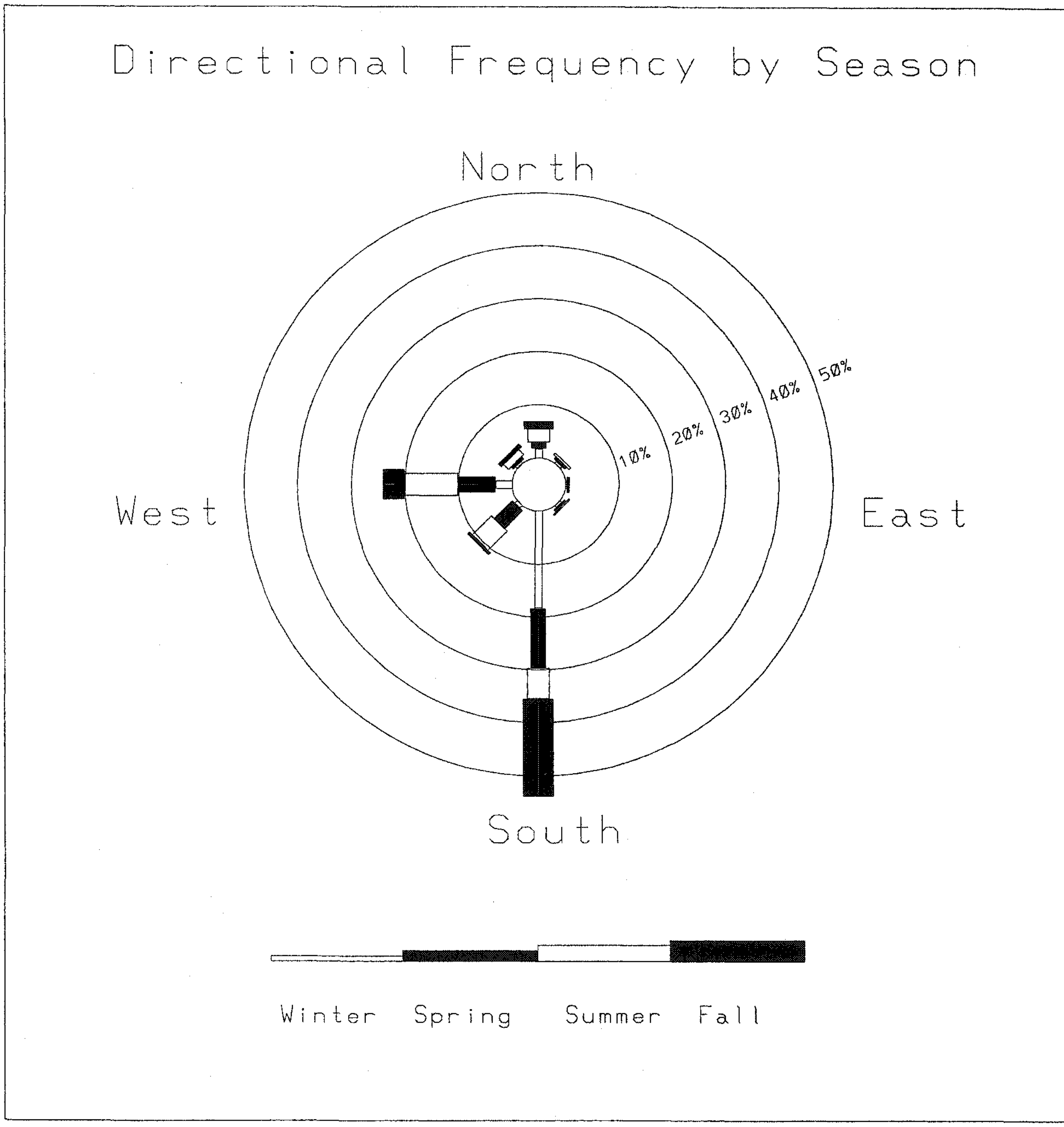

Figure 3.27 Windrose diagram of the monthly extreme gusts at the Prince George Airport (by season): Radial histogram showing directional frequency, and distribution of monthly extreme wind gust directions by time of year during the period 1957-1994. Approximately 40% of all monthly extreme gusts at Prince George are southerly events which occur during the fall or winter.

Table 3.14 Prince George Airport (1956-1994): Directional frequencies of monthly extreme wind gusts by speed class.

Speed Class:						
min	31	51	71	91	111	All
max	50	70	90	110	130	Speeds
Direction:						
E	0.00	0.22	044	0.00	0.00	0.66
NE	0.22	0.44	0.66	0.00	0.00	1.32
N	0.66	3.75	1.99	0.22	0.00	6.62
NW	0.22	1.32	1.32	0.00	0.00	2.87
W	2.21	11.70	6.40	2.65	0.66	23.62
SW	1.10	4.86	3.75	0.22	0.66	10.60
S	2.65	18.54	21.63	9.27	1.10	53.20
SE	0.00	0.88	0.00	0.22	0.00	1.10
All Directions	7.06	41.72	36.20	12.58	2.43	100.00

Table 3.15 Prince George Airport (1956-1994): Directional frequencies of monthly extreme wind gusts by speed season.

Season:	Winter	Spring	Summer	Fall	All Seasons
Direction:					
E	0.00	0.22	0.44	0.00	0.66
NE	0.44	0.44	0.00	0.44	1.32
N	1.77	1.10	2.43	1.32	6.62
NW	0.44	0.44	1.32	0.66	2.87
W	3.09	6.84	9.71	3.97	23.62
SW	0.66	4.64	4.86	0.44	10.60
S	18.32	11.04	5.74	18.10	53.20
SE	0.00	0.44	0.44	0.22	1.10
All Directions	24.72	25.17	24.94	25.17	100.00

Table 3.16 Quesnel Airport (1958-1988): Directional frequencies of monthly extreme wind gusts by speed class.

Speed Class:						
min	31	51	71	91	111	All
max	50	70	90	110	130	Speeds
Direction:						
E	0.56	1.67	0.28	0.00	0.00	2.50
NE	0.00	0.00	0.00	0.00	0.00	0.00
N	4.72	7.50	1.39	0.00	0.00	13.61
NW	8.06	10.54	2.22	0.28	0.28	21.38
W	4.17	3.33	1.94	0.00	0.00	9.44
SW	0.00	1.39	0.00	0.00	0.00	1.39
S	7.78	17.50	5.00	0.83	0.00	31.11
SE	8.06	11.11	1.39	0.00	0.00	20.56
All Directions	33.35	53.04	12.22	1.11	0.28	100.00

Table 3.17 Quesnel Airport (1958-1988): Directional frequencies of monthly extreme wind gusts by season.

Season:	Winter	Spring	Summer	Fall	All Seasons
Direction:					
E	0.56	1.11	0.28	0.56	2.51
NE	0.00	0.00	0.00	0.00	0.00
N	3.06	3.33	4.44	2.78	13.61
NW	6.11	4.44	5.83	5.00	21.38
W	0.56	1.94	5.00	1.94	9.44
SW	0.28	0.28	0.55	0.28	1.39
S	8.06	10.27	5.28	7.50	31.11
SE	6.39	4.44	3.06	6.67	20.56
All Directions	25.02	25.81	24.44	24.73	100.00

Table 3.18 Smithers Airport (1968-1994): Directional frequencies of monthly extreme wind gusts by speed class.

Speed Class:						
min	31	51	71	91	111	All
max	50	70	90	110	130	Speeds
Direction:						
E	1.60	0.96	0.32	0.00	0.00	2.88
NE	0.32	0.64	0.32	0.00	0.32	1.60
N	9.90	4.15	2.56	0.00	0.00	16.61
NW	6.07	2.24	0.96	0.32	0.32	9.91
W	4.79	5.11	3.19	0.00	0.00	13.09
SW	6.39	7.35	2.24	1.60	0.32	17.90
S	12.46	9.58	4.47	1.28	0.32	28.11
SE	4.15	3.83	0.96	0.96	0.00	9.90
All Directions	45.68	33.86	15.02	4.16	1.28	100.00

Table 3.19 Smithers Airport (1968-1994): Directional frequencies of monthly extreme wind gusts by season.

Season:	Winter	Spring	Summer	Fall	All Seasons
Direction:					
E	0.64	0.64	0.95	0.64	2.88
NE	0.32	0.32	0.64	0.32	1.60
N	2.88	7.02	5.43	1.28	16.61
NW	0.64	2.88	4.15	2.24	9.91
W	2.56	1.92	3.83	4.78	13.09
SW	6.08	5.75	3.19	2.88	17.90
S	9.90	4.79	4.47	8.95	28.11
SE	2.56	2.24	1.92	3.18	9.90
All Directions	25.58	25.56	24.59	24.27	100.00

Table 3.20 Williams Lake (1961-1994): Directional frequencies of monthly extreme wind gusts by speed class.

Speed Class:						
min	31	51	71	91	111	All
max	50	70	90	110	130	Speeds
Direction:						
E	0.75	1.00	0.50	0.00	0.00	2.25
NE	0.00	0.00	0.00	0.25	0.00	0.25
N	2.01	4.51	0.25	0.00	0.00	6.77
NW	5.01	7.27	2.26	0.02	0.00	14.56
W	1.50	4.26	1.50	0.75	0.00	8.01
SW	0.50	1.25	1.25	0.00	0.00	3.00
S	3.26	7.27	3.76	0.25	0.00	14.54
SE	5.01	27.07	17.54	1.00	0.00	50.62
All Directions	18.04	52.63	27.06	2.27	0.00	100.00

Table 3.21 Williams Lake (1961-1994): Directional frequencies of monthly extreme wind gusts by season.

Season:	Winter	Spring	Summer	Fall	All Seasons
Direction:					
E	0.25	0.50	1.50	0.00	2.25
NE	0.00	0.00	0.25	0.00	0.25
N	0.50	1.75	3.02	1.50	6.77
NW	1.25	4.54	4.51	4.26	14.56
W	1.25	0.75	5.26	0.75	8.01
SW	0.00	0.75	2.00	0.25	3.00
S	4.26	3.51	3.51	3.26	14.54
SE	17.54	13.03	4.76	15.29	50.62
All Directions	25.05	24.83	24.81	25.31	100.00

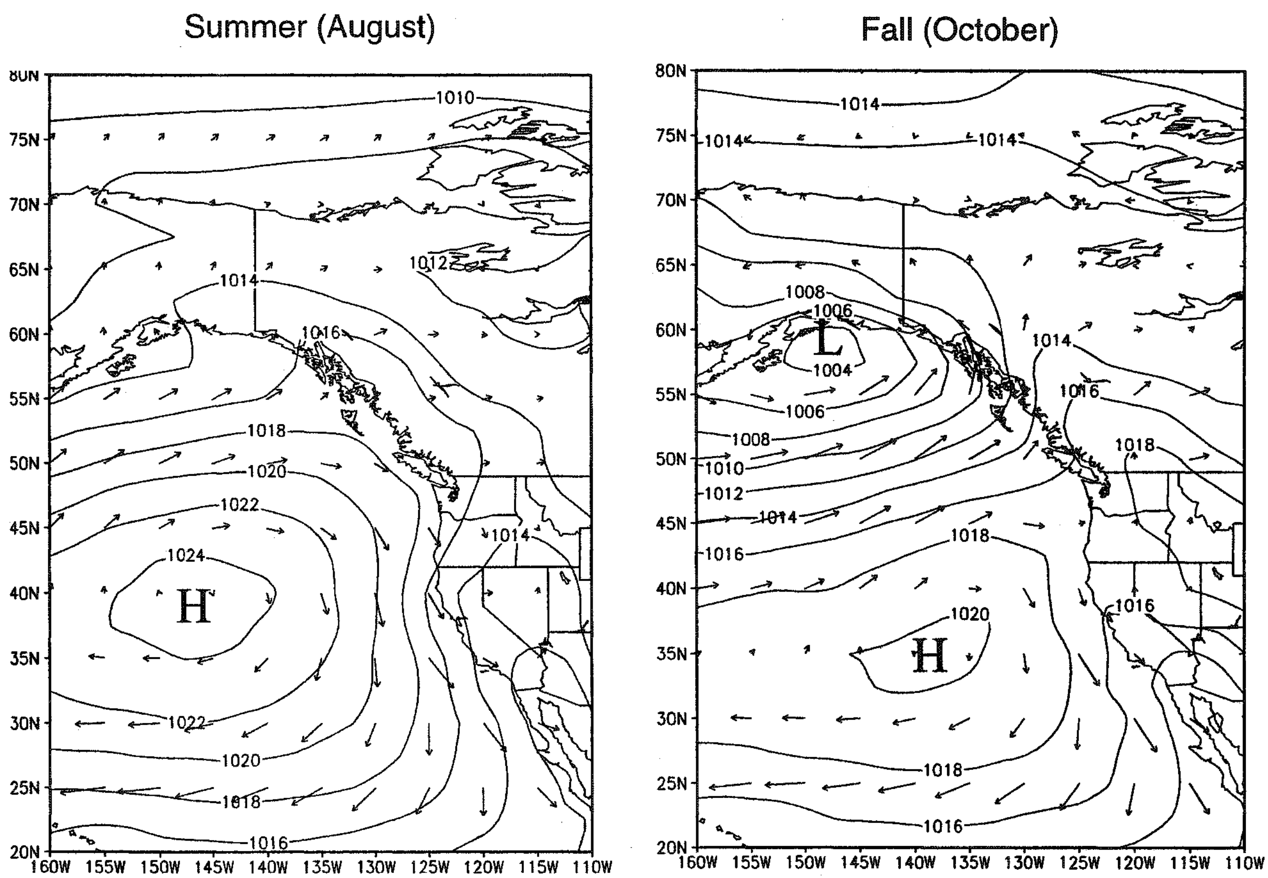

Figure 3.28 Mean Sea-Level Pressure Climatology: Comparison of 25-year average summer and fall mean sea-level pressure patterns and 10-metre winds. Plots were constructed using the Gridded Analysis and Display System (GrADS) using data derived from the NCEP/NCAR Reanalysis Project. (Prince George Airport located at 53° 53' N and 122° 40' W.)

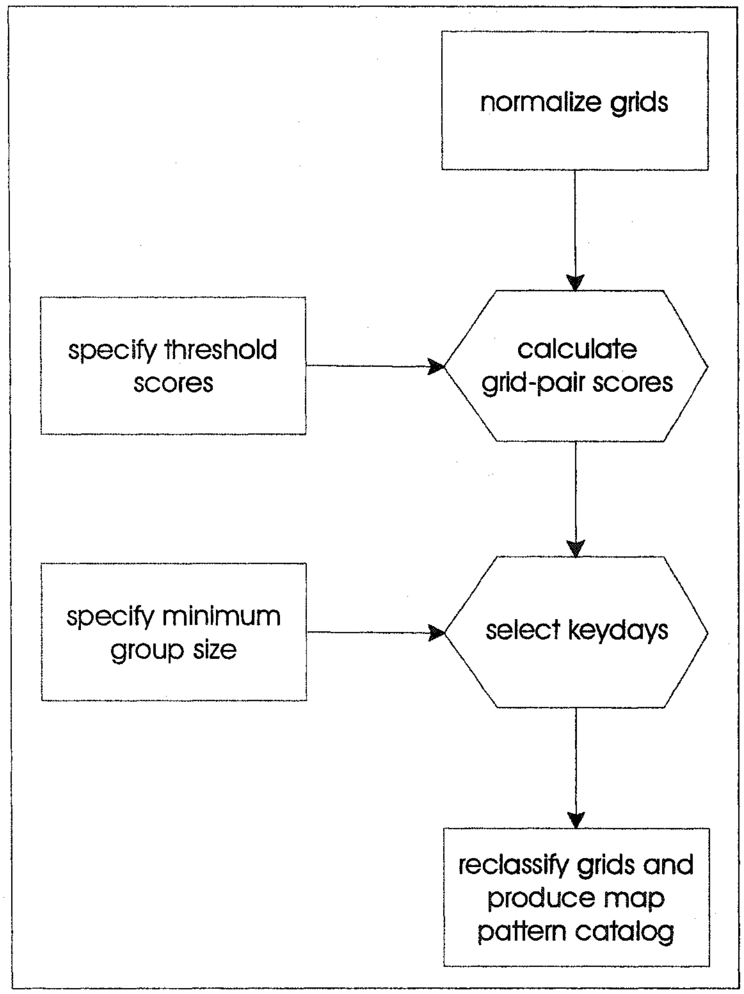

Figure 4.29 Kirchhofer Sums-of-Squares Technique: Flow diagram of keyday map-pattern classification program.

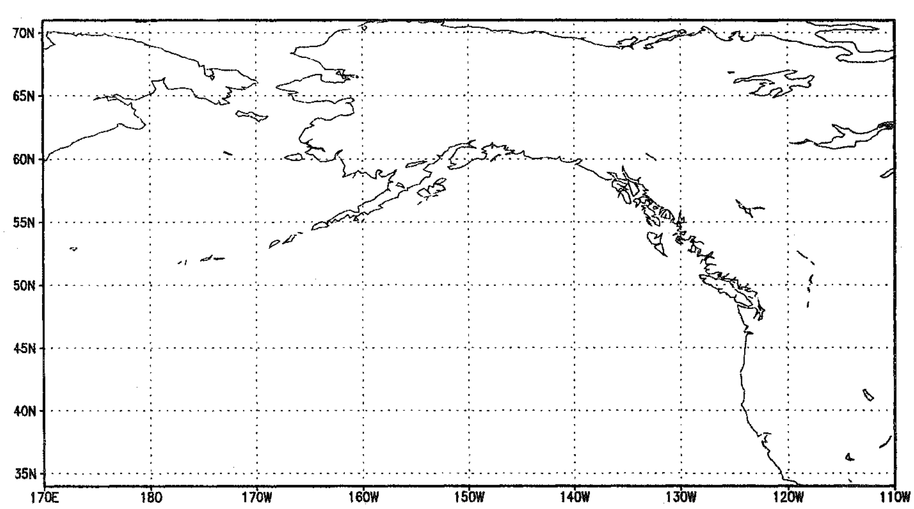

Figure 4.30 Synoptic Climatology Study Area: Map of study area used to develop synoptic-composites of fall and winter cyclones. Prince George Airport located at 53° 53' N and 122° 40' W.

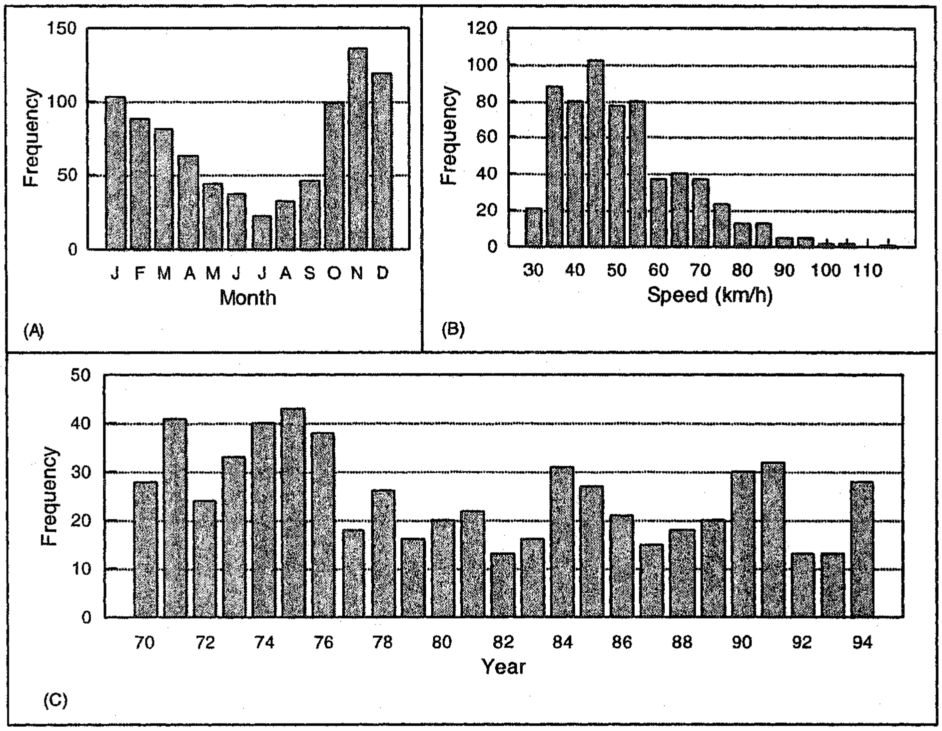

Figure 4.31 Prince George Airport Wind Extreme Distributions: (a) Monthly distribution of all daily extreme wind gusts from a southerly direction recorded during the period 1970-1994. (b) Distribution of southerly gusts occurring during the fall-winter period. (c) Annual distribution of gust events shown in (b).

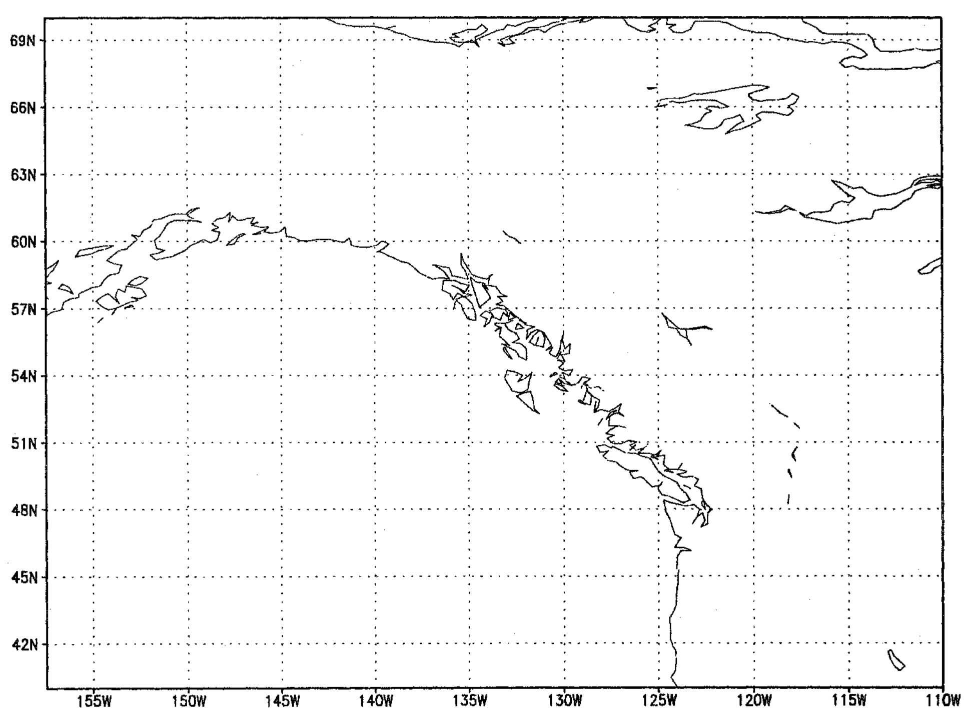

Figure 4.32 Keyday Study Area: Map of gridded area used in map-pattern classification.

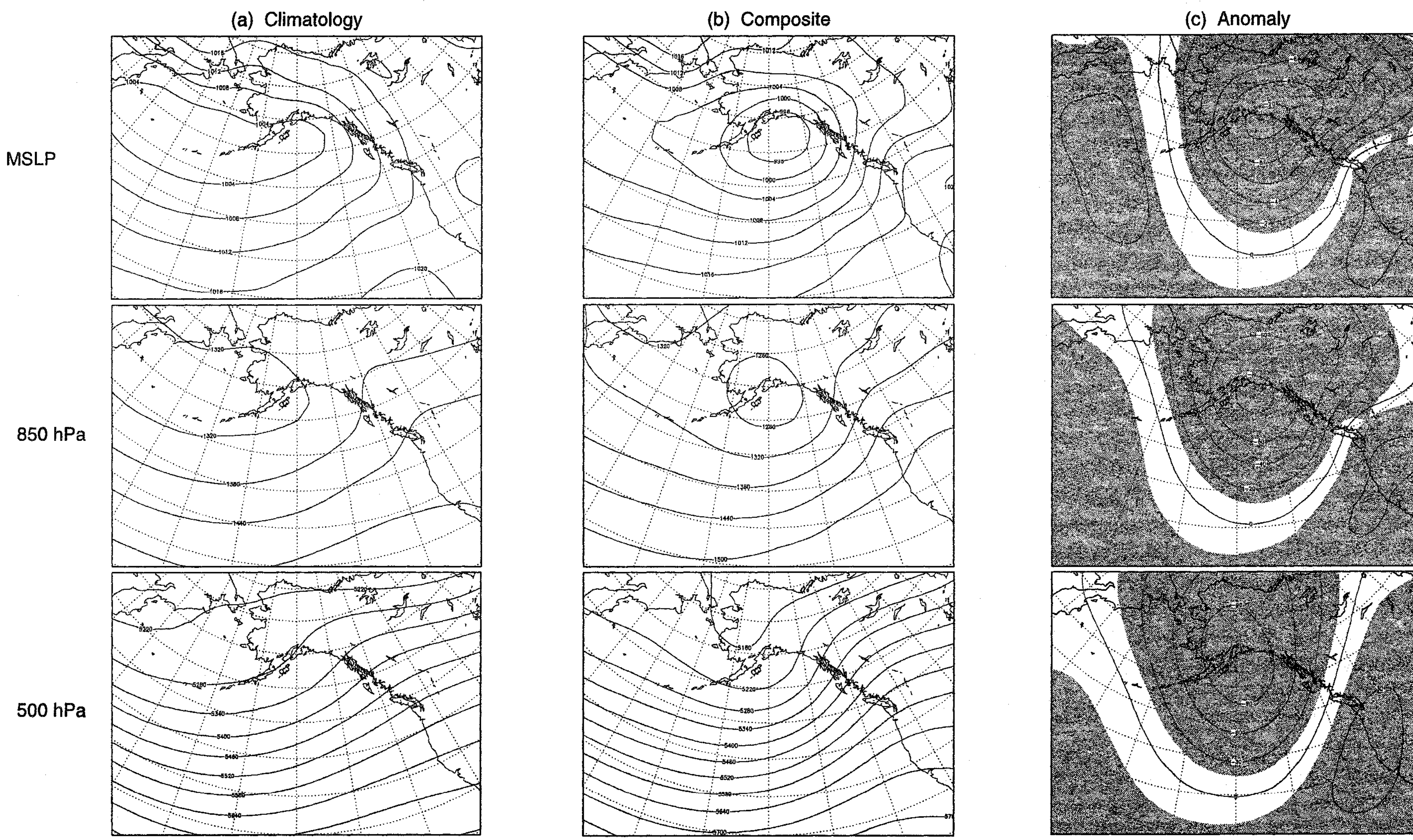

Figure 4.33 Synoptic Climatology: (a) 25-year mean climatological fields (mean sea-level pressure, and 850 hPa and 500 hPa pressure surfaces) for the fall-winter period (1970-1994). (b) Composite fields for all southerly gusts greater than 30 km/hr (1970-1994). (c) Deviation from normal climatology and statistical significance of anomaly at the 99% level (shaded region).

Table 4.22 Summary of Storm Composite Results: Comparison of storm-composite characteristics to climatology for the fall-winter period.

	number of days	mean daily extreme gust speed (km/h)	MSLP (hPa)		relative strength of pressure gradient[a]
			storm centre	criteria-area	
Climatology	4556	-	1004	1016	1
All storms: gusts > 30km/hr	626	52	996	1012	3
Moderate: 51-70 km/h	202	59	992	1010	4
Strong: 71-90 km/h	70	78	984	1008	5
Severe: gusts > 90km/hr	11	99	988	1004	6

[a]The magnitude of the pressure gradient was estimated by counting the number of isobars passing through the area defined by 50°-55° latitude and 120°-125° longitude.

Table 4.23 Summary of Map-Pattern Classification Results: Identification of keyday storms and comparison of storm characteristics.

	% of maps correlated at r = 0.7 or higher	extreme daily gust speed (km/h)	MSLP (hPa)		relative strength of pressure gradient[a]
			storm centre	criteria-area	
Moderate: 88/11/21	45	57	964	1000	5
Strong: 94/10/26	89	74	972	992	5
Severe: 75/11/12	73	98	976	1006	7

[a] See Table 4.22 for explanation

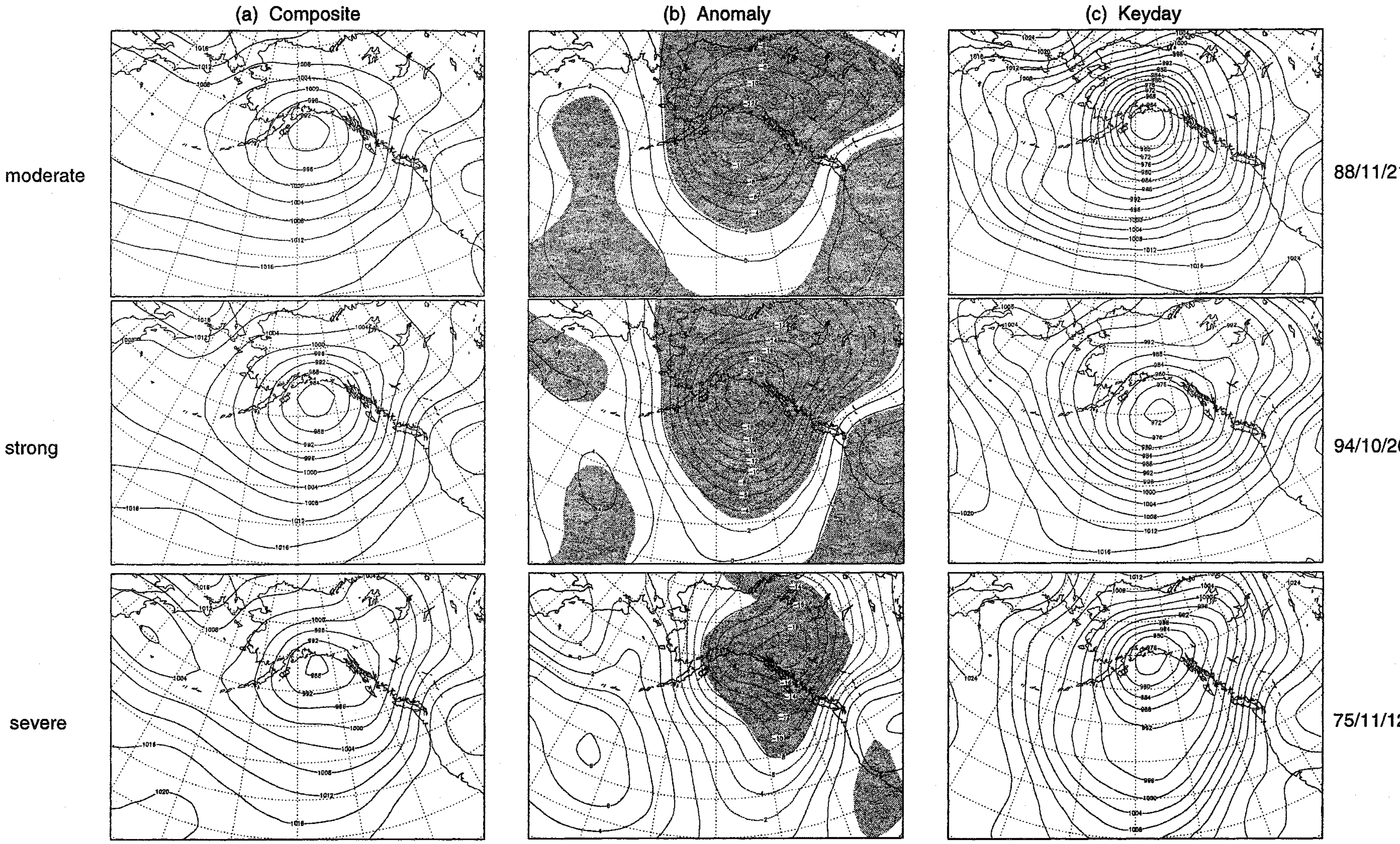

Figure 4.34 Storm Composites and Keyday Events: (a) Mean sea-level pressure storm composites stratified by moderate (51-70 km/h), strong (71-90 km/h) and severe (>90 km/hr) daily extreme gust speeds. (b) Deviation from normal climatology for fall-winter period and statistical significance of anomaly at 99% level (shaded area). (c) Keyday maps identified by map-pattern classification analysis.

Table 4.24 Severe Keyday Storm Weather Properties: Comparison of mean daily weather elements before, during and after severe gust events.

	Day - 1	Day of composite	Day + 1
average daily extreme gust speed (km/h)	55	99	50
average maximum daily temperature °C	4.6	8.2	5.0
average daily mean temperature °C	0.4	3.6	0.5
average daily rainfall (mm)	0.3	1.6	1.0
average daily snowfall (mm)	0.4	1.3	0.4
average total daily precipitation (mm)	0.7	2.9	1.4

Table 4.25 Storm Composite Weather Properties: Comparison of storm composite weather with climatology.

	average maximum	average daily mean	average daily	average daily	average total daily
climatology	0.8	-3.6	0.5	1.2	1.7
all gust	4.7	0.6	0.9	1.3	2.2
moderate	5.4	1.4	0.9	1.0	1.9
strong	6.4	2.1	1.1	0.8	1.9
severe	8.2	3.6	1.6	1.3	2.9

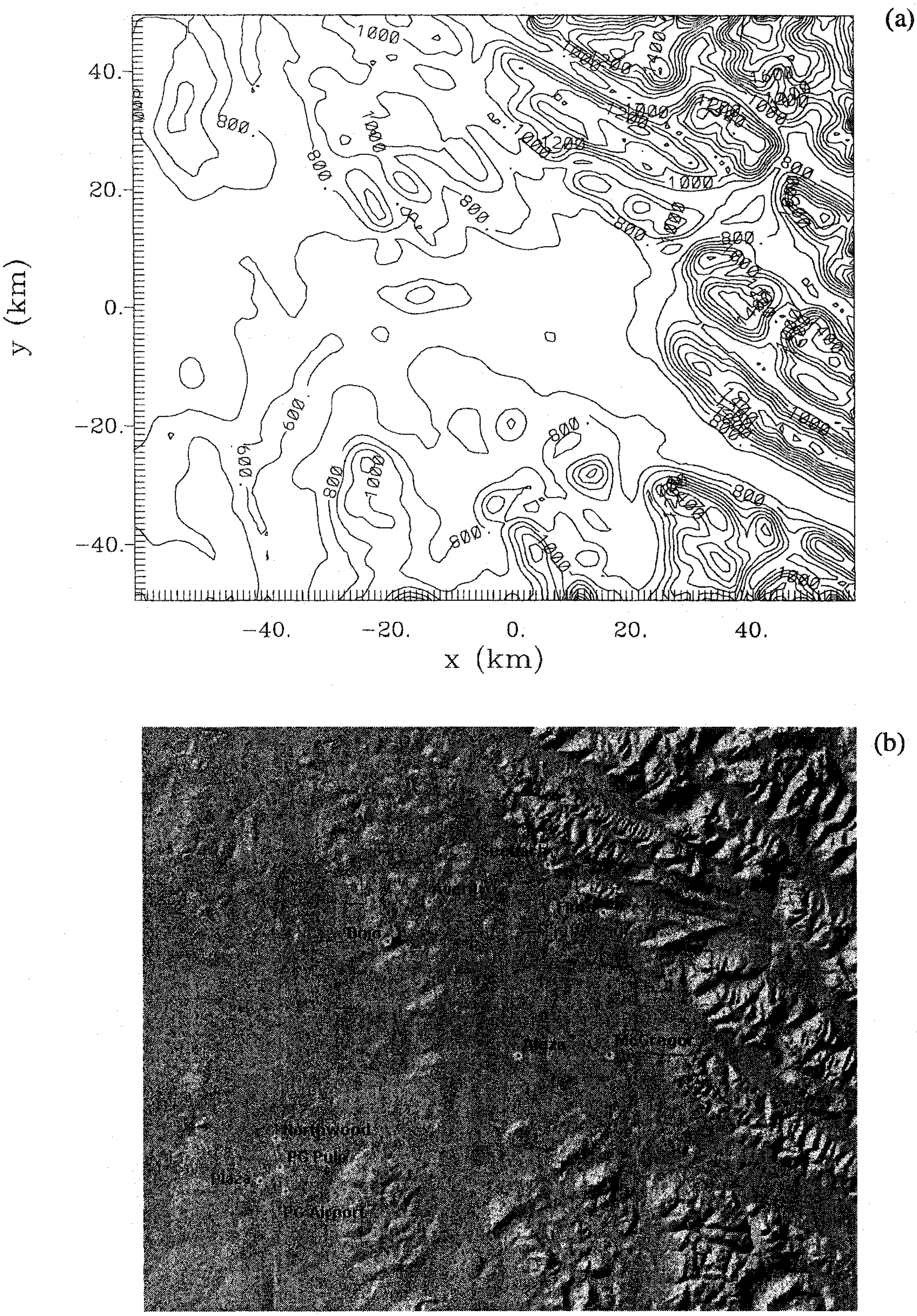

Figure 5.35 Smoothed Topography and Wind Monitoring Network: (a) RAMS model domain smoothed to a 1 km resolution. Terrain elevation contours are shown (above mean sea-level) every 100 m. (b) Digital elevation model (100 m resolution) of area in (a) showing location of wind monitoring stations available for model validation. (Coverage: 100 x 120 km.)

Table 5.26 RAMS Model Configuration: Summary of relevant model configuration parameters used to initialize the keyday and validation numerical simulations.

1. MODEL GRIDS:

Horizontal Grid:

Dimensions:	120 km x 100 km grid
Resolution:	1 kilometre

Vertical Grid:

Levels:	29 levels (16 km top)
Minimum spacing:	50 metre at surface
Stretch factor	1.2
Maximum spacing:	1000 metres

(refer to text for explanation of vertical grid parameters)

Soil Grid:

Levels:	11
Depth:	0.5 metre

2. TIME INTEGRATION:

Equations:	nonhydrostatic
Initialization:	variable (sounding data only)
Duration:	12-hour (12Z to 0Z)
Time step:	5 seconds
Nudging:	strong nudging along lateral boundary (10 grid points from lateral edges) and above 12 km only.

3. MODEL OPTIONS:

uniform surface roughness (coniferous forest)

- moisture as a passive tracer (no clouds or precipitation)
- two passes through topography smoother

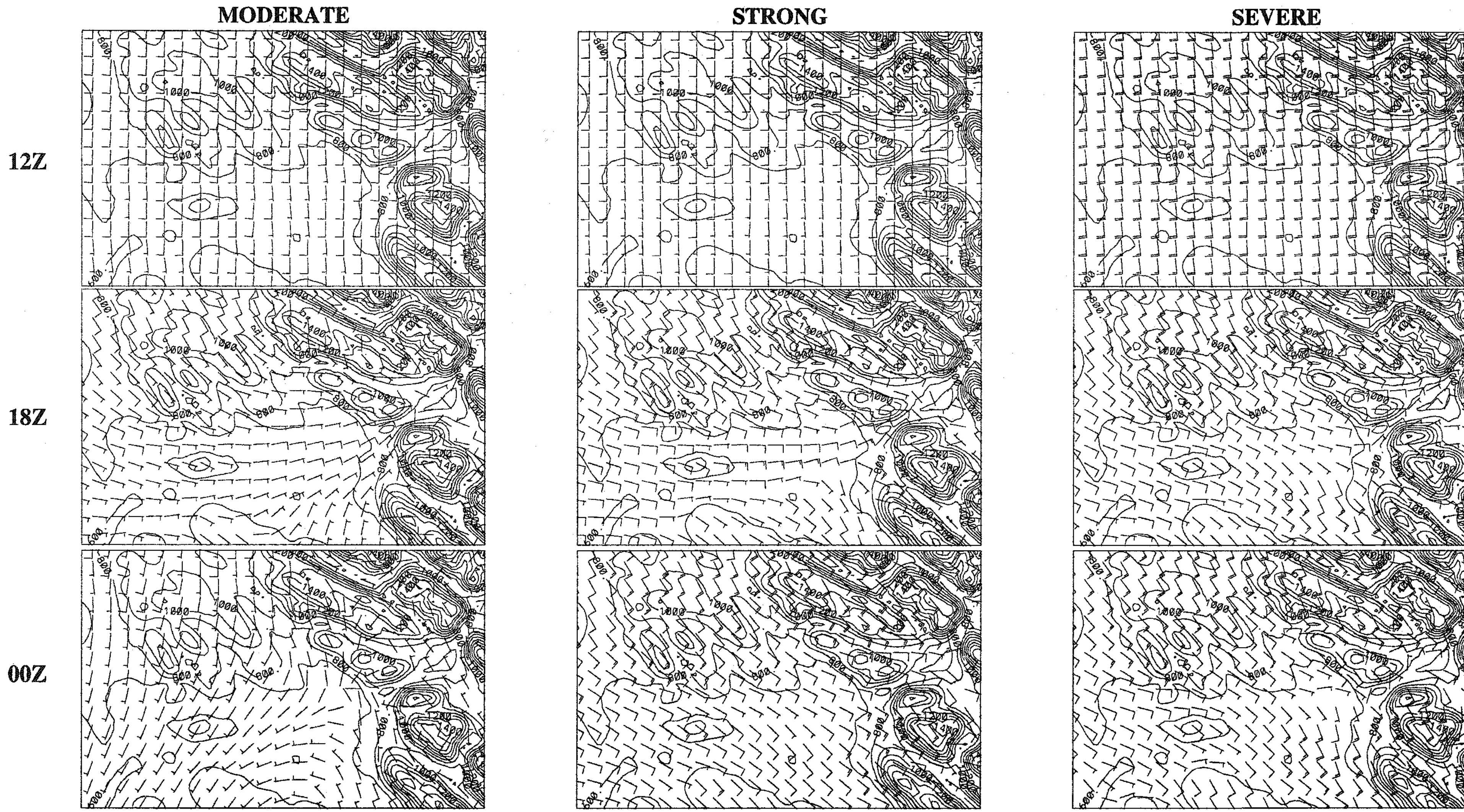

Figure 5.36 Keyday Simulation Results: Results of the three keyday simulations for model level k=3 (corresponding to a mean height of 78.6 metres). Shown from top to bottom is the initialization field (12Z), a snapshot of the windfield after six hours of simulation (18Z) and at the end of the model run (00Z). Wind barbs are shown every four grid points (or 4 km) using speed intervals of 5 and 10 m/s for a half barb and a full barb, respectively. Plots show only the grid interior enclosing the MMF (compare with Fig. 5.35). Elevation contours are shown every 100 m. (Coverage: 60 x 92 km.)

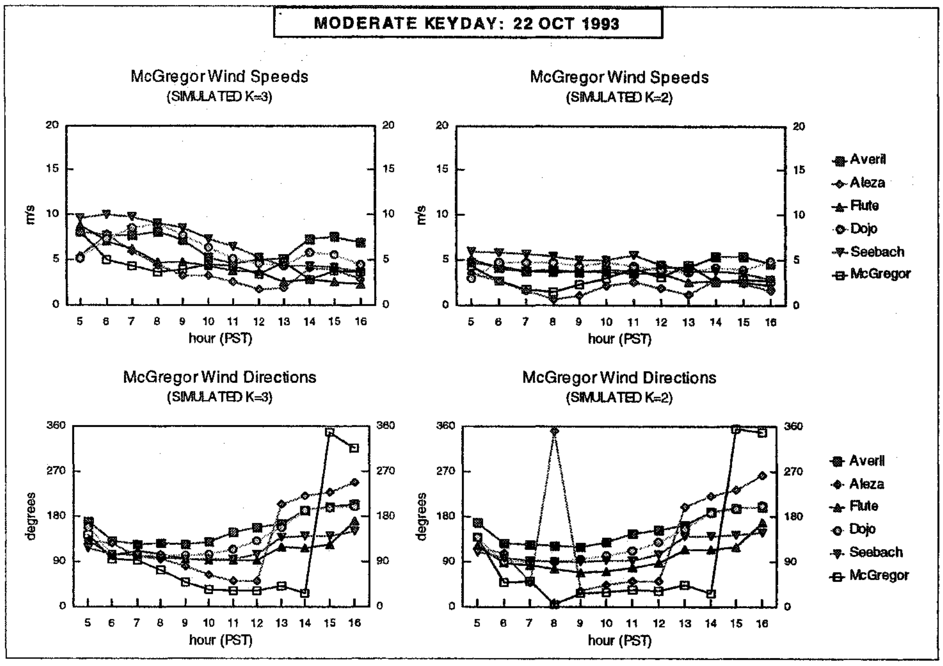

Figure 5.37 (a) Moderate Keyday Simulation Time Series: Temporal evolution of moderate keyday simulated wind speed (top plots) and direction (bottom plots) at grid cells closest to the indicated climate stations for vertical model levels k=3 (left) and k=2 (right).

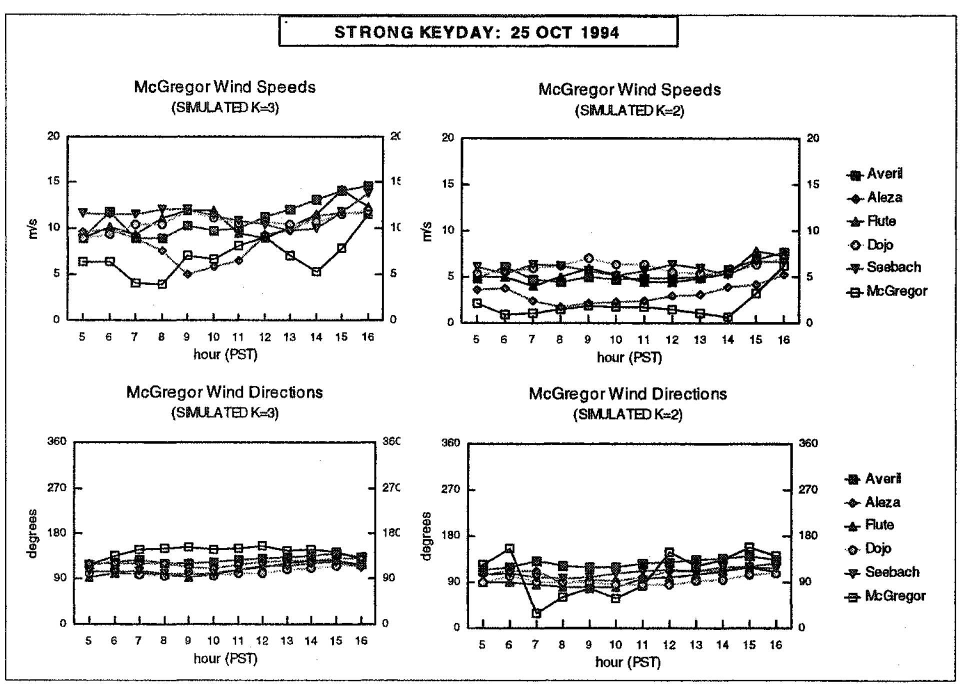

Figure 5.37 (b) Strong Keyday Simulation Time Series.

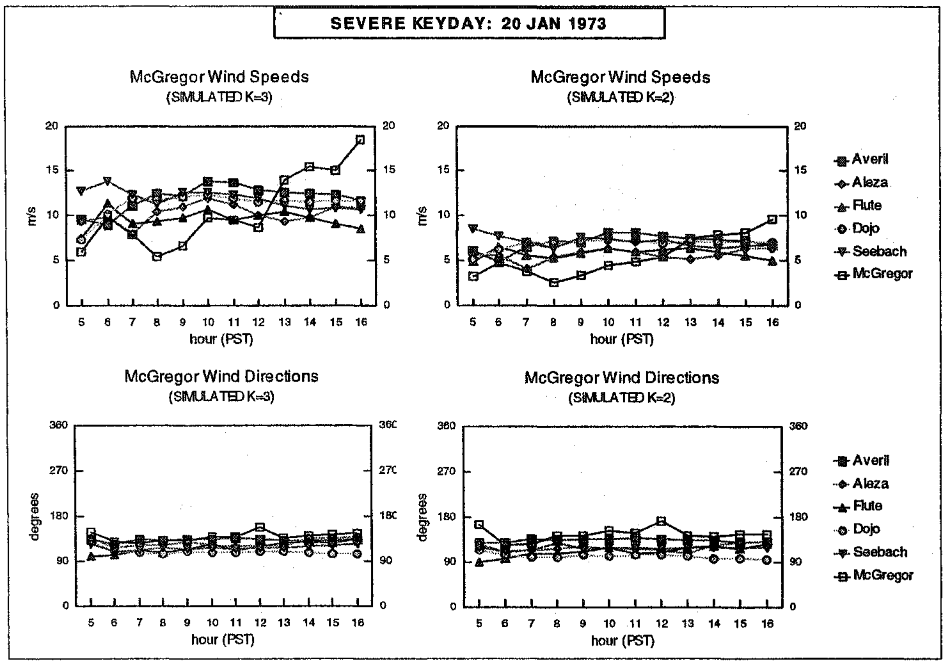

Figure 5.37 (c) Severe Keyday Simulation Time Series.

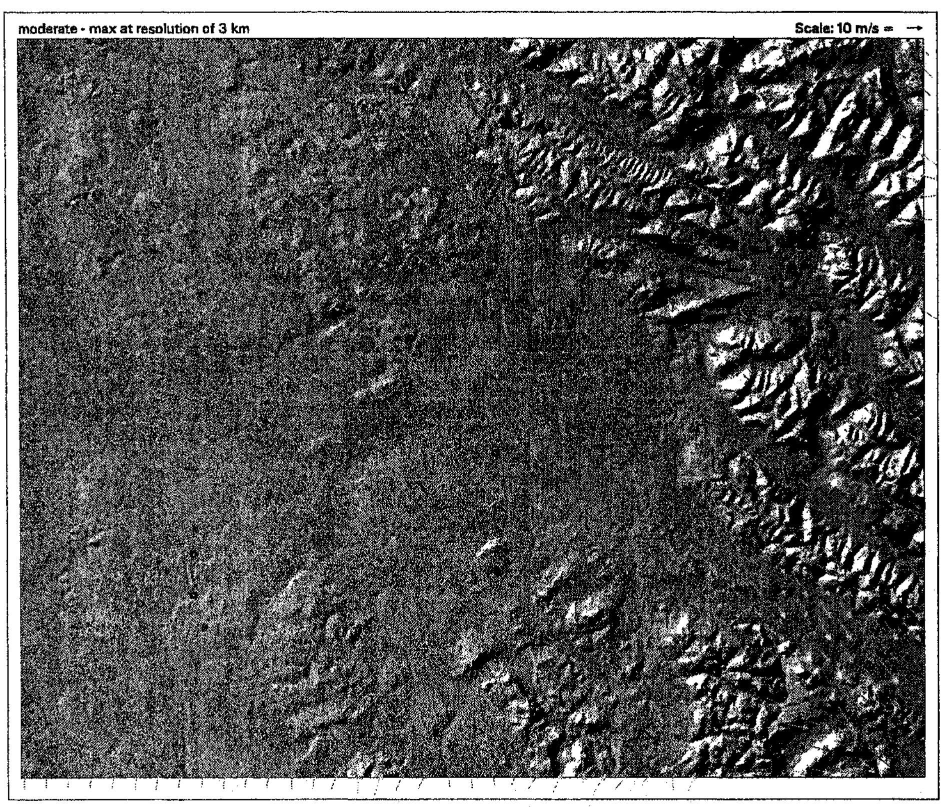

Figure 5.38 (a) Moderate Keyday Wind Maximums: Wind vectors (shown every 3 grid points) are colour coded according storm category, with yellow, orange and red denoting moderate (51-70 km/h), strong (71-90 km/h) and severe (90+ km/h) winds respectively (blue vectors are less than 51 km/h). (Coverage: 100 x 120 km.)

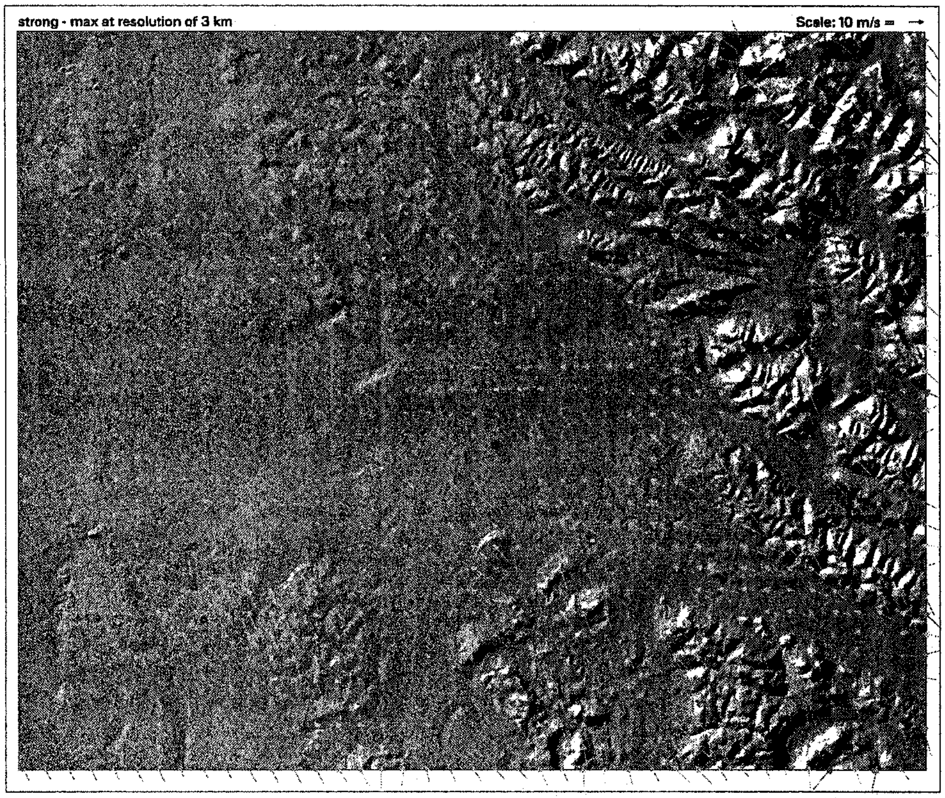

Figure 5.38 (b) Strong Keyday Wind Maximums.

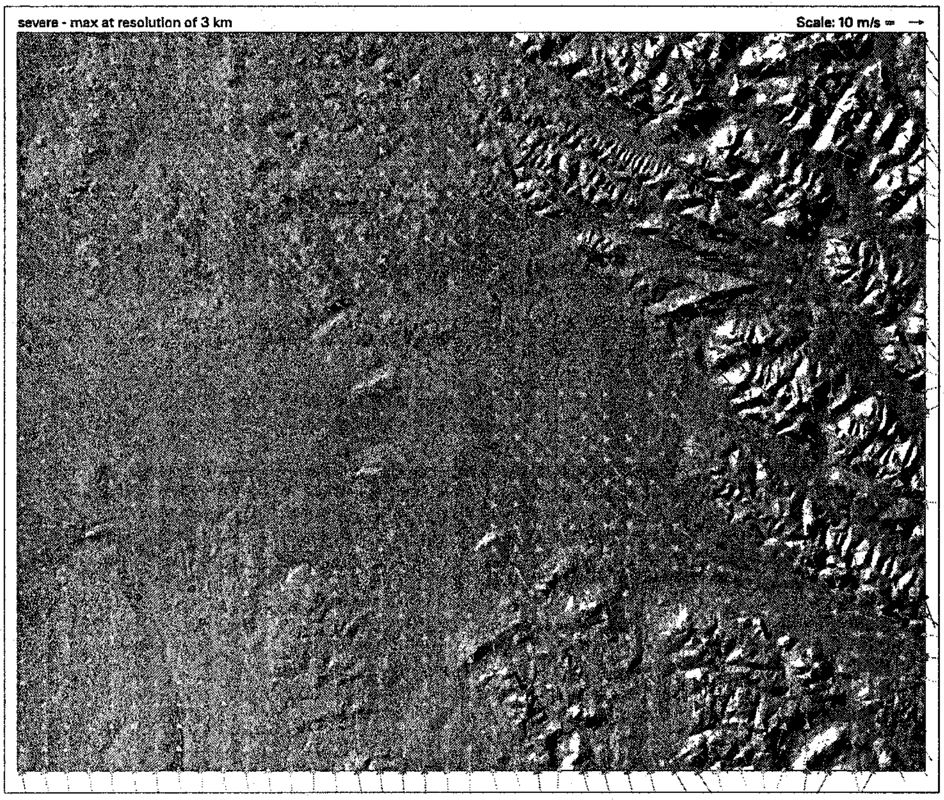

Figure 5.38 (c) Severe Keyday Wind Maximums.

Table 5.27 Validation Storm Characteristics: Observed speed and direction of the daily extreme gust and maximum hourly wind at the Prince George Airport during the validation storm events.

Date	Daily Extreme Gust		Maximum Hourly Wind	
	speed (km/h)	direction (deg)	speed (km/h)	direction (deg)
18 Mar 1997	69	180	43	180
21 Oct 1996	74	190	48	190
04 Dec 1996	82	180	46	190

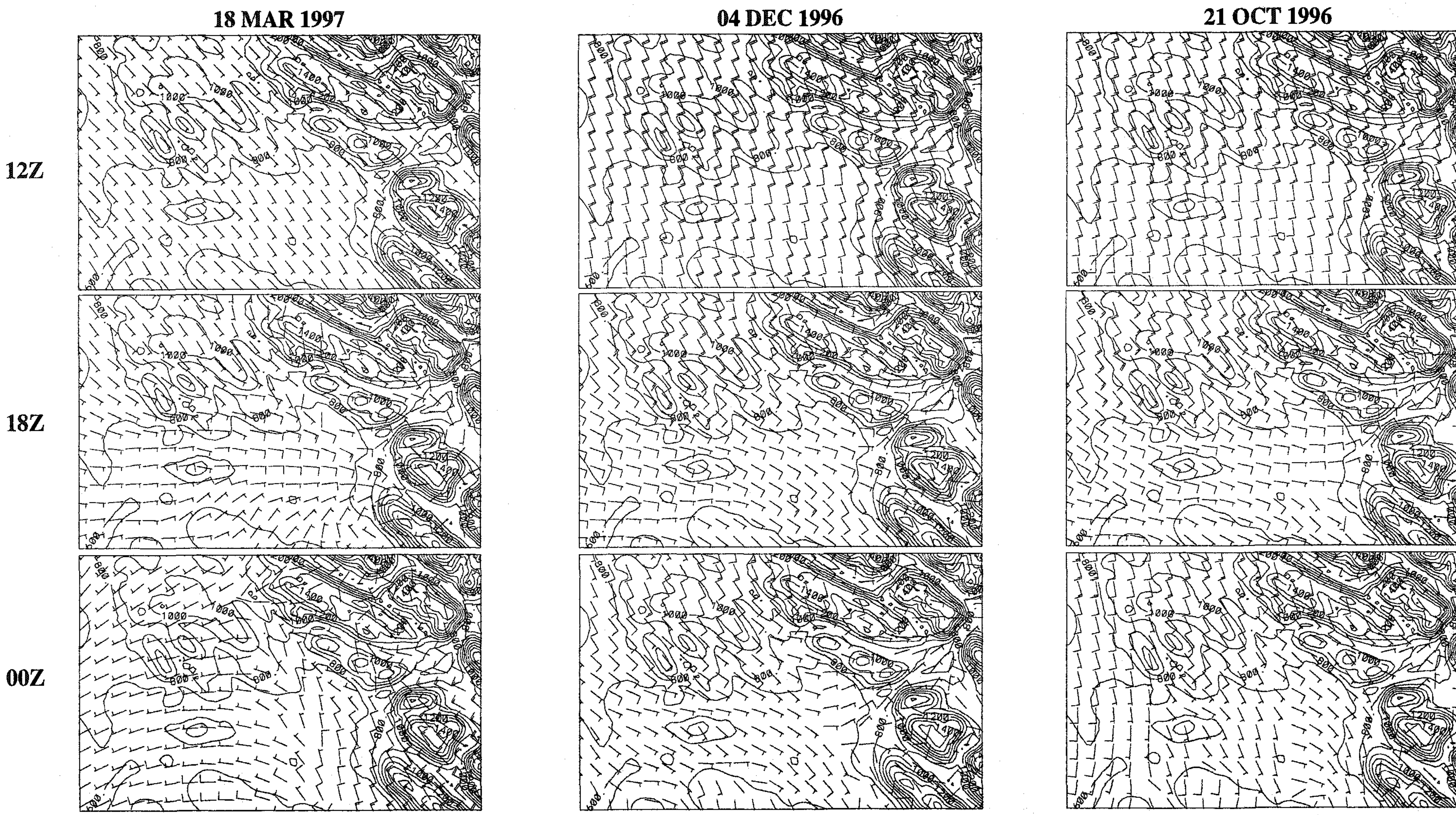

Figure 5.39 Validation Simulation Results: Results of the validation simulations for model level k=3 (corresponding to a mean height of 78.6 metres). Shown from top to bottom is the initialization field (12Z), a snapshot of the windfield after six hours of simulation (18Z) and at the end of the model run (00Z). Wind barbs are shown every four grid points (or 4 km) using speed intervals of 5 and10 for a half barb and full barb, respectively. Plots show only the grid interior encompassing the MMF (compare with Fig. 5.35). Elevation contours are shown every 100 m. (Coverage: 60 x 92 km.)

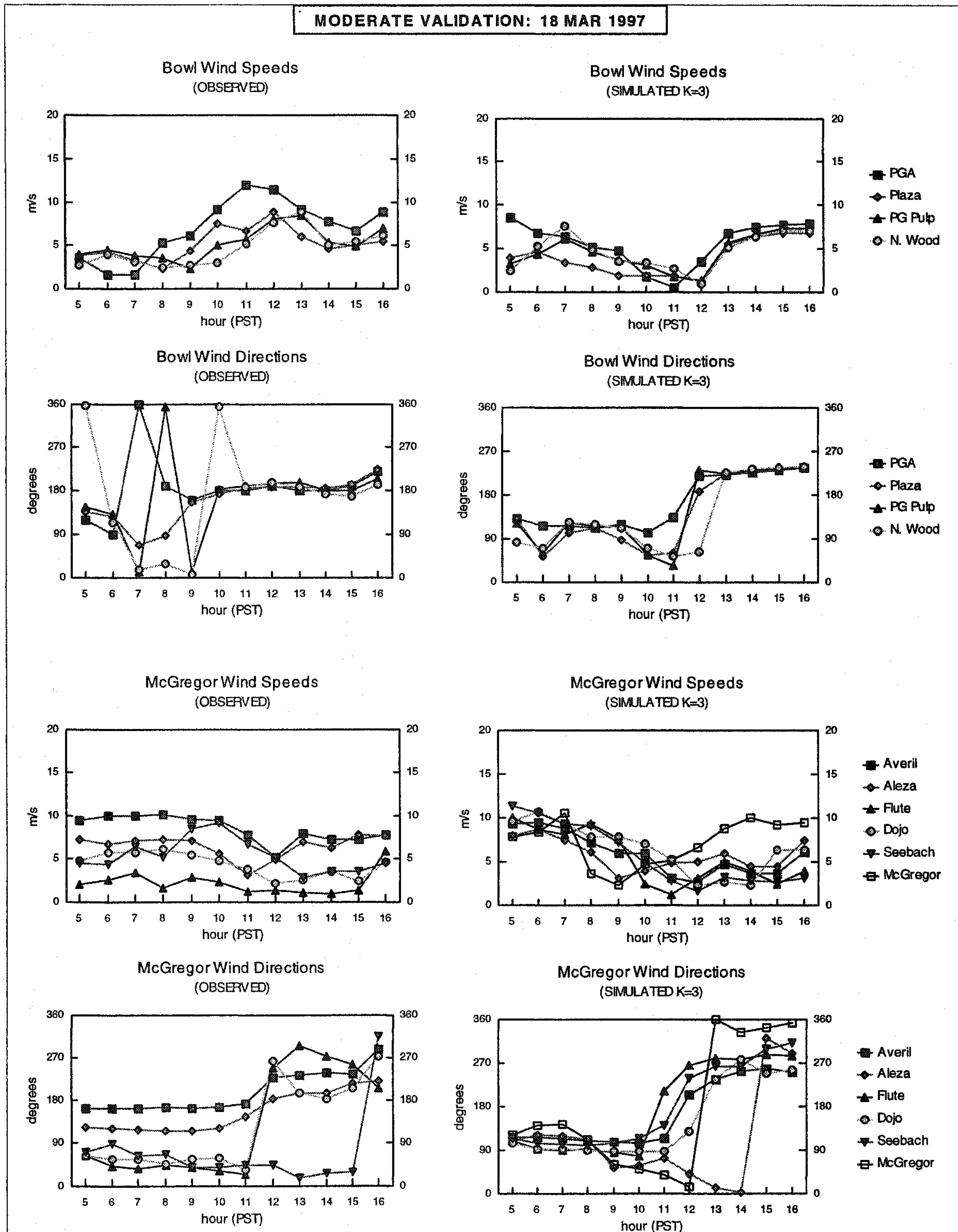

Figure 5.40 (a) 18 March 1997 Validation Time Series: Comparison of observed (left-hand plots) vs. simulated (right-hand plots) wind speed and direction for model level k=3 at grid cells closest to indicated wind monitoring stations in the Prince George Bowl (top plots) and the McGregor Model Forest (bottom plots).

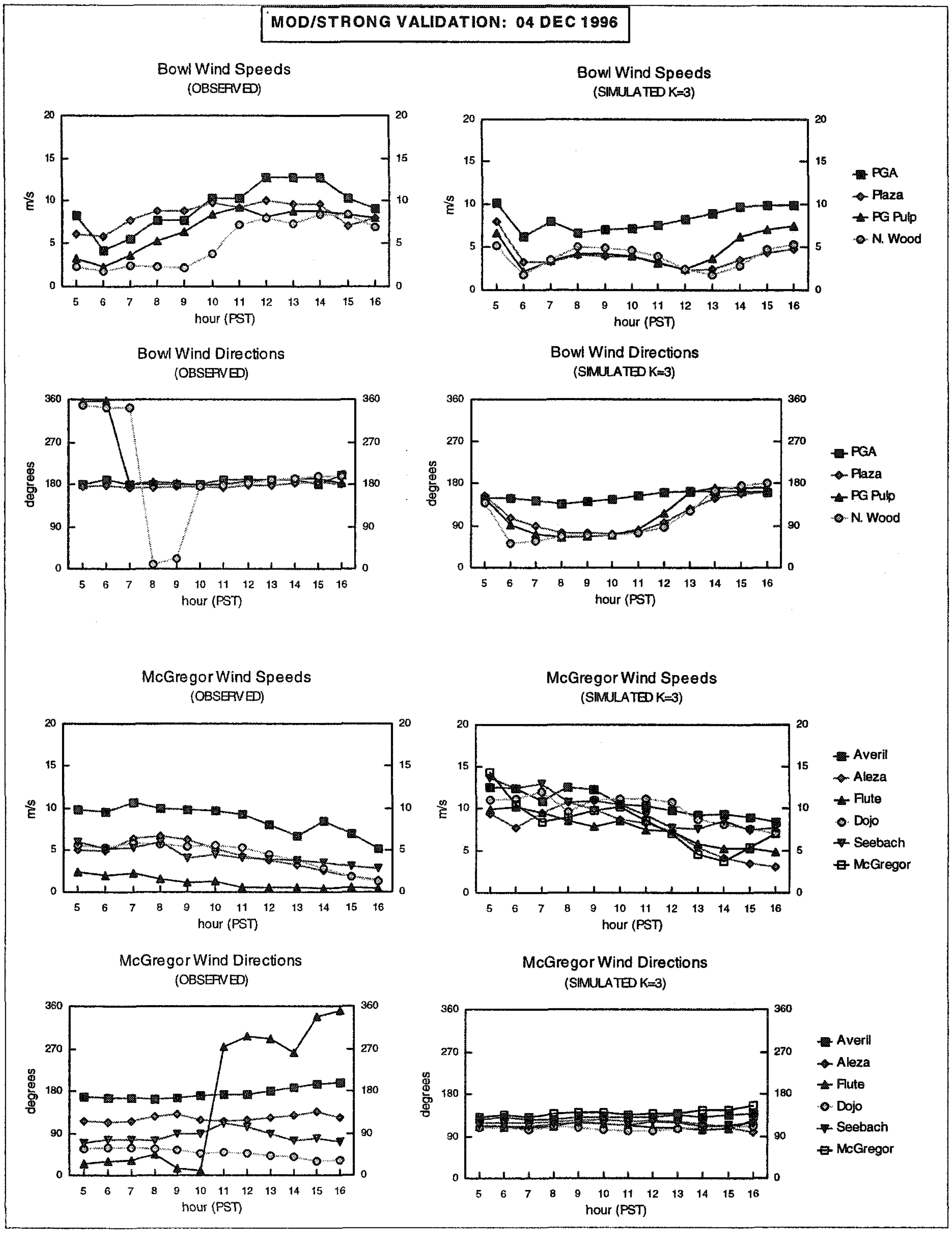

Figure 5.40 (b) 04 December 1996 Validation Time Series.

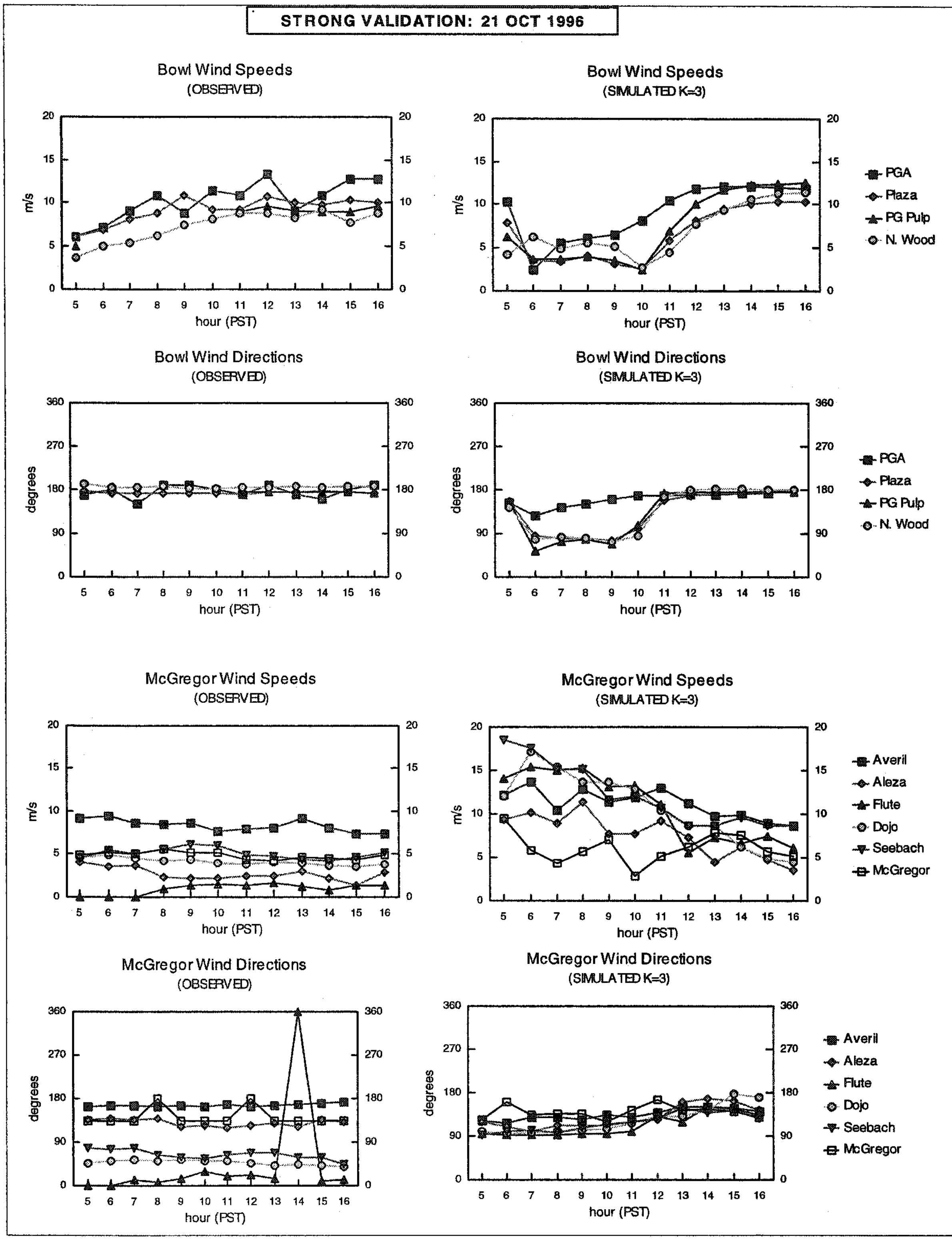

Figure 5.40 (c) 21 October 1996 Validation Time Series.

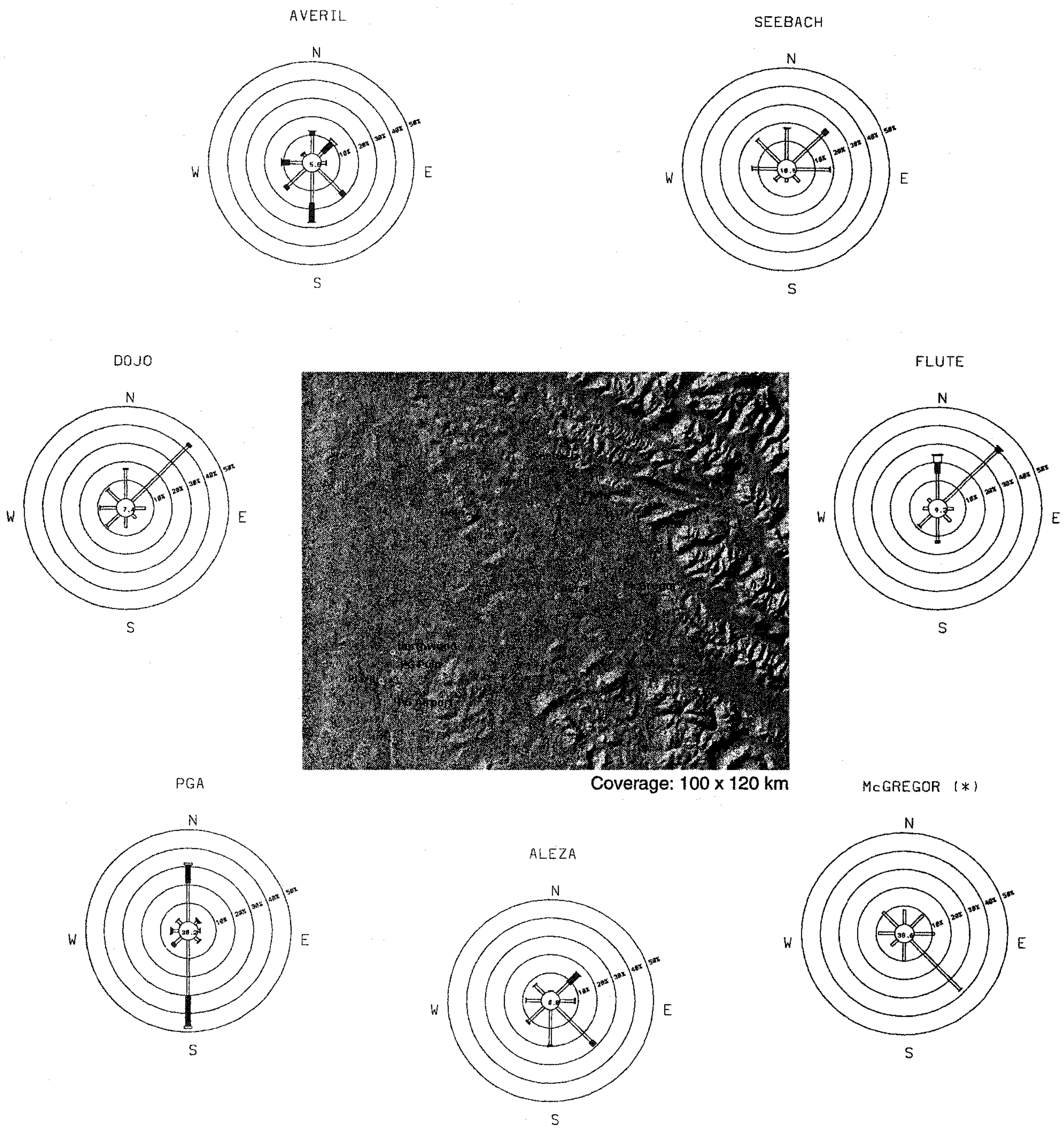

Figure 5.41 Observed Wind Characteristics: Prevailing wind directions measured during the October 1996 to March 1997 windy season. Wind measurements are 1-hour means with the exception of PGA and McGregor. Wind speeds are shown in intervals of 5 m/s. (Note: McGregor data is for the period October 1994 to March 1995.)

Table 6.28 Keyday Wind Speed Ratios at Wind Monitoring Stations: Ratio of simulated wind speed for grid cells nearest available wind monitoring locations, to the wind speed simulated for the grid cell nearest the Prince George Airport, during each of the keyday numerical simulations (model level k=3). Also shown is the length of available wind records for model validation, and the number of southerly gust events which occurred during the period of record.

Station	Speed Ratios			Period of Record	Years	Number of Storms
	moderate	strong	severe			
Averil	0.91	1.19	1.01	1996-1997	2	8
Aleza	0.65	1.08	0.89	1993-1997	5	26
McGregor	0.54	1.14	1.36	1989-1996	8	23
Dojo	0.97	1.02	0.91	1996-1997	2	8
Seebach	1.07	1.16	0.81	1996-1997	2	7
Flute	0.67	1.15	0.85	1996-1997	2	7
Northwood	0.88	0.53	0.77	1993-1997	5	34
PG Pulp	0.9	0.76	0.93	1993-1997	5	32
Plaza	0.85	0.42	0.8	1992-1997	6	3

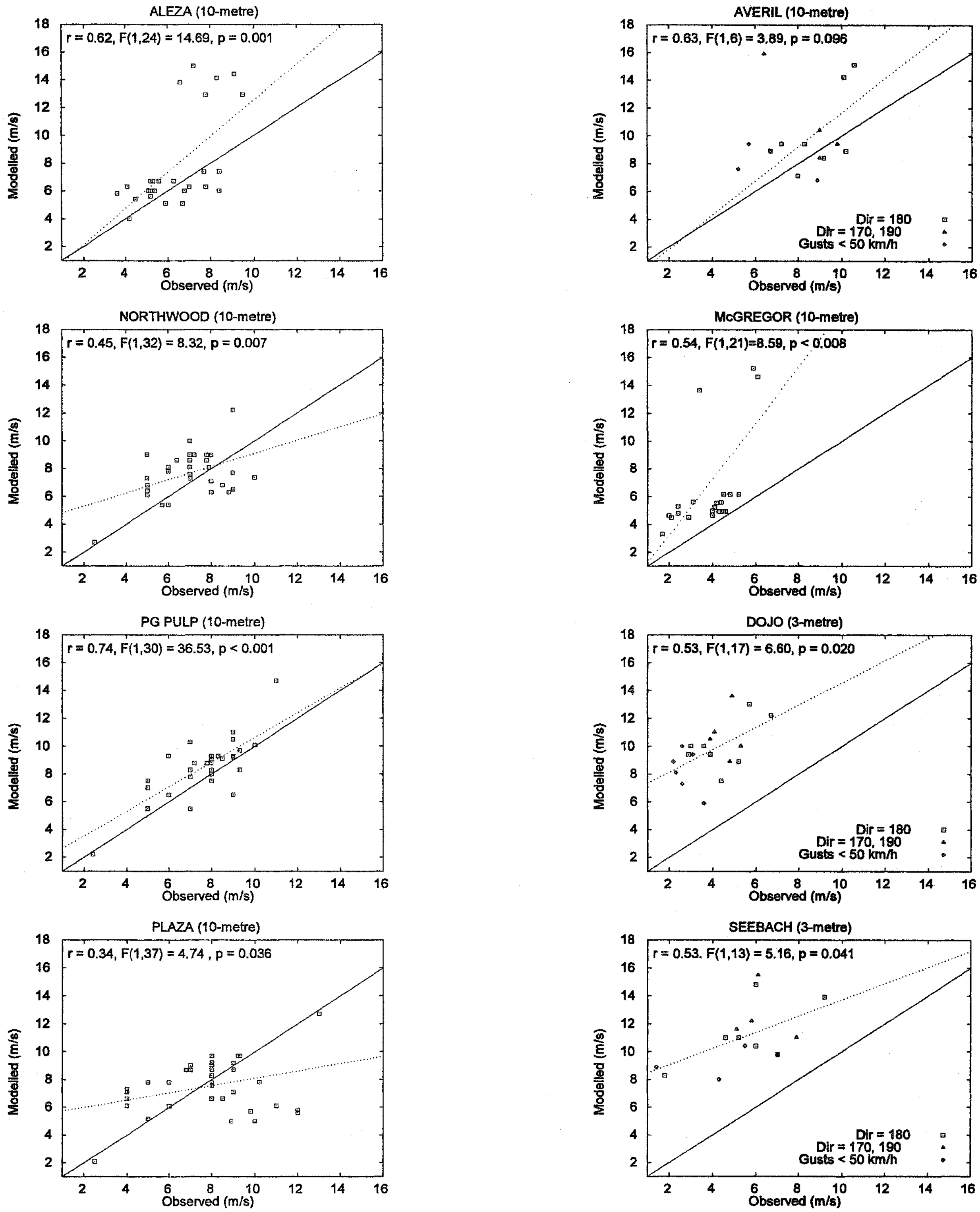

Figure 6.42 All-Keyday Model Validation: Comparison of observed daily maximum hourly wind speed vs. extrapolated wind maximum under a synoptic southerly flow using the set of three keyday speed ratios. Broken line is the regression line and the solid line is the 1:1 line.

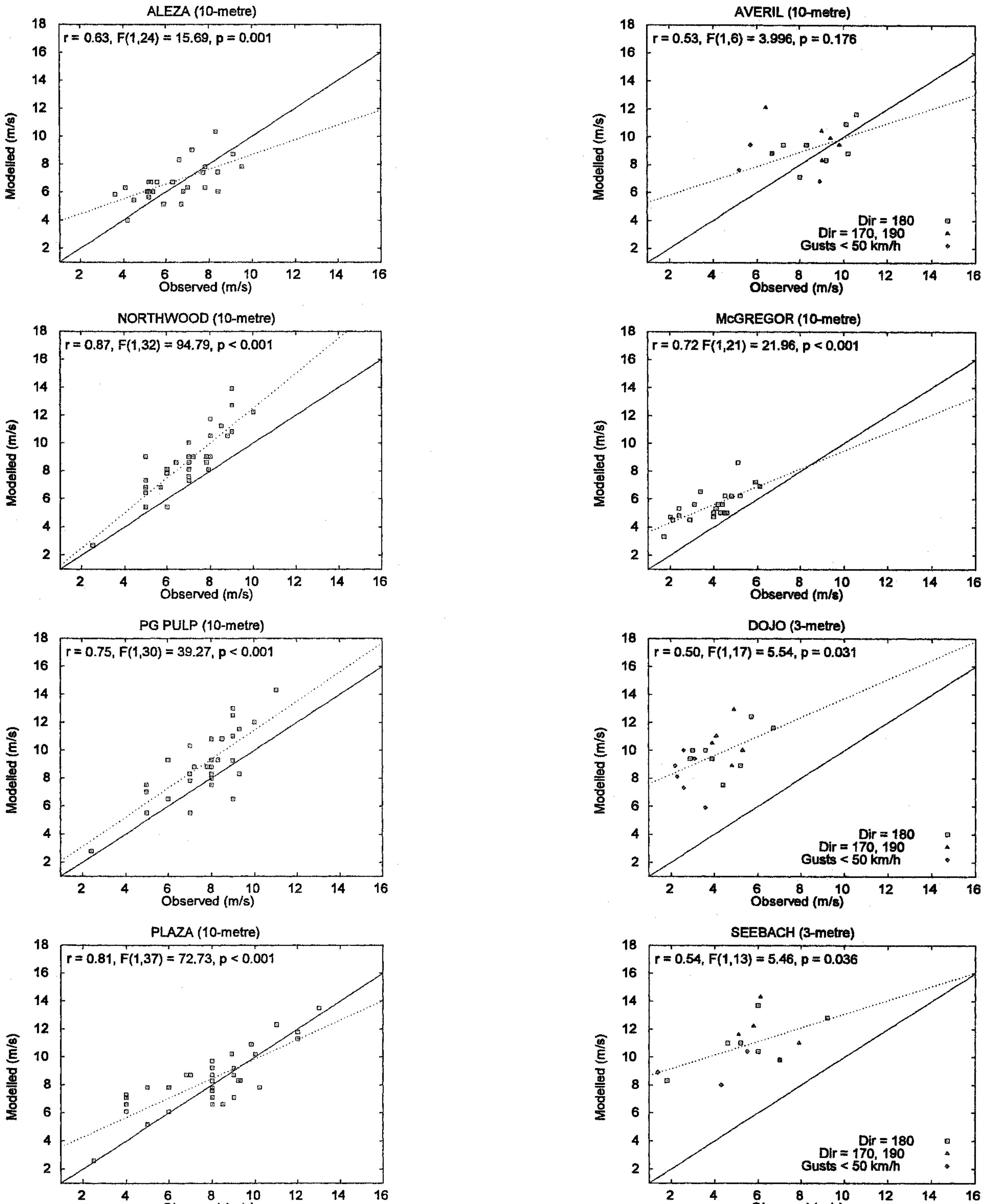

Figure 6.43 Moderate Keyday Validation: Comparison of observed daily maximum hourly wind speed vs. extrapolated wind maximum under a synoptic southerly flow using the moderate keyday speed ratios for all wind classes. Broken line is the regression line and the solid line is the 1:1 line.

Table 6.29 Mean Absolute Error: Comparison of average observed daily maximum hourly wind speed to average extrapolated maximum wind speed, and calculation of mean absolute error using moderate wind speed ratios for all wind classes at each of the wind monitoring stations.

Station	Height (m)	Events N	Observed (m/s)	Modelled (m/s)	Mean Absolute Error [a] (m/s)
Averil	10	17	8.26	9.23	1.72
Aleza	10	26	6.42	6.65	1.13
McGregor	10	23	3.9	5.48	1.59
Northwood	10	34	6.9	8.62	1.76
PG Pulp	10	32	7.59	8.86	1.65
Plaza	10	40	7.77	8.28	1.16
Dojo	3	19	3.94	9.59	5.65
Flute	3	15	3.83	6.81	3.38
Seebach	3	15	5.53	10.88	5.35

[a] Error convention is (modelled - observed).

Table 6.30 Percent Frequency of Mean Absolute Error: Comparison of model error at 10-metre stations, showing frequency of error less than 1 m/s, 2 m/s and 3 m/s, and greater than 3 m/s.

Station	Frequency of Absolute Mean Error [a] (%)			
	≤ 1 m/s	≤ 2 m/s	≤ 3 m/s	> 3 m/s
Averil	20	45	80	20
Aleza	40	85	100	0
McGregor	30	70	90	10
Northwood	20	60	85	15
PG Pulp	35	50	75	25
Plaza	40	80	90	10
Mean Percent Frequency	31	65	87	13

[a] Frequency rounded to nearest 5%.

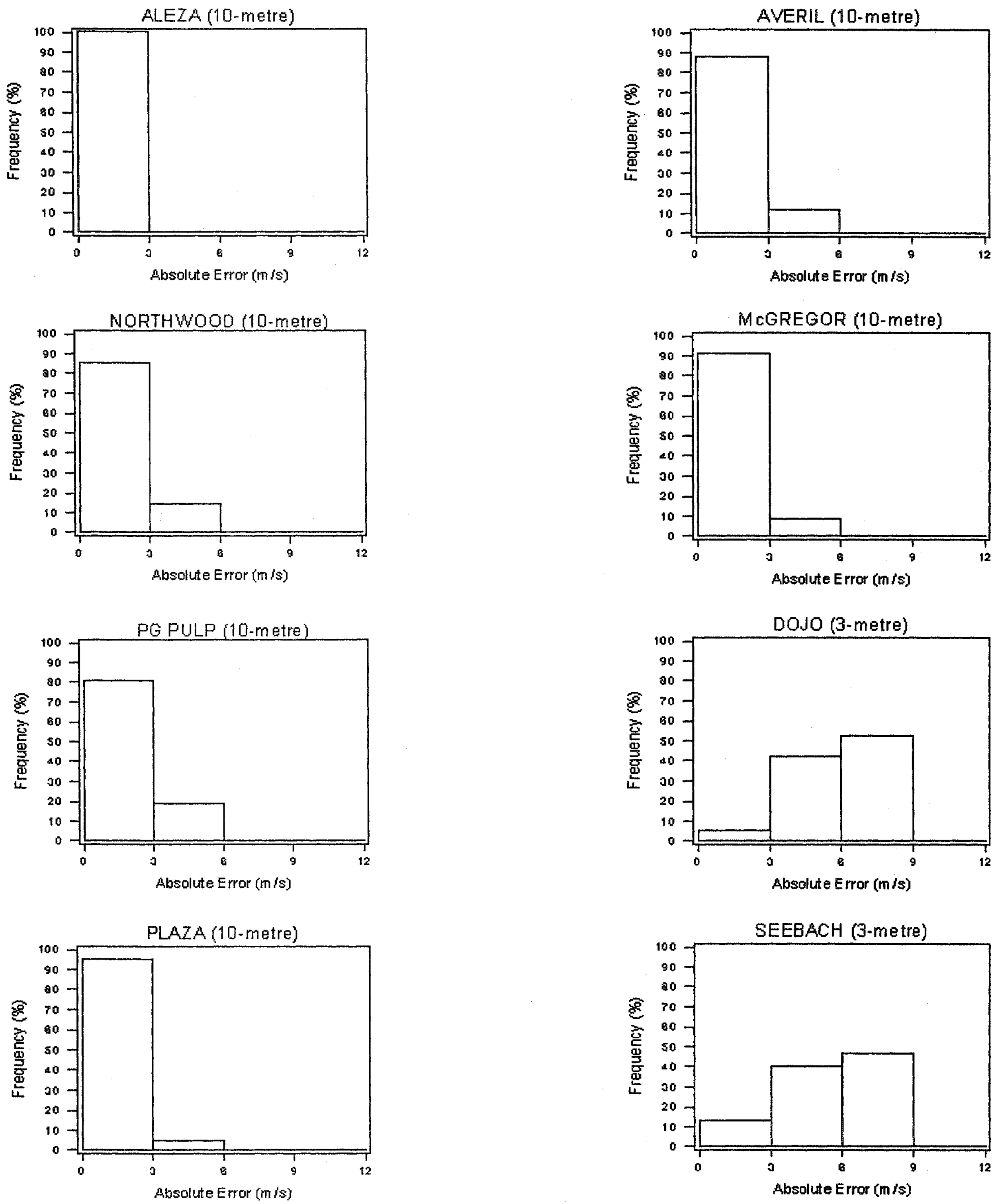

Figure 6.44 Absolute Model Error: Histograms showing frequency distribution of absolute model error at each of the wind monitoring locations.

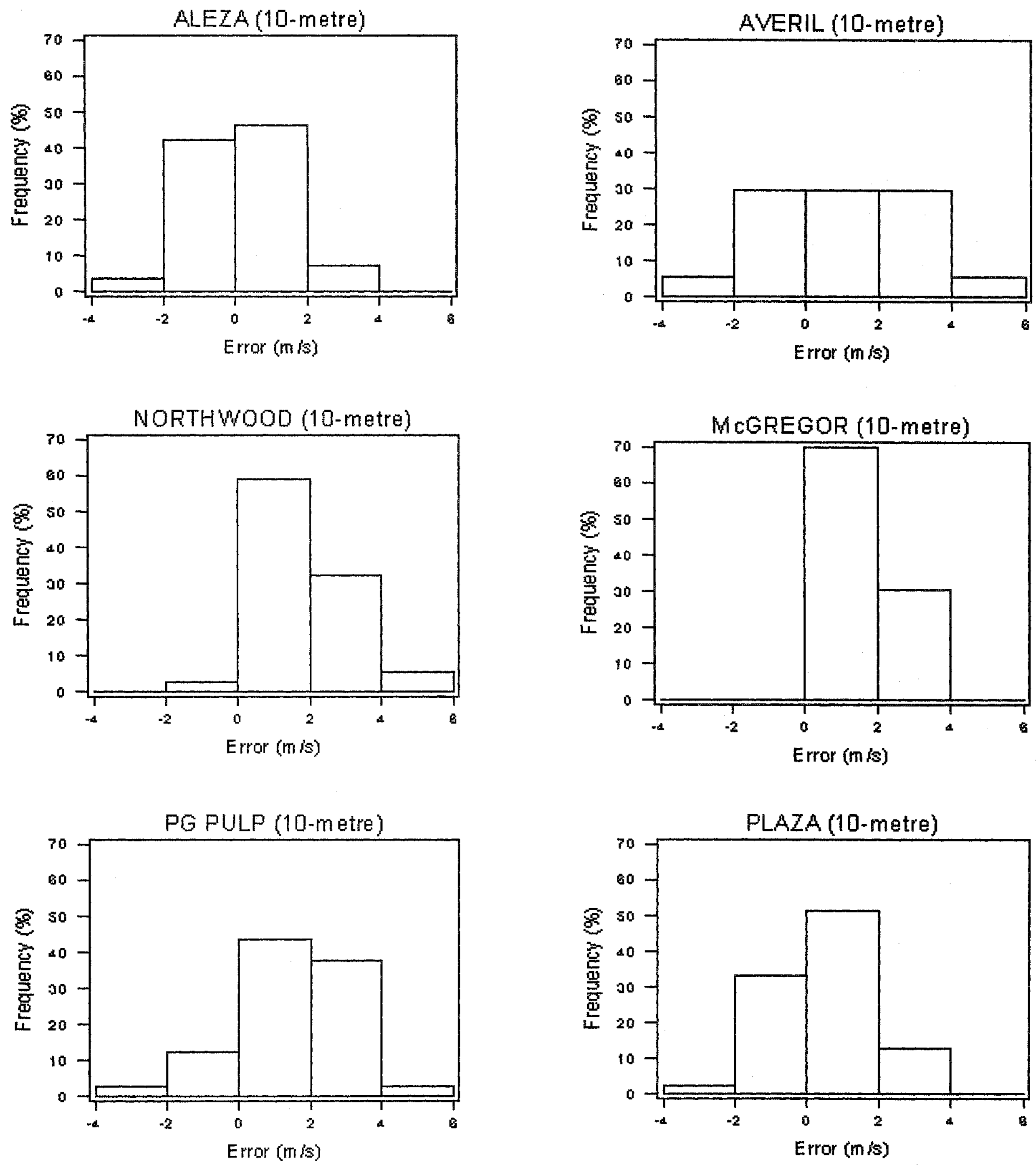

Figure 6.45 Model Error: Histograms showing the frequency distribution of model error at each of the 10-metre wind monitoring stations.

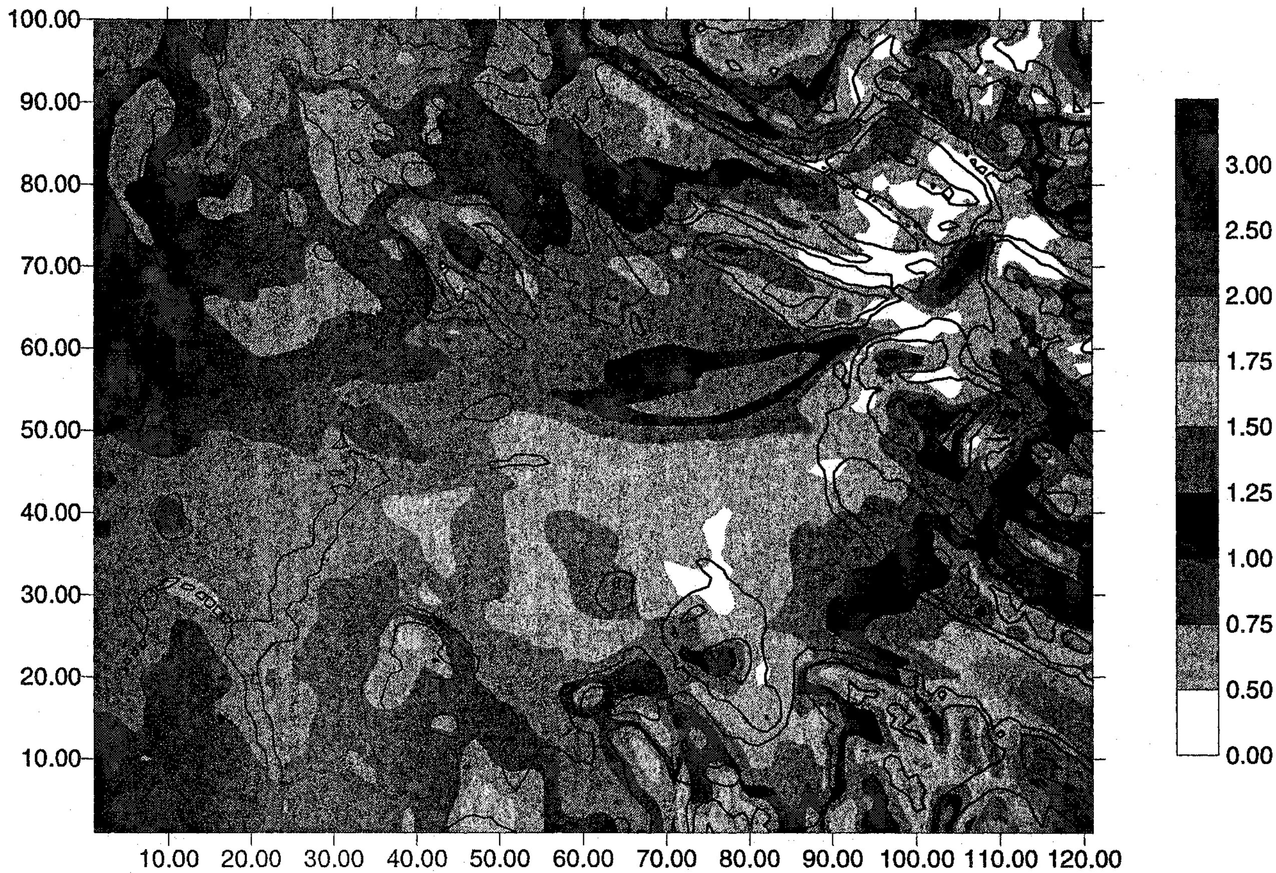

Figure 6.46 Contour Plot of Wind Speed Ratios: Ratio of simulated mean maximum wind speed for each grid cell, to the wind speed simulated for the grid cell nearest the Prince George Airport. Speed ratios were derived from wind maximums simulated for the moderate keyday storm category at a mean height of 70 m and horizontal resolution of 1 km. Topography contours shown in black every 200 m from 600 to 2000 m. Refer to Fig. 6.47 and Fig. 6.48 for corresponding wind directions. (Coverage: 100 x 120 km.)

moderate - max at resolution of 1 km

Scale: 10 m/s =

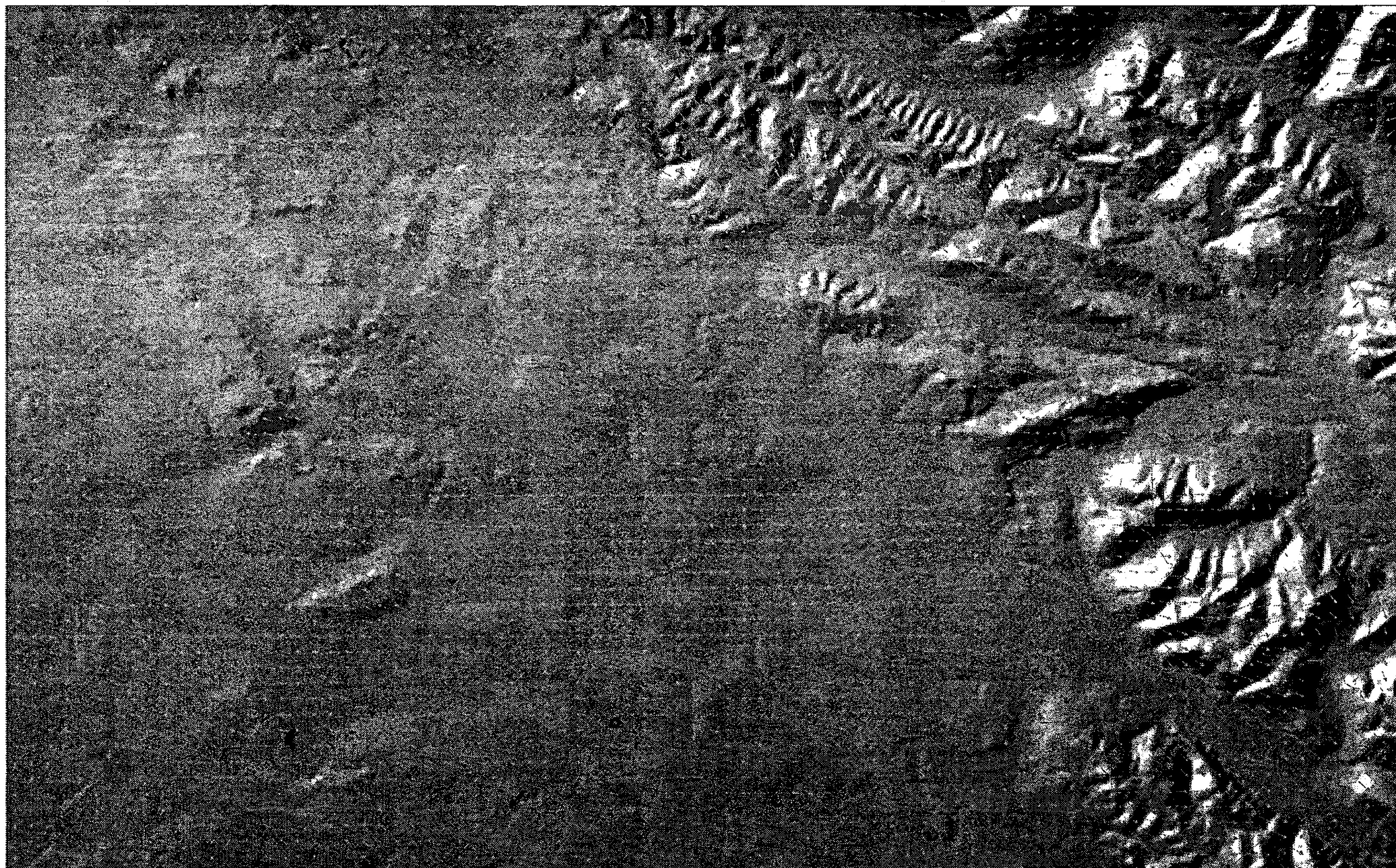

Figure 6.47 Moderate Keyday Wind Directions: Direction of simulated wind maximums for the moderate keyday storm scenario at a mean height of 70 m and horizontal resolution of 1 km. (Coverage: 55 x 85 km.)

average - max at resolution of 1 km

Scale: 10 m/s =

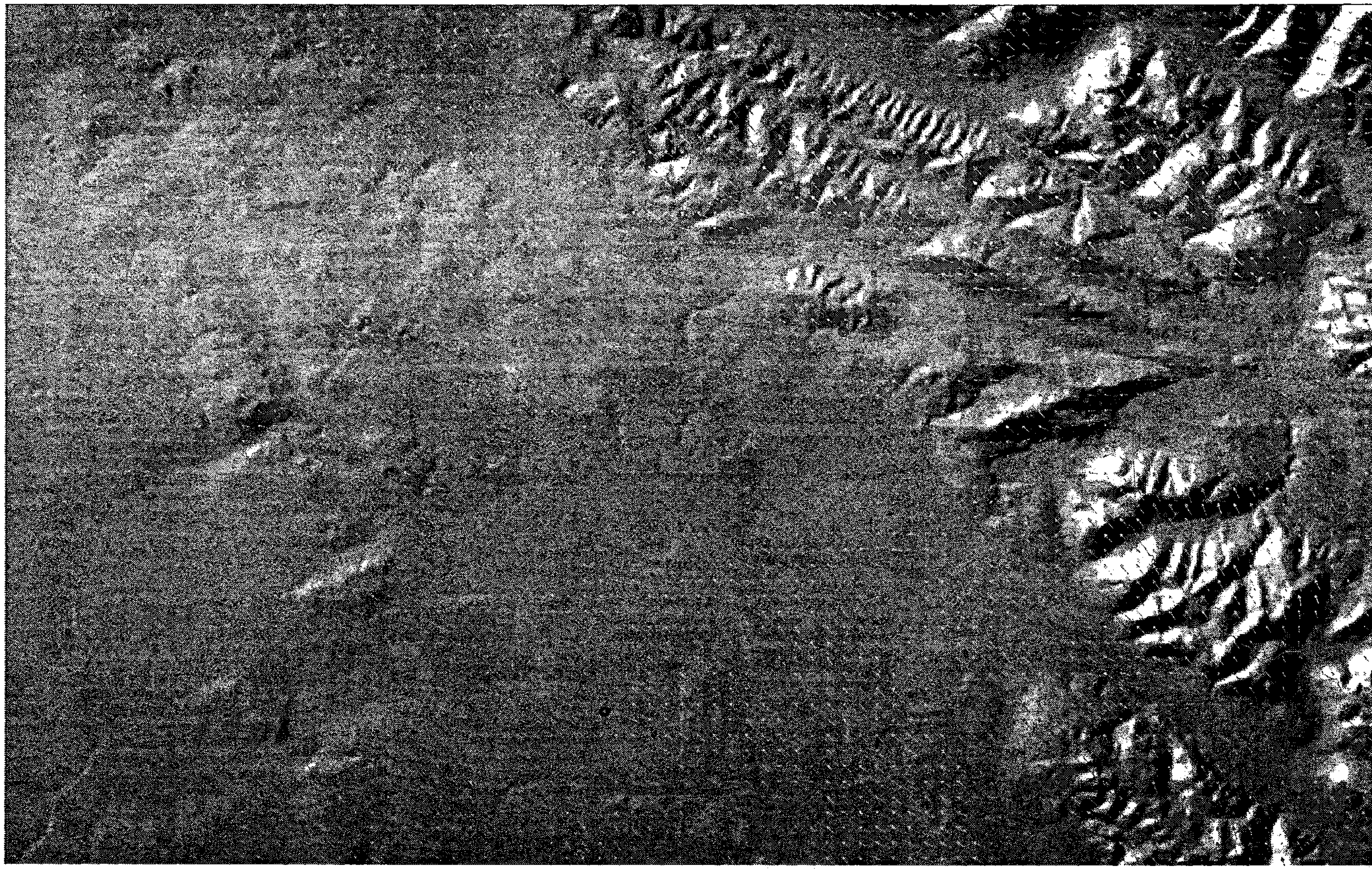

Figure 6.48 Strong-to-Severe Wind Directions: Vector average of simulated wind directions, and scalar average of maximum mean wind speeds, for the strong and severe keyday storm scenarios at a mean height of 70 m and horizontal resolution of 1 km. (Coverage: 55 x 85 km.)

Appendix B - GrADS Scripts

TABLE OF CONTENTS

B.1 INTRODUCTION: The Gridded Analysis and Display System

The Gridded Analysis and Display System (GrADS) is an interactive desktop tool for the analysis and display of earth science data developed by the Center for Ocean-Land-Atmosphere studies, Calverton, MD. The software is GRIB (GRIdded Binary) compatible and is freely distributed over the Internet (http://grads.iges.org). GrADS implements a 4-Dimensional data model, where the dimensions are usually latitude, longitude, level, and time. Operations may be performed on the data directly using a set of built-in functions, or users may add their own functions as external routines written in any language. A programmable scripting language can also be used to automate complex multi-step calculations or displays.

Three GrADS scripts were written in order to construct the synoptic composites developed in Chapter 4 (see **Table B.1**). GrADS was executed with the following command: grads -lc "open /d1/murphyb/grads/daily/mslp/PRESmsl.daily.1970_1994.ctl". The control (.ctl) file, synoptic climatology programs, and supplementary scripts and data files are provided in the sections below.

Table B.1 Synoptic Climatology Scripts:

SCRIPT	DESCRIPTION
CLIMATE.GS	Produces a mean daily map for a specific averaging period.
COMPOSITE.GS	Produces a average map for a discontinuous list of dates/times.
SIGFIG.GS	Computes the statistical significance of climate anomalies.

B.2 GrADS SCRIPT FILES: Synoptic Climatology Programs

```
* SCRIPT:       CLIMATE.GS

* PURPOSE:      Produces a mean daily map for a specific averaging period.

* AUTHOR:       Brendan Murphy, University of Northern B.C.

* DETAILS:      The script as written, computes a 25-year mean for the Fall/Winter period
*               November through March.  It assumes the use of daily data for the 25-year
*               period 1970-1975.  Therefore, t=1 is 01JAN1970 and t=9131 is 31DEC1994.

* CALLS:        Other scripts called are: map.gs and isoplth.gs

* OUTPUT:       The following grids are left in memory:

*               clim - mean climatology map

* VARIABLES WHICH REQUIRE CHANGING BY THE USER:

                MAPPATH     =     '/d1/murphyb/grads/scripts/'
                OUTPATH     =     '/d1/murphyb/grads/results/'

                IMAX        =     9131
                VAR         =     'PRESmsl'
                LEVEL       =     0

************************************************************
*                       START OF SCRIPT                    *
************************************************************

 'c' ; say ' '
 'set grads off'
 'run 'MAPPATH'map'
 'set lev 'LEVEL

* Run climate function (see declared function below)

 climate(VAR,IMAX,LEVEL)
* Output resulting climatology (clim) and standard deviation (sdev) in mb

 'run isoplth 'LEVEL
 if(LEVEL=0) then
   'd clim/100'
 else
   'd clim'
 endif
 'draw title Climatology 1970-1994('VAR'): N='_Nclim

 prompt 'Print Climatology? (y/n) '
 pull ans
 if (ans='y'|ans='Y')
   'enable print 'OUTPATH'clim.gmf'
   'print'
   'disable print'
   say ' FILE PRINTED: 'OUTPATH'clim.gmf'
 endif

************************************************************
*                        END OF SCRIPT                     *
************************************************************
```

```
FUNCTION climate(VAR,IMAX,LEVEL)

 say ' '
 say 'PLEASE WAIT ... building climatology from daily data'
 say ' '

* initialize the average counter
 n=0

* initialize the sum grids to 0
 'define x=const('VAR', 0, -a)'
 'define x2=const('VAR',0,-a)'

* initialize time counter
 I=1

* begin iteration to sum grids
 while(I<=IMAX)

*   *** check date ***
   'set t 'i
   'q time'
   year=substr(result,16,4)
   month=substr(result,13,3)
   day=substr(result,11,2)
   if(month='JAN')|(month='FEB')|(month='MAR')|(month='OCT')|(month='NOV')|(month='DEC')
     if(month='JAN')&(day='01')
       say 'Time = 'day month year '    n = 'n+1
     endif

*     *** check for invalid data ***
     'set gxout stat'
     'd 'VAR
     card=sublin(result,7)
     nvalid=subwrd(card,8)
     'set gxout contour'

*     *** add valid data to running sum ***
     if(nvalid !=0)
       n=n+1
       'define x=x+'VAR
       'define x2=x2+pow('VAR',2)'
     endif
     if(month='DEC')&(day='31')
       'c'
       'run isoplth 'LEVEL
       if(LEVEL=0) then
         'd x/'n'/100'
       else
         'd x/'n'/1'
       endif
       'draw title 1970 to 'year' (n='n')'
     endif
   endif
   i=i+1
 endwhile

* Compute average and standard deviation

 if(n!=0)
  'define clim = x/'n
  'define sdev=sqrt((x2/'n')-(pow(clim,2)))'
 else
  'define clim = const(x,-999,-a)'
```

```
 'define sdev=const(x,-999,-a)'
endif
say 'FINISHED (n= 'n')'; say ' ';
'undefine x'
'undefine x2'
'c'
_Nclim=n

RETURN
```

```
* SCRIPT:        COMPOSITE.GS

* PURPOSE:       Produces a composite (average) map for a list of dates/times which are supplied by the user.

* AUTHOR:        Brendan Murphy, University of Northern B.C.

* DETAILS:       The file containing the list of dates/times to be included in the composite needs to be specified
*                by the user (see INDAT). The first line of INDAT should provide the variable, level and number
*                of dates to be included in the composite. (Note: INDAT must be consistent with the current .ctl)

*                eg.     PRESmsl 0 2          HGTprs 850 2
*                        1                    1
*                        9131                 9131

* CALLS:         Other scripts called are: map.gs and isoplth.gs

* OUTPUT:        The following grids are left in memory:

*                comp - the composite map
*                sdev - the standard deviation of the composite

* VARIABLES WHICH REQUIRE CHANGING BY THE USER:

                 MAPPATh    =    '/d1/murphyb/grads/scripts/'
                 OUTPATH    =    '/d1/murphyb/grads/results/'
                 INDAT      =    '/d1/murphyb/grads/gusts/gusts.dat'

**********************************************************
*                    START OF SCRIPT                     *
**********************************************************

* Allow user to select grid domain

*  say ''
  'run 'MAPPATH'map'

* Obtain variable to be composited

  file   = substr(INDAT,25,10)
  header1 = sublin(read(INDAT),2)
  var    = subwrd(header1,1)
  level  = subwrd(header1,2)
  imax   = subwrd(header1,3)

  'set lev ' level

* Read in list of discontinuous times and echo input data

  say ''
  say 'Reading INDAT: 'INDAT
  say ''
  say ' 'header1
  i=1
  while(i<=imax)
   data=sublin(read(INDAT),2)
   _it.i=subwrd(data,1)
   say ' 'data
   i=i+1
  endwhile

  say ''
  say 'Building composite for: 'var
  say 'Number of fields:      'imax
```

```
  say 'Level:              'level
  say ' '

* Run composite function (see declared function below)

 compo(var,imax,level)

* Output resulting composite (comp) and standard deviation (sdev) in mb

 say ' '
 say 'MAP: COMPOSITE('var') N='_Ncomp
 'c'
 'set grads off'
 'set cstyle 1'
 'set ccolor 1'
 'run isoplth 'level
 if(level=0)
  'd comp/100'
 else
  'd comp'
 endif
 'draw title Comp 'var': 'file' n='_Ncomp
 say ' '
 prompt 'Print Composite? (y/n) '
 pull ans
 if(ans='y' | ans='Y')
  'enable print 'OUTPATH'comp.gmf'
  'print'
  'disable print'
  say 'FILE PRINTED: 'OUTPATH'comp.gmf'
  say ' '
 endif
 prompt 'Plot standard deviation? (y/n) '
 pull ans
 if(ans='y' | ans='Y')
  'c'
  'set cmin 0'
  'set cmax 20'
  'set cint 2'
  'set ccolor 1'
  'd sdev/100'
  'draw title SDEV Comp('var'): 'file' n='_Ncomp
  prompt 'Print Standard Deviation? (y/n) '
  pull ans
  if(ans='y' | ans='Y')
   'enable print 'OUTPATH'sdev.gmf'
   'print'
   'disable print'
   say 'FILE PRINTED: 'OUTPATH'sdev.gmf'
   say ' '
  endif
 endif


*****************************************************************
*                          END OF SCRIPT                        *
*****************************************************************
```

```
FUNCTION compo(var,imax,level)

* Initialize the average counter
 n=0

* Initialize the temporary sum grids (mean and mean square) to zero
   'define x=const('var',0,-a)'
   'define x2=const('var',0,-a)'

* Start iteration

  i=1

  while(i<=imax)

   'set t '_it.i

*    *** check for invalid data ***
    'set gxout stat'
    'd 'var
    card=sublin(result,7)
    nvalid=subwrd(card,8)
    'set gxout contour'

*    *** display valid maps ***
    if(nvalid != 0)
     'c'
     'run isoplth 'level
     if(level=0)
       'd 'var'/100'
       else
         'd 'var
     endif
     'draw title 'var ' (t='_it.i')'

*    *** allow user to exclude displayed map from composite ***
     (Comment this section out for large data sets!)
     prompt 'MAP:' _it.i' Include in composite? (y/n) '
     pull ans
     while (!(ans='y') & !(ans='n') & !(ans='Y') & !(abs='N'))
       say ' '
       prompt 'Please enter (y/n): '
       pull ans
       say ' '
     endwhile

   *** add fields to running sums ***
     if(ans='y' | ans='Y')
       n=n+1
       'define x=x+'var
       'define x2=x2 + pow('var',2)'
     endif
    endif

    i=i+1

  endwhile

* Calculate the mean (composite) of selected maps and their standard deviation
  if(n!=0)
    'define comp = x/'n
    'define sdev = sqrt((x2/'n')-(pow(comp,2)))'
  else
    'define comp = const(x,-999,-a)'
```

```
 'define sdev = const(x2,-999,-a)'
endif

* Assign the number of fields included in composite to a global
* variable for future processing and drop temporary grids
 'undefine x'
 'undefine x2'
 _Ncomp=n
 RETURN
```

```
* SCRIPT:      SIGFIG.GS

* USAGE:       'run sigfig n'  <n = number of fields in the composite>

* PURPOSE:     Computes the statistical significance of climate anomalies using a two-tailed Student's t-test.

* AUTHOR:      Brendan Murphy, University of Northern B.C.

* DETAILS:     The composite (comp), standard deviation (sdev) and climate (clim) fields are used to calculate
*               t-values at each grid point (tvals).  The statisitical significance is tested at the 95% or 99% level
*              by interpolating from an encoded t-table.  Areas of significance are shaded-in over the climate
*              anomaly (comp-clim).

* CALLS:       Grids comp, sdev and clim must be already defined in memory.
*              (See programs climate.gs and composite.gs).

*              Function also requires the external data files t1.dat and t5.dat.

* * * * * * * * * * * * * * * * * * * * * * * * * * * * * * * * * * * * * * * * * * * * * * * * * * * * * * * * * * * * * *
*                                 START OF SCRIPT                              *
* * * * * * * * * * * * * * * * * * * * * * * * * * * * * * * * * * * * * * * * * * * * * * * * * * * * * * * * * * * * * *

FUNCTION sigfig(n)

'define tvals=abs((comp-clim)/(sdev/sqrt('n')))'

* 99% level
 siglev='1'

* 95% level
* siglev='5'

'c'
'set grads off'
'set gxout shaded'
'set clevs 'studt(n,siglev)
'set ccols 0 9'
* 'set clab 99%%'
'd tvals'
'set gxout contour'
'set ccolor 1'
'set cint 2'
'd (comp-clim)/100'
'draw title Anomaly & Statistical Significance (99% level)'

* * * * * * * * * * * * * * * * * * * * * * * * * * * * * * * * * * * * * * * * * * * * * * * * * * * * * * * * * * * * * *
*                                 END OF SCRIPT                                *
* * * * * * * * * * * * * * * * * * * * * * * * * * * * * * * * * * * * * * * * * * * * * * * * * * * * * * * * * * * * * *

FUNCTION studt(n,siglev)

* t-table taken from: Zar, H. Jerrold (1984) Biostatistical Analysis, 2nd ed (pp.484-485).

i=0
while(i<50)
 i=i+1
 if (siglev='1')
  t1.i=sublin(read(t1.dat),2)
 else
  t5.i=sublin(read(t5.dat),2)
 endif
endwhile
```

```
if(n<=50)
 say 'n is less than or equal to 50'
 if (siglev='1')
  tcrit=t1.n
 endif
 if(siglev='5')
  tcrit=t5.n
 endif
else
 say 'n is greater than 50'
 if (siglev='5')
  if (n<=60)
   tcrit=2.009-0.009*(n-50)/10
  endif
  if (n>60 & n<=70)
   tcrit=2.000-0.006*(n-60)/10
  endif
  if (n>70 & n<=90)
   tcrit=1.994-0.007*(n-70)/20
  endif
  if (n>90 & n<=120)
   tcrit=1.987-0.007*(n-90)/30
  endif
  if (n>120 & n<=150)
   tcrit=1.980-0.004*(n-120)/30
  endif
  if (n>150 & n<=200)
   tcrit=1.976-0.004*(n-150)/50
  endif
  if (n>200 & n<=1000)
   tcrit=1.972-0.01*(n-200)/800
  endif
 else
  if (n<=60)
   say 'n is less than or equal to 60 and sgnf is 1%'
   tcrit=2.678-0.018*(n-50)/10)
  endif
  if (n>60 & n<=70)
   tcrit=2.660-0.012*(n-60)/10
  endif
  if (n>70 & n<=90)
   tcrit=2.648-0.009*(n-70)/20
  endif
  if (n>90 & n<=120)
   tcrit=2.632-0.015*(n-90)/30
  endif
  if (n>120 & n<=150)
   tcrit =2.617-0.008*(n-120)/30
  endif
  if (n>150 & n<=200)
   tcrit=2.609-0.008*(n-150)/50
  endif
  if (n>200 & n<=1000)
   tcrit=2.601-0.02*(n-200)/800
  endif
 endif
endif
say 'tcrit='tcrit
return(tcrit)
```

B.3 SUPPLEMENTARY GrADS FILES

B.3.1 Script Files

MAP.GS

```
* Defines Map Area
'set mpdset mres'
'set grads off'
'set poli off'

'set mpvals -170 -120 40 70'
'set mproj nps'
'set lat 20 90'
'set lon -220 -90'
```

ISOPLTH.GS

```
* Defines Contouring Interval
function isoplth(arg)
'set ccolor 1'
'set grads off'
'set cstyle 1'
if(arg=0)
  'set cmin 954'
  'set cint 4'
endif
if(arg=850)
  'set cmin 840'
  'set cint 60'
endif
if(arg=500)
  'set cmin 4760'
  'set cint 60'
endif
```

B.3.2 Sample Control File

PRESmsl.daily.1970_1994.ctl

```
dset ^PRESmsl.daily.b%y20101.e%y21231
dtype grib
options yrev template
index ^PRESmsl.daily.1970_1994.idx
undef -9.99E+33
title MSLP.daily.1970_1994
xdef  144 linear   0  2.5
ydef   73 linear  -90  2.5
tdef       9131 linear 00Z01jan70 1dy
vars        1
PRESmsl  0 1,102,0 ** Pressure :Pa
ENDVARS
zdef 1 linear 1 1
```

B.3.3 Data Files

T1.DAT	T5.DAT
63.657	12.706
9.925	4.303
5.841	3.182
4.604	2.776
4.032	2.571
3.707	2.447
3.499	2.365
3.355	2.306
3.250	2.262
3.169	2.228
3.106	2.201
3.055	2.179
3.012	2.160
2.977	2.145
2.947	2.131
2.921	2.120
2.898	2.110
2.878	2.101
2.861	2.093
2.845	2.086
2.831	2.080
2.819	2.074
2.807	2.069
2.797	2.064
2.787	2.060
2.779	2.056
2.771	2.052
2.763	2.048
2.756	2.045
2.750	2.042
2.744	2.040
2.738	2.037
2.733	2.035
2.728	2.032
2.724	2.030
2.719	2.028
2.715	2.026
2.712	2.024
2.708	2.023
2.704	2.021
2.701	2.020
2.698	2.018
2.695	2.017
2.692	2.015
2.690	2.014
2.687	2.013
2.685	2.012
2.682	2.011
2.680	2.010
2.678	2.009

Appendix C - MMF Climate Monitoring Network

TABLE OF CONTENTS

C.1 OVERVIEW TO MONITORING NETWORK

To provide additional data for validating the numerical simulations in Chapter 5, and the extrapolation model in Chapter 6, three 3-metre tripod-based weather stations were installed in the McGregor Model Forest (MMF) to supplement the existing stations within the study domain (see Dojo, Seebach and Flute in **Fig 1.1, Appendix A**). The three stations were also intended to provide validation data for the model (MMFCliM) developed by Ross Benton for extrapolating temperature and precipitation. The locations were therefore chosen to provide a range of slope, aspect, elevation and wind exposure. The stations were also situated in order to represent the three biogeoclimatic zones (BGCZ) which comprise most of the MMF, and had to be accessible year round. The geographical attributes of the stations are summarized in **Table C.1**.

Table C.1 MMF Climate Monitoring Network: Location of 3-metre climate monitoring stations.

Station	Installed	Location	Elevation	BGCZ	Dismantled
Dojo	Mar 28/96	54° 15' 22" N 122° 24' 31" W	740 m	SBS mk1	Nov 8 /97
Seebach	June 07/96	54° 22' 45" N 121° 59' 14" W	890 m	SBS vk	Oct 22/97
Flute	June 13/96	54° 18' 23" N 121° 50' 35" W	839 m	ESSF wk2	Oct 22/97

Dojo, the western most station, was located on the north leading edge of a narrow trench through which the Fraser flows southwestward. Seebach located in the northeast, was situated mid-way up the western sloping wall of the Seebach River valley. Flute, located in the east on a small knoll south of a east-west gap through the western edge of the Rockies. All three stations were installed in the spring of 1996 in recently planted cutblocks (3-6 years), and remained deployed until the fall of 1997. The station were visited periodically to inspect for damage, and to download data (see Station History, **Table C2.1**). A series of Fortran programs were written to correct clock and wind vane alignment problems documented during the station visits (**Table C2.2**). The parameters measured at each station varied. As a minimum, each station measured wind speed and direction, temperature and rainfall. Daily, hourly and extremes were recorded using a 1-minute sampling interval. A description of the instrumentation is included in the data logger programs given below.

C.2 STATION DOCUMENTATION

Table C.2.1 Station History: Record of station downloads and description of any problems encountered.

FILE*	START	END	COMMENTS
dojo0596.dat	1996,088,1900	1996,128,0900	Data from stn as installed by envs312/mar28 Wnd Monitor North corrected/Time not DST
dojo0696.dat	1996,128,1600	1996,165,0900	Data after stn rebuilt All future Wnd uncorrected/All future time is DST
dojo1296.dat	1996,255,1500	1996,337,1200	SM not plugged in after download 06/96 Missing 3 months
dojo0497.dat	1996,337,1300	1997,113,1000	Okay
dojo0897.dat	1997,113,1100	1997,225,1400	Okay
bach0696.dat	1996,159,1500	1996,165,1800	Okay
bach1196.dat	1996,232,2100	1996,329,1400	SM not plugged in after download (missing 2 months)
bach0497.dat	1996,329,1500	1997,119,1300	Okay
bach0897.dat	1997,119,1400	1997,225,1200	Okay
bend0197.dat	2000,000,0100 (165,1900)	2000,214,1600 (014,0900)	Clock error: stn started June 13 (1900) Wnd Monitor damaged (icing?) four days prior
bend897a.dat	2000,214,1700	2000,241,1600	Wnd Monitor checked on Feb 10/97 - OKAY
bend897b.dat	1997,041,1000	1997,225,1100	Data logger time corrected to 9:12 DST @ 8:12 PST
bach1097.dat	1997,225,1300	1997,295,1000	Station dismantled
bend1097.dat	1997,225,1200	1997,295,1200	Station dismantled
dojo1197.dat	1997,225,1500	1997,312,1300	Station dismantled

* File naming convention gives month/date on which data was downloaded

Table C.2.2 Data Correction: Description of Fortran programs written to correct problems documented in Table C.2.1.

PROGRAM	ACTION
hly_corr.f	correct HOURLY data from DOJO and SEEBACH stations
dly_corr.f	corrects DAILY data from DOJO and SEEBACH stations
bnd_corr.f	corrects HOURLY data from BEND station
mk_dly.f	creates a DAILY data set for BEND from corrected hourly data
bend.dly.f	corrects DAILY data from BEND (post clock correction) in a format consistent with mk_dly.f.

C.3 DATA LOGGER PROGRAMS

DOJO0596.DOC
McGregor Model Forest
Satellite Climate Sation

DOJO Cutblock 4/18, SBSmk1
Lat: 54o 15' 22.43"
Long: 122o 24' 31.16"
Elev.: 740 m

Initial Development: ENVS 312, Mar/96
Modified: Brendan Murphy, May/96

Tripod Base Climate Station:

Equipment	Height	S/N
CM10 Tripod Support Structure	3.0 m	
Vynckier Equipment Shelter	1.5 m	A6614
CSI CR10 DATA LOGGER		20838
CSI SM716 Storage Module		4087
PS12-12V Power Supply		C1608
ICP 5 Watt Solar Panel	3.0 m	9601
RM Young Radiation Sheild	1.3 m	9601
HMP35CF Temp/RH Probe	1.3 m	9601
RM Young Wind Monitor	3.0 m	16978
TE 525M Tipping Bucket	3.0 m	13936
REBS Net Radiometer	3.0 m	Q94250
Li-Cor 200S Pyranometer	3.0 m	19884

Flag Usage:
10 Output

Input Channel Usage:

1L	2	Temp/RH Probe	Orange
2H	3	Temp/RH Probe	Green
2L	4	Wind Monitor	Green
3H	5	Pyranometer	Red
3L	6	Pyranometer	Black
6H	11	Net Radiomer	Red
6L	12	Net Radiometer	Black

Excitation Channel Usage:

E2	2500mV DC	Wind Monitor - direction	Black
E2	2500mV DC	Temp/RH Probe - humidity	Yellow
E3	250mV DC	Temp/RH Probe - temperature	Black

Pulse Input Channel Usage:

P1	Wind Monitor - speed	Red
P2	Tipping Bucket	Black

Input Location Usage:

1	Air Temperature	oC
2	Relative Humidity	%
3	Solar Radiation	MJ/m^2
4	Net Radiation	kW/m^2
5	Wind Speed	m/s
6	Wind Direction	degrees
7	Rainfall	mm
8	Logger Temp	oC

Page 2 Table 1

9	Battery Voltage	volts

Output Array Definitions:

1) Hourly Output Table ID: 60 (minutes)

01	Table ID	060
02	Year	YYYY
03	Julian Day	DDD
04	Time	HHMM
05	Average Air Temperature 1.3 m	oC
06	Average Relative Humidity 1.3 m	%
07	Average Net Radiation 3.0 m	KW/m^2
08	Average Wind Speed 3.0 m	m/s
09	Average Wind Direction	deg
10	Standard Deviation of Wind Direction	deg
11	Standard Deviation of Wind Speed	m/s
12	Maximum Hourly Wind Speed 3.0 m	m/s
13	Time of Maximum Hourly Wind Speed	HHMM
14	Total Solar Radiation	MJ/m^2
15	Total Rainfall	mm

2) Daily Output Table ID: 24 (hours)

01	Table ID	024
02	Year	YYYY
03	Julian Day	DDD
04	Time	HHMM
05	Average Air Temperature 1.3 m	oC
06	Average Relative Humidity 1.3 m	%
07	Average Solar Radiation	MJ/m^2
08	Average Net Radiation 3.0 m	KW/m^2
09	Average Wind Speed 3.0 m	m/s
10	Average Wind Direction	deg
11	Standard Deviation of Wind Directon	deg
12	Maximum Air Temperature 1.3 m	oC
13	Maximum Relative Humidity 1.3 m	%
14	Maximum Solar Radiation	MJ/m^2
15	Maximum Net Radiation 3.0 m	KW/m^2
16	Maximum Wind Speed 3.0 m	m/s
17	Time of Maximum Wind Speed	HHMM
18	Minimum Air Temperature 1.3 m	oC
19	Minimum Relative Humidity 1.3 m	%
20	Minimum Net Radiation 3.0 m	KW/m^2
21	Minimum Wind Speed 3.0 m	m/s
22	Time of Minimum Wind Speed	HHMM
23	Total Solar Radiation	MJ/m^2
24	Total Rainfall	mm
25	Mimimum Panel Temperature	oC
26	Minimum Battery Voltage	V
27	Maximum Battery Voltage	V

* 1 Table 1 Programs
01: 2 Sec. Execution Interval

Page 3 Table 1

01: P4 Excite,Delay,Volt(SE)
01: 1 Rep
02: 4 250 mV slow Range
03: 2 IN Chan
04: 3 Excite all reps w/EXchan 3
05: 0 Delay (units .01sec)
06: 250 mV Excitation
07: 1 Loc [:Temp_oC]
08: .002 Mult
09: 0 Offset

HMP35CF Temp/RH Probe - Temp
Wiring:

black	E3
orange	1L (SE#2)
white	AG

02: P55 Polynomial
01: 1 Rep
02: 1 X Loc Temp_oC
03: 1 F(X) Loc [:Temp_oC]
04: -74.168 C0
05: 646.22 C1
06: -3848.9 C2
07: 16107 C3
08: -34225 C4
09: 30009 C5

03: P4 Excite,Delay,Volt(SE)
01: 1 Rep
02: 5 2500 mV slow Range
03: 3 IN Chan
04: 2 Excite all reps w/EXchan 2
05: 15 Delay (units .01sec)
06: 2500 mV Excitation
07: 2 Loc [:RH_%]
08: .1 Mult
09: 0 Offset

HMP35CF Temp/RH Probe - Humidity
Wiring:

red	12V
yellow	E2
purple	AG
green	2H (SE#3)

04: P2 Volt (DIFF)
01: 1 Rep
02: 25 2500 mV 60 Hz rejection Range
03: 3 IN Chan
04: 3 Loc [:Solar Rad]
05: 0.0077 Mult (60 sec scan rate)
06: 0 Offset

Li-Cor Pyranometer S/N 19884
Cal. 7.78 mV per KW/m^2
Wiring:

red	3H
black	3L
clear	G

If, for some reason, the pyranometer is outputing a value less than zero in darkness hours, then set the value to zero so as to preserve correct daily values

05: P89 If X<=>F
01: 3 X Loc Solar Rad
02: 4 <
03: 0.0000 F
04: 30 Then Do

Page 4 Table 1

```
06: P30 Z=F
01: 0.0000 F
02: 00 Exponent of 10
03: 3 Z Loc [:Solar Rad]
07: P95 End
08: P2 Volt (DIFF)
01: 1 Rep
02: 24 250 mV 60 Hz rejection Range
03: 6 IN Chan
04: 4 Loc [:Q* KW/m^2]
05: 1 Mult
06: 0.0000 Offset
```

RBES Net Radiometer S/N Q19884
Wiring:

red	6H
black	6L

```
09: P89 If X<=>F - Check Flux Direction
01: 4 X Loc Q* KW/m^2
02: 3 >=
03: 0 F
04: 30 Then Do

10: P37 Z=X*F - If positive, use top calibration factor
01: 4 X Loc Q* KW/m^2
02: 0.0085 F
03: 4 Z Loc [:Q* KW/m^2]

11: P94 Else

12: P37 Z=X*F If negative, use bottom calibration factor
01: 4 X Loc Q* KW/m^2
02: 0.1284 F
03: 4 Z Loc [:Q* KW/m^2]

13: P95 End

14: P3 Pulse
01: 1 Rep
02: 1 Pulse Input Chan
03: 21 Low level AC; Output Hz.
04: 5 Loc [:Wspd m/s ]
05: 0.098 Mult
06: 0.0000 Offset
```

RM Young Wind Monitor - Wind Speed
Model: 05103-10 S/N: 16978
Wiring:

red	P1
black (r&b)	G

```
15: P4 Excite,Delay,Volt(SE)
01: 1 Rep
02: 5 2500 mV slow Range
03: 4 IN Chan
04: 2 Excite all reps w/EXchan 2
05: 2 Delay (units .01sec)
06: 2500 mV Excitation
07: 6 Loc [:Wdir deg ]
08: 0.142 Mult
09: 0.0000 Offset
```

RM Young Wind Monitor - Wind Dir
Model: 05103-10 S/N: 16978
Wiring:

black (g&b)	AG
green	2L (SE#4)
black	E2

Page 5 Table 1

TE525M Tipping Bucket S/N 13936-694
Wiring:

black	P2
white	G
clear	G

16: P3 Pulse
01: 1 Rep
02: 2 Pulse Input Chan
03: 2 Switch closure
04: 7 Loc [:Rain mm]
05: 0.1 Mult
06: 0.0000 Offset

17: P17 Module Temperature
01: 8 Loc [:Panel oC]

18: P10 Battery Voltage
01: 9 Loc [:Batt_V]

HOURLY OUTPUT ARRAY
(Table ID: 060)

19: P92 If time is
01: 0 minutes into a
02: 1 minute interval
03: 10 Set high Flag 0 (output)

20: P80 Set Active Storage Area
01: 1 Final Storage Area 1
02: 60 Array ID or location

21: P77 Real Time
01: 1220 Year,Day,Hour-Minute

22: P71 Average Air Temperature & RH
01: 2 Reps
02: 1 Loc Temp_oC

23: P71 Average Net Radiation
01: 1 Rep
02: 4 Loc Q* KW/m^2

24: P69 Wind Vector : Horizontal Wind Speed, Direction, Sigma
01: 1 Rep
02: 0 Samples per sub-interval
03: 0 Polar Sensor/(S, D1, SD1)
04: 5 Wind Speed/East Loc Wspd m/s
05: 6 Wind Direction/North Loc Wdir deg

25: P82 Standard Deviation of Wind Speed
01: 1 Rep
02: 5 Sample Loc Wspd m/s

26: P73 Maximize
01: 1 Rep
02: 10 Value with Hr-Min
03: 5 Loc Wspd m/s

Page 6 Table 1

27: P72 Totalize
01: 1 Rep
02: 3 Loc Solar Rad

28: P72 Totalize
01: 1 Rep
02: 7 Loc Rain mm

DAILY OUTPUT ARRAY
(Table ID: 024)

29: P92 If time is
01: 0 minutes into a
02: 5 minute interval
03: 10 Set high Flag 0 (output)

30: P80 Set Active Storage Area
01: 1 Final Storage Area 1
02: 24 Array ID or location

31: P77 Real Time
01: 1220 Year,Day,Hour-Minute

32: P71 Average Air Temp, RH, Solar & Net Radiation
01: 4 Reps
02: 1 Loc Temp_oC

33: P69 Wind Vector
01: 1 Rep
02: 0 Samples per sub-interval
03: 0 Polar Sensor/(S, D1, SD1)
04: 5 Wind Speed/East Loc Wspd m/s
05: 6 Wind Direction/North Loc Wdir deg

34: P73 Maximize Air Temp, RH, Solar, & Net Rad
01: 4 Reps
02: 0 Value only
03: 1 Loc Temp_oC

35: P73 Maximize
01: 1 Rep
02: 10 Value with Hr-Min
03: 5 Loc Wspd m/s

36: P74 Minimize Air Temp & RH
01: 3 Reps
02: 00 Time Option
03: 1 Loc Temp_oC

37: P74 Minimize Net Radiation
01: 1 Rep
02: 00 Time Option
03: 4 Loc Q* KW/m^2

Page 7 Table 1

38: P74 Minimize
01: 1 Rep
02: 10 Value with Hr-Min
03: 5 Loc Wspd m/s

39: P78 Resolution
01: 1 High Resolution

40: P72 Totalize
01: 1 Rep
02: 3 Loc Solar Rad

41: P78 Resolution
01: 0 Low Resolution

42: P72 Totalize
01: 1 Rep
02: 7 Loc Rain mm

43: P74 Minimize
01: 2 Reps
02: 00 Time Option
03: 8 Loc Panel oC

44: P73 Maximize
01: 1 Rep
02: 00 Time Option
03: 9 Loc Batt_V

45: P96 Serial Output
01: 71 SM192/SM716/CSM1

46: P End Table 1

BACH0596.DOC
McGregor Model Forest
Satellite Climate Sation

SEEBACH Cutblock 11/9, SBSvk
Lat: 54o 22' 44.95"
Long: 121o 59' 13.57"
Elev.: 890 m

Initial Development: Brendan Murphy May/96

Tripod Base Climate Station:

Equipment	Height	S/N
CM10 Tripod Support Structure	3.0 m	
Hoffman Equipment Shelter	1.5 m	A6614
CSI CR10 Datalogger		20340
CSI SM716 Storage Module		3742
PS12-12V Power Supply		7046
ICP 5 Watt Solar Panel	3.0 m	9602
RM Young Radiation Sheild	1.3 m	9602
HMP35CF Temp/RH Probe	1.3 m	C1455
RM Young Wind Monitor	3.0 m	16827
with 50ft cable		C1122
TE 525M Tipping Bucket	3.0 m	694

Flag Usage:
10 Output

Input Channel Usage:

1L	2	Temp/RH Probe	Orange
2H	3	Temp/RH Probe	Green
2L	4	Wind Monitor	Green

Excitation Channel Usage:

E2	2500mV DC	Wind Monitor - direction	Black
E2	2500mV DC	Temp/RH Probe - humidity	Yellow
E3	250mV DC	Temp/RH Probe - temperature	Black

Pulse Input Channel Usage:

P1	Wind Monitor - speed	Red
P2	Tipping Bucket	Black

Input Location Usage:

1	Air Temperature	oC
2	Relative Humidity	%
5	Wind Speed	m/s
6	Wind Direction	degrees
7	Rainfall	mm
8	Logger Temp	oC
9	Battery Voltage	volts

Output Array Definitions:

1)	Hourly Output Table:	
	01 Table ID - Station 2, 60 minutes	2060
	02 Year	YYYY
	03 Julian Day	DDD

Page 2 Table 1

04 Time	HHMM
05 Average Air Temperature 1.3 m	oC
06 Average Relative Humidity 1.3 m	%
07 Average Wind Speed	m/s
08 Average Wind Direction	deg
09 Standard Deviation of Wind Direction	deg
10 Maximum Hourly Wind Speed 3.0 m	m/s
11 Time of Maximum Hourly Wind Speed	HHMM
12 Total Rainfall	mm

2) Daily Output Table ID:

01 Table ID - Station 2, 24 hour	2024
02 Year	YYYY
03 Julian Day	DDD
04 Time	HHMM
05 Average Air Temperature 1.3 m	oC
06 Average Relative Humidity 1.3 m	%
07 Average Wind Speed 3.0 m	m/s
08 Average Wind Direction	deg
09 Standard Deviation of Wind Directon	deg
10 Maximum Air Temperature 1.3 m	oC
11 Maximum Relative Humidity 1.3 m	%
12 Maximum Wind Speed 3.0 m	m/s
13 Time of Maximum Wind Speed	HHMM
14 Minimum Air Temperature 1.3 m	oC
15 Minimum Relative Humidity 1.3 m	%
16 Minimum Wind Speed 3.0 m	m/s
17 Time of Minimum Wind Speed	HHMM
18 Total Rainfall	mm
19 Mimimum Panel Temperature	oC
20 Minimum Battery Voltage	V
21 Maximum Battery Voltage	V

* 1 Table 1 Programs
01: 60 Sec. Execution Interval

01: P4 Excite,Delay,Volt(SE)
01: 1 Rep
02: 4 250 mV slow Range
03: 2 IN Chan
04: 3 Excite all reps w/EXchan 3
05: 0 Delay (units .01sec)
06: 250 mV Excitation
07: 1 Loc [:Temp_oC]
08: .002 Mult
09: 0 Offset

HMP35CF Temp/RH Probe - Temp
Wiring:

black	E3
orange	1L (SE#2)
white	AG

Page 3 Table 1

02: P55 Polynomial
01: 1 Rep
02: 1 X Loc Temp_oC
03: 1 F(X) Loc [:Temp_oC]
04: -74.168 C0
05: 646.22 C1
06: -3848.9 C2
07: 16107 C3
08: -34225 C4
09: 30009 C5

03: P4 Excite,Delay,Volt(SE)
01: 1 Rep
02: 5 2500 mV slow Range
03: 3 IN Chan
04: 2 Excite all reps w/EXchan 2
05: 15 Delay (units .01sec)
06: 2500 mV Excitation
07: 2 Loc [:RH_%]
08: .1 Mult
09: 0 Offset

HMP35CF Temp/RH Probe - Humidity
Wiring:

red	12V
yellow	E2
purple	AG
green	2H (SE#3)

04: P3 Pulse
01: 1 Rep
02: 1 Pulse Input Chan
03: 21 Low level AC; Output Hz.
04: 5 Loc [:Wspd m/s]
05: 0.098 Mult
06: 0.0000 Offset

RM Young Wind Monitor - Wind Speed
Model: 05103-10 S/N: 16978
Wiring:

red	P1
black (r&b)	G

05: P4 Excite,Delay,Volt(SE)
01: 1 Rep
02: 5 2500 mV slow Range
03: 4 IN Chan
04: 2 Excite all reps w/EXchan 2
05: 2 Delay (units .01sec)
06: 2500 mV Excitation
07: 6 Loc [:Wdir deg]
08: 0.142 Mult
09: 0.0000 Offset

RM Young Wind Monitor - Wind Dir
Model: 05103-10 S/N: 16978
Wiring:

black (g&b)	AG
green	2L (SE#4)
black	E2

06: P3 Pulse
01: 1 Rep
02: 2 Pulse Input Chan
03: 2 Switch closure
04: 7 Loc [:Rain mm]
05: 0.1 Mult
06: 0.0000 Offset

TE525M Tipping Bucket S/N 13936-694
Wiring:

black	P2
white	G
clear	G

07: P17 Module Temperature
01: 8 Loc [:Panel oC]

08: P10 Battery Voltage
01: 9 Loc [:Batt_V]

Page 4 Table 1

HOURLY OUTPUT ARRAY

09: P92 If time is
01: 0 minutes into a
02: 60 minute interval
03: 10 Set high Flag 0 (output)

10: P80 Set Active Storage Area
01: 1 Final Storage Area 1
02: 2060 Array ID or location

11: P77 Real Time
01: 1220 Year,Day,Hour-Minute

12: P71 Average Air Temperature & RH
01: 2 Reps
02: 1 Loc Temp_oC

13: P69 Wind Vector : Horizontal Wind Speed, Direction, Sigma
01: 1 Rep
02: 0 Samples per sub-interval
03: 0 Polar Sensor/(S, D1, SD1)
04: 5 Wind Speed/East Loc Wspd m/s
05: 6 Wind Direction/North Loc Wdir deg

14: P73 Maximize
01: 1 Rep
02: 10 Value with Hr-Min
03: 5 Loc Wspd m/s

15: P72 Totalize
01: 1 Rep
02: 7 Loc Rain mm

DAILY OUTPUT ARRAY

16: P92 If time is
01: 0 minutes into a
02: 1440 minute interval
03: 10 Set high Flag 0 (output)

17: P80 Set Active Storage Area
01: 1 Final Storage Area 1
02: 2024 Array ID or location

18: P77 Real Time
01: 1220 Year,Day,Hour-Minute

19: P71 Average Air Temp & RH
01: 2 Reps
02: 1 Loc Temp_oC

Page 5 Table 1

20: P69 Wind Vector
01: 1 Rep
02: 0 Samples per sub-interval
03: 0 Polar Sensor/(S, D1, SD1)
04: 5 Wind Speed/East Loc Wspd m/s
05: 6 Wind Direction/North Loc Wdir deg

21: P73 Maximize Air Temp & RH
01: 2 Reps
02: 0 Value only
03: 1 Loc Temp_oC

22: P73 Maximize
01: 1 Rep
02: 10 Value with Hr-Min
03: 5 Loc Wspd m/s

23: P74 Minimize Air Temp & RH
01: 2 Reps
02: 00 Time Option
03: 1 Loc Temp_oC

24: P74 Minimize
01: 1 Rep
02: 10 Value with Hr-Min
03: 5 Loc Wspd m/s

25: P72 Totalize
01: 1 Rep
02: 7 Loc Rain mm

26: P74 Minimize
01: 2 Reps
02: 00 Time Option
03: 8 Loc Panel oC

27: P73 Maximize
01: 1 Rep
02: 00 Time Option
03: 9 Loc Batt_V

28: P96 Serial Output
01: 71 SM192/SM716/CSM1

29: P End Table 1

BEND0696.DOC
McGregor Model Forest
Satellite Climate Sation

FLUTE Cutblock 10/16, ESSFwk2
Lat: 54o 18' 22.59"
Long: 121o 50' 34.73"
Elev: 839 m

Initial Development: Brendan Murphy June/96

Tripod Base Climate Station:

Equipment	Height	S/N
CM10 Tripod Support Structure	3.0 m	
Hoffman Equipment Shelter	1.5 m	
CSI CR10 Datalogger		20323
CSI SM716 Storage Module		3743
PS12-12V Power Supply		7052
ICP 5 Watt Solar Panel	3.0 m	9603
Shop Fabricated Radiation Sheild	1.3 m	
107B Temperature Probe (25t)	1.3 m	C3465
RM Young Wind Monitor	3.0 m	21672
with 50ft cable		C1121
BCFS Tipping Bucket Rain Gauge	3.0m	BCFS01

Flag Usage:
10 Output

Input Channel Usage:

2H	3	Temp Probe	Red
2L	4	Wind Monitor	Green

Excitation Channel Usage:

E2	2500mV DC	Wind Monitor - direction	Black
E3	250mV DC	Temp Probe	Black

Pulse Input Channel Usage:

P1	Wind Monitor - speed	Red
P2	Tipping Bucket	Red

Input Location Usage:

1	Air Temperature	oC
5	Wind Speed	m/s
6	Wind Direction	degrees
7	Rainfall	mm
8	Logger Temp	oC
9	Battery Voltage	volts

Output Array Definitions:

Hourly Output Table:

01	Table ID - Station 3, 60 minutes	3060
02	Year	YYYY
03	Julian Day	DDD
04	Time	HHMM
05	Average Air Temperature 1.3 m	oC
06	Average Wind Speed	m/s

page 2 Table 1

07 Average Wind Direction	deg
08 Standard Deviation of Wind Direction	deg
09 Maximum Hourly Wind Speed 3.0 m	m/s
10 Time of Maximum Hourly Wind Speed	HHMM
11 Total Rainfall	mm

Haily Output Table:	
01 Table ID - Station 3, 24 hour	3024
02 Year	YYYY
03 Julian Day	DDD
04 Time	HHMM
05 Average Air Temperature 1.3 m	oC
06 Average Wind Speed 3.0 m	m/s
07 Average Wind Direction	deg
08 Standard Deviation of Wind Directon	deg
09 Maximum Air Temperature 1.3 m	oC
10 Maximum Wind Speed 3.0 m	m/s
11 Time of Maximum Wind Speed	HHMM
12 Minimum Air Temperature 1.3 m	oC
13 Minimum Wind Speed 3.0 m	m/s
14 Time of Minimum Wind Speed	HHMM
15 Total Rainfall	mm
16 Mimimum Panel Temperature	oC
17 Minimum Battery Voltage	V
18 Maximum Battery Voltage	V

* 1 Table 1 Programs
01: 60 Sec. Execution Interval

01: P11 Temp 107 Probe
01: 1 Rep
02: 3 IN Chan
03: 3 Excite all reps w/EXchan 3
04: 1 Loc [:Temp_oC]
05: 1 Mult
06: 0.0000 Offset

Air Temperature
Model: 107B S/N: C3465
Wiring:

red	2L (SE#3)
black	E3
purple	AG

02: P3 Pulse
01: 1 Rep
02: 1 Pulse Input Chan
03: 21 Low level AC; Output Hz.
04: 5 Loc [:Wspd m/s]
05: 0.098 Mult
06: 0.0000 Offset

RM Young Wind Monitor - Wind Speed
Model: 05103-10 S/N: 16978
Wiring:

red	P1
black (r&b)	G

Page 3 Table 1

03: P4 Excite,Delay,Volt(SE)
01: 1 Rep
02: 5 2500 mV slow Range
03: 4 IN Chan
04: 2 Excite all reps w/EXchan 2
05: 2 Delay (units .01sec)
06: 2500 mV Excitation
07: 6 Loc [:Wdir deg]
08: 0.142 Mult
09: 0.0000 Offset

RM Young Wind Monitor - Wind Dir
Model: 05103-10 S/N: 16978
Wiring:

black (g&b)	AG
green	2L (SE#4)
black	E2

04: P3 Pulse Tipping Bucket
01: 1 Rep
02: 2 Pulse Input Chan
03: 2 Switch closure
04: 7 Loc [:Rain mm]
05: 0.25 Mult
06: 0.0000 Offset

BCFS01
Wiring:

red	P2
black	G
"unshielded"	

05: P17 Module Temperature
01: 8 Loc [:Panel oC]

06: P10 Battery Voltage
01: 9 Loc [:Batt_V]

HOURLY OUTPUT ARRAY

07: P92 If time is
01: 0 minutes into a
02: 1 minute interval
03: 10 Set high Flag 0 (output)

08: P80 Set Active Storage Area
01: 1 Final Storage Area 1
02: 3060 Array ID or location

09: P77 Real Time
01: 1220 Year,Day,Hour-Minute

10: P71 Average Air Temperature
01: 1 Rep
02: 1 Loc Temp_oC

11: P69 Wind Vector : Horizontal Wind Speed, Direction, Sigma
01: 1 Rep
02: 0 Samples per sub-interval
03: 0 Polar Sensor/(S, D1, SD1)
04: 5 Wind Speed/East Loc Wspd m/s
05: 6 Wind Direction/North Loc Wdir deg

12: P73 Maximize
01: 1 Rep
02: 10 Value with Hr-Min
03: 5 Loc Wspd m/s

Page 4 Table 1

13: P72 Totalize
01: 1 Rep
02: 7 Loc Rain mm

DAILY OUTPUT ARRAY

14: P92 If time is
01: 0 minutes into a
02: 5 minute interval
03: 10 Set high Flag 0 (output)

15: P80 Set Active Storage Area
01: 1 Final Storage Area 1
02: 3024 Array ID or location

16: P77 Real Time
01: 1220 Year,Day,Hour-Minute

17: P71 Average Air Temp
01: 1 Rep
02: 1 Loc Temp_oC

18: P69 Wind Vector
01: 1 Rep
02: 0 Samples per sub-interval
03: 0 Polar Sensor/(S, D1, SD1)
04: 5 Wind Speed/East Loc Wspd m/s
05: 6 Wind Direction/North Loc Wdir deg

19: P73 Maximize Air Temp
01: 1 Rep
02: 0 Value only
03: 1 Loc Temp_oC

20: P73 Maximize
01: 1 Rep
02: 10 Value with Hr-Min
03: 5 Loc Wspd m/s

21: P74 Minimize Air Temp
01: 1 Rep
02: 00 Time Option
03: 1 Loc Temp_oC

22: P74 Minimize
01: 1 Rep
02: 10 Value with Hr-Min
03: 5 Loc Wspd m/s

23: P72 Totalize
01: 1 Rep
02: 7 Loc Rain mm

Page 5 Table 1

24: P74 Minimize
01: 2 Reps
02: 00 Time Option
03: 8 Loc Panel oC

25: P73 Maximize
01: 1 Rep
02: 00 Time Option
03: 9 Loc Batt_V

26: P96 Serial Output
01: 71 SM192/SM716/CSM1

27: P End Table 1